UNIVERSITY OF ALBERTA

THE NATURE OF DIAMONDS AND THEIR MINERAL INCLUSIONS: A STUDY ON DIAMONDS FROM THE PANDA (CANADA) AND JAGERSFONTEIN (SOUTH AFRICA) KIMBERLITES AND FROM PLACER DEPOSITS IN BRAZIL

by

Ralf Tappert ©

A thesis submitted to the Faculty of Graduate Studies and Research in partial fulfillment of the requirements for the degree of DOCTOR OF PHILOSOPHY

DEPARTMENT OF EARTH AND ATMOSPHERIC SCIENCES

EDMONTON, ALBERTA

FALL 2005

Library and
Archives Canada

Published Heritage
Branch

395 Wellington Street
Ottawa ON K1A 0N4
Canada

Bibliothèque et
Archives Canada

Direction du
Patrimoine de l'édition

395, rue Wellington
Ottawa ON K1A 0N4
Canada

0-494-08744-7

Your file Votre référence
ISBN:
Our file Notre reterence
ISBN:

NOTICE:
The author has granted a non-exclusive license allowing Library and Archives Canada to reproduce, publish, archive, preserve, conserve, communicate to the public by telecommunication or on the Internet, loan, distribute and sell theses worldwide, for commercial or non-commercial purposes, in microform, paper, electronic and/or any other formats.

The author retains copyright ownership and moral rights in this thesis. Neither the thesis nor substantial extracts from it may be printed or otherwise reproduced without the author's permission.

AVIS:
L'auteur a accordé une licence non exclusive permettant à la Bibliothèque et Archives Canada de reproduire, publier, archiver, sauvegarder, conserver, transmettre au public par télécommunication ou par l'Internet, prêter, distribuer et vendre des thèses partout dans le monde, à des fins commerciales ou autres, sur support microforme, papier, électronique et/ou autres formats.

L'auteur conserve la propriété du droit d'auteur et des droits moraux qui protège cette thèse. Ni la thèse ni des extraits substantiels de celle-ci ne doivent être imprimés ou autrement reproduits sans son autorisation.

In compliance with the Canadian Privacy Act some supporting forms may have been removed from this thesis.

While these forms may be included in the document page count, their removal does not represent any loss of content from the thesis.

Conformément à la loi canadienne sur la protection de la vie privée, quelques formulaires secondaires ont été enlevés de cette thèse.

Bien que ces formulaires aient inclus dans la pagination, il n'y aura aucun contenu manquant.

Canada

ABSTRACT

This thesis contains the results of detailed studies on diamonds and their mineral inclusions from the Panda kimberlite in Canada; from three alluvial diamond deposits in Brazil (Arenapolis, Boa Vista and Canastra); and, from the Jagersfontein kimberlite in South Africa. The results give insights into the composition and evolution of major parts of the Earth's mantle.

Incorporated are data on the physical, chemical and isotopic characteristics of the diamonds as well as data on the major-, minor- and trace-element composition of the inclusions.

The studied diamonds formed at various depths in the Earth's mantle, including the subcratonic lithospheric upper mantle (150-250 km), the asthenosphere (>250 km) and the transition zone (>410 km), and the lower mantle (>660 km). Depending on the depths of their origin, diamonds and their mineral inclusion indicate distinct chemical source environments and diamond formation processes.

The majority of lithospheric diamonds formed in a depleted peridotitic environment, which experienced an early stage of extensive melt extraction and to different degrees, subsequent re-enrichment. An overall smaller portion of diamonds formed in an eclogitic environment, which at least in some cases can be linked to subducted oceanic crust. Peridotitic and eclogitic diamond sources in the lithospheric mantle, however, are heterogeneously distributed. Diamond formation in the lithospheric mantle is in most cases related to the precipitation of CHO-rich fluids.

Unlike diamonds from the lithosphere and the lower mantle, diamonds from asthenosphere and transition zone reflect predominantly eclogitic sources. The trace-element composition of their inclusions and the carbon stable isotope characteristic of the diamond hosts indicate that these deep diamonds formed exclusively in subducting oceanic crust, most likely from graphite derived from various carbon sources within the slab.

ACKNOWLEDGEMENTS

First of all I would like to thank my supervisor, Thomas Stachel, not only for giving me the opportunity to work on such amazing projects at such a nice place (as it turned out), but also for his constant support throughout the last years.

I would also like to thank Gerhard Brey for cultivating my interest in the Earth's mantle and his support during my studies in Frankfurt and Edmonton.

Thanks to Jeff Harris for introducing me into the secrets of diamonds and for giving me the chance to work on diamond samples from so many different deposits.

I am grateful to Karlis Muehlenbachs, who in his enthusiasm and support is truly an inspiration.

Thanks to the members of my examining committee: Bob Luth, Larry Heaman, Tom Chacko and Ron Cavell, who not only took the time to read the thesis and sit through the exams, but who also taught, motivated and supported me on various occasions. Special thanks to Dan Schulze for coming to Edmonton as external examining committee member and for giving many valuable comments which greatly improved this thesis.

For his excellent analytical work with the ionprobe at the Universität Heidelberg, thanks to Thomas Ludwig and additional thanks to Rainer Altherr for enabling and supporting the measurements right away. I am grateful to Nobu Shimizu for his help with the ionprobe at the Woods Hole Oceanographic Institutions. Thanks to Lutz Nasdala at the Universität Mainz for his effort with the Micro-Raman spectrometer. I would also like to thank Heidi Höfer and Sergei Matveev for their help with the electron microprobes in Frankfurt and Edmonton and for their constantly good spirits. Thanks to Yann Lahaye for his help in the attempts to produce LA-ICP-MS data.

DeBeers Consolidated Mines Ltd is thanked for providing diamond samples.

I am thankful to Derek Robinson for providing valuable information about the locations of the Brazilian diamond deposits. The support by Kenneth Tainton, who supplied me with maps and difficult to access literature from Brazil, is greatly acknowledged. Special thanks to Pedro Jugo for helping me with the translations of the Brazilian literature.

Jan Heliosch and Franz Kneissl are thanked for their help in many instances and for the good times at the tool shop in Frankfurt.

I would also like to thank my colleagues and friends at the University of Alberta for making grad school an “awesome” experience: particularly Anetta Banas and Steven Creighton, “worthy” members of the DRG, for their help and for the good times; Jason “Jay” French for the “rock-spirit”; Hilary Corlett; Trevor MacHattie (special thanks for the comments on the Jagersfontein paper) and Shannon Zurevinski.

Thanks also to my colleagues and friends in Germany and other places in the world: Nina Simon, Sonja Aulbach, Sascha Staubach and Stephan Buhre.

The biggest thanks go to Michelle Goryniuk who not only made the last years a very enjoyable experience, but also helped with her editing skills to finish this project.

Last but not least: Thanks to my family and friends in Germany, who always supported me kept the connection to me alive, even over the great distances.

TABLE OF CONTENTS

CHAPTER 1: INTRODUCTION 1

1.1 BACKGROUND 1
1.2 INTENT AND ORGANIZATION OF THIS THESIS 3
BIBLIOGRAPHY 5

CHAPTER 2: DIAMONDS AND THEIR MINERAL INCLUSIONS FROM THE PANDA KIMBERLITE, SLAVE PROVINCE, CANADA 9

2.1 INTRODUCTION 9
2.1.1 Analytical methods and sample preparation 11
2.1.2 Database 13
2.2 MAJOR ELEMENT COMPOSITION OF MINERAL INCLUSIONS 13
2.2.1 Peridotitic inclusion suite 13
2.2.2 Eclogitic inclusion suite 15
2.2.3 Inclusion assemblages with ferropericlase 16
2.3 TRACE ELEMENT COMPOSITION OF MINERAL INCLUSIONS 18
2.4 GEOTHERMOBAROMETRY 19
2.5 PHYSICAL AND CHEMICAL CHARACTERISTICS OF THE HOST DIAMONDS 20
2.5.1 Morphology and color 20
2.5.2 Nitrogen contents and aggregation levels 21
2.6 DISCUSSION AND CONCLUSIONS 22
2.6.1 Composition of diamond sources beneath the Slave 22
2.6.2 Evolution of the thermal regime in the deep lithosphere 27
BIBLIOGRAPHY 29
TABLES 40
FIGURES 48

CHAPTER 3: PLACER DIAMONDS FROM BRAZIL: INDICATORS OF THE COMPOSITION OF THE EARTH'S MANTLE AND OF THE ORIGIN OF THEIR KIMBERLITE SOURCE 61

3.1 INTRODUCTION 61
3.2 GEOLOGICAL AND GEOGRAPHICAL BACKGROUND OF THE DIAMOND DEPOSITS 62
3.2.1 Arenapolis 63
3.2.1 Boa Vista 63
3.2.3 Canastra 64
3.3 SAMPLE PREPARATION AND ANALYTICAL TECHNIQUES 65
3.4 PHYSICAL CHARACTERISTICS OF THE DIAMONDS 67
3.4.1 Shapes and surface textures 67
3.4.2 Color 68
3.5 MINERAL INCLUSIONS 68
3.5.1 Peridotitic Suite 69
3.5.2 Eclogitic Suite 70
3.6 GEOTHERMOBAROMETRY 71
3.7 COMPOSITIONAL ZONING AND NITROGEN CHARACTERISTICS OF THE DIAMONDS 72

3.8 CARBON ISOTOPE COMPOSITION OF THE DIAMONDS 73
3.9 DISCUSSION 74
3.9.1 Diamond characteristics 74
3.9.2 Characteristics of the mantle source 75
3.10 CONCLUSIONS 77
BIBLIOGRAPHY 78
TABLES 85
FIGURES 90
PLATES 100

CHAPTER 4: DIAMONDS FROM JAGERSFONTEIN (SOUTH AFRICA): MESSENGERS FROM THE SUBLITHOSPHERIC MANTLE 102

4.1 INTRODUCTION 102
4.2 SAMPLE PREPARATION AND ANALYTICAL TECHNIQUES 104
4.3 RESULTS 106
4.3.1 Lithospheric inclusion suite 106
4.3.2 Sublithospheric inclusion suite 108
4.3.3 Chemical and isotopic characteristics of the host diamonds 109
4.4 DISCUSSION 110
4.4.1 Major and trace element compositions 110
4.4.2 Carbon Isotopes 114
4.4.3 Age and geological framework for the sublithospheric diamonds 117
4.5 CONCLUSIONS 119
BIBLIOGRAPHY 120
TABLES 128
FIGURES 134

CHAPTER 5: SUBDUCTING OCEANIC CRUST: THE SOURCE OF DEEP DIAMONDS 147

5.1 INTRODUCTION 147
5.2 METHODS 148
5.3 RESULTS 148
5.4 DISCUSSION 140
5.5 CONCLUSIONS 149
BIBLIOGRAPHY 151
FIGURES 155

CHAPTER 6: GENERAL DISCUSSION AND CONCLUSIONS 158

6.1 DIAMOND FORMATION IN THE LITHOSPHERIC MANTLE 158
6.2 DIAMOND FORMATION IN THE SUBLITHOSPHERIC MANTLE 160
BIBLIOGRAPHY 162

APPENDIX A: METHODOLOGY 165

DIAMOND CRUSHING AND POLISHING 166
ELECTRON-PROBE MICROANALYSIS (EPMA) 167
SECONDARY ION MASS SPECTROMETRY (SIMS) 170

FOURIER TRANSFORM INFRARED (FTIR) SPECTROSCOPY 172
CARBON STABLE ISOTOPE ANALYSIS 176
BIBLIOGRAPHY 177

APPENDIX B: PANDA 178

APPENDIX C: BRAZIL 187

APPENDIX D: JAGERSFONTEIN 205

LIST OF TABLES

Table 2-1: Summary of morphological, paragenetic and nitrogen characteristics of Panda diamonds....40

Table 2-2: Mineral inclusions recovered from Panda diamonds separated into paragenetic groups (based on the major element composition)....42

Table 2-3: Major- and trace element composition of peridotitic and eclogitic inclusions in Panda diamonds....44

Table 2-4: Major element composition of selected sulfide inclusions in diamonds from Panda....45

Table 2-5: Major element composition of inclusions of lower mantle origin in diamonds from Panda....46

Table 2-6: Major element composition of inclusions of uncertain parageneses (lithospheric dunites?)....47

Table 3-1: Summary of morphological, compositional and isotopic characteristics of diamonds from Arenapolis, Boa Vista and Canastra....85

Table 3-2: Mineral inclusions recovered from the studied Brazilian diamonds; separated into paragenetic groups....87

Table 3-3: Major- element composition of selected mineral inclusions in diamonds from Arenapolis, Boa Vista and Canastra....88

Table 3-4: Major- and trace element composition of garnet inclusions in diamonds from Boa Vista....89

Table 4-1: Abundance of inclusions in diamonds from Jagersfontein....128

Table 4-2: Comparison of REE concentrations of PN-garnet megacrysts determined by secondary ion mass spectrometry methods used in this study with independent results....129

Table 4-3: Composition of selected silicate inclusions in lithospheric diamonds from Jagersfontein....130

Table 4-4: Major and trace element composition of lithospheric inclusions in diamonds from Jagersfontein....131

Table 4-5: Major and trace element composition of majoritic garnet inclusions in diamonds from Jagersfontein....133

LIST OF FIGURES

Figure 2-1: Outline of the Slave craton. 48

Figure 2-2: CaO versus Cr_2O_3 for garnet inclusions in diamonds from Panda. 49

Figure 2-3: CaO (wt%) versus molar Mg number for olivine inclusions in diamonds from Panda. 50

Figure 2-4: Diagram of Cr# versus ferric iron ratio of magnesiochromite inclusions in diamonds from Panda. 51

Figure 2-5: Composition of Fe and Fe-Ni sulfide inclusions from Panda diamonds in the Fe-Ni-Cu system. 52

Figure 2-6: Composition of the Cu-Fe sulfide from diamond PA-76 in the Cu-Fe-S system. 53

Figure 2-7: NiO (wt%) versus Mg# for ferropericlase inclusions from Panda diamonds. 54

Figure 2-8: Backscattered-electron image of inclusion from diamond PA-54. 55

Figure 2-9: REE concentrations of harzburgitic garnet inclusions in diamonds from Panda. 56

Figure 2-10: REE concentrations of lherzolitic garnet inclusions in diamonds from Panda. 57

Figure 2-11: Results of geothermobarometric calculations for garnet-opx and garnet-olivine inclusion pairs from Panda diamonds. 58

Figure 2-12: Aggregation level versus nitrogen concentration in Type I diamonds from the Panda kimberlite. 59

Figure 2-13: Diagram of experimentally determined Fe-Mg partitioning between ferropericlase and $(Mg,Fe)_2SiO_4$ polymorphs as function of the composition of the $(Mg,Fe)_2SiO_4$ polymorph. 60

Figure 3-1: Map of South America showing the main tectonic structures and the locations of the studied placer deposits. 90

Figure 3-2: Histogram showing the distribution of surface radiation spots on diamonds from Arenapolis, Boa Vista and Canastra. 91

Figure 3-3: CaO (wt%) versus molar Mg number for olivine inclusions from Arenapolis, Boa Vista and Canastra diamonds. 92

Figure 3-4: CaO versus Cr_2O_3 for garnet inclusions in diamonds from Boa Vista and Canastra. 93

Figure 3-5: Rare earth element concentrations of garnet inclusions in diamonds from Boa Vista. 94

Figure 3-6: FFM ($100*Fe^{2+}/Fe^{2+}+Mg$) versus Cr# (100*Cr/Cr+Al) of magnesiochromite inclusions from Arenapolis, Boa Vista and Canastra diamonds... 95

Figure 3-7: Pressure and temperature conditions calculated for non-touching inclusion pairs from Boa Vista. 96

Figure 3-8: Histograms showing temperature estimates for magnesiochromite inclusions in diamonds from Arenapolis, Boa Vista and Canastra. 97

Figure 3-9: Aggregation state versus nitrogen concentration of Type I diamonds from Brazil. 98

Figure 3-10: Carbon isotopic composition of diamonds from Arenapolis, Boa Vista and Canastra. 99

Figure 4-1: Locality of the Jagersfontein kimberlite and other diamond deposits on the Kaapvaal cratonic block. 134

Figure 4-2: The composition of CaO versus Cr_2O_3 of garnet inclusions in diamonds from Jagersfontein. 135

Figure 4-3: Rare earth element composition of peridotitic garnet inclusions from Jagersfontein diamonds. 136

Figure 4-4: Chondrite normalized rare earth element composition of eclogitic garnet inclusions in diamonds from Jagersfontein. 137

Figure 4-5: Chondrite normalized rare earth element composition of websteritic and high-calcium eclogitic garnet inclusions in diamonds from Jagersfontein. 138

Figure 4-6: Chondrite normalized rare earth element composition of clinopyroxene inclusions in diamonds from Jagersfontein. 139

Figure 4-7: P-T diagram showing the results of geothermobarometric calculations for mineral inclusion pairs in diamonds from Jagersfontein. 140

Figure 4-8: Al+Cr versus Si (pfu) composition of garnet inclusions from Jagersfontein diamonds. 141

Figure 4-9: Chondrite normalized rare earth element composition of majoritic garnet inclusions in diamonds from Jagersfontein. 142

Figure 4-10: Aggregation level versus nitrogen concentration in Jagersfontein diamonds. 143

Figure 4-11: Carbon isotopic composition of peridotitic, eclogitic, websteritic and majoritic garnet bearing, sublithospheric diamonds from Jagersfontein. 144

Figure 4-12: Si versus Mg and Ca composition of majoritic garnet inclusions in diamonds from Jagersfontein and worldwide. 145

Figure 4-13: Cross section of southwestern Gondwanaland showing the processes that may have led to the formation of the deep diamonds 146

Figure 5-1: Atomic proportions of Al+Cr versus Si of majoritic garnet inclusions in diamonds from the Jagersfontein kimberlite. 155

Figure 5-2: Chondrite normalized rare earth element composition of majoritic garnet inclusions in Jagersfontein diamonds. 156

Figure 5-3: Carbon isotope composition of diamonds from the Jagersfontein kimberlite 157

LIST OF PLATES

Plate 3-1: [A] SEI overview image of the surface of abraded diamond.
[B] Close-up of the surface of abraded diamond.
[C] CL image of diamond with oscillatory growth zoning.
[D] CL image of unzoned diamond .100

Plate 3-2: CL images of diamonds from Arenapolis, Boa Vista and Canastra with typical zoning patterns.
[A] Irregular growth zoning.
[B] Sector zoning.
[C],[D] Low nitrogen outer octahedral layer of Boa Vista diamonds. .101

LIST OF ABBREVIATIONS

BSE	Backscattered Electron
CL	Cathodoluminescence
EPMA	Electron Probe Microanalysis
FTIR	Fourier Transform Infrared
HFSE	High Field Strength Element
INAA	Instrumental Neutron Activation Analysis
LA-ICP-MS	Laser Ablation Inductively Coupled Plasma Mass Spectrometry
pfu	per formula unit
REE	Rare Earth Element
REE_N	Rare Earth Element (normalized to chondritic)
SEI	Secondary Electron Image
SIMS	Secondary Ion Mass Spectrometry

In Tables:

,	non-touching pair with
-	touching pair with
amph	amphibole
chr	chromite
cor	corundum
cpx	clinopyroxene
ex	exposed to the surface
grt, gt	garnet
maj	majoritic
ol	olivine
opx	orthopyroxene
qz	quartz
rut	rutile

f	flattened
o	octahedra
d	dodecahedra
i	irregular
m	macle twin
a	aggregate
c	colorless
b	brown
y	yellow

CHAPTER 1

Introduction

1.1 Background

Diamonds attract attention not only because of their monetary value as a gemstone and their brilliant luster when cut to a jewel, but also because they represent samples from the interior of the Earth, from depths that are otherwise inaccessible.

Impurities within diamonds, in the form of mineral inclusions, were found to be particularly important sources of information; protected by the host diamond from alteration, they represent pristine samples of the chemical environment in which the diamond grew. Diamonds and their mineral inclusions, therefore, have been extensively used to reconstruct the chemical composition and the evolution of their source regions in the Earth's mantle.

The results of these studies show that the formation of the vast majority of diamonds took place at depths of ~150-200 kilometers, within the *lithospheric* Earth's mantle underneath the oldest parts of the continents, the Archean cratons (Clifford, 1966). Based on the mineralogy of the diamond inclusions, two main rock types have been identified to be the source of these diamonds (Meyer and Boyd, 1972; Gurney, 1984; Meyer, 1987). The most common source rock is peridotite, which is considered to be the main component of the Earth's mantle in general (Ringwood, 1975). Less abundant on average, are inclusions that indicate an eclogitic source rock. These eclogitic sources, which chemically resemble basaltic compositions, appear to be heterogeneously distributed within the lithospheric mantle. The origin of these eclogitic sources in the lithospheric mantle remains in many cases a subject of debate and may be related to crystallization of mafic magmas at high pressures within the lithosphere (Smyth et al. 1989; Taylor and Neal, 1989; Snyder et al. 1997) or to subduction processes that introduced crustal rocks into the lithospheric mantle (Jacob et al., 1994; Schulze et al., 1997; Jacob and Foley, 1999).

Chapter 1

Peridotitic and eclogitic diamonds are not only distinct in the composition of their inclusions, but they also show differences in their stable carbon isotope composition, which may reflect distinct carbon sources or formation mechanisms (Deines, 2001).

Detailed studies on lithospheric diamonds and their inclusions can reveal the chemical and thermal characteristics of their specific diamond source region. In addition they can also contribute to the understanding of the principles of the formation and evolution of the lithospheric mantle as well as diamond formation processes.

Within the last two decades a small number of diamonds have been discovered that contained mineral inclusions indicating a significantly deeper, *sublithospheric* origin. Among these inclusions two very distinct groups were identified, which indicate not only distinct depths of origin, but also chemically different sources.

One group is characterized by the occurrence of majoritic garnet inclusions, which were experimentally shown to form at depths of >250 kilometers by continuous dissolution of pyroxene into the garnet structure (Ringwood, 1967; Akaogi and Akimoto, 1977; Irifune, 1987). In contrast to an expected mainly peridotitic composition of the Earth's mantle at these depths, most of the majoritic garnet inclusions were found to be eclogitic (Stachel, 2001). The nature of these deep eclogitic sources has been interpreted in different ways. It was suggested that it reflects a large scale primordial layering within the Earth's mantle (Gasparik, 2002), but is has also been interpreted as being caused by the crystallization of basaltic melts at great depth (Moore et al., 1991) or to reflect subducted oceanic crust (Stachel et al., 2000a). It is also debated whether the formation of majoritic garnet is restricted to the asthenosphere or whether it reaches into the *transition zone*, to depths of >410 kilometers. Because majoritic garnet inclusions in diamonds are the only available pristine samples from the asthenosphere and potentially the transition zone, it is crucial to understand their origin.

The second group of sublithospheric diamonds comprises diamonds that contain inclusion of an even deeper origin, within the *lower mantle*, at depths of >660 kilometers. These diamonds are characterized by the occurrence of distinct inclusion assemblages, including ferropericlase, MgSi-Perovskite and CaSi-Perovskite (Scott Smith et al., 1984; Wilding, 1990; Harte and Harris, 1994; Hutchison, 1997; Stachel et al., 2000b). Unlike majoritic garnet-bearing diamonds, lower mantle diamonds are dominated by inclusions that indicate formation in an environment with broadly peridotitic bulk chemistry.

Diamonds that contain mineral inclusions of potential lower mantle origin have been discovered in diamond deposits worldwide, but in many cases it appears difficult to prove unequivocally such a deep origin. It is important therefore to test in each case whether the diamonds formed in the lower mantle.

1.2 Intent and organization of this thesis

This thesis contains the detailed study of diamonds and their mineral inclusions from:

1.) The **Panda** kimberlite, Lac de Gras-area, Northwest Territories, Canada (Chapter 2)

2.) Placer diamond deposits in Brazil: **Arenapolis**, Mato Grosso; **Boa Vista,** Roraima; and **Canastra**, Minas Gerais (Chapter 3)

3.) The **Jagersfontein** kimberlite, South Africa (Chapter 4)

The Panda kimberlite in the Achaean Slave Province is the location of the first diamond mine in Canada. Diamonds and their mineral inclusions from this deposit represent samples from a mantle region, which could not have been accessed prior to the discovery of the diamondiferous kimberlites in the early 1990s. Although a small number of studies on diamonds from the Slave Province have been published since that time (Chinn et al., 1998; Davies et al., 1999; Pokhilenko et al., 2001; Westerlund et al., 2003a,b; Davies et al., 2004; Promprated et al., 2004), knowledge about diamond formation processes and the chemical characteristics of the Earth's mantle beneath the Slave province is still incomplete.

This study of 90 Panda diamonds is intended to reveal the characteristics of the diamond sources beneath the central Slave province.

Diamonds in Brazil have been found in placer deposits since the early 18th century. Although these placer deposits are widespread throughout Brazil (Svisero, 1995), primary kimberlitic sources are very scarce. The absence of primary diamond sources has been interpreted as being the result of erosion or a derivation of the diamonds from sources outside of Brazil. More recently an increasing number of discoveries of diamondiferous kimberlites in Brazil and adjacent countries like Venezuela shows that primary sources are more common than previously suggested, but their identification appears difficult because of a lack of indicator minerals in many parts of South America.

The detailed study of 68 diamonds and their mineral inclusions in this study from placer deposits in Brazil will provide information about the chemical characteristics of their mantle sources and the location of their kimberlitic sources.

The Jagersfontein kimberlite in South Africa is not only noteworthy because it is the oldest diamond mine of this kind in South Africa (start of mining in 1871) and delivered during its production (until 1972) some of the largest rough diamonds in the world (e.g. the "Excelsior" with 995 ct.), but it is also a deposit with a high frequency of majoritic garnet-bearing diamonds (Deines et al., 1991).

Diamonds recovered in 2001 during a re-evaluation of the historic dumps of the Jagersfontein mine by DeBeers provide a unique opportunity to carry out this study. One hundred and twenty-two inclusion-bearing diamonds (from a total of ~4500 ct. examined) were selected for this project. The results of this study are intended to reveal the nature of sublithospheric, majoritic garnet-bearing diamonds.

Chapter 1

Bibliography

Akaogi, M. and Akimoto, S., 1977. Pyroxene-garnet solid-solution equilibria in the systems $Mg_4Si_4O_{12}$-$Mg_3Al_2Si_3O_{12}$ and $Fe_4Si_4O_{12}$-$Fe_3Al_2Si_3O_{12}$ at high pressures and temperatures. Physics of the Earth and Planetary Interiors, 15: 90-106.

Chinn, I.L., Gurney, J.J. and Kyser, K.T., 1998. Diamonds and Mineral Inclusions from the NWT, Canada, VIIth International Kimberlite Conference, Cape Town, pp. not paginated.

Clifford, T.N., 1966. Tectono-metallogenic units and metallogenic provinces of Africa. Earth and Planetary Science Letters, 1: 421-434.

Davies, R.M. et al., 1999. Diamonds from the deep: pipe DO-27, Slave Craton, Canada. In: J.J. Gurney, J.L. Gurney, M.D. Pascoe and S.H. Richardson (Editors), The J.B. Dawson Volume, Proceedings of the VIIth International Kimberlite Conference. Red Roof Design, Capetown, pp. 148-155.

Davies, R.M., Griffin, W.L., O'Reilly, S.Y. and Doyle, B.J., 2004. Mineral inclusions and geochemical characteristics of microdiamonds from the DO27, A154, A21, A418, DO18, DD17 and Ranch Lake kimberlites at Lac de Gras, Slave Craton, Canada. Lithos, 77: 39-55.

Deines, P., 2001. The carbon isotope geochemistry of mantle xenoliths. Earth-Science Reviews, 58: 247-278.

Deines, P., Harris, J.W. and Gurney, J.J., 1991. The carbon isotopic composition and nitrogen content of lithospheric and asthenospheric diamonds from the Jagersfontein and Koffiefontein kimberlite, South Africa. Geochimica et Cosmochimica Acta, 55: 2615-2625.

Gasparik, T., 2002. Experimental investigation of the origin of majoritic garnet inclusions in diamonds. Physics and Chemistry of Minerals, 29: 170-180.

Gurney, J.J., 1984. A correlation between garnets and diamonds in kimberlites. Publication of the Geology Department & University of Extension, University of Western Australia, 8: 143-166.

Harte, B. and Harris, J.W., 1994. Lower mantle associations preserved in diamonds. Mineralogical Magazine, 58A: 384-385.

Hutchison, M.T., 1997. Constitution of the deep transition zone and lower mantle shown by diamonds and their inclusions. PhD Thesis, University of Edinburgh, 340, 306 pp.

Irifune, T., 1987. An experimental investigation of the pyroxene-garnet transformation in a pyrolite composition and its bearing on the constitution of the mantle. Physics of the Earth and Planetary Interiors, 45: 324-336.

Jacob, D., Jagoutz, E., Lowry, D., Mattey, D. and Kudrjavtseva, G., 1994. Diamondiferous eclogites from Siberia - remnants of Archean oceanic- crust. Geochimica et Cosmochimica Acta, 58(23): 5191-5207.

Jacob, D.E. and Foley, S.F., 1999. Evidence for Archean ocean crust with low high field strength element signature from diamondiferous eclogite xenoliths. Lithos, 48(1-4): 317-336.

Meyer, H. and Boyd, F., 1972. Composition and origin of crystalline inclusions in natural diamonds. Geochimica et Cosmochimica Acta, 36: 1255-1273.

Meyer, H.O.A., 1987. Inclusions in diamond. In: P.H. Nixon (Editor), Mantle xenoliths. John Wiley & Sons, Chichester, pp. 501--522.

Moore, R.O., Gurney, J.J., Griffin, W.L. and Shimizu, N., 1991. Ultra-high pressure garnet inclusions in Monastery diamonds - Trace-element abundance patterns and conditions of origin. European Journal of Mineralogy, 3(2): 213-230.

Pokhilenko, N.P. et al., 2001. Crystalline inclusions in diamonds from kimberlites of the Snap Lake Area (Slave Craton, Canada): New evidences for the anomalous lithospheric structure. Doklady Earth Science, 380(7): 806-811.

Promprated, P. et al., 2004. Multiple-mineral inclusions in diamonds from the Snap Lake/King Lake kimberlite dike, Slave craton, Canada: a trace-element perspective. Lithos, 77: 69-81.

Ringwood, A.E., 1967. The pyroxene garnet transformation in the earth's mantle. Earth and Planetary Science Letters, 2: 255-263.

Chapter 1

Ringwood, A.E., 1975. Composition and petrology of the earth's upper mantle. McGraw-Hill, London, 618 pp.

Schulze, D.J., Valley, J.W., Viljoen, K.S., Stiefenhofer, J. and Spicuzza, M., 1997. Carbon isotope composition of graphite in mantle eclogites. Journal of Geology, 105(3): 379-386.

Scott Smith, B.H., Danchin, R.V., Harris, J.W. and Stracke, K.J., 1984. Kimberlites near Orroroo, South Australia. In: J. Kornprobst (Editor), Kimberlites I: Kimberlites and related rocks. Elsevier, Amsterdam, pp. 121-142.

Smyth, J.R., Caporuscio, F.A. and McCormick, T.C., 1989. Mantle eclogites: evidence of igneous fractionation in the mantle. Earth and Planetary Science Letters, 93: 133-141.

Snyder, G.A. et al., 1997. The origins of Yakutian eclogite xenoliths. Journal of Petrology, 38(1): 85-113.

Stachel, T., 2001. Diamonds from the asthenosphere and the transition zone. European Journal of Mineralogy, 13: 883-892.

Stachel, T., Brey, G.P. and Harris, J.W., 2000a. Kankan diamonds (Guinea) I: from the lithosphere down to the transition zone. Contributions to Mineralogy and Petrology, 140: 1-15.

Stachel, T., Harris, J.W., Brey, G.P. and Joswig, W., 2000b. Kankan diamonds (Guinea) II: lower mantle inclusion parageneses. Contributions to Mineralogy and Petrology, 140: 16-27.

Svisero, D.P., 1995. Distribution and Origin of Diamonds in Brazil - an Overview. Journal of Geodynamics, 20(4): 493-514.

Taylor, L.A. and Neal, C.R., 1989. Eclogites with oceanic crustal and mantle signatures from the Bellsbank kimberlite, South Africa, Part I: mineralogy, petrography, and whole rock chemistry. Journal of Geology, 97: 551-567.

Westerlund, K.J., Hauri, E.H. and Gurney, J.J., 2003a. FTIR absorption and stable nitrogen and carbon isotope microanalysis of Mid- Archean diamonds from the Panda Kimberlite, Slave Craton, VIIth International Kimberlite Conference, Extended Abstracts, Victoria, Canada.

Westerlund, K.J., Shirey, S.B., Richardson, S.H., Gurney, J.J. and Harris, J.W., 2003b. Re–Os Isotope systematics of peridotitic diamond inclusion sulfides from the Panda kimberlite, Slave Craton, VIIIth International Kimberlite Conference, Extended Abstracts, Victoria, Canada.

Wilding, M.C., 1990. PhD thesis, University of Edinburgh, 281 pp.

CHAPTER 2

Diamonds and their mineral inclusions from the Panda kimberlite, Slave Province, Canada

The content of this chapter, in modified form, has been accepted for publication in the *European Journal of Mineralogy* as:
Tappert, R., Stachel, T., Harris, J.W., Shimizu, N., Brey, G.P.(2005): Diamonds and their mineral inclusions from the Panda kimberlite, Slave Province, Canada.

2.1 Introduction

Syngenetic mineral inclusions in diamonds have been employed as probes into the deep lithospheric mantle (>140 km) for virtually all cratonic areas where diamonds are mined. With the discovery of diamondiferous kimberlites on the Slave Craton in the early 1990s and the subsequent opening of Canada's first diamond mines (Ekati and Diavik), similar studies suddenly became possible for an ancient building block of the North American Shield that actually contains the oldest rocks presently known on Earth (Acasta Gneiss, ≥4.02 Ga; Bowring *et al.*, 1989; Bowring and Williams, 1999). Consequently, diamonds and their syngenetic mineral inclusions from the Slave craton rapidly became the focal point of an intense research effort. A first preliminary survey of diamonds from the Lac de Gras area (central Slave craton, Fig. 2-1) by Chinn *et al.* (1998) showed that diamonds from the Misery, Sable and Jay pipes on the Ekati property are largely derived from peridotitic sources with a minor eclogitic component. A study of diamonds from the Cambrian Snap Lake kimberlite dyke, in the southern part of the Slave craton (Fig. 2-1) also yielded mostly peridotitic and only few eclogitic inclusions (Pokhilenko *et al.*, 2001).

However, during a detailed study on diamonds from pipe DO27 (Davies *et al.*, 1999) in the Tli Kwi Cho kimberlite cluster located on the south-east side of Lac de Gras (Fig. 2-1), Davies *et al.* (1999) recorded not only an unusually high proportion of eclogitic diamonds, but also a number of inclusions that they interpreted to indicate an ultradeep "sublithospheric" origin ranging from the asthenosphere through the transition zone into the lower mantle. More recently, Davies *et al.* (2004), reported similarly high abundances of eclogitic and sublithospheric diamonds for seven other Lac de Gras kimberlites. Stachel *et al.* (2003) completed the first comparison of major element data on peridotitic inclusions in diamonds from the Slave and Kapvaal cratons, and concluded that the diamondiferous subcratonic lithospheric mantle beneath the Slave craton is chemically less depleted than beneath the Kapvaal craton.

In the present paper we report the results of a detailed study on diamonds from the Panda kimberlite, the diatreme where operations at the Ekati Mine started in 1998. Panda is located just north of Lac de Gras, ~300 km NNE of Yellowknife, Northwest Territories, (Fig. 2-1), and is part of a kimberlite field within the Central Slave Province that comprises more than 200 individual pipes. Radiometric age dating shows that the kimberlites in the Lac de Gras area are Upper Cretaceous (oldest: 74 Ma, C13 kimberlite; Heaman *et al.*, 2003) to Eocene (youngest: 45 Ma, Aaron kimberlite; Creaser *et al.*, 2004) in age. For Panda itself, Rb-Sr dating of phlogopite macrocrysts gave an age of 53.2 ± 3.8 Ma (Carlson *et al.*, 1999) whereas a somewhat older age of 59.0 ± 0.4 Ma was obtained by U-Pb dating of a single zircon megacryst (Richardson *et al.*, 1999b).

The physical and chemical properties of the host diamonds from Panda and the major- and trace-element composition of their syngenetic mineral inclusions have been examined in this study. In addition, the new results including trace element data for peridotitic, eclogitic and sublithospheric diamonds will be compared with already published major element analyses of peridotitic Panda inclusions (Stachel *et al.*, 2003).

Recent studies employing mantle xenoliths (MacKenzie & Canil, 1999; Kopylova *et al.*, 1999; Pearson *et al.*, 1999; Doyle *et al.*, 2003; Grütter & Moore, 2003; Menzies *et al.*, 2004) and xenocrysts (Griffin *et al.*, 1999; Grütter *et al.*, 1999) as well as geophysical experiments (Bostock, 1998; Bank *et al.*, 2000; Jones *et al.*, 2001) provide a rather detailed picture of the structure and composition of the lithospheric mantle beneath the Slave craton. Panda diamonds supply complementary information to these studies by providing information on an ancient stage in the thermal and chemical evolution of the lithospheric mantle that predates, by billions of years in some cases, kimberlite emplacement events and the time-slices represented by xenolith and xenocryst material. The results of this study are intended to establish better constraints for the origin and the evolution of the lithospheric mantle beneath the central Slave. The sublithospheric diamonds from Panda also play an important role in this comparative study, as they may be used to test models for unique processes of lithospheric growth during the Archean, as suggested by Griffin *et al.* (1999 and 2003).

2.1.1 Analytical methods and sample preparation

Ninety inclusion-bearing diamonds from Panda in the size range 2-5 mm were selected for this study and their characteristic features (overall shape, surface characteristics, color, and signs of plastic deformation) were described in detail (Tab. 2-1). After breakage, six diamonds were found to contain only inclusions of graphite or of a soft whitish or orange material of probable epigenetic origin. Initially, 118 mineral inclusions ranging in size between 50-350 μm were recovered from the remaining 84 diamonds, but three of these inclusions were lost during sample preparation.

Twenty "inclusions" were not completely enclosed within their host diamonds and thus may have continuously re-equilibrated with the surrounding mantle at depth or may have become metasomatized by the kimberlite magma during ascent to the Earth's surface. No evidence for the latter has been found; because these "exposed inclusions" did not show compositional gradients indicative of inward or outward diffusion. However, some of the inclusions were affected by alteration processes occurring after kimberlite emplacement, possibly resulting from the acid cleaning of the diamonds prior to sale, leading to the formation of very thin (10-20 microns) alteration rims. As the central portions of these samples are regarded as well equilibrated mantle samples, they have been included into the data set, but denoted them with a special symbol when plotted.

After extraction, the inclusions were embedded individually in brass rings using Araldite® resin. Subsequently, the samples were ground on a glass plate using SiC powder and then polished on a Pb-Sb plate with 0.25 µm diamond powder. Major-element compositions were determined with a JEOL JXA-8900 RL electron microprobe at Frankfurt University at 20 kV acceleration voltage and 20 nA beam current. Synthetic and natural silicates, oxides and metals were used as standards. The counting times for single elements ranged from 30 to 100 seconds for the peak and 30 to 200 seconds for the background. Three analytical points were averaged to ensure detection limits of 100 ppm or better for all oxides except Na_2O (ca. 200 ppm). Analytical accuracy and precision were tested using secondary standards (see Appendix: Table A1) and was shown to be better than 1% (relative) for major elements.

The complete set of microprobe analyses of the mineral inclusions is given in Appendix B (silicate and oxide inclusions: Tab. B1, sulfide inclusions: Tab. B2-3).

Trace-element concentrations in 10 peridotitic garnets were determined with a CAMECA IMS-3f ion microprobe at the Woods Hole Oceanographic Institution. The analyses included selected rare earth elements (REE: La, Ce, Nd, Sm, Eu, Dy, Er, Yb), Ti, Sr, Y and Zr. A primary beam of negatively charged oxygen ions was focused to a spot size of ~30 µm diameter for the REE, for the other trace elements a spot size of ~5 µm was used. To suppress molecular interferences, an energy offset of -60V for the REE and -90 V for the remaining trace elements was applied (Shimizu & Hart, 1982). Trace-element concentrations were calculated using empirical relationships between concentration and secondary ion yields in well-characterized standards (working curves) and by normalization to silicon as an internal standard. For the compositional ranges observed here analytical uncertainties are, based on ion counting statistics, in the order of 10-30 % (relative) for the REE and 5-15 % for the other trace elements.

The concentration and aggregation state of nitrogen impurities of the host diamonds were determined on inclusion free, transparent fragments by Fourier transform infrared spectroscopy (FTIRS) using a Nicolet Magna IR 550 spectrometer with Spectra Tech IR microscope. The deconvolution of IR-spectra and the determination of nitrogen concentrations followed the protocol described in Stachel *et al.* (2003). Further details are also given in Appendix A. The detection limits are dependent on the quality of the fragments, but are generally in the range 10-20 ppm. The errors on concentration and aggregation state are in the order 10-20%.

2.1.2 Database

The analytical results from this study are compared against a database of published and unpublished analyses of mineral inclusions in diamonds from worldwide sources referenced in Stachel & Harris (1997); Stachel *et al.* (1998a) and Stachel *et al.* (2000a). This worldwide database has been expanded by incorporation of inclusion analyses presented by Aulbach (1999); Daniels & Gurney (1999); Davies *et al.* (1999); Richardson *et al.* (1999a); Kaminsky *et al.* (2000) and Pokhilenko *et al.* (2001).

2.2 Major-element composition of mineral inclusions

2.2.1 Peridotitic inclusion suite

The major-element chemistry of the peridotitic inclusion suite at Panda, (85 % of the diamonds, see Tab. 2-2 and Table B1, Appendix B) has already been discussed by Stachel *et al.* (2003) in their comparison of peridotitic diamond sources beneath the Slave craton in Canada and the Kaapvaal craton in southern Africa. These results are briefly summarized before providing new data. An additional, detailed list of new and already published data is given in Table B1, Appendix B.

Five out of 27 diamonds contained peridotitic *garnet* inclusions of lherzolitic paragenesis (Fig. 2-2), the remaining 22 reflect a harzburgitic source composition. Characteristically, all garnet inclusions have both relatively high Cr_2O_3 (up 13.6 wt%) and CaO-contents (up to 5.2 wt%), (Fig. 2-2). Unusually high Na_2O contents (0.10-0.31 wt%) are observed in three of the harzburgitic garnets from Panda (Tab. 2-3, see also Tab.2 in Stachel *et al.*, 2003). The harzburgitic garnet from diamond PA-40 has a slight excess in Si (6.11 Si a.f.u. at [O]=24) perhaps indicating the presence of a majorite component in the garnet structure (Ringwood & Major, 1971). However, with an analytical uncertainty for Si of about 0.06 cations, the observed silicon excess (0.11 cations) is regarded as only marginally significant. Similar compositions were found in peridotitic xenoliths from Panda (Menzies *et al.*, 2004) and other Lac de Gras kimberlites (Pearson *et al.*, 1998; MacKenzie & Canil, 1999) as well as in xenocrystic garnets from the Central Slave (Grütter *et al.*, 1999).

Olivine inclusions from 23 of the 25 olivine-bearing diamonds belong to the "normal" peridotitic suite, i.e. are not associated with ferropericlase (see discussion below). These olivines have forsterite contents (91.9-93.2 mol%) coinciding with the lower half of the Mg-numbers (100*Mg/(Mg+Fe)) comprising the worldwide data base. Within this set, four olivines are of lherzolitic paragenesis, as indicated by the composition of coexisting garnets. Approximately two thirds of the remaining peridotitic olivines fall into the same narrow range of CaO (0.04-0.05 wt%) content and Mg-number (91.9-93.2; Fig. 2-3). The majority of olivine inclusions from DO-27 diamonds (Davies *et al.*, 1999) is compositionally similar to Panda olivines (Fig. 2-3).

Only two *orthopyroxenes* were found, one intergrown with garnet (PA-19) and the other as part of a four-phase inclusion (PA-05) together with garnet, olivine, and Mg-chromite (see Tab. 2 in Stachel *et al.*, (2003) and Tab. B1, Appendix B for compositional data). Their Mg-number of about 94 is typical of the worldwide database for orthopyroxene inclusions, excluding those from the Kaapvaal craton, which are more Mg-rich.

All eight recovered peridotitic *clinopyroxene* inclusions were partially exposed to the surface before they were released from their host diamond (Tab. 2-2 and 2-3) and the results are therefore of limited validity (see above). With Mg numbers between 90.8 and 93.3 and Ca-numbers (100Ca/[Ca+Mg+Fe^{total}]) in the range 42.4-44.8, these clinopyroxene inclusions are slightly less magnesian and more Ca-rich than the worldwide average.

Mg-Chromites have total iron contents (14.9-16.7 wt% FeO) that plot near the high end of the worldwide database. In relative terms Fe^{2+}/Fe^{3+} ratios, calculated after Droop (1987), indicate the presence of more "oxidized" and a more "reduced" group

(Fig. 2-4). The Cr-number (100*Cr/(Cr+Al)) is generally around 85, but can be as high as 91.5. No compositional differences were observed between "true" inclusions and the five Mg-chromites that were partially exposed at the surface of their host diamonds (Fig. 2-4). A possible Mg-chromite inclusion was observed as part of a four-phase inclusion with garnet, olivine and orthopyroxene in diamond PA-05. The small size of this crystal did not allow for a compositional analysis.

Fe-Ni mono-sulfides (Tab. 2-4) occur in 14 diamonds from Panda. An association with the peridotitic suite is inferred from high-Ni contents (Yefimova *et al.*, 1983), but is also confirmed by the presence of Mg-chromite (PA-79) and olivine (PA-57) as additional inclusions in two diamonds (Fig. 2-5). Fe contents range from 38.0-42.0 wt% and Ni varies from 18.8-22.6 wt%, which is common for peridotitic sulfide inclusions. Among the minor elements, Cu (0.56-2.34 wt%) is somewhat elevated relative to the worldwide average and also relative to sulfide inclusions from nearby DO27 (Davies *et al.*, 1999) (Fig. 2-5). Co (0.45-0.52 wt%) and Cr (0.07-0.17 wt%) are similar. All sulfides show some variability in composition during EMPA analysis, which is most pronounced in the copper-rich samples and relates to exsolution from Fe-Ni monosulfides during cooling.

2.2.2 Eclogitic inclusion suite

Eclogitic inclusions were found in eight diamonds, but only six inclusions (from four diamonds) were fully enclosed in their hosts, whereas the remaining four diamonds contained partially exposed phases (Tab. 2-2). The "true" inclusions are sulfide only (two diamonds), sulfide together with a clinopyroxene-rutile intergrowth (PA-66), and two individual garnet inclusions in diamond PA-65.

The two individual *garnet* inclusions have almost identical compositions with 0.03 wt% Cr_2O_3, 12.8 wt% CaO and 0.9 wt% TiO_2 (Tab. 2-3). Overall, eclogitic garnets from Panda, including the partially exposed samples, are similar to garnet inclusions from DO27 (Davies *et al.*, 1999) and lie well within the ranges defined by the worldwide E-type garnet database.

The one eclogitic *clinopyroxene* is low in Na (0.20 cations at [O]=6) and Al (0.21 cations) resulting in a low jadeite component (21 mol %) relative to eclogitic clinopyroxene inclusions from DO27 (Davies *et al.*, 1999), Snap Lake (Pokhilenko *et al.*, 2001) and occurrences worldwide. Its Mg-number of 74, however, is typical for eclogitic clinopyroxene inclusions.

Three eclogitic *sulfides* were recovered: two *Fe-monosulfides* (Fig. 2-5) and one Cu-Fe-sulfide (Tab. 2-4). The Fe-monosulfides are composed of about 56 wt% Fe with minor Ni (~3 wt%), Cu (~2 wt%) and Co (~0.3 wt%). One of the two Fe-monosulfides (diamond PA-71) is associated with two surface exposed eclogitic garnets and appears partially altered and replaced by an unidentified mass of silicates which occurs in patches and streaks. The other Fe-monosulfide occurs together with clinopyroxene-rutile intergrowth in diamond PA-66.

The *Cu-Fe-sulfide* from diamond PA-76 shows exsolution lamellae (Appendix B, Fig. B1). An original composition on the chalcopyrite-bornite join prior to exsolution was estimated from 21 point analyses (Fig. 2-6). Noteworthy is an average Pb content of 0.2 wt% (see Tab. 2-4). Because of the small size of the exsolutions, the composition of the exsolved phases could not be determined directly, but plotting individual analyses (Appendix B, Tab. B3) into a ternary Cu-Fe-S diagram (Fig. 2-6) clearly shows exsolution of bornite from chalcopyrite.

2.2.3 Inclusion assemblages with ferropericlase

$CaSiO_3$ plus ferropericlase: In diamond PA-50, $CaSiO_3$ 99.5% pure (Tab. 2-5) was found together with two ferropericlase inclusions. Contents of Al_2O_3 (0.09 wt%), MgO (0.10 wt%), SrO (0.10 wt%), K_2O (0.10 wt%) and P_2O_5 (0.09 wt%) are similar to $CaSiO_3$ inclusions in diamonds from Brazil (Harte *et al.*, 1999; Kaminsky *et al.*, 2000) and Guinea (Stachel *et al.*, 2000b). The two separate, but compositionally identical ferropericlases are characterized by high Mg-numbers (~86) and high NiO (~1.3 wt%, Fig. 2-7). Na_2O contents of <0.07 wt% are at the low end of the worldwide data-base, which extends to concentrations of >1.3 wt% Na_2O for ferropericlase from the Juina area (Kaminsky *et al.*, 2001). Aluminum, chromium and

manganese are within normal ranges for ferropericlase inclusions. Diamonds with coexisting $CaSiO_3$ and ferropericlase are generally considered to originate from the lower mantle. However, Liu (1979) showed that $CaSiO_3$-perovskite plus ferropericlase form a stable paragenesis at pressures as low as 15 GPa and thus an origin in the transition zone cannot be excluded, depending on the existence of appropriate (non-peridotitic) bulk compositions.

SiO_2 plus ferropericlase: The occurrence of ferropericlase together with an SiO_2 phase as separate inclusions in diamond PA-55 also points to an origin in the lower mantle or the lower part of the transition zone, in which case the SiO_2 was most likely originally included as stishovite. The ferropericlase, which was optically identified by its characteristic iridescent, metallic luster within the diamond and a transparent brown color, was lost during polishing. According to experimental results, for a peridotitic bulk composition, a ferropericlase with a maximum Mg# of approximately 70 can be expected in the presence of SiO_2 (Liu, 1975; Yagi *et al.*, 1979; Fei *et al.*, 1996). Yet, such a mineral association has only been reported so far in a few instances. There is one analysis recorded in diamonds from the Juina-São Luiz deposits in Brazil (Kaminsky *et al.*, 2001), a pair from Kankan diamonds in Guinea (Stachel *et al.*, 2000b), and two pairs from the Central Slave craton (Davies *et al.*, 2004). The Mg-numbers of the ferropericlases are, respectively, 78, 86, 84 and 86, which means that the Mg-number of the ferropericlase is too high to be in equilibrium with stishovite. Only one ferropericlase with an Mg-number of 70 was described in a diamond from São Luiz (Harte *et al.*, 1999).

Olivine, spinel and ferropericlase: Two colorless and one dark brown inclusion were observed inside diamond PA-54. After breakage, the dark brown inclusion was identified as touching ferropericlase-spinel pair (Fig. 2-8), one of the "colorless" inclusions was a touching pair ferropericlase-olivine (with ferropericlase being modally more abundant) and the second colorless inclusion was a single olivine. The touching and the single olivine are identical in chemical composition within analytical error (Tab. 2-6) and have the highest Mg-number (~95) and Al_2O_3 content (~0.05 wt %) and the lowest Cr_2O_3 (~0.015 wt%), MnO (~0.07 wt%) and

NiO (~0.2 wt%) concentrations of all Panda olivine inclusions. The two ferropericlases (touching with olivine or spinel, respectively) are characterized by low Mg-numbers (~80) compared to other Panda ferropericlases (Tab. 2-5), but also have the highest nickel contents (>2.1 wt% NiO) observed for ferropericlase inclusions worldwide (Fig. 2-7). Compositional differences between the two ferropericlases are minor with the sample in contact with spinel being slightly higher in Al_2O_3, Cr_2O_3 and Mg-number (Tab. 2-6). The spinel in this touching paragenesis is small compared to the ferropericlase (Fig. 2-8) and has a composition (57 wt% Al_2O_3, 8.5 wt % Cr_2O_3, 24 wt% MgO) similar in Cr-number to spinels from primitive spinel-lherzolites. The association of Mg-Al spinel, olivine and ferropericlase as inclusions in one diamond has not been observed before.

Olivine plus ferropericlase: Diamond PA-39 contains olivine and ferropericlase as separate inclusions. Their compositions are similar to an olivine-ferropericlase pair described in diamond KK-84 from Guinea (Stachel *et al.*, 2000b) and the ferropericlase also compares well to the two inclusions in diamond PA-50, which coexists with $CaSiO_3$. Compared to diamond PA-54 the Mg-number of olivine is lower (~94; Fig. 2-3) whereas ferropericlase has a higher Mg-number (~85; Tab. 2-6 and Fig. 2-7).

2.3 Trace-element composition of mineral inclusions

Ten peridotitic garnets have been analyzed for rare earth elements (REE), Ti, Zr, Y and Sr. Six of these garnets belong to the harzburgitic and four to the lherzolitic suite. Rare earth element contents are normalized (REE_N) to the C1-chondrite composition of McDonough & Sun (1995).

Four garnets were selected to test homogeneity in the distribution of Ti, Zr, Y and Sr with up to 15 analytical spots per grain. In all cases the variation was within the 2 σ error derived from counting statistics, indicating that trace element zoning is absent.

With one exception, the harzburgitic garnets have sinusoidal REE_N patterns with a hump in the $LREE_N$ and a trough in the $MREE_N$ (Fig. 2-9). These features are characteristics of both harzburgitic garnet inclusions from other localities worldwide (e.g. Shimizu & Richardson, 1987; Stachel *et al.*, 1998b) and from peridotite xenoliths (e.g. Menzies *et al.*, 1987; Hoal *et al.*, 1994). The garnet from diamond PA-04 in Fig. 2-9 exhibits a completely different REE_N pattern with a steep positive slope from the LREE_N to the MREE_N ($\mathrm{La}_N/\mathrm{Sm}_N=0.007$) and high HREE_N, similar to patterns described for Ti-rich lherzolitic garnet inclusions in diamonds from Ghana (Stachel & Harris, 1997) and Guinea (Stachel *et al.*, 2000a). This garnet also has extremely high Zr (152 ppm) and Y (39 ppm) contents. Similar Zr (151 ppm) and even higher Y (48 ppm) have been previously observed for a lherzolitic garnet inclusion in a diamond (L12) from Pipe 50 in Liaoning, China (Wang *et al.*, 2000). Strontium ranges from 2.1 to 30 ppm and such "high" contents are characteristic of garnet in the absence of clinopyroxene, that otherwise would scavenge all strontium.

The lherzolitic garnet from diamond PA-23 (see Fig. 2-10) shows a positive slope within the LREE_N and flat MREE_N-HREE_N. Two more garnets have similar concentrations for La-Eu but their REE_N patterns are mildly sinusoidal with a low at Er. Similar REE_N patterns are frequently found for lherzolitic inclusions worldwide (Stachel *et al.*, 2004). The REE_N pattern of the garnet recovered from diamond PA-40 is similar to the pattern of the harzburgitic garnet inclusions from Panda (Fig. 2-9). However, in the case of the two lherzolitic garnets that are mildly sinusoidal, (see Fig. 2-10), the hump in REE_N is shifted towards the MREE, peaking at Sm, compared to a peak at Ce-Nd (Pr not analyzed) for the harzburgitic garnets (Fig. 2-9). Strontium contents are low (0.6-2.3 ppm Sr) in accordance with a lherzolitic paragenesis. A less depleted character of the lherzolitic garnets is also reflected by Zr contents (14.5-23.6 ppm) that are high compared to harzburgitic garnets (with the exception of PA-04).

2.4 Geothermobarometry

The composition of ten garnet-olivine pairs was used to estimate temperatures based on Mg-Fe exchange between these two minerals (O'Neill & Wood, 1979; O'Neill, 1980). Temperatures between 1061 and 1233°C are calculated for an assumed pressure of 5 GPa (Fig. 2-11). The two touching garnet-olivine inclusion pairs as well as a garnet in contact with Mg-chromite (PA-20) give the lowest temperatures (1061-1076°C), whereas all non-touching pairs fall in the range 1111-1233°C. The average temperature of 1140°C for Panda inclusions is similar to the average garnet-olivine temperature from worldwide sources (~1150°C; Stachel *et al.*, 2003).

Garnet-orthopyroxene geothermobarometry (combination of Harley, 1984 with Brey & Köhler, 1990) for the four-phase inclusion in diamond PA-05 indicates equilibration at 1101°C and 6.5 GPa, which compares very well with the result of garnet-olivine thermometry (1136°C for a fixed pressure of 6.5GPa). A second touching pair of garnet- orthopyroxene (PA-19) gives 1029°C at 5.5 GPa (Fig. 2-11).

For Mg-chromite inclusions temperatures were calculated using the empirical thermometer of Ryan *et al.* (1996), based on the Zn content of spinel in equilibrium with olivine. Despite a large spread from 960 to 1300°C, the average Zn in spinel temperature of 1160°C compares well with the results of garnet-olivine thermometry (1140°C).

2.5 Physical and chemical characteristics of the host diamonds

2.5.1 Morphology and color

Based on an overall assessment of the Panda production shipped through the DTC (London) in 2000-2001, diamonds from this kimberlite typically have as primary crystal shapes, the octahedron and the related spinel twin, the triangular macle, throughout all common sizes. In the smaller size ranges (<2.5 mm), dark single cubes, interpenetrant cubes, or more complex shapes such a cubo-octahedra are observed as well. Polycrystalline boart is not present at Panda. Secondary, resorbed crystal shapes like dodecahedra and flattened dodecahedral macles correspond to less than 10% of the production. Another characteristic feature is the occurrence of fibrous diamond coats. These coats may be so thin that they are almost transparent, but usually they occur as an opaque cover over a clear diamond.

Irrespective of size, the dominant body color of the diamonds from Panda is colorless, followed by brown. Yellow diamonds are extremely rare. For diamond, a brown body color results from plastic deformation (Orlov, 1977; Wilks &Wilks, 1991; Harris, 1992) and accordingly the brown color may be unevenly distributed within the crystal. Fibrous coats are grey to dark grey-black, some of the wholly opaque diamonds appear green-grey. In the absence of fluorescence analyses of the diamonds, no data linking the characteristics of the external and internal morphology to the inclusion type are available.

2.5.2 Nitrogen contents and aggregation levels

The determination of nitrogen contents and aggregation levels in Panda diamonds were performed on single cleavage chips and thus small scale variations within individual diamonds, as previously found for Panda by Westerlund *et al.* (2001), cannot be assessed.

The nitrogen contents are in the range <10 (detection limit) to 1100 atomic ppm (Fig. 2-12). With one exception, an eclogitic diamond with unusually high nitrogen of 2700 atomic ppm. Fourteen diamonds (16%) were found to be Type-II (no detectable nitrogen), nine diamonds from this group contain inclusions of peridotitic or eclogitic paragenesis. The remaining five diamonds comprise either mineral associations including ferropericlase (3) or are of unknown origin (2).

Nitrogen aggregation levels are highly variable and scatter over the full range from poorly aggregated (all nitrogen in A-centers, Type-IaA) to fully aggregated (all nitrogen in B-centers, Type-IaB) (Fig. 2-12). However, if all diamonds that show signs of plastic deformation are excluded, which comprises diamonds with brown body color and diamonds that show deformation lines, this apparent scatter disappears. Figure 2-12 illustrates that nitrogen aggregation in diamonds with no visible signs of plastic deformation, except of four samples, is restricted to a relative proportion of less than 30% nitrogen in B-centers.

2.6 Discussion and Conclusions

2.6.1 Composition of diamond sources beneath the Slave

Based on the observations at Panda and the data of Chinn *et al.* (1998) for three other Ekati kimberlites, the vast majority of inclusion-bearing diamonds on the north side of Lac de Gras come from moderately depleted peridotitic sources. In accordance with xenolith data (e.g. Griffin et al., 1999) this may be taken as a direct reflection of the overall composition of the lithosphere at depths greater than 140 km. However, different results were obtained by Davies *et al.* (1999 and 2004), based largely on diamonds from pipe DO27 (south side of Lac de Gras) where about 50% of the inclusions belong to the eclogitic suite. This either reflects strong lateral variations in the composition of the deep lithosphere, which is not consistent with xenolith and concentrate data (Griffin *et al.*, 1999), or indicates that individual kimberlites sample the diamondiferous lithosphere in a very selective manner.

Based on the compositions of peridotitic xenoliths and xenocrysts, Griffin *et al.* (1999) suggested that the lithosphere beneath Lac de Gras is chemically and thermally stratified with an ultra-depleted shallow layer (<145 km) and a less depleted, predominantly lherzolitic deeper layer. This lower layer is interpreted as a frozen plume head in accordance with the model of Haggerty (1994), who proposed superplumes ascending from the core-mantle boundary to initiate kimberlite magmatism. In the model of Griffin et al. (1999), Archean plumes not only generated the deep cratonic lithosphere beneath the central Slave but also transported diamonds with lower mantle inclusions to shallower levels of the mantle. Consequently, a "high proportion" of diamonds with suspected lower mantle inclusions (13 % in the study of Davies *et al.*, 2004) was presented as key evidence for a plume origin of the diamondiferous lithosphere beneath the central Slave. However, "indisputable" evidence for a lower mantle origin exists only for very few Lac de Gras diamonds that contained ferropericlase coexisting with inclusions of Mg- and Ca-silicate perovskite or stishovite chemistries (Davies *et al.*,1999 and 2004; this study). The depth of origin for these diamonds appears to be in a narrow window around the 660 km discontinuity, based on; I) low Al contents in Mg-silicate perovskite (Wood &

Rubie, 1996; Frost & Langenhorst, 2002) and II) coexisting "ringwoodite", ferropericlase, Mg- and Ca-silicate perovskite (Davies *et al.*, 2004). There is no indication that any of these lower mantle diamonds formed significantly deeper and, therefore, their existence does not provide clear evidence for an origin of plumes in deeper parts of the lower mantle.

At some stage during the formation of the mantle lithosphere beneath the central Slave, these "ultra-deep" diamonds were transported and incorporated into the cratonic root (Griffin *et al.*, 1999) before they were eventually carried to the surface during kimberlite eruptions. Upward transport from the lower mantle may have occurred in a plume, as envisaged by Griffin *et al.* (1999), but may also be related to diapirs rising from megaliths formed at the top of the lower mantle (Ringwood, 1991) or to upwelling branches of mantle convection cells.

The presence of single ferropericlase inclusions, such as those from DO27 (Davies *et al.*, 1999) and other Lac de Gras kimberlites (Davies *et al.*, 2004; Chinn *et al.*, 1999), is not conclusive evidence for a lower mantle origin, in that mineral is also stable in the upper mantle (Stachel *et al.*, 2000b). Experimental work by Brey *et al.* (2004) showed that ferropericlase formed in the lower mantle cannot be distinguished from upper mantle ferropericlase using chemical criteria. In the present study, based on coexisting inclusion phases, there is evidence that two Panda diamonds containing ferropericlase inclusions (PA-54 and 39) are of upper mantle origin. PA-54 contained touching pairs of ferropericlase-spinel and ferropericlase-olivine as well as a single olivine. High-pressure experiments (Liu, 1978; Irifune *et al.*, 1991) show that a spinel phase can be stable at pressures exceeding 25 GPa and could be an important host of aluminum in the lower mantle. The mineral assemblage of PA-54 could for that reason indicate a lower mantle origin. However, if this was the case, the observed inclusion assemblage had to be entrapped in the lower mantle as touching pairs of; (i) ferropericlase and $MgAl_2O_4$, (ii) ferropericlase and Mg-silicate perovskite with a modal overabundance of ferropericlase, and (iii) ferropericlase and Mg-silicate perovskite in exactly the modal proportions equivalent to olivine. During ascent from the lower mantle and adjustment to ambient PT-conditions in the upper mantle, the individual inclusion pairs then would have re-equilibrated to (i) ferropericlase + $MgAl_2O_4$-spinel (a structural adjustment), (ii) ferropericlase + olivine and (iii) a pure olivine inclusion. Ferropericlase and olivine that form as a result of such a re-equilibration would certainly have distinct compositions. Yet, this is not the case and uniformity in the composition of the ferropericlase and olivine inclusions is observed instead. Therefore, re-equilibration of the touching pair ferropericlase-olivine did not occur, but the inclusions were entrapped in the upper mantle under PT-conditions that were fairly stable until the moment the diamond was picked up by rapidly rising kimberlite magma. Further evidence for an upper mantle origin of diamond PA-54 comes from the observed Fe-Mg partition coefficient of ~5.0 between ferropericlase and olivine (Fig. 2-13), which is too high to agree with experimental partitioning data for ferropericlase and the high pressure polymorphs of olivine: wadsleyite and ringwoodite (Fei *et al.*, 1991; Ito & Yamada, 1982; Ito & Takahashi, 1989; Wood & Rubie, 1996; Akaogi *et al.*, 1998; Frost *et al.*, 2001; Frost, 2003). The chemical evidence, therefore, indicates that diamond PA-54 formed within the cratonic lithosphere in a region of very low silica activity, either through reduction of magnesite-bearing dunite by a methane-rich fluid, or in the course of degassing and reduction of a carbonatitic melt, with both processes leading to the crystallization of olivine and ferropericlase (Stachel *et al.*, 2000b; Brey *et al.*, 2004). The presence of $MgAl_2O_4$-spinel (with a Cr/Al ratio typical for spinel peridotites), also indicates a lithospheric origin, because at very low silica activity, aluminum is hosted in spinel rather than garnet.

With diamond PA-39 containing two mono-mineralic inclusions of ferropericlase and olivine, a lower mantle origin would be feasible, but only if the olivine had formed from a precursor consisting of a touching pair of ferropericlase and Mg-silicate perovskite with an exact molar ratio of 1:1. Although theoretically possible, this is not very likely and a mono-mineralic precursor with olivine composition is favored instead. One possibility would be a primary paragenesis of ringwoodite and ferropericlase trapped at the transition zone / lower mantle boundary. However, a low Cr and Al content and the absence of spinel exsolutions in the olivine from PA-39 are not in support of a silicate spinel precursor (cf. Stachel *et al.*, 2000b). Thus, PA-39 probably also formed in the upper mantle in a similar manner to diamond PA-54. The observed Fe-Mg partition coefficient of ~2.4 is in fact low enough to agree with the experimental partitioning data for ringwoodite and ferropericlase (see Fig. 2-13), but the value of the partition coefficient is not conclusive, because in this compositional range, it is also similar to the values that could be expected for wadsleyite and olivine. The preference for a formation in the olivine stability field, (with a maximum depth of approximately 400 km), therefore, rests entirely on the supposition that ringwoodite is distinct from olivine in its minor element chemistry (see Akaogi & Akimoto, 1979).

Peridotitic inclusions in diamonds from the central and southern Slave craton are characterized by garnets with relatively high Ca and intermediate to high Cr-contents (Davies *et al.*, 1999; Pokhilenko *et al.*, 2001; Stachel *et al.*, 2003). The absence of very low-Ca harzburgitic (dunitic) garnets at Panda (Fig. 2-2) is an important chemical difference to similar inclusions in diamonds from, for example, the De Beers Pool Mines in South Africa and indicates that the diamondiferous lithosphere beneath the central and southern Slave craton is chemically less depleted than beneath the Kaapvaal craton (Stachel *et al.*, 2003). This moderate degree of depletion noted from the inclusions is very similar to that recorded for the lower layer beneath the central Slave, first recognized by Pearson *et al.* (1999) and Griffin *et al.* (1999). Griffin et al. (1999) also found evidence for the presence of lenses of highly depleted low-Ca harzburgite/dunite within the lower layer. Thus the presence of ferropericlase-bearing dunites in the deep Slave lithosphere, as recorded by the inclusions in diamonds, is not in conflict with garnet concentrate data. In their model Griffin *et al.* (1999) propose that the deeper, less depleted lithospheric layer beneath Lac de Gras represents the residue of high pressure partial melting in a rising mantle plume, a proposal developed in detail by Herzberg (1999). However, as already discussed by Stachel *et al.* (2003), generation of the deep lithospheric mantle beneath the central Slave as a residue of high pressure melting, fails to provide an explanation for the observed high chromium contents in peridotitic garnets. Experimental data show that the high Cr/Al ratio of the bulk rocks implied by high-Cr garnets, not only from the Slave but from cratonic garnet peridotites worldwide, can only be generated during melt extraction in the spinel stability field (Bulatov *et al.*, 1991; Stachel *et al.*, 1998b). The overall fairly undepleted character of the deeper lithosphere beneath Lac de Gras thus is not entirely a primary characteristic but is at least in part due to metasomatic re-enrichment after emplacement of this former melting residue into the cratonic lithosphere. The LREE enriched signature of the peridotitic garnet inclusions from Panda provides clear evidence for such metasomatic modification. Harzburgitic garnets typically have distinctly sinusoidal REE_N whereas lherzolitic garnets exhibit flat or slightly sinusoidal REE_N patterns. The continuous enrichment trend in the major elements from harzburgitic towards lherzolitic garnets is obviously also reflected in the trace element composition. The evolution from almost exclusive LREE enrichment as the cause of highly sinusoidal harzburgitic garnet patterns to increasing MREE and HREE enrichment for moderately sinusoidal or "normal" (i.e. flat $MREE_N$-$HREE_N$) lherzolitic garnet patterns corresponds to a shift from fluid dominated to melt dominated metasomatism (Stachel & Harris, 1997; Stachel *et al.*, 2004). The harzburgitic garnet from diamond PA-04, with its evidence for enrichment not only in LREE but also in MREE-HREE, Y and Zr, shows that melt dominated metasomatism may in some cases also affect harzburgitic diamond sources. Garnets from peridotite xenoliths from Panda (Menzies *et al.*, 2004) and other kimberlites in the Lac de Gras area (Doyle *et al.*, 2003; Menzies *et al.*, 2004) show, in respect to major- and trace-element composition, similar characteristics to those found in the inclusion garnets. Similar to the garnet inclusion in the diamonds, garnets from xenolith are not strongly Ca-depleted (Fig. 2-2) and their trace-element composition correlates with their major-element composition. This correlation is apparent in the trend from flat REE pattern of lherzolitic garnets towards sinusoidal patterns of high-Cr harzburgitic garnets from xenoliths (Menzies *et al.*, 2004).

Re-Os data for mantle xenoliths from the central Slave craton indicate that the formation of the lithospheric mantle, the subsequent metasomatic modification and the diamond formation are Archean events (see Fig. B2, Appendix B). Gurney *et al.*

(2003) determined Re-depletion ages between 2.7 and 3.1 Ga and a model age between 2.8 and 3.4 Ga for seven garnet harzburgites from Panda. Aulbach *et al.* (2001) and Aulbach *et al.* (2003) obtained Re-Os model ages of >3 Ga for the lithospheric mantle beneath Lac de Gras through in-situ dating of sulfide inclusions in olivine xenocrysts and eleven of their samples define an isochron at 3.27 ± 0.34 Ga. Overall, the xenolith and xenocryst data approach the 3.4 Ga isochron age obtained for peridotitic sulfide inclusions in diamonds from Panda (Westerlund *et al.*, 2003b).

2.6.2 Evolution of the thermal regime in the deep lithosphere

Inclusion-based PT estimates of the conditions of diamond formation generally indicate geothermal gradients corresponding to 40-42 mW/m^2 surface heat flow (e.g. Boyd & Gurney, 1986; Griffin *et al.*, 1992; Stachel *et al.*, 2003). Based on the data from Panda and recent results for DO-27 (Davies *et al.*, 2004) and for Snap Lake (Pokhilenko *et al.*, 2001), the central and southern Slave Province are no exception to this rule.

Based on the study of xenoliths and xenocrysts, geothermal gradients at the time of kimberlite eruption for the northern Slave have been constrained by the Jurassic Jericho kimberlite (37-38 mW/m^2 calculated after Pollack & Chapman, 1977; based on the data from Kopylova *et al.*, 1999) and for the central Slave by various Cretaceous to Tertiary kimberlites in the Lac de Gras area (Griffin *et al.*, 1999; Pearson *et al.*, 1999; MacKenzie & Canil, 1999; Doyle *et al.*, 2003; Grütter & Moore, 2003; Menzies *et al.*, 2004). For the Lac de Gras area these studies indicate a significantly cooler paleo-geotherm of about 35-37 mW/m^2 for the upper part of the lithospheric mantle, compared to 40 mW/m^2 for the deeper part. In contrast to Pearson *et al.* (1999) and Griffin *et al.* (1999), who proposed a stepped geotherm corresponding to the observed compositional layering, more recent data (Doyle *et al.*, 2003; Grütter & Moore, 2003; Menzies *et al.*, 2004) appear to indicate a more continuous transition from a cooler geotherm in the upper part to a hotter geothermal regime in the lower part of the mantle lithosphere.

The PT estimates for two touching garnet-orthopyroxene pairs from Panda plot close to a 37 mW/m^2 geothermal gradient (Fig. 2-11), which is in good agreement with the Jurassic paleo-geotherm from Jericho and data for the upper layer at Lac de Gras. Separate olivine-garnet pairs give higher temperatures, consistent with 40-42 mW/m^2 surface heat flow. Similarly, Phillips & Harris (1995 and 2003) found for the DeBeers Pool Mines that touching inclusion pairs yield lower temperatures than non-touching pairs and suggested re-equilibration of touching inclusions in response to lithospheric cooling as the probable cause. The diamond data from Panda imply cooling by about 150°C for the deep lithosphere beneath the central Slave between the time of diamond formation and equilibration of the lithosphere to geothermal conditions similar to those observed at Jericho and preserved during Cretaceous and Tertiary kimberlite activity at Lac de Gras in the shallow lithospheric mantle only. Alternatively, diamond formation may have taken place under conditions where the regional geotherm was only locally perturbed, implying that cooling to ambient conditions may have occurred soon after diamond formation.

Additional constraints on the thermal evolution of the deep lithosphere can be gleaned from the nitrogen characteristics of Panda diamonds. For a given nitrogen content the aggregation level of the nitrogen atoms (single substitutional, A-center, B-center) depends on mantle residence time and temperature. This relationship was examined by Evans & Harris (1989) and Taylor *et al.* (1990) and can be applied as a thermo-chronometer, bearing in mind the yet unquantified effect of plastic deformation on nitrogen aggregation (Evans, 1990). The observation at Panda that exclusion of diamonds with visible signs of plastic deformation leads to a dramatic reduction in average aggregation level (Fig. 2-12) may be an indication that plastic deformation indeed facilitates nitrogen aggregation significantly. However, deformed Panda diamonds may also represent a specific geological environment where elevated temperature and strain are directly connected, with an extreme example being the hot and sheared peridotites found in kimberlites on the Kaapvaal craton (Boyd, 1987). The bulk of undeformed diamonds from Panda have less than 30% of its nitrogen occurring in the fully aggregated state (B-center). Similarly low nitrogen aggregation was also reported by Davies *et al.* (1999) for DO27 and by Westerlund *et al.* (2003a) for sulfide inclusion bearing diamonds from Panda used for Re-Os isotopic studies. Taking the 3.4 Ga age of sulfide inclusions from Panda (Westerlund *et al.*, 2003b) as the time of diamond formation (see Richardson *et al.*, 2004 for a detailed discussion of inclusion versus diamond ages) then such low aggregation states require mantle residence at "low" ambient temperature (1000-1100°C, Fig. 2-12). However, three highly aggregated, colorless diamonds seem to be exceptions and indicate formation under higher temperatures (up to ≤1250°C). No further information could be obtained due to the lack of sufficient inclusion phases in these diamonds. The low temperature range for the bulk of the diamonds is consistent with the results obtained from touching inclusion pairs in Panda diamonds. At higher temperatures, similar to the conditions during diamond formation derived from non-touching inclusions, low aggregation states could not be preserved over time periods exceeding tens to hundreds of millions of years. Consequently, soon after diamond formation temperatures must have dropped by about 100-150°C. A rapid temperature drop of this scale is only feasible, if the elevated temperatures during diamond formation were a transient feature (e.g. magmatic intrusions; see Fig. B3, Appendix B) and the stable geotherm for the Slave mantle lithosphere was already in the range of 37 mW/m^2 during the Archean. A stable geotherm of 35-37 mW/m^2 for the Slave mantle lithosphere would also account for the "low temperature group" of xenoliths from Lac de Gras, whereas the deeper "high temperature group" may just reflect another transient heating event associated with Cretaceous-Tertiary kimberlite activity.

Bibliography

Akaogi, M. & Akimoto, S. (1979): High-pressure phase equilibria in a garnet lherzolite, with special reference to Mg^{2+}-Fe^{2+} partitioning among constituent minerals. *Phys. Earth Planet. Inter.*, **19**, 31-51.

Akaogi, M., Kojitani, H., Matsuzaka, K., Suzuki, T., Ito, E. (1998): Post spinel transformation in the system Mg_2SiO_4-Fe_2SiO_4: Element partitioning, calorimetry and thermodynamic calculation. *in* "Property of earth and planetary materials at high pressure and temperature" M.H. Manghnani & T. Yagi, ed. Am. Geophys. Union, Washington, 373-384.

Aulbach, S. (1999): The chemistry of syngenetic mineral inclusions in diamonds from Venetia and the stable isotope composition of diamonds from Mwadui and the Kankan district. Diplom-Thesis, Universität Frankfurt, Frankfurt, 104 p.

Aulbach, S., Griffin, W.L., Pearson, N.J., O'Reilly, S.Y., Doyle, B.J., Kivi, K. (2001): Re-Os isotope evidence for Meso-Archaean mantle beneath 2.7 Ga Contwoyto Terrane, Slave Craton, Canada: Implications for the tectonic history of the Slave Craton. The Slave-Kapvaal Workshop, Merrickville, Ontario, 5 p.

Aulbach, S., Griffin, W.L., Pearson, N.J., O'Reilly, S.Y., Kivi, K., Doyle, B.J., (2004): Constraints on mantle formation and evolution from HSE abundances and Re-Os isotope systematics of sulfide inclusions in mantle xenocrysts. *Chem. Geol.*, **208**, 61-88

Bank, C.G., Bostock, M.G., Ellis, R.M., Cassidy, J.F. (2000): A reconnaissance teleseismic study of the upper mantle and transition zone beneath the Archean Slave craton in NW Canada. *Tectonophysics*, **319**, 151-166.

Bleeker, W. & Davis, W.J. (1999): The 1991-1996 NATMAP Slave Province Project: Introduction. *Canad. J. Earth Sci.*, **36(7)**, 1033-1042.

Bostock, M.G. (1998): Seismic stratigraphy and evolution of the Slave Province. *J. Geophys. Res.*, **103**, 21183-21200.

Bowring, S.A. & Williams, I.S. (1999): Priscoan (4.00-4.03 Ga) orthogneisses from northwestern Canada. *Contrib. Mineral. Petrol.*, **134**, 3-16.

Bowring, S.A., Williams, I.S., Compston, W. (1989): 3.96 Ga gneisses from the Slave Province, Northwest Territories, Canada. *Geology*, **17**, 971-975.

Boyd, F.R. (1987): High- and low-temperature garnet peridotite xenoliths and their possible relation to the lithosphere-asthenosphere boundary beneath Southern Africa. *in* "Mantle Xenoliths". P.H. Nixon, ed. John Wiley, New York, 403-412.

Boyd, F.R. & Gurney, J.J. (1986): Diamonds and the African lithosphere. *Science*, **232**, 472-477.

Brey, G.P. & Köhler, T. (1990): Geothermobarometry in four-phase lherzolites II. New thermobarometers, and practical assessment of existing thermobarometers. *J. Petrol.*, **31**, 1353-1378.

Brey, G.P., Bulatov, V., Girnis, A., Harris, J.W., Stachel, T. (2004): Ferropericlase - a lower mantle phase in the upper mantle. *Lithos*, **77**, 655-663

Bulatov, V., Brey, G.P., Foley, S.F. (1991): Origin of low-Ca, high-Cr garnets by recrystallization of low-pressure harzburgites. 5th International Kimberlite Conference, Extended Abstracts, *CPRM Spec. Publ.*, **2/91**: 29-31.

Carlson, J.A., Kirkley, M.B., Thomas, E.M., Hillier, W.D. (1999): Recent Canadian kimberlite discoveries. ***in*** "The J.B Dawson Volume, Proceedings of the 7th International Kimberlite Conference", J.J. Gurney, J.L. Gurney, M.D. Pascoe, S.H. Richardson, eds. Red Roof Design, Capetown, 81-89.

Chinn, I.L., Gurney, J.J., Kyser, K.T. (1998): Diamonds and mineral inclusions from the NWT, Canada. 7th International Kimberlite Conference, Cape Town, not paginated.

Creaser, R.A., Grütter, H.S., Carlson, J.A., Crawford, B. (2004): Macrocrystal phlogopite Rb-Sr dates for the Ekati property kimberlites, Slave Province, Canada: Evidence for multiple intrusive episodes in the Paleocene and Eocene. *Lithos*, **77**, 399-414.

Daniels, L.R.M. & Gurney, J.J. (1999): Diamond inclusions from the Dokolwayo kimberlite, Swaziland. ***in*** "The J.B Dawson Volume, Proceedings of the 7th International Kimberlite Conference", J.J. Gurney, J.L. Gurney, M.D. Pascoe, S.H. Richardson, eds. Red Roof Design, Capetown, 134-142.

Davies, R.M., Griffin, W.L., Pearson, N.J., Andrew, A.S., Doyle, B.J., O'Reilly, S.Y. (1999): Diamonds from the deep: pipe DO-27, Slave Craton, Canada. ***in*** "The J.B Dawson Volume, Proceedings of the 7th International Kimberlite Conference", J.J. Gurney, J.L. Gurney, M.D. Pascoe, S.H. Richardson, eds. Red Roof Design, Capetown, 148-155.

Davies, R.M., Griffin, W.L., O'Reilly, S.Y., Doyle, B.J. (2004): Mineral inclusions and geochemical characteristics of microdiamonds from the DO27, A154, A21, A418, DO18, DD17 and Ranch Lake kimberlites at Lac de Gras, Slave craton, Canada. *Lithos*, **77**, 39-55.

Doyle, P.M., Gurney, J.J., Le Roex, A. (2003): Xenoliths from the Arnie, Misery and Pigeon kimberlites, Ekati mine, NWT, Canada, 8th International Kimberlite Conference, Extended Abstracts, Victoria, Canada.

Droop, G.T.R. (1987): A general equation for estimating Fe^{3+} concentrations in ferromagnesian silicates and oxides from microprobe analyses, using stoichiometric criteria. *Min. Mag.*, ***51***, 431–435.

Evans, T. (1992): Aggregation of nitrogen in diamonds. *in* "The properties of natural and synthetic diamond" J.E. Field, ed. Academic Press, pp. 259-290.

Evans, T. & Harris, J. (1989): Nitrogen aggregation, inclusion equilibration temperatures and the age of diamonds. *in* "Kimberlites and related rocks" J. Ross *et al.* eds. Blackwell, Carlton, 1001-1006.

Fei, Y., Mao, H.K., Mysen, B. (1991): Experimental determination of element partitioning and calculation of phase relations in the MgO-FeO-SiO_2 system at high pressure and high temperature. *J. Geophys. Res.*, **96**, 2157-2169.

Fei, Y.W., Wang, Y.B., Finger, L.W. (1996): Maximum solubility of FeO in (Mg,Fe)SiO_3-perovskite as a function of temperature at 26 GPa: Implication for FeO content in the lower mantle. *J. Geophys. Res.* **101**, 11525-11530.

Frost, D.J. (2003): Fe^{2+}-Mg partitioning between garnet, magnesiowüstite, and $(Mg,Fe)_2SiO_4$ phases of the transition zone. *Am. Mineral.*, **88**, 387-397.

Frost, D.J. & Langenhorst, F. (2002): The effect of Al_2O_3 on Fe-Mg partitioning between magnesiowüstite and magnesium silicate perovskite. *Earth Planet Sci. Lett.*, **199**, 227-241.

Frost, D.J., Langenhorst, F., Van Aken, P.A. (2001): Fe-Mg partitioning between ringwoodite and magnesiowüstite and the effect of pressure, temperature and oxygen fugacity. *Phys. Chem. Mineral.*, **28**, 455-470.

Griffin, W.L., Gurney, J.J., Ryan, C.G. (1992): Variations in trapping temperatures and trace-elements in peridotite-suite inclusions from African diamonds - Evidence for two inclusion suites, and implications for lithosphere stratigraphy. *Contrib. Mineral. Petrol.*, **110**, 1-15.

Griffin, W. L., O'Reilly, S. Y., Abe, N., Aulbach, S., Davies, R.M., Pearson, N. J., Doyle, B. J., Kivi, K. (2003): The origin and evolution of Archean lithospheric mantle. *Precambrian Res.*, **127**, 19-41.

Griffin, W. L., Doyle, B. J., Ryan, C. G., Pearson, N. J., O'Reilly, S. Y., Davies, R., Kivi, K., VanAchterbergh, E., Natapov, L. M. (1999):

Grütter, H.S. & Moore, R.O. (2003): Pyroxene geotherms revisited - an empirical approach based on Canadian xenoliths. 8th International Kimberlite Conference, Extended Abstracts, Victoria, Canada.

Grütter, H.S., Apter, D.B., Kong, J. (1999): Crust-mantle coupling: Evidence from mantle-derived garnets. *in* "The J.B Dawson Volume, Proceedings of the 7th International Kimberlite Conference", J.J. Gurney, J.L. Gurney, M.D. Pascoe, S.H. Richardson, eds. Red Roof Design, Capetown, 307-313.

Gurney, J.J., Westerlund, K.J., Carlson, R.W., Shirey, S.B. (2003): Mineral compositions and Re-Os isotope systematics of harzburgitic nodules from the Panda kimberlite, Slave craton. 8th International Kimberlite Conference, Extended Abstracts, Victoria, Canada.

Haggerty, S.E. (1994): Superkimberlites - a geodynamic diamond window to the Earth's core. *Earth Planet. Sci. Lett.*, **122**, 57-69.

Harley, S. (1984): An experimental study of the partitioning of iron and magnesium between garnet and orthopyroxene. *Contrib. Mineral. Petrol.*, **86**, 359-373.

Harris, J. (1992): Diamond geology. *in* "The properties of natural and synthetic diamond" J.E. Field, ed. Academic Press, London, 345-393.

Harte, B., Harris, J.W., Hutchinson, M.T., Watt, G.R., Wilding, M.C. (1999): Lower mantle mineral associations in diamonds from São Luiz, Brazil. *in* "Mantle Petrology: Field observations and high pressure experimentation: A tribute to

Francis R. (Joe) Boyd", Y. Fei, C.M. Bertka, B.O. Mysen eds. The Geochemical Society Special Publication No.6, Houston, 125-153.

Heaman, L.M., Kjarsgaard, B.A., Creaser, R.A. (2003): The timing of kimberlite magmatism in North America: Implications for global kimberlite genesis and diamond exploration. *Lithos*, **71**, 153-184.

Herzberg, C. (1999): Phase equilibrium constraints on the formation of cratonic mantle. *in* "Mantle Petrology: Field observations and high pressure experimentation: A tribute to Francis R. (Joe) Boyd", Y. Fei, C.M. Bertka, B.O. Mysen eds. The Geochemical Society Special Publication No.6, Houston, 241-258.

Hoal, K.E.O., Hoal, B.G., Erlank, A.J., Shimizu, N. (1994): Metasomatism of the mantle lithosphere recorded by rare-earth elements in garnets. *Earth Planet. Sci. Lett.*, **126**, 303-313.

Irifune, T., Fujino, K., Ohtani, E. (1991): A new high pressure form of $MgAl_2O_4$. *Nature*, **349**, 409-411.

Ito, E. & Takahashi, E. (1989): Postspinel transformations in the system Mg_2SiO_4-Fe_2SiO_4 and some geophysical implications. *J. Geophys. Res.*, **94**, 10637-10646.

Ito, E. & Yamada, H. (1982): Stability relations of silicate spinel ilmenites and perovskites. *in* "High pressure research in geophysics", S. Akimoto & M.H. Manghnani eds. Center for Acad. Publ., Tokyo, 405-419.

Jones, A.G., Ferguson, A.J., Chave, A.D., Evans, R.L., McNeice, G.W. (2001): Electric lithosphere of the Slave craton. *Geology*, **29**, 423-426.

Kaminsky, F.V., Zakharchenko, O.D., Griffin, W.L., Channer, D.M.D., Khachatryan-Blinova, G.K. (2000): Diamond from the Guaniamo area, Venezuela. *Canad. Mineral.*, **38**, 1347-1370.

Kaminsky, F.V., Zakharchenko, O.D., Davies, R.M., Griffin, W.L., Khachatryan-Blinova, G.K., Shiryaev, A.A.. (2001): Superdeep diamonds from the Juina area, Mato Grosso State, Brazil. *Contrib. Mineral. Petrol.*, **140**, 734-753.

Kennedy, C.S., Kennedy, G.C. (1976): The equilibrium boundary between graphite and diamond. *J. Geophys. Res.*, **81**, 2467-2470.

Kopylova, M.G., Russell, J.K., Cookenboo, H. (1999): Petrology of peridotite and pyroxenite xenoliths from the Jericho kimberlite: Implications for the thermal state of the mantle beneath the Slave craton, Northern Canada. *J. Petrol.*, **40**, 79-104.

Liu, L.G (1975): Post-oxide phases of forsterite and enstatite. *Geophys. Res. Lett.*, **2**, 417-419.

– (1978). A new high pressure phase of spinel. *Earth Planet. Sci. Lett.*, **41**, 398-404.

– (1979): High pressure phase transformations in the joins Mg_2SiO_4-Ca_2SiO_4 and MgO-$CaSiO_3$, *Contrib. Mineral. Petrol.*, **69**, 245-247.

MacKenzie, J.M. & Canil, D. (1999): Composition and thermal evolution of cratonic mantle beneath the central Archean Slave Province, NWT, Canada. *Contrib. Mineral. Petrol.*, **134**, 313-324.

McDonough, W. & Sun, S.S. (1995): The composition of the Earth. *Chemical Geol.*, **120**, 223-253.

Menzies, M.A., Rogers, N., Tindle, A., Hawkesworth, C.J. (1987): Metasomatic and enrichment processes in lithospheric peridotites, an effect of asthenosphere-lithosphere interaction. *in*: "Mantle Metasomatism", M.A. Menzies, C.J. Hawkesworth, eds. Academic Press, London, 313-364.

Menzies, A.H., Westerlund, K.J., Gurney, J.J., Carlson, J.A., Fung, A., Nowicki, T. (2003): Peridotitic mantle xenoliths from kimberlites on the Ekati Diamond Mine property, N.W.T., Canada: major element compositions and applications for the lithosphere beneath the central Slave craton. *Lithos*, **77**, 395-412

Morimoto, N. (1988): Nomenclature of pyroxenes. *Mineral. Mag.*, **52**, 535-550.

O'Neill, H.StC. (1980): An experimental study of the iron-magnesium partitioning between garnet and olivine and its calibration as a geothermometer: corrections. *Contrib. Mineral. Petrol.*, **72**, 337.

O'Neill, H.StC. & Wood, B. (1979): An experimental study of the iron-magnesium partitioning between garnet and olivine and its calibration as a geothermometer. *Contrib. Mineral. Petrol.*, **70**, 59-70.

Orlov, Y.L. (1977): The mineralogy of the diamond. John Wiley & Sons, Chichester, 235 p.

Pearson, N.J., Griffin, W.L., Doyle, B.J., O'Reilly, S.Y., Van Achtenberg, E., Kivi, K. (1999): Xenoliths from kimberlite pipes of the Lac de Gras area, Slave Craton, Canada. *in* "The P.H. Nixon Volume, Proceedings of the 7th International Kimberlite Conference", J.J. Gurney, J.L. Gurney, M.D. Pascoe, S.H. Richardson, eds. Red Roof Design, Capetown, 644-658.

Phillips, D. & Harris, J.W. (1995): Geothermobarometry of diamond inclusions from the De Beers Pool Mines, Kimberley, South Africa. 6th International Kimberlite Conference, Extended Abstracts, Novosibirsk, 441-443.

Phillips, D. & Harris, J.W. (2003): The effect of differential mineral compressibility on diamond inclusion thermobarometry, 8th International Kimberlite Conference, Extended Abstracts, Victoria, Canada.

Pokhilenko, N.P. Sobolev, N.V., McDonald, J.A., Hall, A.E., Yefimova, E.S., Zedgenizov, D.A., Logvinova, A.M., Reimers, L.F. 2001. Crystalline inclusions in diamonds from kimberlites of the Snap Lake area (Slave Craton, Canada): New evidences for the anomalous lithospheric structure. *Dokl. Earth Sci.*, **380**, 806-811.

Pollack, H.N. & Chapman, D.S. (1977): On the regional variation of heat flow, geotherms, and lithospheric thickness. *Tectonophysics*, **38**, 279-296.

Richardson, S.H., Chinn, I.L., Harris, J.W. (1999a): Age and origin of eclogitic diamonds from the Jwaneng kimberlite, Botswana. *in* "The P.H. Nixon Volume, Proceedings of the 7th International Kimberlite Conference", J.J. Gurney, J.L. Gurney, M.D. Pascoe, S.H. Richardson, eds. Red Roof Design, Capetown, 709-713.

Richardson, S.H., Zartman, R.E., Carlson, J.A., (1999b): Old zircon megacrysts from young NWT kimberlites. 9th Annual V.M.Goldschmidt Conference, Abstract

#7250. LPI Contribution No.971 (CD-ROM), Lunar and Planetary Institute, Houston.

Richardson, S.H., Shirey, S.B., Harris, J.W. (2003): Episodic diamond genesis at Jwaneng, Botswana, and implications for Kaapvaal craton evolution. *Lithos*, **77**, 143-154

Ringwood, A.E. (1991): Phase transformations and their bearing on the constitution and dynamics of the mantle. *Geochim. Cosmochim. Acta*, **55**, 2083-2110.

Ringwood, A.E. & Major, A. (1971): Synthesis of majorite and other high pressure garnets and perovskites. *Earth Planet. Sci. Lett.*, **12**, 411-418.

Ryan, C.G., Griffin, W.L., Pearson, N.J. (1996): Garnet geotherms - pressure-temperature data from Cr-pyrope garnet xenocrysts in volcanic rocks. *J. Geophys. Res.*, **101**, 5611-5625.

Shimizu, N. & Hart, S.R. (1982): Applications of the ion microprobe to geochemistry and cosmochemistry. *Ann. Rev. Earth Planet. Sci.*, **10**, 483-526.

Shimizu, N. & Richardson, S.H. (1987): Trace-element abundance patterns of garnet inclusions in peridotite- suite diamonds. *Geochim. Cosmochim. Acta*, **51**, 755-758.

Stachel, T. & Harris, J.W. (1997): Syngenetic inclusions in diamond from the Birim field (Ghana) - A deep peridotitic profile with a history of depletion and re-enrichment. *Contrib. Mineral. Petrol.*, **127**, 336-352.

Stachel, T., Harris, J.W., Brey, G.P. (1998a): Rare and unusual mineral inclusions in diamonds from Mwadui, Tanzania. *Contrib. Mineral. Petrol.*, **132**, 34-47.

Stachel, T., Viljoen, K.S., Brey, G., Harris, J.W. (1998b): Metasomatic processes in lherzolitic and harzburgitic domains of diamondiferous lithospheric mantle: REE in garnets from xenoliths and inclusions in diamonds. *Earth Planet. Sci. Lett.*, **159**, 1-12.

Stachel, T., Brey, G.P., Harris, J.W. (2000a): Kankan diamonds (Guinea) I: from the lithosphere down to the transition zone. *Contrib. Mineral. Petrol.*, **140**, 1-15.

Stachel, T., Harris, J.W., Brey, G.P., Joswig, W. (2000b): Kankan diamonds (Guinea) II: lower mantle inclusion parageneses. *Contrib. Mineral. Petrol.*, **140**, 16-27.

Stachel, T., Harris, J.W., Tappert, R., Brey, G.P. (2003): Peridotitic inclusions in diamonds from the Slave and the Kaapvaal cratons - similarities and differences based on a preliminary data set. *Lithos*, **71**, 489-503.

Stachel, T., Aulbach, S., Brey, G.P., Harris, J.W., Leost, I., Tappert, R., Viljoen, K.S. (2004): The trace element composition of silicate inclusions in diamonds: a review, *Lithos*, **77**, 1-19.

Taylor, W.R., Jaques, A.L., Ridd, M. (1990): Nitrogen-defect aggregation characteristics of some Australasian diamonds: Time-temperature constraints on the source regions of pipe and alluvial diamonds. *Am. Mineral.*, **75**, 1290-1310.

Wang, W., Sueno, S., Takahashi, E., Yurimoto, H., Gasparik, T. (2000): Enrichment processes at the base of the Archean lithospheric mantle: observations from trace element characteristics of pyropic garnet inclusions in diamonds. *Contrib. Mineral. Petrol.*, **139**, 720-733.

Westerlund, K.J., Gurney, J.J., Shirey, S.B., Hauri, E. (2001): Nitrogen aggregation and stable nitrogen and carbon isotope characteristics of diamonds from the Panda kimberlite, Slave craton, Canada. The Slave-Kapvaal Workshop, Merrickville, Ontario, 4 p.

Westerlund, K.J., Hauri, E.H., Gurney, J.J. (2003a): FTIR absorption and stable nitrogen and carbon isotope microanalysis of mid-Archean diamonds from the Panda kimberlite. 8th International Kimberlite Conference, Extended Abstracts, Victoria, Canada.

Westerlund, K.J., Shirey, S.B., Richardson, S.H., Gurney, J.J., Harris, J.W. (2003b): Re-Os systematics of diamond inclusion sulfides from the Panda kimberlite, Slave craton. 8th International Kimberlite Conference, Extended Abstracts, Victoria, Canada.

Wilks, E.M. & Wilks, J. (1991): Properties and applications of diamond. Butterworth-Heinemann, Oxford, 525 p.

Wood, B.J. & Rubie, D.C. (1996): The effect of alumina on phase transformations at the 660-kilometer discontinuity from Fe-Mg partitioning experiments. *Science*, **273**, 1522-1524.

Yagi, T., Bell, P.M., Mao, H.K. (1979): Phase relations in the system MgO-FeO-SiO_2 between 150 and 700 kbar at 1000°C. *Carnegie Inst. of Washington Yr. Bk.*, **78**, 614-618.

Yefimova, E.S., Sobolev, N.V., Pospelova, L.N. (1983): Sulfide inclusions in diamonds and specific features of their paragenesis. *Zapiski Vsesoyuznogo Mineralogicheskogo Obshchestva*, **112**, 300-310.

Table 2-1: Summary of morphological, paragenetic and nitrogen characteristics of Panda diamonds.

Sample	Assemblage	Paragenesis	Shape	Color	Def.	Type	N (at.ppm)	Aggr. (%B)
PA-01	grt,grt-ol	Peridotitic	O	Brown	Yes	IaAB	347	21.9
PA-02	grt	Peridotitic	TM	Brown	No	IaAB	372	11.4
PA-03	grt	Peridotitic	TM	Brown	Yes	II	0	0
PA-04	grt	Peridotitic	TM	Brown	Yes	IaAB	225	19.2
PA-05	grt-ol-opx	Peridotitic	FD	Brown	Yes	IaAB	243	75.6
PA-06	grt	Peridotitic	O	Brown	Yes	IaA	26	2.7
PA-07	grt	Peridotitic	O	Brown	Yes	IaAB	67	46.5
PA-08	2grt	Peridotitic	O	Brown	Yes	II	0	0
PA-09	grt	Peridotitic	O	Brown	Yes	IaAB	631	89
PA-10	grt,ol	Peridotitic	IM	Brown	Yes	IaAB	125	55.8
PA-11	2grt	Peridotitic	D	Brown	Yes	IaAB	345	80.2
PA-12	grt	Peridotitic	O	Brown	Yes	II	0	0
PA-13	grt,chr	Peridotitic	O	Brown	Yes	IaAB	56	40
PA-14	grt	Peridotitic	O	Brown	Yes	IaAB	296	41.2
PA-15	grt	Peridotitic	O	Brown	Yes	II	0	0
PA-16	grt	Peridotitic	O	Brown	Yes	IaAB	131	61
PA-17	grt	Peridotitic	FD	Brown	Yes	IaA	17	0
PA-18	grt	Peridotitic	D	Brown	Yes	IaAB	106	71.3
PA-19	grt-opx,ol	Peridotitic	O	Brown	Yes	IaAB	65	47.1
PA-20	grt,chr,chr-ol	Peridotitic	O	Brown	Yes	IaAB	118	61.7
PA-21	grt,ol	Peridotitic	O	Brown	Yes	IaAB	73	50.8
PA-22	grt,ol	Peridotitic	I	Brown	Yes	IaAB	192	79.4
PA-23	grt,ol	Peridotitic	O	Brown	Yes	IaAB	543	56.5
PA-24	chr,chr(ex)	Peridotitic	I	Colorless	No	IaA	464	7
PA-25	chr	Peridotitic	D	Brown	Yes	IaAB	544	85.1
PA-26	chr	Peridotitic	D	Colorless	No	IaAB	268	10.7
PA-27	chr(ex)	Peridotitic	IM	Brown	No	IaA	27	0
PA-28	chr(ex)	Peridotitic	I	Brown	Yes	IaA	174	5.7
PA-29	chr	Peridotitic	I	Brown	Yes	IaA	292	0
PA-30	chr(ex)	Peridotitic	I	Brown	No	IaA	78	9.3
PA-31	chr,chr(ex)	Peridotitic	I	Brown	Yes	IaA	237	8.4
PA-32	chr	Peridotitic	I	Brown	No	IaA	148	2.2
PA-33	chr	Peridotitic	I	Brown	No	IaA	74	0
PA-34	chr	Peridotitic	I	Brown	No	IaAB	271	12.9
PA-35	chr	Peridotitic	I	Brown	No	IaAB	184	14.1
PA-36	ol	Peridotitic	O	Brown	Yes	IaA	609	8.1
PA-37	ol	Peridotitic	O	Brown	Yes	IaAB	79	44.8
PA-38	ol	Peridotitic	O	Colorless	No	IaAB	404	26.4
PA-39	fper,ol	?	I	Brown	Yes	II	0	0
PA-40	grt,ol	Peridotitic	FDM	Brown	Yes	II	0	0
PA-41	ol	Peridotitic	I	Brown	Yes	IaAB	55	61.6
PA-42	grt,ol	Peridotitic	TM	Brown	Yes	IaAB	333	81.4
PA-43	ol	Peridotitic	TM	Brown	No	IaAB	118	37.3
PA-44			I	Brown	Yes	IaAB	57	34.2
PA-45	3ol	Peridotitic	I	Brown	Yes	IaAB	70	39.9

O: octahedra, D: dodecahedra, C: cube, I: irregular, F: flattened, M: macle, A: aggregate, T: triangular

grt: garnet, *cpx*: clinopyroxene, *chr*: chromite, *ol*: olivine, *fper*: ferropericlase, *sulf*: sulfide, *(ex)*: surface exposed

comma: non-touching pair with..., *minus*: touching pair with..., *number*: number of separate crystals recoverd

Table 2-1 continued

Sample	Assemblage	Paragenesis	Shape	Color	Def.	Type	N (at.ppm)	Aggr. (%B)
PA-46	ol	Peridotitic	I	Brown	No	IaAB	57	49
PA-47			O	Colorless	No	IaA	782	7.4
PA-48	ol	Peridotitic	O	Colorless	No	IaAB	834	22.4
PA-49	ol	Peridotitic	O	Brown	Yes	IaAB	494	85.4
PA-50	2fper,$CaSiO_3$	Lower Mantle	I	Brown	No	II	0	0
PA-51	ol	Peridotitic	O	Colorless	No	IaA	608	7.4
PA-52	2ol	Peridotitic	FDM	Brown	Yes	IaAB	341	46
PA-53			I	Brown	Yes	II	0	0
PA-54	fper-spin,fper-ol,ol	?	I	Brown	Yes	II	0	0
PA-55	fper,SiO_2	?	O	Brown	Yes	IaA	16	0
PA-56	ol	Peridotitic	O	Brown	No	IaB	859	91.9
PA-57	ol,sulf	Peridotitic	I	Colorless	No	IaAB	337.9	13.4
PA-58	grt	Peridotitic	TM	Brown	No	IaAB	72	51.8
PA-59	cpx(ex)	Peridotitic	I	Brown	Yes	II	0	0
PA-60	cpx(ex),grt(ex)	Peridotitic	I	Colorless	No	IaAB	620	85.7
PA-61	cpx(ex)	Peridotitic	I	Colorless	No	II	0	0
PA-62	cpx(ex)	Peridotitic	I	Brown	Yes	II	0	0
PA-63	grt(ex)	Eclogitic	IA	Brown	No	II	0	0
PA-64	grt(ex)	Eclogitic	CA	Colorless	No	IaA	648	2.7
PA-65	2grt	Eclogitic	TM	Colorless	No	IaB	2720	100
PA-66	cpx-rut, sulf	Eclogitic	OM	Colorless	No	IaAB	638	69
PA-67	cpx(ex)	Peridotitic	IA	Colorless	No	IaB	197	100
PA-68	cpx(ex)	Peridotitic	IA	Colorless	No	IaB	262	100
PA-69	cpx(ex)	Peridotitic	OA	Colorless	No	IaAB	1028	13.7
PA-70	cpx(ex)	Peridotitic	I	Brown	No	IaAB	64	10.9
PA-71	2grt,sulf	Eclogitic	I	Brown	No	IaA	14	0
PA-72			I	Brown	Yes	II	0	0
PA-73	grt(ex)	Eclogitic	CA	Colorless	No	IaA	881	3.2
PA-74	grt(ex)	Eclogitic	CA	Colorless	No	IaA	1084	3.9
PA-75	2sulf	Peridotitic	O	Colorless	No	IaA	700	3.5
PA-76	sulf	Eclogitic	O	Colorless	No	IaAB	985	10.7
PA-77			O	Colorless	No	IaAB	881	16.6
PA-78	sulf	Peridotitic	O	Colorless	No	IaA	424	7.6
PA-79	chr,sulf	Peridotitic	I	Colorless	No	IaA	242	0
PA-80	2sulf	Peridotitic	IM	Colorless	No	IaA	663	9
PA-81	sulf	Peridotitic	O	Brown	Yes	IaAB	114	22.6
PA-82	sulf	Peridotitic	O	Colorless	No	IaA	123	5
PA-83	sulf	Peridotitic	O	Brown	No	IaA	474	6.4
PA-84	sulf	Peridotitic	O	Brown	No	IaAB	86	22
PA-85	2sulf	Peridotitic	O	Brown	Yes	IaA	333	0
PA-86			I	Brown	Yes	IaA	291	0
PA-87	2sulf	Peridotitic	I	Brown	Yes	IaA	23	0
PA-88	sulf	Peridotitic	I	Colorless	No	IaA	468	9
PA-89	sulf	Peridotitic	O	Colorless	No	IaA	552	1.8
PA-90	sulf	Peridotitic	I	Brown	No	IaA	12	0

O: octahedra, D: dodecahedra, C: cube, I: irregular, F: flattened, M: macle, A: aggregate, T: triangular
grt: garnet, *cpx*: clinopyroxene, *chr*: chromite, *ol*: olivine, *fper*: ferropericlase, *sulf*: sulfide, *(ex)*: surface exposed
comma: non-touching pair with…, *minus*: touching pair with…, *number*: number of separate crystals recoverd

Table 2-2: Mineral inclusions recovered from Panda diamonds separated into paragenetic groups (based on the major element composition). Numbers represent diamonds, not inclusions.

Paragenesis	Single Phase		Multiple Phases		Exposed	
Peridotitic (72)	garnet	15	garnet-olivine	7	clinopyroxene	7
	olivine	12	olivine-sulfide	1	garnet-clinopyroxene	1
	chromite	9	chromite-sulfide	1	chromite	3
	sulfide	12	garnet-chromite	1		
			garnet-olivine-orthopyroxene-spinel	1		
			garnet-olivine-orthopyroxene	1		
			garnet-olivine-chromite	1		
Eclogitic (8)	garnet	1	clinopyroxene-rutile-sulfide	1	garnet	4
	CuFe-sulfide	1				
	Fe-sulfide	1				
Lower Mantle + Uncertain (4)			ferropericlase-$CaSiO_3$	1		
			ferropericlase-SiO_2	1		
			ferropericlase-spinel-olivine	1		
			ferropericlase-olivine	1		

Note: 6 diamonds did not contain inclusions or yielded only soft/epigenetic material

Table 2-3: Major- and trace element composition of peridotitic and eclogitic inclusions in Panda diamonds. Major element compositions (EPMA-analyses) are given as wt%.

Mineral	Harzburgitic garnet	Harzburgitic garnet	Lherzolitic garnet	Lherzolitic garnet	Harzburgitic garnet	Harzburgitic garnet	Harzburgitic garnet	Harzburgitic garnet	Lherzolitic garnet	Lherzolitic garnet	Harzburgitic garnet
Sample	PA-04	PA-08	PA-10	PA-11	PA-12	PA-13	PA-17	PA-20	PA-23	PA-40	PA-58
Assemblage	grt	2grt	grt,ol	2grt	grt	gt,chr	grt	gt,chr,chr-ol	grt,ol	grt,ol	grt
Paragenesis	peridotitic	peridotitic	peridotitic	peridotitic	peridotitic	peridotitic	peridotitic	peridotitic	peridotitic	peridotitic	peridotitic
P_2O_5	0.02	0.02	0.00	0.02	0.00	0.04	0.00	0.00	0.00	0.03	0.02
SiO_2	41.9	42.1	41.6	41.7	42.2	41.0	41.9	42.2	41.8	42.4	41.6
TiO_2	0.04	0.05	0.05	0.14	0.00	0.09	0.03	0.02	0.16	0.13	0.07
Al_2O_3	18.0	15.8	16.3	16.6	16.0	13.9	15.6	14.3	16.9	16.3	16.1
Cr_2O_3	7.61	10.01	9.03	8.58	10.8	12.7	10.3	12.6	8.14	8.59	8.99
FeO	5.98	6.30	6.29	6.51	5.81	6.71	6.16	6.19	6.10	5.95	6.27
MnO	0.29	0.30	0.29	0.32	0.29	0.37	0.29	0.33	0.29	0.28	0.30
NiO	0.00	0.02	0.02	0.00	0.00	0.02	0.00	0.00	0.00	0.00	0.02
MgO	22.4	21.0	20.6	20.3	22.3	19.4	21.5	22.5	20.8	20.7	21.2
CaO	3.15	5.17	5.41	5.81	3.61	6.14	4.33	3.14	5.51	5.79	4.87
Na_2O	0.00	0.10	0.00	0.00	0.00	0.00	0.00	0.28	0.00	0.03	0.00
K_2O	0.00	0.00	0.00	0.00	0.00	0.00	0.00	0.00	0.00	0.00	0.00
Total	99.5	100.8	99.5	100.1	101.1	100.4	100.2	101.46	99.8	100.2	99.5
Ti [ppm]	331		331	635	174	1063	217	186	1023	1070	964
Sr [ppm]	1.83		0.55	1.40	5.12	21.5	2.10	29.6	0.94	2.32	5.45
Y [ppm]	38.7		1.88	2.59	1.73	0.56	2.03	2.96	11.7	5.65	12.2
Zr [ppm]	152		23.6	14.5	7.10	4.14	8.64	26.8	20.6	23.2	13.4
La [ppm]	0.01		0.17	0.19	0.19	0.83	0.13	0.28	0.16	0.03	0.23
Ce [ppm]	0.65		1.06	2.07	1.37	5.46	2.20	3.46	1.30	0.57	2.10
Nd [ppm]	1.68		0.83	2.08	1.10	3.33	1.52	4.38	1.60	3.37	2.31
Sm [ppm]	0.74		0.75	0.67	0.13	0.47	0.42	1.25	0.82	1.66	0.46
Eu [ppm]	0.51		0.28	0.26	0.06	0.07	0.12	0.37	0.28	0.53	0.08
Dy [ppm]	4.41		0.51	0.69	0.13	0.05	0.23	0.33	1.59	0.73	0.58
Er [ppm]	0.93		0.22	0.31	0.08	0.05	0.16	0.15	1.28	0.36	0.30
Yb [ppm]	0.81		0.36	0.46	0.12	0.13	0.26	0.25	1.16	0.56	0.63

Table 2-3 continued

Mineral	Chromite*	Chromite**	Chromite***	Clinopyroxene (exposed)	Clinopyroxene (exposed)	Clinopyroxene (exposed)	Eclogitic Garnet	Eclogitic Garnet	Clinopyroxene (-rutile)	Rutile (-cpx)
Sample	PA-20	PA-25	PA-29	PA-61a	PA-67a	PA-70a	PA-65	PA-65	PA-66	PA-66
Assemblage	grt,chr,chr-ol	chr	chr	cpx	cpx	cpx	2grt	2grt	cpx-rut,sulf	cpx-rut,sulf
Paragenesis	peridotitic	peridotitic	peridotitic	peridotitic	peridotitic	peridotitic	eclogitic	eclogitic	eclogitic	eclogitic
P_2O_5	0.00	0.00	0.00	0.00	0.00	0.00	0.08	0.07	0.02	0.00
SiO_2	0.17	0.19	0.09	54.3	54.1	54.1	40.0	40.3	53.6	0.00
TiO_2	0.03	0.09	0.22	0.06	0.14	0.01	0.91	0.90	0.38	100.3
Al_2O_3	4.99	4.89	7.20	1.62	2.58	1.08	22.5	22.3	4.78	0.15
Cr_2O_3	66.1	66.1	63.7	0.89	1.01	1.65	0.03	0.03	0.08	0.21
FeO	15.2	15.4	14.9	2.60	2.87	2.27	13.63	13.40	8.61	0.29
MnO	0.26	0.27	0.25	0.10	0.10	0.10	0.27	0.26	0.13	0.00
NiO	0.10	0.10	0.10	0.06	0.05	0.06	0.00	0.00	0.03	0.00
MgO	13.5	13.4	13.8	17.7	15.8	17.7	10.1	10.1	13.4	0.00
CaO	0.00	0.00	0.00	19.8	19.2	19.6	12.7	12.9	14.5	0.20
Na_2O	0.00	0.00	0.04	1.31	2.21	1,22	0.31	0.28	2.75	0.00
K_2O	0.00	0.00	0.00	0.06	0.07	0.15	0.00	0.00	0.19	0.00
Total	100.7	100.7	100.7	98.5	98.2	98.0	100.6	100.6	98.6	101.2

* ZnO: 0.40, V_2O_3: 0.25

** ZnO: 0.42, V_2O_3: 0.20

*** ZnO: 0.46, V_2O_3: 0.24

Table 2-4: Major element composition (EPMA-analyses, wt%) of selected sulfide inclusions in diamonds from Panda

Mineral	Fe-Ni sulfide	Fe-Ni sulfide	Fe-Ni sulfide	Fe-Ni sulfide	Fe-Ni sulfide	Fe-Ni sulfide	Fe-Ni sulfide	Fe-Ni sulfide	Fe-Ni sulfide	Fe-Ni sulfide	Fe-sulfide	Fe-sulfide	Fe-Cu Sulfide (average)
Sample	PA-78	PA-83	PA-84	PA-88	PA-75	PA-80	PA-85	PA-87	PA-79	PA-57	PA-66	PA-71	PA-76
Assemblage	sulf	sulf	sulf	sulf	2 sulf	2 sulf	2 sulf	2 sulf	chr,sulf	ol,sulf	cpx-rut,sulf	sulf, 2gl(ex)	sulf
Paragenesis	peridotitic	peridotitic	peridotitic	peridotitic	peridotitic	peridotitic	peridotitic	peridotitic	peridotitic	peridotitic	eclogitic	eclogitic	eclogitic
Mg	n.a.	n.a.	n.a.	n.a.	n.a.	n.a.	n.a.	n.a.	n.a.	n.a.	≤ 0.01	0.09	n.a.
Si	n.a.	n.a.	n.a.	n.a.	n.a.	n.a.	n.a.	n.a.	n.a.	n.a.	≤ 0.01	0.02	n.a.
S	36.6	36.8	37.2	37.0	36.7	36.6	36.3	37.0	36.7	36.6	37.7	37.9	31.6
Cr	0.13	0.13	0.16	0.17	0.08	0.09	0.11	0.13	0.12	0.10	0.00	0.00	n.a.
Mn	≤ 0.01	≤ 0.01	≤ 0.01	≤ 0.01	≤ 0.01	≤ 0.01	≤ 0.01	≤ 0.01	≤ 0.01	≤ 0.01	≤ 0.01	≤ 0.01	≤ 0.01
Fe	39.9	38.6	40.0	39.1	42.0	40.7	38.9	41.3	38.4	39.9	56.0	54.9	24.7
Co	0.47	0.49	0.46	0.47	0.49	0.46	0.51	0.50	0.52	0.48	0.32	0.41	0.08
Ni	20.4	21.5	20.6	21.5	18.8	19.8	21.6	19.8	22.3	20.7	3.26	2.94	0.69
Cu	1.37	1.86	0.97	0.59	0.89	1.19	2.09	0.56	0.66	1.29	1.88	2.35	41.0
Zn	≤ 0.01	≤ 0.01	≤ 0.01	≤ 0.01	≤ 0.01	≤ 0.01	≤ 0.01	≤ 0.01	≤ 0.01	≤ 0.01	≤ 0.01	≤ 0.01	n.a.
As	≤ 0.01	≤ 0.01	≤ 0.01	≤ 0.01	≤ 0.01	≤ 0.01	≤ 0.01	≤ 0.01	≤ 0.01	≤ 0.01	≤ 0.01	≤ 0.01	0.01
Ag	n.a.	n.a.	n.a.	n.a.	n.a.	n.a.	n.a.	n.a.	n.a.	n.a.	n.a.	n.a.	0.05
Pb	n.a.	n.a.	n.a.	n.a.	n.a.	n.a.	n.a.	n.a.	n.a.	n.a.	n.a.	n.a.	0.20
Bi	n.a.	n.a.	n.a.	n.a.	n.a.	n.a.	n.a.	n.a.	n.a.	n.a.	n.a.	n.a.	0.10
Total	98.9	99.3	99.4	98.9	99.0	98.8	99.6	99.4	98.6	99.0	99.2	98.6	98.5

Table 2-5: Major element composition (EPMA-analyses, wt%) of inclusions of lower mantle origin in diamonds from Panda

Mineral	Ferropericlase	Ferropericlase	$CaSiO_3$	SiO_2
Sample	PA-50	PA-50	PA-50	PA-55
Assemblage	2fper,$CaSiO_3$	2fper,$CaSiO_3$	2fper,$CaSiO_3$	fper,SiO_2
P_2O_5	≤ 0.01	≤ 0.01	≤ 0.01	≤ 0.01
SiO_2	0.02	0.03	51.13	99.5
TiO_2	≤ 0.01	≤ 0.01	≤ 0.01	≤ 0.01
Al_2O_3	0.07	0.07	0.08	0.05
Cr_2O_3	0.75	0.74	≤ 0.01	≤ 0.01
FeO	21.4	21.4	0.04	≤ 0.01
MnO	0.23	0.24	0.04	≤ 0.01
NiO	1.35	1.34	0.00	≤ 0.01
MgO	75.3	75.2	0.10	≤ 0.01
CaO	≤ 0.01	≤ 0.01	47.9	≤ 0.01
Na_2O	≤ 0.02	0.07	0.02	≤ 0.02
K_2O	≤ 0.01	0.02	0.10	≤ 0.01
Total	99.1	99.1	99.5	99.6

Table 2-6: Major element composition (EPMA-analyses, wt%) of inclusions of uncertain parageneses (lithospheric dunites) in diamonds from Panda

Mineral	Ferropericlase (-spinel)	Spinel (-fper)	Ferropericlase (-ol)	Olivine (-fper)	Olivine	Olivine	Ferropericlase
Sample	PA-54	PA-54	PA-54	PA-54	PA-54	PA-39	PA-39
Assemblage	fper-sp,fper-ol,ol	fper-sp,fper-ol,ol	fper-sp,fper-ol,ol	fper-sp,fper-ol,ol	fper-sp,fper-ol,ol	fper,ol	fper,ol
P_2O_5	≤ 0.01	≤ 0.01	≤ 0.01	≤ 0.01	0.02	≤ 0.01	≤ 0.01
SiO_2	0.08	0.40	0.04	40.8	41.2	40.9	0.02
TiO_2	≤ 0.01	0.10	≤ 0.01	≤ 0.01	≤ 0.01	≤ 0.01	≤ 0.01
Al_2O_3	0.41	57.4	0.11	0.05	0.05	0.02	≤ 0.01
Cr_2O_3	0.71	8.47	0.64	0.02	≤ 0.01	0.03	0.61
FeO	28.9	9.10	29.6	4.61	4.63	5.90	20.9
MnO	0.12	0.07	0.14	0.06	0.08	0.09	0.16
NiO	2.11	0.23	2.14	0.20	0.19	0.22	1.34
MgO	67.9	23.8	66.7	51.51	51.7	50.8	75.0
CaO	≤ 0.01	≤ 0.01	≤ 0.01	0.09	0.08	0.03	≤ 0.01
Na_2O	0.15	≤ 0.02	0.12	≤ 0.02	≤ 0.02	≤ 0.02	≤ 0.02
K_2O	≤ 0.01	≤ 0.01	≤ 0.01	≤ 0.01	≤ 0.01	≤ 0.01	≤ 0.01
Total	100.4	99.6	99.5	97.4	98.0	98.1	98.1

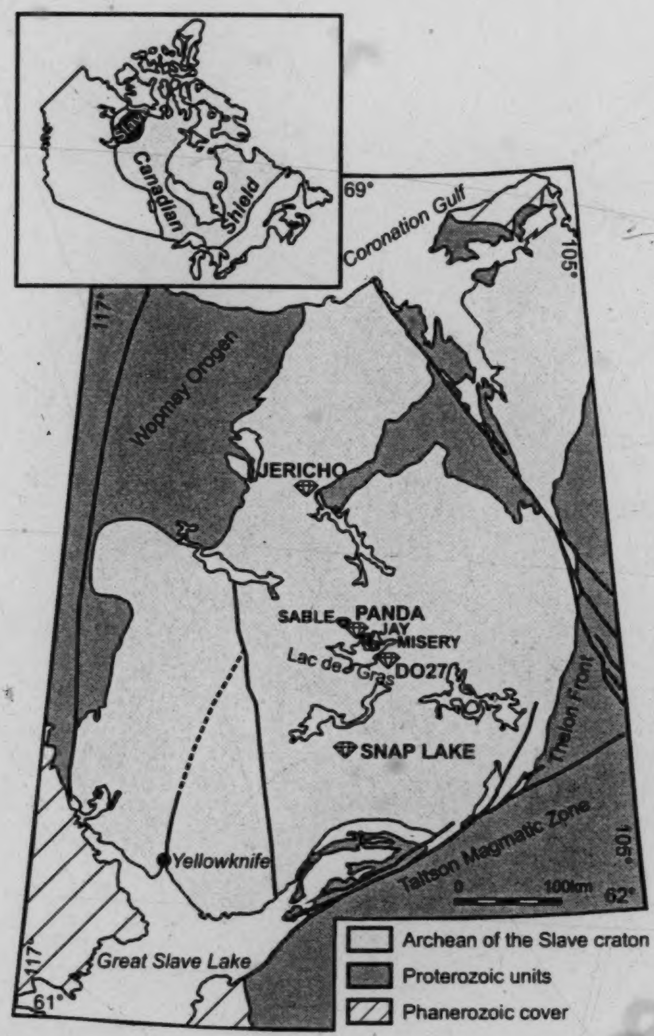
Canadian
Shield
Slave
69°
Coronation Gulf
105°
117°
Wopmay Orogen
JERICHO
SABLE
PANDA
JAY
MISERY
Lac de Gras
DO27
SNAP LAKE
Thelon Front
Taltson Magmatic Zone
106°
0
100km
62°
Yellowknife
Great Slave Lake
117°
61°
Archean of the Slave craton
Proterozoic units
Phanerozoic cover

Figure 2-1: Outline of the Slave craton after Bleeker (1999), showing the locations of the kimberlites mentioned in the text.

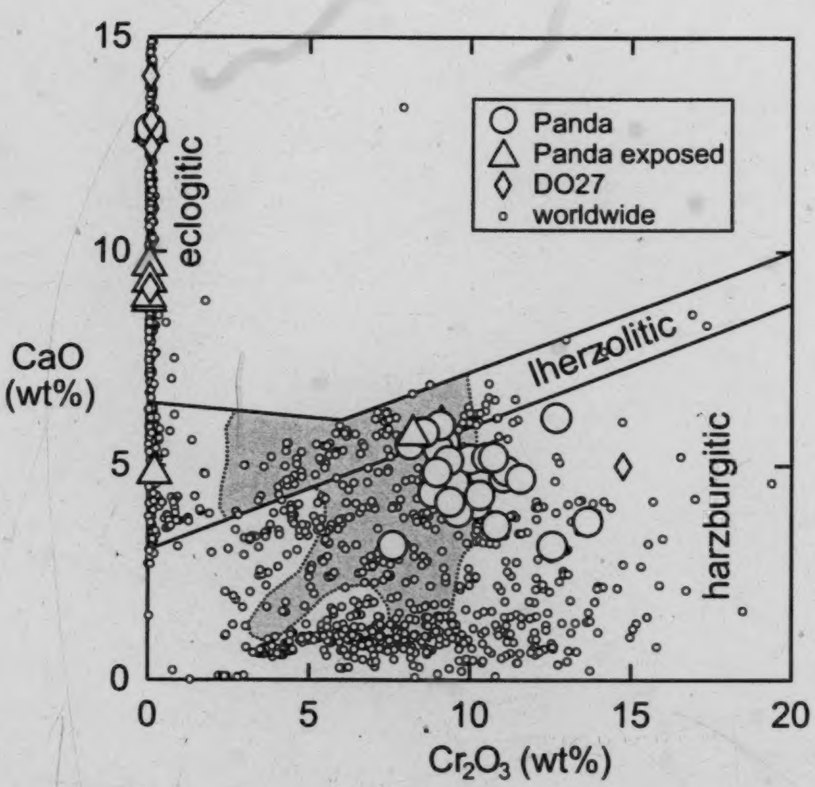

Figure 2-2: CaO versus Cr_2O_3 for garnet inclusions in diamonds from Panda (*open triangles*: surface exposed garnets; *open circles* represent garnets fully included in the diamond). Also shown are garnet compositions given by Davies *et al.* (1999) for DO27 (*open diamonds*) and the field (*grey area*) for garnets from xenoliths from Panda (Menzies *et al.*, 2003). Garnet compositions of the database for mineral inclusions in diamonds worldwide are shown as *small circles*. The compositional field for lherzolitic garnets is taken from Sobolev *et al.* (1973).

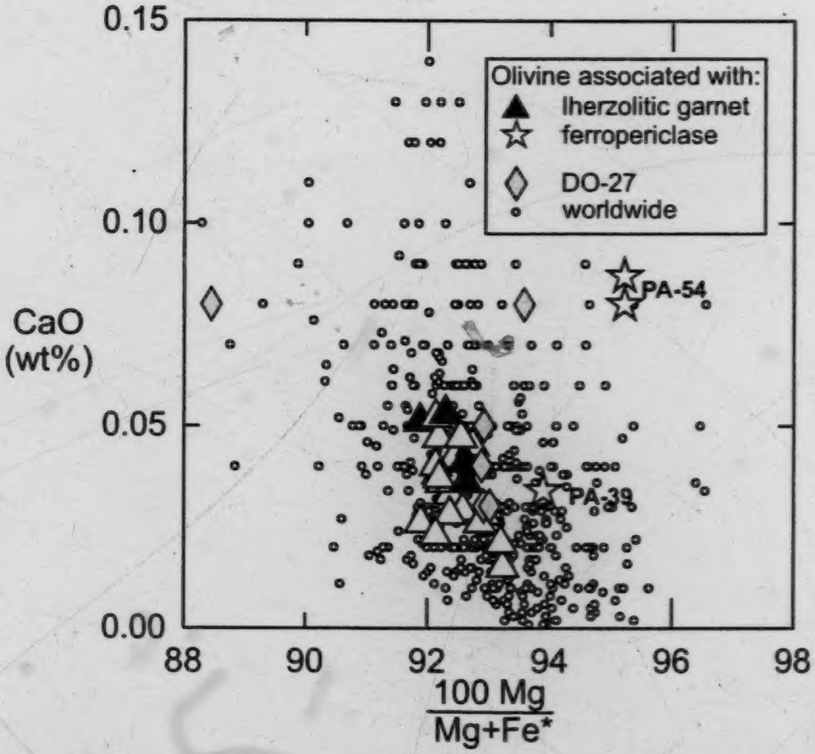

Figure 2-3: CaO (wt%) versus molar Mg number for olivine inclusions (*open triangles*). *Black triangles* indicate olivines associated with lherzolitic garnets. *Stars* mark the composition of olivines associated with ferropericlase. The compositional data for DO-27 olivines are taken from Davies *et al.* (1999). *Small circles*: worldwide data.

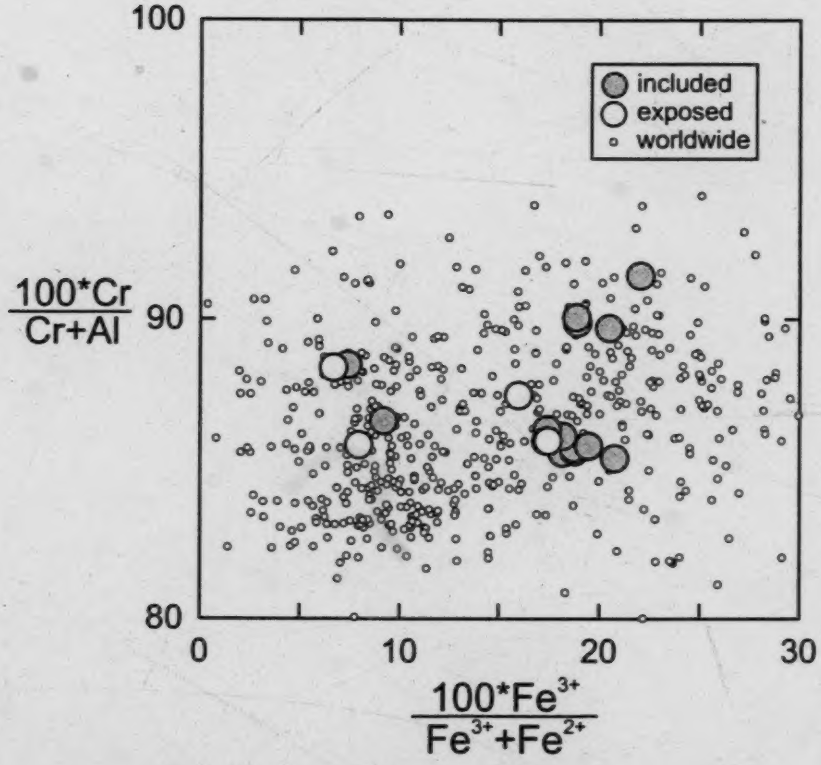

Figure 2-4: Diagram of Cr# versus ferric iron ratio (Fe^{3+} calculated after Droop, 1987) of magnesiochromite inclusions (*grey circles*); *open circle*: surface exposed chromites; *small circles*: worldwide data.

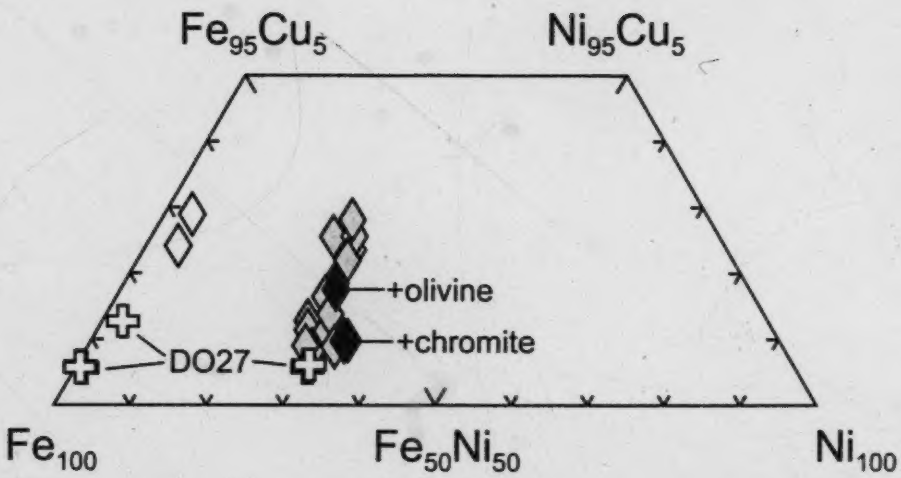

Figure 2-5: Composition of Fe and Fe-Ni sulfide inclusions from Panda diamonds (in atomic %) in the Fe-Ni-Cu system. *Grey diamonds*: Fe-Ni (peridotitic) sulfide inclusions (inclusions with olivine/chromite as coexisting phase are filled in black). *Open diamonds*: Fe-sulfides (eclogitic). *Crosses*: Sulfides from DO27 (Davies *et al.*, 1999).

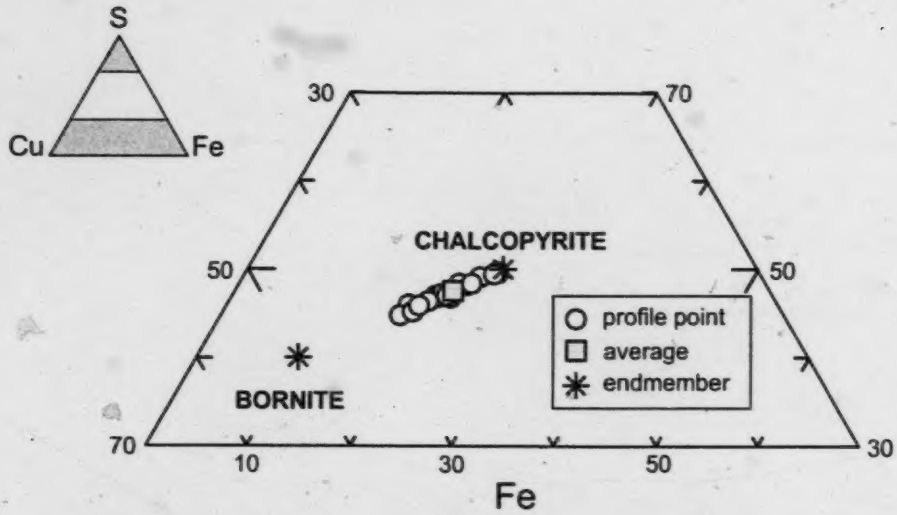

Figure 2-6: Composition of the Cu-Fe sulfide from diamond PA-76 (in atomic %) in the Cu-Fe-S system. Individual analyses were performed along a compositional profile.

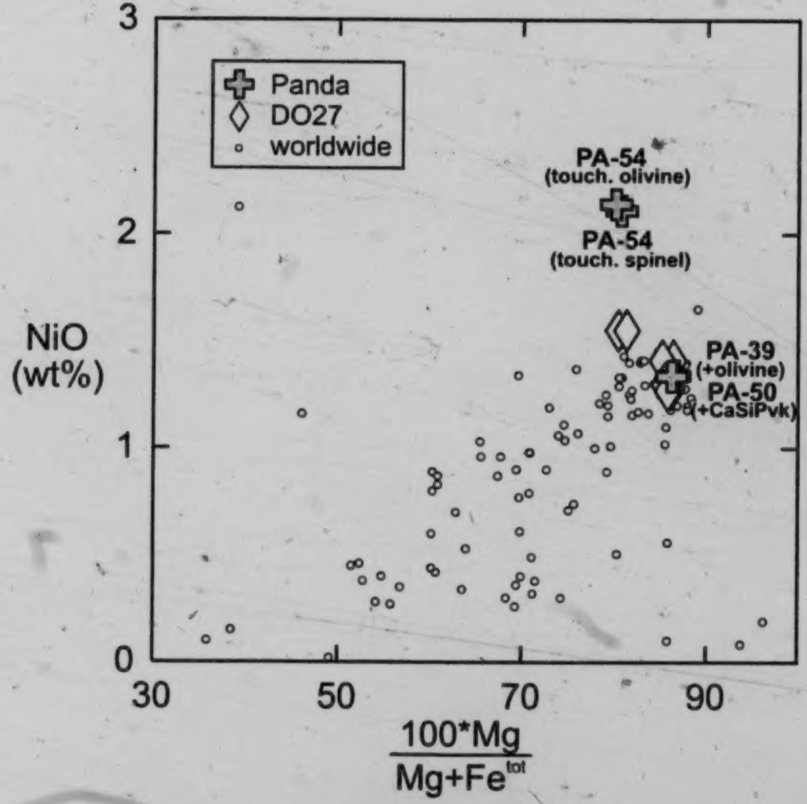

Figure 2-7: NiO (wt%) versus Mg# for ferropericlase inclusions from Panda diamonds (*crosses*). Additional phases within the same diamond are indicated. For comparison compositional data for ferropericlase inclusions from the worldwide database are shown (*small circles*). Ferropericlase inclusions from the DO27 (Davies *et al.*, 1999) are marked with an *open diamond symbol*.

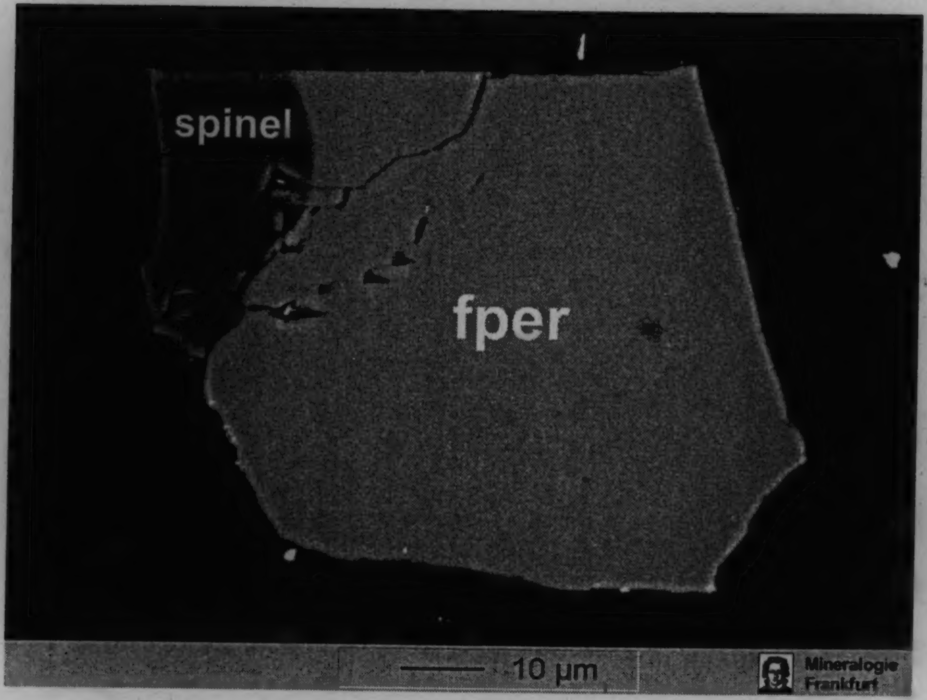
spinel
fper
10 µm
Mineralogie
Frankfurt

Figure 2-8: Backscattered-electron image of inclusion from diamond PA-54 consisting of ferropericlase and a phase of spinel chemistry.

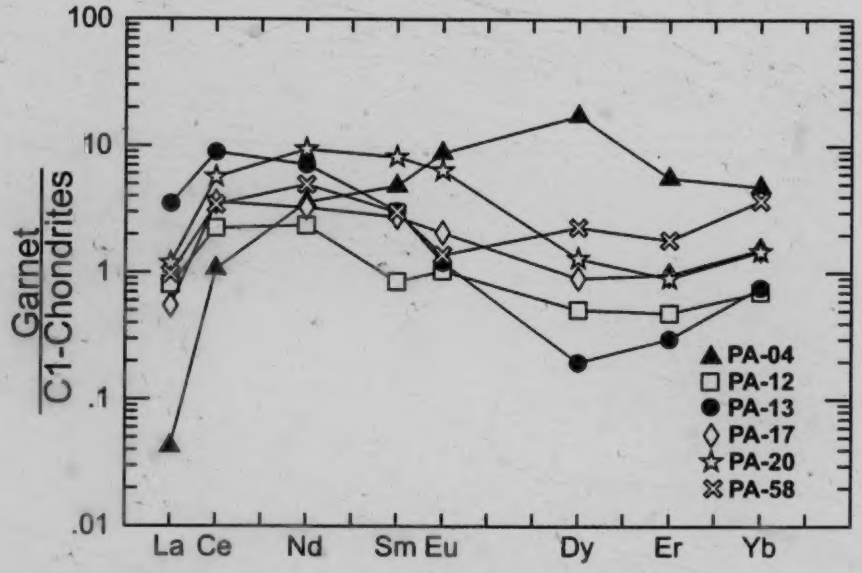

Figure 2-9: REE concentrations of harzburgitic garnet inclusions normalized to C1 (McDonough & Sun, 1995).

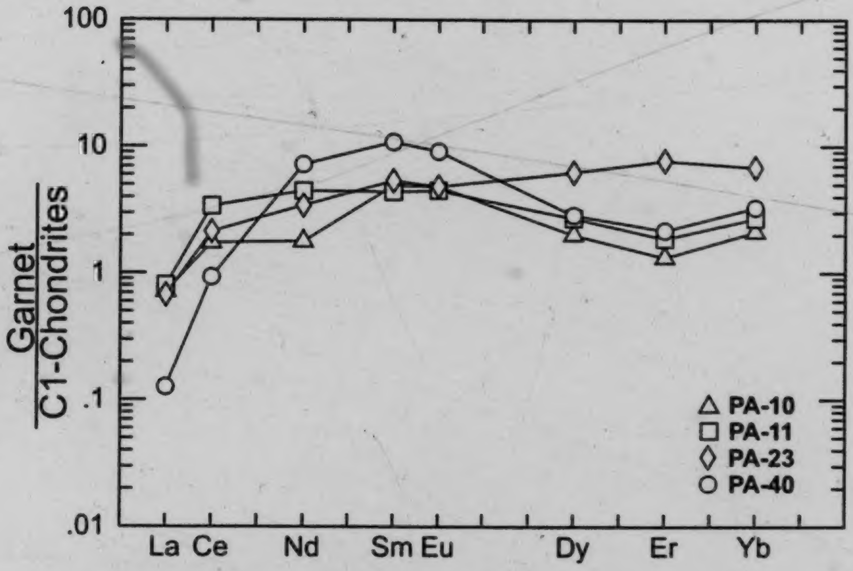

Figure 2-10: REE concentrations of lherzolitic garnet inclusions normalized to C1 (McDonough & Sun, 1995).

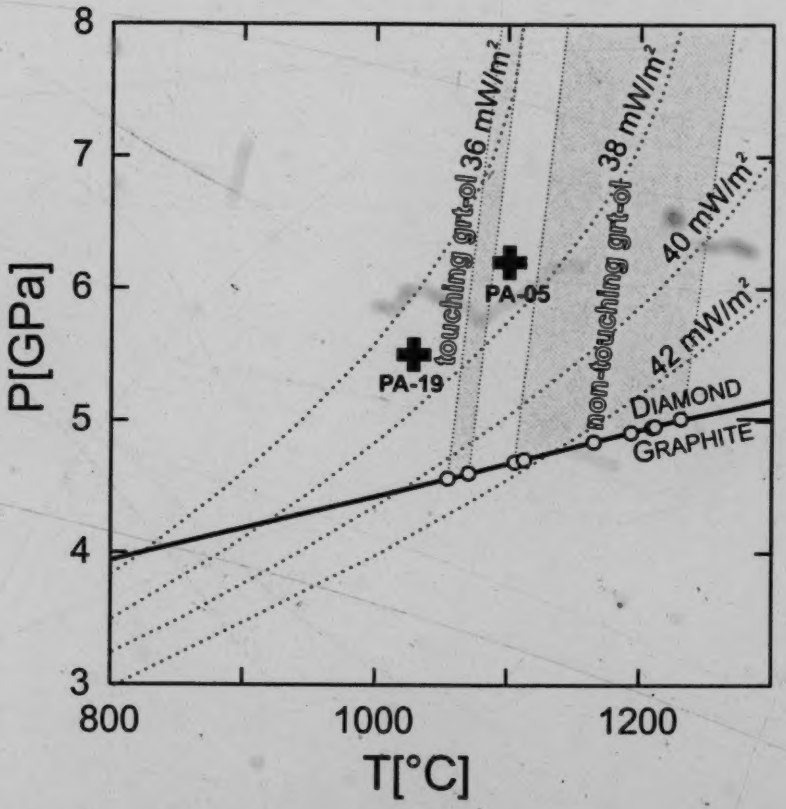

Figure 2-11: Results of geothermobarometric calculations for garnet-opx and garnet-olivine inclusion pairs from Panda diamonds. The P-T conditions for *touching* garnet-opx pairs from diamonds PA-19 and PA-05 (*crosses*) were calculated after Brey & Köhler (1990) and Harley (1984). The dotted lines indicate conductive geotherms for various surface heat flow values (calculated after Pollack & Chapman (1977)). The *shaded area* represents the range of temperatures at given pressures calculated for *touching and non-touching* garnet-olivine pairs (O'Neill & Wood, 1979; O'Neill, 1980) recovered from Panda diamonds. *Open circles*: Individual results for touching and non-touching garnet-olivine pairs projected on the diamond-graphite boundary. Graphite-diamond phase boundary from Kennedy & Kennedy (1976).

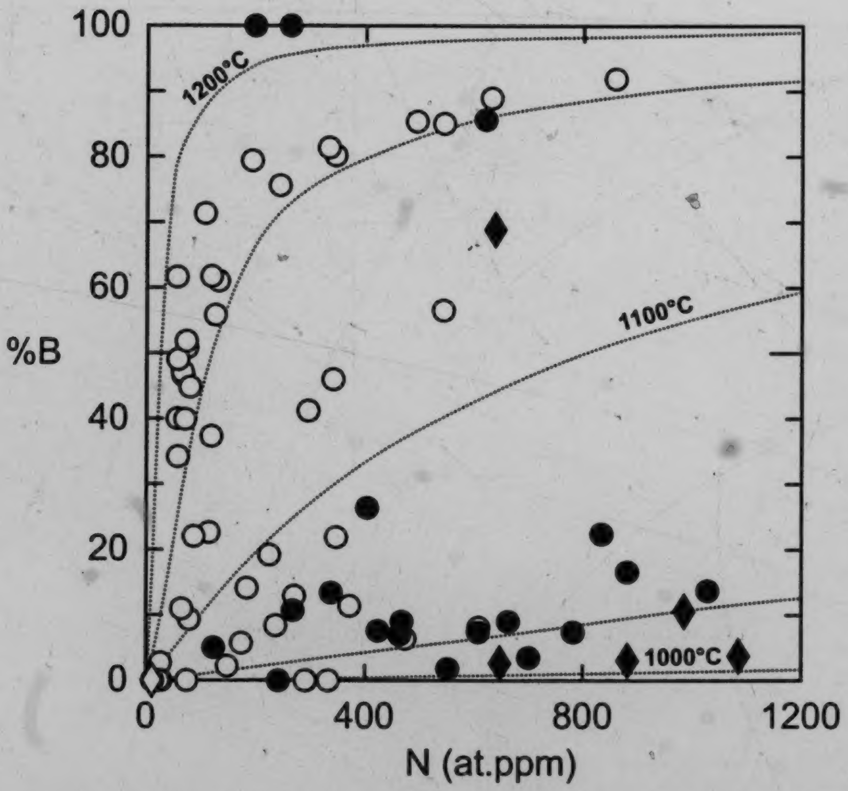

Figure 2-12: Aggregation level (percentage of higher aggregated B-center relative to the A-center) versus nitrogen concentration (atomic ppm) in Type I diamonds from the Panda kimberlite. Dotted lines are isotherms of ambient mantle temperatures calculated using the activation energy for the conversion of the A- to B-center derived by Taylor *et al.* (1990). A residence time of 3.4 billion years was assumed for the calculations, which is consistent with isochron ages found for sulfides inclusions in Panda diamonds (Westerlund *et al.*, 2003) and a Teriary kimberlite eruption age. *Circles*: peridotitic diamonds, *diamond symbol*: eclogitic diamonds. *Black symbols* mark diamonds that do not show signs of plastic deformation. Note that one eclogitic diamond with a nitrogen content of 2720 at.ppm (100% B-centers) is not shown in the diagram.

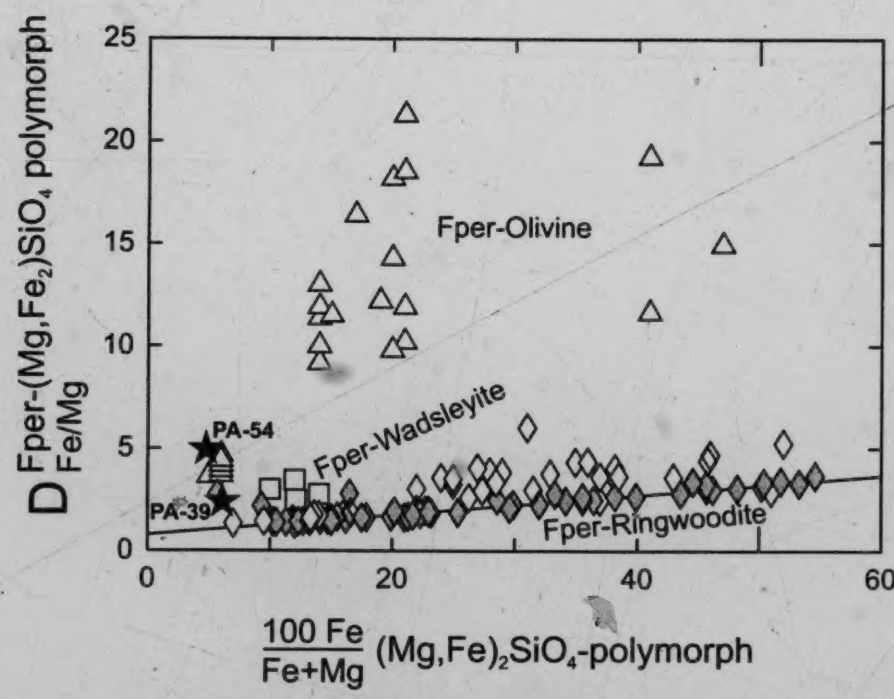

Figure 2-13: Diagram of experimentally determined Fe-Mg partitioning between ferropericlase and $(Mg,Fe)_2SiO_4$ polymorphs (olivine: *triangles*, wadsleyite: *squares*, ringwoodite: *diamonds*) as function of the composition of the $(Mg,Fe)_2SiO_4$ polymorph, shown as molar Fe number. The data are from Ito & Yamada (1982); Ito & Takahashi (1989); Fei *et al.* (1991); Wood & Rubie (1996); Akaogi *et al.* (1998); Frost *et al.* (2001) and Frost (2003). Results for the ferropericlase-ringwoodite compositions from experiments in Fe-capsules (Frost *et al.*, 2001) are indicated by *grey diamonds*. Observed Fe-Mg partitioning between ferropericlase and olivine inclusions in diamond PA-39 and PA-54 is marked as *stars*.

CHAPTER 3

Placer diamonds from Brazil: Indicators of the composition of the Earth's mantle and of the origin of their kimberlite source

The content of this chapter is in preparation to be submitted for publication to *Economic Geology* as:

Tappert, R., Stachel, T., Harris, J.W., Muehlenbachs, K., Brey, G.P.: Placer diamonds from Brazil: Indicators of the composition of the Earth's mantle and of the origin of their kimberlite source.

3.1 Introduction

Despite the fact that diamonds have been mined in Brazil since the early 18th century and the status of Brazil as the main diamond producer in the world until 1870, the knowledge about the mantle origin of the diamonds and their kimberlitic sources is still incomplete. Diamonds in Brazil generally occur in widespread placer deposits (see Svisero, 1995). In the past, the lack of known diamondiferous kimberlites has led to suggestions that diamonds in Brazil were derived from ancient kimberlites that are completely eroded, metamorphosed, or buried underneath younger sedimentary rocks (Chaves et al., 1993). It was also suggested that some Brazilian diamonds originate from remote sources, e.g. West Africa (Reid, 1974). More recently, an increasing number of kimberlites and associated rocks, which are in part diamondiferous, have been discovered in Brazil (see e.g. Svisero et al., 1984; Tompkins, 1994; Bizzi et al., 1994). Theses discoveries show that primary diamond sources exist, but so far their small number does not account for the presence of the widespread placer deposits in Brazil and suggests that further discoveries of primary diamond deposits in Brazil are likely. However, deep reaching tropical weathering, which in many cases destroyed indicator minerals associated with diamonds, and re-deposition of diamonds over geologically long periods of time make it difficult to locate the kimberlitic sources if they still exist. One way to obtain information about the primary sources of placer diamonds is to carry out detailed studies of the diamonds and their associated mineral inclusions. Considering the extent of alluvial diamond sources in Brazil, previous studies of this type are surprisingly scarce.

A description of diamonds and their mineral inclusions from alluvial deposits in southern Brazil from Meyer and Svisero (1975) indicates inclusion assemblages very similar to other deposits worldwide, but few other studies on diamonds from Brazil have been published. One exception is the diamond suite from the Juina area, which includes the original placer deposits of the São Luiz River. These diamonds have attracted attention because of a unusually high abundance of diamonds that indicate a sublithospheric origin (Wilding, 1990; Harte and Harris, 1994; Harte et al., 1999; Hutchison et al., 1999; Kaminsky et al., 2001). However, the mineral assemblages recovered from this deposit appear not to be representative for the bulk of the Brazilian diamonds (Meyer and Svisero, 1975), and maybe therefore of limited significance for the interpretation of the large scale composition of the Earth's mantle beneath Brazil.

In this paper a detailed description and compositional data for sixty-eight diamonds and their mineral inclusions from three alluvial deposits in Brazil are presented. The results are intended to constrain the processes of diamond formation, the composition of diamond sources in the Earth's mantle beneath different parts of Brazil, and the history of the diamonds after their emplacement on the Earth's surface. This is particularly important, because it may indicate if diamonds within a deposit are derived from an undiscovered, proximal kimberlite source, or if they represent a mixture of diamonds from various sources.

3.2 Geological and Geographical Background of the Diamond Deposits

The diamonds for this study were recovered from three alluvial deposits, Arenapolis, Boa Vista and Canastra (Fig. 3-1). The deposits are located in different diamond-producing regions in Brazil, which are in different geological settings.

3.2.1 Arenapolis

The Arenapolis deposit is located at the headwaters of the Paraguay River, close to the village of the same name, approximately 170 km north of Cuiabá, in the province of Mato Grosso in western Brazil (Fig. 3-1).

The first discoveries in this region dates back to the 1970s, when diamonds were found in rivers that drain into the Rio Santana outside of Nortelândia. In small-scale operations within riverbeds, the diamonds were mined from quaternary alluvial deposits until industrial mining started in the early 1980s (De Carvalho et al., 1991). Diamonds in these alluvial deposits are most likely derived from Cretaceous, diamondiferous conglomerates of the Parecis Formation, which overlies Precambrian basalts and sediments of the Alto Paraguay-Group in this area. Due to regional uplift in the Tertiary, the Parecis Formation became exposed to erosion, which subsequently led to the deposition of sediments with elevated diamond contents. Further reworking of these sediments and continued erosion led to the concentration of the diamonds in quaternary alluvial deposits within the local riverbeds (De Carvalho et al., 1991).

The primary origin of the diamonds in this region remains unknown due to the lack of potential kimberlitic hosts and the absence of kimberlitic tracer minerals (Weska et al., 1984). However, diamondiferous kimberlites have been discovered to the north, on the adjacent Guapore Shield, which is the southern part of the Amazon craton. These discoveries include the kimberlites in the Juina area (Tompkins, 1992), which is located ~500 km north-northwest of Cuiabá (Fig. 1).

3.2.2 Boa Vista

The second set of diamonds was recovered from a Quaternary alluvial deposit in the Rio Branca, in northern Brazil. The deposit is located north of Boa Vista, in the state of Roraima, close to the Venezuelan border (Fig. 3-1). The diamonds have been interpreted as being derived from clastic sediments (in particular conglomerates) of the Mesoproterozoic Roraima Supergroup. The Roraima Supergroup overlies major parts of the Guyana Shield, the northern part of the Amazon craton, and extends north into Venezuela, where similar diamond placer deposits have been found (Sidder, 1995). The Roraima Supergroup itself has been considered a paleoplacer (Gibbs and Barron, 1983, Meyer and McCallum, 1993), but the primary origin of the diamonds remains controversial. An origin post-dating the deposition of the Roraima Supergroup and relating to the emplacement of the Avanavero basalts, which intrude the Roraima sediments, has also been suggested. Other ideas include an origin of the diamonds relating to kimberlite volcanism during the Paleoproterozoic Uatuma event, which produced volcanic rocks that underlie the Roraima Supergroup (see Da Silva Rodrigues, 1991 and references therein).

The lack of kimberlitic indicator minerals in the alluvial deposits and the absence of potential kimberlitic host rocks on the Guyana Shield have been used as argument against a primary origin for the diamonds within the Guyana Shield. As an alternative, Reid (1974) suggested that the source of the diamonds remained in Ghana, West Africa, where similar placer diamond deposits and associated kimberlites were found. Kimberlitic diamond sources, until now, have not been found on the Brazilian part of the Guyana Shield, but the more recent discoveries of Neoproterozoic (730 Ma) diamondiferous kimberlites in the Guaniamo area of Venezuela (Nixon, 1988; Nixon et al., 1992; Channer et al., 1998), ~ 600 km northwest of Boa Vista (Fig. 1), show that diamond source rocks are present on the Guyana Shield and it has been demonstrated that these kimberlites are the source of local placer diamonds (Kaminsky et al., 2000).

3.2.3 Canastra

The third set of diamonds for this study was recovered from a placer deposit within the Serra de Canastra, which is located in central-eastern Brazil in the state of Minas Gerais (Fig. 3-1). It is an alluvial deposit in the São Francisco River, approximately 60 km north of the town of Vargem Bonita. The region around the São Francisco Craton, which includes the Coromandel region, is historically the most important diamond source in Brazil and established its status as the world's main diamond producer in the 18th and 19th century. Diamond mining within the alluvial deposits of the São Francisco River goes back into the 1930s. As in the case of Arenapolis and Boa Vista, the origin of the placer diamonds in the Serra de Canastra remains unknown. It was suggested that the diamonds were derived from sediments of the Canastra Group or from an undiscovered kimberlite, which may have been eroded down to the root zone (Chaves et al., 1993). Over the 1960-70s, systematic exploration revealed the existence of a number of kimberlites in the western part of the São Francisco craton. For example, kimberlites were found and related rocks in the Alto Paranaiba igneous province in the region of the headwaters of the Paranaiba River, near Coromandel. Most of the kimberlites, however, were only marginally diamondiferous and, therefore, an unlikely source of the rich alluvial deposits in the region. Also, kimberlites were discovered in the vicinity of Bambui, just east of the Serra de Canastra (Tompkins and Gonzaga, 1989). Some of these kimberlites, in particular "Canastra 1", are diamondiferous and are a potential source for the alluvial diamonds of this study.

3.3 Sample Preparation and Analytical Techniques

All diamonds were examined microscopically to determine visible morphological features, colors and surface textures. This was followed by systematic secondary electron imagery (SEI) of the diamond surfaces and a high resolution cathodoluminescence (CL) study, to reveal information about zoning patterns within the diamonds. CL was performed on a JEOL JXA-8900 RL electron microprobe at Frankfurt University at 20 kV acceleration voltage and beam currents of ~1-5 mA.

The diamonds were subsequently cracked in a hardened steel piston crusher to release the mineral inclusions, which were then individually mounted in brass rings using Epoxy resin. The mounted inclusions were abraded using SiC powder and then polished on a Pb-Sb plate with 0.25 μm diamond powder.

The major-element compositions of the inclusions were determined on the electron microprobe at Frankfurt University at 20 kV acceleration voltage and 20 nA beam current. Synthetic and natural silicates, oxides, and metals were used as standards. The counting times for single elements ranged from 30 to 100 seconds for the peak and 30 to 200 seconds for the background. Three analytical points were averaged to ensure detection limits of 100 ppm or better for all oxide-species except Na_2O (ca. 200 ppm). Analytical accuracy and precision were tested using secondary standards and were shown to be better than 1% (relative) for major elements. The complete set of microprobe analyses of the mineral inclusions is given in Appendix C, Table C1.

Garnet inclusions were analyzed for trace elements using a CAMECA IMS-3f ion microprobe at the Woods Hole Oceanographic Institution. The analyses included the rare earth elements (REE) La, Ce, Nd, Sm, Eu, Dy, Er and Yb; other high field strength elements (HFSE) Ti, Y, Zr as well as Sr. A primary beam of negatively charged oxygen ions was focused to a spot size of ~30 μm diameter for the REE, for all other trace elements a spot size of ~5 μm was used. To suppress molecular interferences, an energy offset of -60V for the REE and -90 V for the other trace elements was applied (Shimizu and Hart, 1982). Trace element concentrations were calculated using empirical relationships between concentration and secondary ion yields in well-characterized standards (working curves) and by normalization to silicon as an internal standard. For the compositional ranges observed here, analytical uncertainties based on ion counting statistics are in the order of 10-30 % (relative) for the REE and 5-15 % for the other trace elements.

The concentration and the aggregation state of nitrogen impurities in the host diamonds were determined by Fourier transform infrared (FTIR) spectroscopy, using a Thermo Nicolet Nexus 470 FT-IR Spectrometer equipped with a Nicolet Continuum IR microscope at the University of Alberta. The measurements were collected on inclusion free, transparent diamond cleavage chips with thickness of 0.2-1.0 millimeter. The beam size was set to 50x50 μm. The detection limits, which strongly depend on the quality of the fragments, are generally in the range 10-20 ppm. The errors on the nitrogen concentration and the aggregation state are in the order 10-20%.

The carbon isotope composition of each diamond was determined using a Finnigan MAT 252 gas flow mass spectrometer, at the University of Alberta, after combusting ~1 mg of inclusion free diamond fragments. The fragments were combusted together with ~1g CuO as oxygen-source in a sealed and evacuated quartz tube at 1000°C for ~12 hours.

3.4 Physical Characteristics of the Diamonds

The sixty eight studied diamonds (Arenapolis: 20, Boa Vista: 34, Canastra: 14) have a size range of 2-4 mm (0.03-0.25 carats).

3.4.1 Shapes and surface textures

Diamonds from the three deposits show similar shape distributions. The dominant shape is the dodecahedron, which comprises approximately half of the studied diamonds. Combinations of octahedra and dodecahedra, pure octahedral and irregular shapes make up the remaining half, and are present in almost equal proportions. Besides these dominant shapes, more complex growth forms such as twins, in particular triangular macles, and aggregates occur at Boa Vista and Canastra, but their number is limited (<10% macles and <5% aggregates). Examples of the different crystal shapes are shown in Appendix C (Fig. C1).

Most of the diamonds show surface textures that are either related to processes that took place within in the Earth's mantle (i.e. growth, deformation) or on the way to the surface (i.e. resorption in a kimberlitic melt). These surface textures include shield-shaped laminae and negatively oriented trigonal pits (trigons) on octahedral diamond faces, as well as terraces, hillocks, and deformation lines on dodecahedral faces. Surface textures that are not restricted to certain diamond faces include inclusion cavities and frosting (see Robinson, 1979). Examples of the surface textures are shown in Appendix C: Figs. C2-6.

In addition, some of the diamonds exhibit abrasion textures that are related to transport on the Earth's surface, after their release from the original source. These include percussion marks, edge abrasions and network patterns, which in many cases were found to occur together on single diamonds (Plate 3-1A,B and Appendix C: Figs. C7-8). Percussion marks are caused by the impact of particles on the diamond surface in relatively high energy environments, such as fast flowing rivers, where particle transportation allows grains to saltate. Edge abrasions and network patterns are caused by steady abrasion of the diamond surface in fluvial or aeolian environments, respectively.

The number of diamonds that show abrasion textures varies significantly between the deposits. Approximately 70% of the diamonds from Arenapolis exhibit abrasion textures, but these were not observed on diamonds from Boa Vista and are rare on diamonds from Canastra (2 diamonds = 14 %, see Table 3-1) (Appendix C: Fig. C9).

3.4.2 Color

The majority of the diamonds studied are colorless; however, brown and yellow body colors are also present in all three deposits (Tab. 3-1). A common feature is the presence of transparent green or brown radiation spots on the crystal surface (Appendix C: Fig. C10). The spots range in intensity from pale to dark, and are present as single spots and as clusters covering large areas of the diamond surface.

Figure 3-2 illustrates the frequency of spotted diamonds within the studied suites, showing that Boa Vista has the highest abundance (~75%) and Arenapolis and Canastra have abundances of 40% or less. Green is the predominant color of the surface spots at Boa Vista, whereas at Arenapolis and Canastra green, brown, and combinations of green and brown spots occur in approximately equal proportions.

3.5 Mineral Inclusions

Inclusions from fifty four diamonds were recovered. Diamonds that did not yield recoverable inclusions usually contained sulfide, which was dispersed into thin cracks surrounding an original sulfide inclusion or thin graphite flakes.

Inclusions abundances are summarized in Table 3-2. The majority of diamonds from each deposit belong to the peridotitic suite. Eclogitic inclusions are present in only two diamonds, one from Boa Vista and one from Canastra.

3.5.1 Peridotitic Suite

Olivine is the most common silicate inclusion and the only silicate phase that is present in diamonds from all three deposits. Olivine commonly occurs with magnesiochromite as touching and non-touching inclusion pair in the same diamond (Tab. 3-2). Combinations of olivine with garnet and orthopyroxene (plus magnesiochromite) are restricted to diamonds from Boa Vista. Forsterite contents range from 91.5 to 94.4 mol%, and CaO contents are <0.07 wt% (Tab. 3-3, Fig. 3-3). The broadest compositional range is found in olivines from Canastra, whereas olivines from Arenapolis are compositionally restricted (Fig. 3-3).

A single peridotitic *garnet* recovered from a diamond from Arenapolis was lost during polishing. Other inclusions of peridotitic *garnet* were found only in diamonds from Boa Vista, where garnets not only occur as single inclusions, but also in association with olivine and orthopyroxene. With CaO contents between 0.9 and 4.8 wt%, all recovered garnets are calcium undersaturated harzburgitic (Fig. 3-4). Cr_2O_3 contents are in the range 6.2 to 11.9 wt% and Mg- numbers ((100*Mg/(Mg+Fe)) between 84.9 and 89.1. The chondrite normalized rare earth element (REE_N) compositions of nine peridotitic garnet inclusions show, with one exception, sinusoidal patterns with humps between Ce and Eu and troughs at Dy or Er (Fig. 3-5). Sinusoidal REE_N patterns are a common feature for Ca-undersaturated garnet inclusions from diamonds worldwide (e.g. Shimizu and Richardson, 1987; Shimizu et al., 1997; Stachel and Harris, 1997a). Only one harzburgitic garnet inclusion, recovered from diamond BV-16, does not show a sinusoidal REE_N pattern. This inclusion is characterized by flat (~5-10 times chondritic) middle to heavy REE and is also distinct from the rest of the garnets by higher Zr (111 ppm) and Y (31.4 ppm) contents (see Tab. 3-4).

Orthopyroxene inclusions were found only in diamonds from Boa Vista, where they occur as single inclusions or in combination with garnet, olivine or magnesiochromite (Tab. 3-3). The orthopyroxene inclusions have Mg-numbers of 93.2-94.5, CaO contents of 0.12-0.46 wt%, and Cr_2O_3 contents of 0.25-0.56 wt%. As might be expected, the orthopyroxenes with the highest Mg-numbers have the lowest calcium and highest chromium contents.

The most abundant mineral inclusion is *magnesiochromite*, which was found in diamonds from all three deposits. Magnesiochromite was recovered as separate inclusions or in association with olivine (plus orthopyroxene in one case). Magnesiochromite inclusions display a wide compositional range (Tab. 3-3), with Cr-numbers [100*Cr/(Cr+Al)] of 67.1-98.4 and FFM ratios [100*Fe^{2+}/(Fe^{2+}+Mg)] of 22.3-38.9 (Fig. 3-6).

Signs of alteration were found in magnesiochromite inclusions in two diamonds from Arenapolis and one from Canastra. The inclusions were connected to the surface of their host diamond through large visible fractures. These altered magnesiochromites are characterized by heterogeneous compositions and unusually high zinc contents (~2-15 wt% ZnO). Backscattered electron images and compositional profiles show that alteration proceeds along fractures from the rims into the centers of the inclusion crystals.

In addition to syngenetic mineral inclusions, two diamonds from Arenapolis contained mineral phases that indicate a secondary, epigenetic origin. A *quartz* "inclusion", recovered along with olivine from the same diamond, belongs to this group. This quartz "inclusion", which was connected to the diamond surface by a fracture, is characterized by a high proportion of impurities. in one case could be identified as chromite. The preserved cubo-octahedral crystal shape indicates that the quartz either filled a preexisting dissolution cavity within the diamond, similar to what was proposed for quartz inclusions in diamonds from Minas Gerais (Correns, 1931), or it completely replaced an original inclusion mineral through fractures within the diamond. *Pargasitic amphibole,* which was found along a fracture through the host diamond, is the second epigenetic mineral recovered.

3.5.2 Eclogitic Suite

The eclogitic suite is restricted to two diamonds, one from Boa Vista (BV-34) and one from Canastra (CA-14), and in both cases *garnet* was the only inclusion mineral recovered. The composition of the two eclogitic garnets is very distinctive. The garnet from Boa Vista is characterized by higher calcium (11.9 wt% CaO) and titanium (0.97 wt% TiO_2) contents and a lower Mg-number (#38) compared to the garnet from Canastra (4.90 wt% CaO, 0.21 wt% TiO_2, Mg# 64). The REE_N composition was only determined for the garnet from Boa Vista and shows an increase from subchondritic La towards flat, 20-30 times chondritic middle and heavy REE_N (Fig. 3-5).

3.6 Geothermobarometry

The pressure and temperature conditions during diamond formation were determined using the composition of two non-touching (i.e. separate) garnet-orthopyroxene and four non-touching garnet-olivine pairs recovered from Boa Vista diamonds. For the garnet-orthopyroxene inclusions pressures and temperatures were determined iteratively using the experimental calibrations from Brey and Köhler (1990) and Harley (1984). In the case of the garnet-olivine pairs, for which a pressure determination is not possible, temperatures based on the Mg-Fe exchange (after O'Neill and Wood, 1979) were determined for a range of assumed pressures within the diamond stability field. The results for the garnet-orthopyroxene pairs (1040°C at 4.1 GPa and 1200°C at 6.0 GPa; see Fig. 3-7) show a temperature and pressure difference of ~200°C and ~2 GPa, respectively and are consistent with formation along a 40-42mW/m^2 (surface heat flow) geotherm, a common value for diamond formation worldwide (Boyd and Gurney, 1986; Griffin et al., 1992; Stachel and Harris, 1997b). Temperature results for the four garnet-olivine pairs vary by ~100°C. At pressures below ~6 GPa, which marks the maximum pressure for the two garnet-orthopyroxene pairs, temperature conditions for garnet-olivines are also consistent with formation along a 40-42mW/m^2 geotherm.

Further temperature estimates for diamond formation are based on the zinc content in magnesiochromite inclusions (Ryan et al., 1996). The results for all analyzed samples cover a large temperature range of 1100-1600°C and even within single deposits temperature estimates extend over 300-400°C (Fig. 3-8).

Magnesiochromite inclusions from Arenapolis show the highest average temperature (1340°C) of the three deposits, followed by Canastra (1290°C) and Boa Vista (1210°C). These temperatures estimates are higher than average diamond formation temperatures determined for other regions e.g. the Kaapvaal craton (average ~1200°C, see Stachel et al., 2003)

3.7 Compositional Zoning and Nitrogen Characteristics of the Diamonds

Nitrogen is the most common impurity in natural diamonds and can reach concentrations of >2500 atomic ppm (Cartigny et al., 2001). Studies on the distribution of nitrogen in diamond have revealed that strong variations in the nitrogen contents within a single diamond can occur and that complex nitrogen zoning patterns are common (e.g. Fitzsimons et al., 1999). These studies are generally based on observations from a small number of specifically prepared polished diamond plates. In order to obtain information about the zoning patterns of the whole set of studied diamonds, high resolution cathodoluminescence imagery in combination with secondary electron imagery was used on the rough diamonds. This method, however, reveals only information about zoning along secondary crystal faces, e.g. resorption related dodecahedral faces or breakages that cut across the primary growth zoning.

With few exceptions (Appendix C: Fig.11) all studied diamonds show compositional zoning of variable degree under cathodoluminescence. The types of zoning are variable and range from simple, oscillatory growth zoning parallel to the octahedral faces (Plate 3-1C and Appendix C: Fig.12) and sector zoning (Plate 3-2B) to more complex zoning patterns (Plate 3-2A and Appendix C: Fig.13). A distinctive zoning pattern that characterizes diamonds from a certain deposit could not be established. However, it appears that unresorbed, octahedral faces of diamonds from Boa Vista generally show an outer layer of a few micron thickness with low nitrogen concentrations (Plate 3-2C,D).

To minimize the effects of zoning on the determination of average nitrogen concentration and aggregation states of the studied diamonds, multiple (2-4) diamond cleavage chips of each diamond were analyzed. Nitrogen concentrations range from <10 (detection limit) to 1856 atomic ppm (Fig. 3-9). Six Type II diamonds (no detectable nitrogen) were found. Aggregation states of nitrogen are highly variable and range from poorly aggregated with all nitrogen in A-centre (Type IaA diamond) to highly aggregated with all nitrogen in B-center (Type IaB diamond). A comparison of the nitrogen concentrations and aggregation states of the studied deposits (Fig. 3-9) shows almost complete overlap.

3.8 Carbon Isotope Composition of the Diamonds

The carbon isotope composition of the diamonds for each of the Brazilian deposits is shown in Figure 3-10. The results for the peridotitic diamonds for all three deposits fall within the range of -2.0‰ to -8.9‰, in accordance with the range established by Sobolev et al. (1979) for peridotitic diamonds worldwide. The isotopic composition of the peridotitic diamond suite of each deposit is characterized by a slightly different position of the mode (Fig. 3-10). In the case of Arenapolis and Boa Vista the mode is at -5‰ to -6‰, whereas in the case of Canastra it is at [illegible]‰ (Fig. 3-10). Compared to the other Brazilian deposits, peridotitic diamonds from Boa Vista have the broadest isotopic range, from -2.1 to -8.9‰ and a distribution that is skewed towards isotopically light compositions. The resulting isotopic distributions within single deposit may not be fully representative, because of the small number of samples.

The isotopic composition of -4.4‰ of the single eclogitic diamond from Boa Vista (BV-34, see Tab.3-1) is indistinguishable from the peridotitic diamonds, whereas the eclogitic diamond from Canastra (CA-14) is characterized by isotopically light carbon, with a $\delta^{13}C$ of -16.1‰ (Tab.3-1). Such isotopically light carbon is generally restricted to diamonds of eclogitic paragenesis (Sobolev et al., 1979; Galimov, 1991; Kirkley et al., 1991). At Canastra, a diamond of unknown paragenesis (CA-11) yielded a $\delta^{13}C$ value of -19.7‰ (Tab.3-1) and thus is likely to belong to the eclogitic suite. The remaining diamonds of unknown paragenesis fall into the range of the peridotitic diamonds.

3.9 Discussion

3.9.1 Diamond characteristics

The similarity of crystal shapes of the diamonds among the deposits shows that simple morphological criteria are inadequate to distinguish these diamond populations. A predominance of dodecahedral shapes has also been observed in other placer deposits in Brazil and Venezuela (Meyer and Svisero, 1975; Kaminsky et al., 2000; Kaminsky et al., 2001).

Surface textures relating to growth or resorption are common and found in similar proportions on diamonds from all three deposits, but there is a significant difference in the abundance of diamonds that show abrasion textures. Differences in the abundance of abraded diamonds may indicate a contribution of diamonds from more than one source to a single placer deposit, and may help to constrain whether these diamond sources are distal or proximal. The high abundance of abrasion textures on diamonds from Arenapolis is consistent with the majority of diamonds from this deposit being derived from a distal source. The complete absence of abrasion textures on diamonds from Boa Vista, on the other hand, is a strong indication that the primary kimberlitic source of these diamonds is in close proximity to the placer deposit, but has not yet been located. In the case of Canastra, the small percentage of diamonds with abrasion textures also indicates a proximal primary source, which is in accordance with the discovery of kimberlitic sources in the adjacent Serra de Canastra, from which at least part of the diamond population may have been derived.

Diamonds from all three deposits have similar body colors showing that the color alone cannot be used to distinguish diamond populations. However, the green/brown surface spotting distinguishes Boa Vista diamonds, which have a higher abundance and a higher percentage of green spots, compared to Arenapolis and Canastra diamonds (Fig.3-2).

The appearance of green surface spots is the result of damage to the diamond surface by α-particle radiation (Meyer et al., 1965). Radiation damage on diamonds has been shown to occur within the host kimberlite, particularly within the upper oxidized zones, where radioactive-element enriched groundwater can infiltrate the kimberlite. This type of radiation results in most cases in a uniform, transparent, pale green surface coating (Vance et al., 1973). Radiation damage on diamonds can also be caused by the presence of radioactive-element-rich minerals, such as zircon, close to the diamond surface over extended periods of time. In this case, radiation results in the formation of green surface spots or clusters of variable color intensity. These spots or clusters are commonly observed on the surface of diamonds from placer deposits, which has been attributed to the high abundance of radioactive-element-rich minerals in the sediments of placer deposits (Vance et al., 1973). Green surface spots may change into a brown color in response to heating after irradiation. Heating is commonly attributed to a metamorphic event. The occurrence of green and brown surface spots on the same diamond indicates that irradiation continued after the end of a heating event.

High abundances (55-89%) of spotted diamonds have previously been described from the Guaniamo area in Venezuela (Kaminsky et al., 2000). In this case, diamonds with surface spots are not only abundant in the placer deposits (70-89%), but also in the kimberlites (55-78%), which indicates that the bulk of the diamonds received radiation damage already within their kimberlitic source. This radiation damage may be caused by radioactive-element-rich minerals derived from crustal xenoliths that occur in kimberlites from the Guaniamo area (Nixon et al., 1992).

The similarity between the Boa Vista and Guaniamo placer diamonds indicates that a high proportion of green spots is a common feature of diamonds from the Guyana Shield. As it has been shown that the surface spotting on diamonds from the Guaniamo area is caused by irradiation in the kimberlite source, it seems reasonable to assume the same for the diamonds from Boa Vista.

3.9.2 Characteristics of the mantle source

Although separated by large lateral distances, diamonds from all three deposits have similar mineral inclusion assemblages and similar compositions. This indicates that they all formed in similar chemical environments in the Earth's mantle. The predominance of peridotitic inclusions, which is consistent with previous observations on Brazilian diamonds (Meyer and Svisero, 1975), indicates a mantle source that is similar in composition to other diamond deposits worldwide. A peridotitic mantle source is, however, in stark contrast to observations on diamonds from the Juina (Wilding, 1990; Harte et al., 1999; Hutchison, 1997; Kaminsky et al., 2001) and the Guaniamo area, which are almost exclusively eclogitic (Sobolev et al., 1998; Kaminsky et al., 2000; Schulze et al., 2004). Consistently high Mg-numbers and low calcium contents of olivine and orthopyroxene inclusions, as well as the absence of clinopyroxene, indicates that the peridotitic diamonds from all three studied deposits largely formed in depleted, harzburgitic source rocks. This conclusion is supported by the composition of garnet inclusions in diamonds from Boa Vista, which are exclusively subcalcic (Fig. 3-4).

Depleted peridotitic sources have been identified for a large portion of diamonds worldwide (e.g. Sobolev, 1977; Gurney, 1984; Meyer, 1987), which shows that the mantle source of the Brazilian diamonds is chemically similar to the source of other diamond deposits. This is also consistent with the sinusoidal REE_N patterns for the bulk of the garnet inclusions from Boa Vista, which are characteristic for harzburgitic garnet inclusions worldwide (e.g. Shimizu and Richardson, 1987; Shimizu et al., 1997; Stachel and Harris, 1997a). They have been interpreted as being the result of metasomatism by strongly fractionated CHO-fluids (Stachel et al., 2004). The one harzburgitic garnet recovered from diamond BV-16, however, shows a very distinct REE_N pattern with enriched middle to heavy REE (Fig. 3-5). Such REE_N patterns are common in lherzolitic garnet inclusions in diamonds, for example from Akwatia, Ghana, (Stachel and Harris, 1997a) and Kankan, Guinea, (Stachel et al., 2000), but have been observed in very few harzburgitic garnet inclusions (e.g. Mwadui, Tanzania: Stachel et al., 1999). It has been suggested that such REE_N patterns are the result of melt metasomatism, which in a harzburgitic environment would take place at subsolidus conditions, therefore requiring proximity to a magmatic intrusion or to the base of the lithosphere (Stachel et al., 2004).

The P-T conditions calculated for peridotitic silicate inclusion pairs from Boa Vista are consistent with observations from other diamond sources worldwide (Stachel et al., 2004), indicating that diamond formation generally occurs on a geothermal gradient of 40-42 mW/m^2 (surface heat flow). The temperature range for the non-touching garnet-olivine inclusion pairs from Boa Vista (1200-1300°C at 5.5 GPa) is slightly higher than the average temperature of ~1200°C (at 5.5 GPa) for diamond formation worldwide. This suggests that diamond formation beneath Brazil occurred at higher temperatures, i.e. slightly deeper, than on most other cratons.

The unreasonably large range in temperatures calculated using the Zn in spinel thermometry indicates that the temperature results of this method are of limited viability.

The low abundance of eclogitic inclusions among the diamonds indicates that diamond source rocks with basaltic chemistries are a minor constituent of the lithospheric mantle underneath major parts of Brazil. Similar observations have been made on other cratons (e.g. Meyer, 1987; Gurney, 1989).

3.10 Conclusions

Comparison of the diamond populations from Arenapolis, Boa Vista and Canastra shows that many of the diamond properties, including crystal shape, body color, and the development of growth and resorption textures are very similar among the deposits. This similarity also applies to the nitrogen characteristics and carbon isotope compositions of the diamonds, which resemble results from other diamond deposits worldwide. The distribution of abrasion texture on diamond surfaces, however, is distinctive, and indicates that the majority of diamonds from Arenapolis are derived from distal kimberlitic sources, whereas diamonds from Boa Vista and Canastra are close to their primary source. So far, diamondiferous kimberlites have only been located in vicinity of the Canastra alluvial deposits. The high proportion of diamonds with green radiation spots at Boa Vista is consistent with a derivation of these diamonds from a proximal kimberlitic source on the Guyana Shield and shows that the diamonds have not experienced extensive metamorphism.

Mineral inclusion chemistry reveals similarities among the deposits and indicates strong to moderately depleted peridotitic mantle sources. Diamond formation took place in a geothermal regime following a gradient of 40-42 mW/m^2 surface heat flow. Temperatures, however, appear to be higher than the worldwide average, indicating that the diamonds formed at slightly greater depths.

The low abundance of eclogitic mineral inclusions suggests that diamond source rocks with basaltic compositions are scarce in the lithospheric mantle underneath major parts of Brazil.

Bibliography

Bizzi, L.A., Smith, C.B., de Wit, M.J., Armstrong, R.A. and Meyer, H.O.A. (Editors), 1994. Mesozoic kimberlites and related alkalic rocks in south-western São Francisco craton, Brazil: a case for local mantle reservoirs and their interaction. Kimberlites, Related Rocks and Mantle Xenoliths. CPRM, Brasilia, 156-171 pp.

Boyd, F.R. and Gurney, J.J., 1986. Diamonds and the African lithosphere. Science, 232: 472-477.

Brey, G.P. and Köhler, T., 1990. Geothermobarometry in four-phase lherzolites II. New thermobarometers, and practical assessment of existing thermobarometers. Journal of Petrology, 31: 1353-1378.

Cartigny, P., Harris, J.W. and Javoy, M., 2001. Diamond genesis, mantle fractionations and mantle nitrogen content: a study of δ^{13}C-N concentrations in diamonds. Earth and Planetary Science Letters, 185: 85-98.

Channer, D.M.D., Cooper, R. and Kaminsky, F.V., 1998. The Guaniamo region, Bolivar state, Venezuela: a new kimberlite province, 7th International Kimberlite Conference, Extended Abstract, Cape Town, pp. 144-146.

Chaves, M.L.C.S., Dupont, H., Karfunkel, J. and Svisero, D.P., 1993. Depósitos diamantíferos de Minas Gerais: Uma revisão. Anais I Simpósio Brasileiro de Geologia do Diamante: 79-100.

Chapter 3

Correns, C.W., 1931. Über Diamanten mit Quarzeinlagerungen. Zeitschrift für Kristallographie, 80: 37-44.

Da Silva Rodrigues, A.F., 1991. Depósitos diamantíferos de Roraima. In: C. Schobbenhaus, E.T. Queiroz and C.E.S. Coelho (Editors), Principais depósitos minerais do Brasil. Rochas e minerais industriais. Gemas e rochas ornamentais. DNPM/CPRM, Brasilia, pp. 177-198.

De Brito Neves, B.B. and Cordani, U.G., 1991. Tectonic evolution of South America during the Late Proterozoic. Precambrian Research, 53: 23-40.

De Carvalho, M.S., Akabane, T., Tesser, M.A. and Filho, L.T.D.S., 1991. Depósitos de diamante da fazenda camargo, Nortelândia, Mato Grosso. In: C. Schöbbenhaus, E.T. Queiroz and C.E.S. Coelho (Editors), Principais depósitos minerais do Brasil. Rochas e minerais industriais. Gemas e rochas ornamentais. DNPM/CPRM, Brasília, pp. 161-176.

Droop, G.T.R., 1987. A general equation for estimating Fe^{3+} concentrations in ferromagnesian silicates and oxides from microprobe analyses, using stoichiometric criteria. Geological Magazine, 51: 431-435.

Fitzsimons, I.C.W., Harte, B., Chinn, I.L., Gurney, J.J. and Taylor, W.R., 1999. Extreme chemical variation in complex diamonds from George Creek, Colorado: a SIMS study of carbon isotope composition and nitrogen abundance. Mineralogical Magazine, 63(6): 857-880.

Galimov, E.M., 1991. Isotope fractionation related to kimberlite magmatism and diamond formation. Geochimica et Cosmochimica Acta, 55(6): 1697-1708.

Gibbs, A.K. and Barron, C.N., 1983. The Guiana shield reviewed. Episodes, 1983(2): 7-14.

Griffin, W.L., Gurney, J.J. and Ryan, C.G., 1992. Variations in trapping temperatures and trace-elements in peridotite- suite inclusions from African diamonds - Evidence for two inclusion suites, and implications for lithosphere stratigraphy. Contributions to Mineralogy and Petrology, 110(1): 1-15.

Gurney, J.J., 1984. A correlation between garnets and diamonds in kimberlites. Publications of the Geological Department & University of Extension, University of Western Australia, 8: 143-166.

Gurney, J.J., 1989. Diamonds. In: J. Ross and et al. (Editors), Kimberlites and related rocks. GSA Special Publication 14. Blackwell, Carlton, pp. 935-965.

Harley, S.L., 1984. An experimental study of the partitioning of iron and magnesium between garnet and orthopyroxene. Contributions to Mineralogy and Petrology, 86: 359-373.

Harte, B. and Harris, J.W., 1994. Lower mantle associations preserved in diamonds. Mineralogial Magazine, 58A: 384-385.

Harte, B., Harris, J.W., Hutchison, M.T., Watt, G.R. and Wilding, M.C., 1999. Lower mantle mineral associations in diamonds from São Luiz, Brazil. In: Y. Fei, C.M. Bertka and B.O. Mysen (Editors), Mantle Petrology: Field Observations and High Pressure Experimentation: A tribute to Francis R. (Joe) Boyd. Special Publication. The Geochemical Society, Houston, pp. 125-153.

Hutchison, M.T., 1997. Constitution of the deep transition zone and lower mantle shown by diamonds and their inclusions. PhD Thesis, University of Edinburgh, 340, 306 pp.

Hutchison, M.T., Cartigny, P. and Harris, J.W., 1999. Carbon and nitrogen composition and physical characteristics of transition zone and lower mantle diamonds from São Luiz, Brazil. In: J.J. Gurney, J.L. Gurney, M.D. Pascoe and S.H. Richardson (Editors), The J.B. Dawson, Proceedings of the VIIth International Kimberlite Conference. Red Roof Design, Capetown, pp. 372-382.

Kaminsky, F.V. et al., 2001. Superdeep diamonds from the Juina area, Mato Grosso State, Brazil. Contributions to Mineralogy and Petrology, 140: 734-753.

Kaminsky, F.V., Zakharchenko, O.D., Griffin, W.L., Channer, D.M.D. and Khachatryan-Blinova, G.K., 2000. Diamond from the Guaniamo area, Venezuela. The Canadian Mineralogist, 38: 1347-1370.

Kennedy, C. and Kennedy, G., 1976. The equilibrium boundary between graphite and diamond. Journal of Geophysical Research, 81: 2467-2470.

Kirkley, M.B., Gurney, J.J., Otter, M.L., Hill, S.J. and Daniels, L.R., 1991. The application of C isotope measurements to the identification of the sources of C in diamonds - a review. Applied Geochemistry, 6(5): 477-494.

McDonough, W.F. and Sun, S.S., 1995. The composition of the Earth. Chemical Geology, 120: 223-253.

Meyer, H.O.A., 1987. Inclusions in diamond. In: P.H. Nixon (Editor), Mantle xenoliths. John Wiley & Sons, Chichester, pp. 501--522.

Meyer, H.O.A. and McCallum, M.E., 1993. Diamonds and their sources in the Venezuelan portion of the Guyana shield. Economic Geology, 88(5): 989-998.

Meyer, H.O.A. and Svisero, D.P., 1975. Mineral inclusions in Brazilian diamonds. Physics and Chemistry of the Earth, 9: 785-795.

Meyer, H.O.A., Milledge, H.J. and Nave, E., 1965. Natural irradiation damage in Ivory Coast diamonds. Nature, 206: 392.

Nixon, P.H., 1988. Diamond source rocks from Venezuela, Industrial Diamond Quarterly, pp. 23-29.

Nixon, P.H., Davies, G.R., Rex, D.C. and Gray, A., 1992. Venezuela Kimberlites. In: K.G. Cox and P.E. Baker (Editors), Essays on magmas and other Earth fluids (a volume in appreciation of Professor P.G.Harris). Journal of Volcanology and Geothermal Research, pp. 101-115.

O'Neill, H.S. and Wood, B.J., 1979. An experimental study of the iron-magnesium partitioning between garnet and olivine and its calibration as a geothermometer. Contributions to Mineralogy and Petrology, 70: 59-70.

Pollack, H.N. and Chapman, D.S., 1977. On the regional variation of heat flow, geotherms, and lithospheric thickness. Tectonophysics, 38: 279-296.

Reid, A.R., 1974. Proposed origin for Guianian diamonds. Geology, 2(2): 67-68.

Robinson, D.N., 1979. Surface textures and other features of diamonds (Volume I), University of Cape Town, Cape Town, 221 pp.

Ryan, C.G., Griffin, W.L. and Pearson, N.J., 1996. Garnet geotherms - pressure-temperature data from Cr-pyrope garnet xenocrysts in volcanic rocks. Journal of Geophysical Research, 101, B3: 5611-5625.

Schulze, D.J., Harte, B., Valley, J.W. and Channer, D.M.D., 2004. Evidence of subduction and crust-mantle mixing from a single diamond. Lithos, 77: 349-358.

Shimizu, N. and Hart, S.R., 1982. Applications of the ion microprobe to geochemistry and cosmochemistry. Annual Review of Earth and Planetary Sciences, 10: 483-526.

Shimizu, N. and Richardson, S.H., 1987. Trace-element abundance patterns of garnet inclusions in peridotite- suite diamonds. Geochimica et Cosmochimica Acta, 51(3): 755-758.

Shimizu, N., Sobolev, N.V. and Yefimova, E.S., 1997. Chemical heterogeneity of garnet inclusions and juvenility of peridotite diamonds from Siberia. Geologiya I Geofizika, 38(2): 337-352.

Sidder, G.B., 1995. Mineral deposits of the Venezuelan Guyana Shield. In: G.B. Sidder, A.E. García and J.W. Stoeser (Editors), Geology and mineral deposits of the Venezuelan Guyana Shield. U.S. Geological Survey Bulletin 2124. United States Government Printing Office, Washington.

Sobolev, N.V., 1977. Deep-seated inclusions in kimberlites and the problem of the composition of the upper mantle. (Translated from the Russian edition, 1974). AGU, Washington, 279 pp.

Sobolev, N.V., Lavrentev, Y.G., Pokhilenko, N.P. and Usova, L.V., 1973. Chrome-rich garnets from the kimberlites of Yakutia and their paragenesis. Contributions to Mineralogy and Petrology, 40: 39-52.

Sobolev, N.V., Galimov, E.M., Ivanovskaya, I.N. and Yefimova, E.S., 1979. Isotope composition of carbon of diamonds containing crystalline inclusions. Doklady Akademii Nauk SSSR, 249: 1217-1220.

Sobolev, N.V., Yefimova, E.S., Channer, D.M.D., Anderson, P.F.N. and Barron, K.M., 1998. Unusual upper mantle beneath Guaniamo, Guyana shield, Venezuela: Evidence from diamond inclusions. Geology, 26(11): 971-974.

Stachel, T. et al., 2004. The trace element composition of silicate inclusions in diamonds: a review. Lithos, 77: 1-19.

Stachel, T., Brey, G.P. and Harris, J.W., 2000. Kankan diamonds (Guinea) I: from the lithosphere down to the transition zone. Contributions to Mineralogy and Petrology, 140: 1-15.

Stachel, T., Harris, J.W. and Brey, G.P., 1999. REE patterns of peridotitic and eclogitic inclusions in diamonds from Mwadui (Tanzania). In: J.J. Gurney, J.L. Gurney, M.D. Pascoe and S.H. Richardson (Editors), Proceedings of the 7th International Kimberlite Conference. Red Roof Design, pp. 829-835.

Stachel, T. and Harris, J.W., 1997a. Diamond precipitation and mantle metasomatism - evidence from the trace element chemistry of silicate inclusions in diamonds from Akwatia, Ghana. Contributions to Mineralogy and Petrology, 129(2-3): 143-154.

Stachel, T. and Harris, J.W., 1997b. Syngenetic inclusions in diamond from the Birim field (Ghana) - A deep peridotitic profile with a history of depletion and re-enrichment. Contributions to Mineralogy and Petrology, 127(4): 336-352.

Stachel, T., Harris, J.W., Tappert, R. and Brey, G.P., 2003. Peridotitic inclusions in diamonds from the Slave and the Kaapvaal cratons - similarities and differences based on a preliminary data set. Lithos, 71: 489-503.

Svisero, D.P., 1995. Distribution and Origin of Diamonds in Brazil - an Overview. Journal of Geodynamics, 20(4): 493-514.

Svisero, D.P., Meyer, H.O.A., Haralyi, N.L.E. and Hasui, Y., 1984. A note on the geology of some Brazilian kimberlites. Journal of Geology, 92: 331-338.

Tompkins, L.A., 1994. Tectono-structural environments of primary diamond source rocks in Brazil: a review, 5th International Kimberlite Conference. Vompanhia de Pesquisa de Recursos Minerais, Special Publication 1B, Minas Gerais, Brazil, pp. 259-267.

Chapter 3

Tompkins, L.A. and Gonzaga, G.M., 1989. Diamonds in Brazil and a proposed model for the origin and distribution of diamonds in the Coromandel region, Minas Gerais, Brazil. Economic Geology, 84: 591-602.

Tompkins, L.A., 1992. Kimberlite structural environments and diamond productivity of Brazil. Russian Geology and Geophysics, 33: 91-98.

Vance, E.R., Harris, J.W. and Milledge, H.J., 1973. Possible origins of α-damage in diamonds from kimberlite and alluvial sources. Mineralogical Magazine, 39: 349-360.

Weska, K.R., Perin, A.L. and Ferreira, I.A., 1984. Placers diamantíferos da bacia do alto Paraguai -MT- caracterizaçâo geologica como critérios e guias de prospecçâo, Anais do XXXIII congresso brasileiro de geologia, Rio de Janeiro.

Wilding, M.C., 1990. PhD Thesis, University of Edinburgh, 281 pp.

Table 3-1: Summary of morphological, compositional and isotopic characteristics of diamonds from Arenapolis, Boa Vista and Canastra.

Sample	Shape	Color	Def.	Radiation Spots	Abrasion textures	δ^{13}C (‰)	Type	N conc. (at. ppm)	N agg. (%B)	Parag.	Inclusion Assemblage
AR-01	d	c	no		yes	-4.06	IaAB	567	38.5	unknown	
AR-02	d	c	no		yes	-4.14	IaAB	118	42.6	unknown	
AR-03	i	b	no		no	-5.24	IaAB	30	14.8	unknown	
AR-04	d	c	no		yes	-3.06	IaAB	68	65.4	peridotitic	ol
AR-05	d	c	no		yes	-4.93	IaAB	29	24.9	peridotitic	ol,qz(chr)
AR-06	o	y	no	brown	no	-4.57	II			unknown	
AR-07	f/o	b	no	green/brown	yes	-4.95	IaAB	86	39.3	peridotitic	chr
AR-08	o/d	b	no	brown	yes	-5.02	IaAB	484	83.6	peridotitic	chr
AR-09	d	b	no	brown	yes	-4.55	IaAB	346	15.0	peridotitic	chr
AR-10	d	c	no		yes	-5.04	IaB	20	95.5	peridotitic	chr
AR-11	o	c	no	green	no	-5.19	IaAB	119	70.7	peridotitic	chr,amph
AR-12	i	c	no		yes	-6.20	IaAB	144	70.4	peridotitic	chr
AR-13	f/d	c	no	green	yes	-2.04	IaAB	32	38.4	peridotitic	chr
AR-14	f/d	c	no		yes	-3,06	II			peridotitic	ol, chr
AR-15	f/d	c	no	green/brown	no	-5.97	IaAB	772	83.3	unknown	
AR-16	o/d	c	no		yes	-3.94	IaAB	774	65.4	peridotitic	chr
AR-17	o/d	y	no	brown	yes	-3.08	IaA	770	8.2	peridotitic	
AR-18	f/d	c	no	green	yes	-4.07	IaAB	316	71.3	peridotitic	chr
AR-19	i	c	no		no	-3.92	IaAB	209	33.8	peridotitic	chr
AR-20	i	c	no		yes	-5.86	Ib	488	97.8	peridotitic	chr
BV-01	d/m	c	no	green	no	-2.97	IaAB	15	19.9	peridotitic	gt,ol
BV-02	f/d	c	no	green	no	-4.03	IaAB	167	31.1	peridotitic	gt
BV-03	o/d	c	no	green	no	-3.87	IaAB	303	17.2	peridotitic	gt
BV-04	o	c	no	green/brown	no	-3.00	IaA	186	1.1	peridotitic	ol,chr
BV-05	o/d	c	no	green	no	-4.79	IaA	196	2.7	peridotitic	chr
BV-06	o	c	no	green	no	-7.48	IaAB	191	74.4	peridotitic	chr
BV-07	i	c	no	green	no	-5.00	IaA	116	0.0	peridotitic	chr
BV-08	i	c	no	green	no	-3.12	IaAB	13	59.8	peridotitic	chr
BV-09	f/d	c	no	green/brown	no	-7.61	IaAB	273	58.4	peridotitic	ol
BV-10	f/d	c	no	green	no	-5.98	IaAB	550	33.9	peridotitic	ol
BV-11	d	c	no		no	-4.40	IaAB	701	46.8	peridotitic	opx
BV-12	d	c	no	green	no	-4.87	IaAB	47	75.9	peridotitic	ol
BV-13	o/d	c	no	green/brown	no	-2.96	IaAB	321	29.9	peridotitic	ol
BV-14	o/d	c	no		no	-5.22	IaAB	618	37.8	unknown	
BV-15	o/d	c	no		no	-4.49	IaAB	364	69.1	unknown	
BV-16	i	b	no		no	-6.14	IaB	53	100.0	peridotitic	gt,ol
BV-17	d	b	yes	brown	no	-3.29	IaAB	79	17.4	peridotitic	gt,ol
BV-18	f/d	c	no		no	-3.74	II			unknown	
BV-19	d	c	no	green	no	-2.12	IaAB	188	36.7	peridotitic	gt,opx
BV-20	o/d	c	no	green/brown	no	-3.83	II			peridotitic	gt,ol
BV-21	f/d/m	c	no	green	no	-3.78	IaAB	284	34.2	peridotitic	gt,opx
BV-22	o	c	no	green	no	-3.93	IaAB	46	42.0	peridotitic	gt
BV-23	o	c	no	green	no	-5.72	II			peridotitic	gt
BV-24	d	c	yes	green	no	-4.16	IaAB	382	73.0	peridotitic	gt
BV-25	o	c	no	green	no	-4.69	IaAB	1392	19.4	peridotitic	gt
BV-26	o/m/a	c	no	green	no	-4.28	IaA	91	3.1	peridotitic	ol-chr,opx,chr
BV-27	o	c	no		no	-4.33	IaAB	929	85.1	peridotitic	ol,chr
BV-28	i/a	c	no	green/brown	no	-5.21	IaAB	278	54.7	peridotitic	chr
BV-29	d/m	c	no	green	no	-8.89	IaAB	941	86.2	peridotitic	chr
BV-30	d	y	no		no	-2.36	IaAB	1856	82.2	peridotitic	chr
BV-31	i	c	no		no	-4.25	IaA	62	0.0	peridotitic	chr
BV-32	o	c	no		no	-4.18	IaAB	220	38.9	peridotitic	chr
BV-33	f/d	c	no	green	no	-5.17	IaAB	473	30.1	peridotitic	chr
BV-34	d	c	no	green	no	-4.44	IaAB	391	69.3	eclogitic	gt

Table 3-1 continued

Sample	Shape	Color	Def.	Radiation Spots	Abrasion textures	$\delta^{13}C$ (‰)	Type	N conc. (at. ppm)	N agg. (%B)	Parag.	Inclusion Assemblage
CA-01	d	c	yes		no	-3.71	IaA	139	4.0	peridotitic	ol
CA-02	o/d	c	no		no	-6.08	IaAB	301	15.5	peridotitic	ol
CA-03	o/d	c	no		no	-6.40	IaAB	316	32.3	peridotitic	ol
CA-04	o	c	no		no	-6.67	IaA	74	7.7	unknown	
CA-05	f/d	c	no	green	yes	-5.00	IaAB	368	66.7	peridotitic	chr
CA-06	d	b	no		yes	-4.91	IaAB	190	60.1	unknown	
CA-07	o/m	c	no	green	no	-4.79	IaAB	440	80.9	unknown	
CA-08	d	c	no		no	-5.86	IaAB	143	52.9	unknown	
CA-09	i	c	no		no	-6.15	IaA	521	2.8	unknown	
CA-10	o/d	y	no	green/brown	no	-5.40	IaA	14	0.0	peridotitic	ol,chr
CA-11	d	y	yes		no	-19.70	II			unknown	
CA-12	d	c	no	brown	no	-5.36	IaAB	157	67.1	peridotitic	ol,chr
CA-13	o/d	c	no		no	-5.80	IaA	564	5.9	peridotitic	chr
CA-14	i	c	no		no	-16.08	IaA	43	4.4	eclogitic	gt

Abbrevations:

Def.: Visible signs of plastic deformation of the diamond

"Shape"- o: octahedra, d: dodecahedra, i: irregular, f: flattened, m: macle, a: aggregate

"Color"- c: colorless, y: yellow, b: brown

"Assemblege"- ol: olivine, gt: garnet, opx: orthopyroxene, chr: chromite, amph: amphibole, qz: quartz

Table 3-2: Mineral inclusions recovered from the studied Brazilian diamonds; separated into paragenetic groups. Numbers represent diamonds, not inclusions

	Arenapolis		**Boa Vista**		**Canastra**	
peridotitic	olivine	1	garnet	6	olivine	3
	olivine, quartz (ex)	1	olivine	4	Mg-chromite	2
	olivine, Mg-chromite	1	orthopyroxene	1	olivine-Mg-chromite	2
	Mg-chromite	8	Mg-chromite	10		
	chromite (ex)	2	garnet, orthopyroxene	2		
	Mg-chromite, amphibole (ex)	1	garnet, olivine	4		
			olivine, Mg-chromite	2		
			olivine-Mg-chromite, orthopyroxene, Mg-chromite	1		
eclogitic			garnet	1	garnet	1
no recovery		6		3		6

Table 3-3: Major- element composition of selected mineral inclusions in diamonds from Arenapolis, Boa Vista and Canastra Major element compositions (EPMA-analyses) are given as wt%.

Deposit	Arenapolis	Boa Vista	Boa Vista	Boa Vista	Boa Vista	Canastra	Canastra	Boa Vista	Boa Vista	Arenapolis	Arenapolis	Arenapolis	Boa Vista	Canastra	Canastra	Canastra
Mineral	olivine	olivine	olivine	olivine	olivine	olivine	olivine	opx	opx	chromite	chromite	chromite	chromite	chromite	chromite	chromite
								n=2		n=4		n=2				n=2
Sample	AR-04	BV-01	BV-16	BV-17	BV-20	CA-01	CA-12	BV-19	BV-21	AR-09	AR-10	AR-16	BV-27	CA-10	CA-12	CA-13
Assemblage	ol	gt,ol	gt,ol	gt,ol	gt,ol	ol	ol,chr	gt,opx	gt,opx	chr	chr	chr	ol,chr	ol,chr	ol,chr	chr
Paragenesis	peridotitic	peridotitic	peridotitic	peridotitic	peridotitic	peridotitic	peridotitic	peridotitic	peridotitic	peridotitic	peridotitic	peridotitic	peridotitic	peridotitic	peridotitic	peridotitic
P_2O_5	≤ 0.01	0.02	≤ 0.01	≤ 0.01	≤ 0.01	≤ 0.01	≤ 0.01	≤ 0.01	≤ 0.01	≤ 0.01	≤ 0.01	≤ 0.01	≤ 0.01	≤ 0.01	≤ 0.01	≤ 0.01
SiO_2	41.5	40.0	40.5	40.8	40.3	39.8	40.6	57.0	57.5	0.19	0.14	0.20	0.31	0.32	0.20	0.14
TiO_2	≤ 0.01	≤ 0.01	≤ 0.01	≤ 0.01	≤ 0.01	≤ 0.01	≤ 0.01	≤ 0.01	≤ 0.01	0.03	0.08	0.32	0.34	0.54	0.01	0.13
Al_2O_3	0.01	0.05	0.03	0.02	0.01	0.02	0.02	0.66	0.51	7.94	8.76	17.55	4.69	4.68	0.78	3.74
Cr_2O_3	0.04	0.06	0.10	0.07	0.03	0.05	0.20	0.55	0.25	63.4	64.1	53.8	64.5	65.2	71.4	67.0
V_2O_3										0.21	0.11	0.20	0.26	0.25	0.10	0.18
FeO	7.03	8.00	7.27	7.20	6.80	8.38	5.66	4.18	4.21	13.9	10.4	11.8	17.2	11.7	11.3	15.8
MnO	0.09	0.11	0.11	0.11	0.10	0.10	0.08	0.11	0.11	0.24	0.20	0.20	0.29	0.22	0.24	0.29
NiO	0.40	0.40	0.39	0.38	0.39			0.13	0.13	0.10	0.10	0.12	0.11	0.12	0.10	0.09
MgO	50.6	50.0	50.7	51.1	50.4	50.7	53.4	35.3	35.7	14.0	15.9	17.0	13.1	16.0	14.8	12.6
CaO	0.02	0.04	0.07	0.02	≤ 0.01	0.03	≤ 0.01	0.38	0.43	≤ 0.01	≤ 0.01	≤ 0.01	≤ 0.01	≤ 0.01	≤ 0.01	≤ 0.01
ZnO										0.05	0.03	0.05	0.06	0.04	0.04	0.06
Na_2O	≤ 0.02	≤ 0.02	≤ 0.02	≤ 0.02	≤ 0.02	≤ 0.02	≤ 0.02	0.05	≤ 0.02	≤ 0.02	≤ 0.02	≤ 0.02	0.07	≤ 0.02	≤ 0.02	≤ 0.02
K_2O	≤ 0.01	≤ 0.01	≤ 0.01	≤ 0.01	≤ 0.01	≤ 0.01	0.04	≤ 0.01	≤ 0.01	≤ 0.01	≤ 0.01	≤ 0.01	≤ 0.01	≤ 0.01	≤ 0.01	≤ 0.01
Total	99.6	98.7	99.2	99.7	98.0	99.1	100.0	98.3	98.8	100.0	99.8	101.2	101.0	99.0	99.0	100.1

Table 3-4: Major- and trace element composition of garnet inclusions in diamonds from Boa Vista. Major element compositions (EPMA-analyses) are given as wt%.

Mineral	Garnet	Garnet	Garnet (n=2)	Garnet	Garnet (n=2)	Garnet (n=2)	Garnet (n=2)	Garnet	Garnet	Garnet	Garnet	Garnet	Garnet (n=2)	Garnet (n=2)
Sample	BV01	BV02	BV03	BV16	BV17	BV19	BV20	BV21	BV22	BV23	BV24	BV25	BV34	CA14
Assemblage	grt,ol	grt	grt	grt,ol	grt,ol	grt,opx	grt,ol	grt,opx	grt	grt	grt	grt	grt	grt
Paragenesis	peridotitic	peridotitic	peridotitic	peridotitic	peridotitic	peridotitic	peridotitic	peridotitic	peridotitic	peridotitic	peridotitic	peridotitic	eclogitic	eclogitic
P_2O_5	0.02	0.01	0.01	0.12	0.01	0.01	0.01	0.02	0.02	0.02	0.00	0.01	0.15	0.10
SiO_2	40.7	41.8	41.4	41.4	41.6	41.1	42.3	42.7	40.2	42.0	42.6	41.1	39.1	40.4
TiO_2	0.02	0.03	0.00	0.08	0.02	0.03	0.01	0.01	0.22	0.13	0.01	0.08	0.97	0.21
Al_2O_3	15.9	17.2	18.5	18.8	18.4	14.8	19.3	18.3	15.8	18.8	18.2	14.8	21.1	22.2
Cr_2O_3	9.10	9.73	7.82	7.29	7.83	11.9	6.18	6.47	9.84	6.80	7.72	10.0	0.05	0.18
FeO	6.55	5.76	6.04	6.44	5.86	6.06	5.67	6.13	5.88	5.73	5.38	6.54	19.9	15.4
MnO	0.30	0.28	0.29	0.30	0.28	0.30	0.26	0.27	0.26	0.26	0.25	0.29	0.39	0.45
NiO	≤ 0.01	0.02	≤ 0.01	≤ 0.01	≤ 0.01	0.02	≤ 0.01	≤ 0.01	0.02	≤ 0.01	0.02	0.02	≤ 0.01	≤ 0.01
MgO	20.7	23.5	21.1	21.9	23.2	21.7	23.8	23.5	21.8	23.0	24.7	21.6	6.71	15.6
CaO	4.83	1.71	4.76	3.28	2.24	3.43	1.81	2.68	2.93	2.66	0.86	4.10	11.9	4.90
Na_2O	≤ 0.02	≤ 0.02	≤ 0.02	0.04	≤ 0.02	≤ 0.02	≤ 0.02	≤ 0.02	≤ 0.02	≤ 0.02	≤ 0.02	0.04	0.26	0.16
K_2O	≤ 0.01	≤ 0.01	≤ 0.01	≤ 0.01	≤ 0.01	≤ 0.01	≤ 0.01	≤ 0.01	≤ 0.01	≤ 0.01	≤ 0.01	≤ 0.01	≤ 0.01	≤ 0.01
Total	98.1	100.0	99.9	99.7	99.5	99.4	99.5	100.1	96.9	99.4	99.7	98.4	100.6	99.7
Ti [ppm]		183	154	798	271	463	20.2	13.2		661	24.3		5921	
Sr [ppm]		2.37	4.83	9.16	17.28	8.65	3.98	2.69		5.14	5.35		5.28	
Y [ppm]		0.85	3.75	31.4	1.86	4.17	0.09	0.08		2.00	0.09		53.6	
Zr [ppm]		2.84	41.4	111	7.23	4.51	1.05	0.43		14.9	1.69		63.2	
La [ppm]		0.17	0.07	0.09	0.16	0.25	0.22	0.16		0.33	0.20		0.05	
Ce [ppm]		1.88	0.61	1.18	2.48	1.88	2.34	2.53		3.69	3.24		1.19	
Nd [ppm]		2.74	1.46	2.56	2.99	0.70	2.35	2.70		4.92	1.63		7.40	
Sm [ppm]		0.40	1.15	1.26	1.06	0.39	0.23	0.25		0.94	0.08		4.54	
Eu [ppm]		0.08	0.44	0.34	0.13	0.08	0.04	0.00		0.24	0.02		2.03	
Dy [ppm]		0.22	0.36	1.73	0.18	0.20	0.03	0.04		0.42	0.03		8.19	
Er [ppm]		0.12	0.15	1.61	0.04	0.14	0.02	0.03		0.18	0.01		5.30	
Yb [ppm]		0.20	0.29	1.56	0.20	0.31	0.10	0.16		0.23	0.10		5.37	

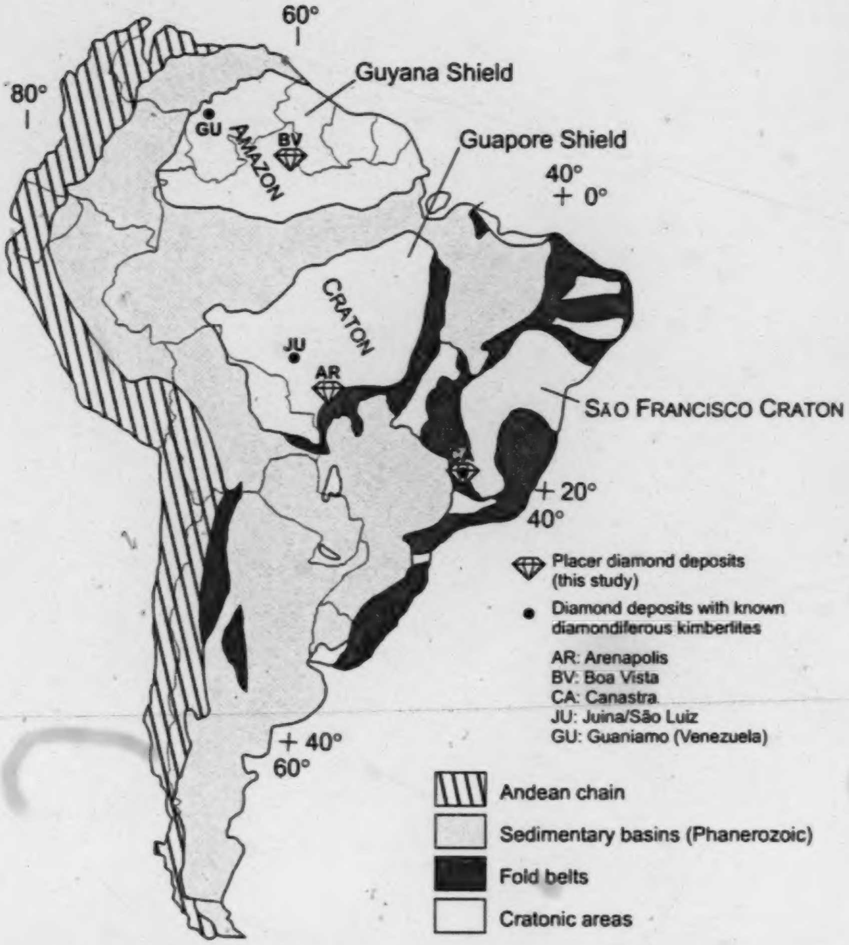
60°
Guyana Shield
80°
GU
AMAZON
BV
Guapore Shield
40°
0°
CRATON
JU
AR
SÃO FRANCISCO CRATON
CA
20°
40°
Placer diamond deposits (this study)
Diamond deposits with known diamondiferous kimberlites
AR: Arenapolis
BV: Boa Vista
CA: Canastra
JU: Juina/São Luiz
GU: Guaniamo (Venezuela)
40°
60°
Andean chain
Sedimentary basins (Phanerozoic)
Fold belts
Cratonic areas

Figure 3-1: Map of South America showing the main tectonic structures (based on De Brito Neves and Cordani, 1991) and the locations of the studied placer deposits.

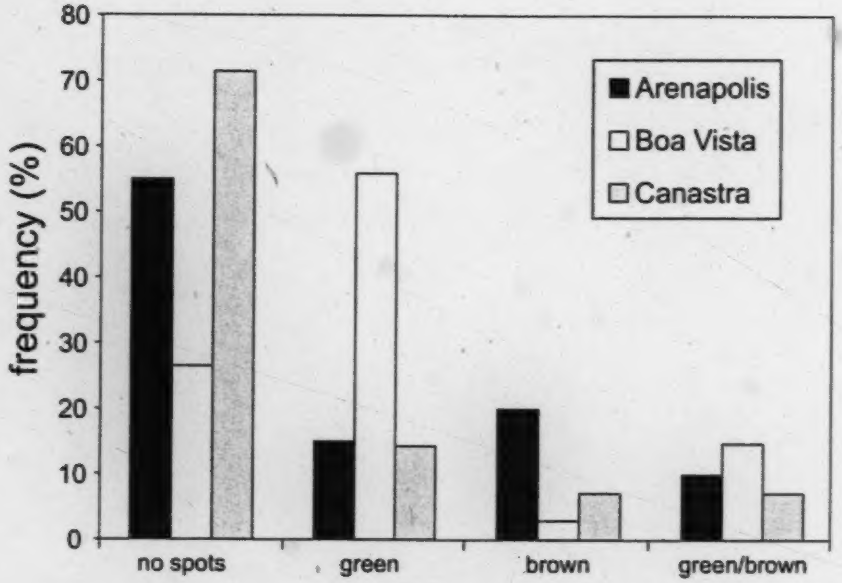

Figure 3-2: Histogram showing the distribution of surface radiation spots on diamonds from Arenapolis, Boa Vista and Canastra.

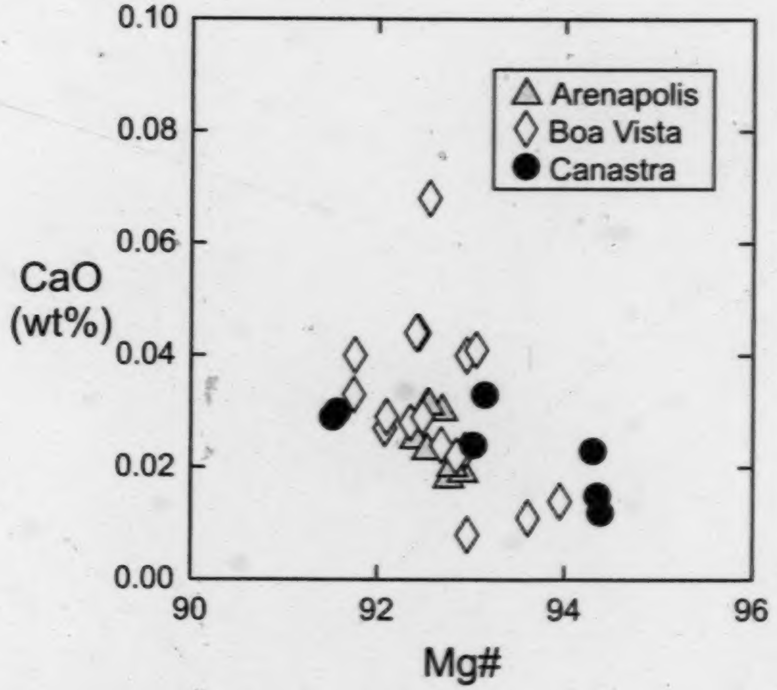

Figure 3-3: CaO (wt%) versus molar Mg number for olivine inclusions from Arenapolis, Boa Vista and Canastra diamonds.

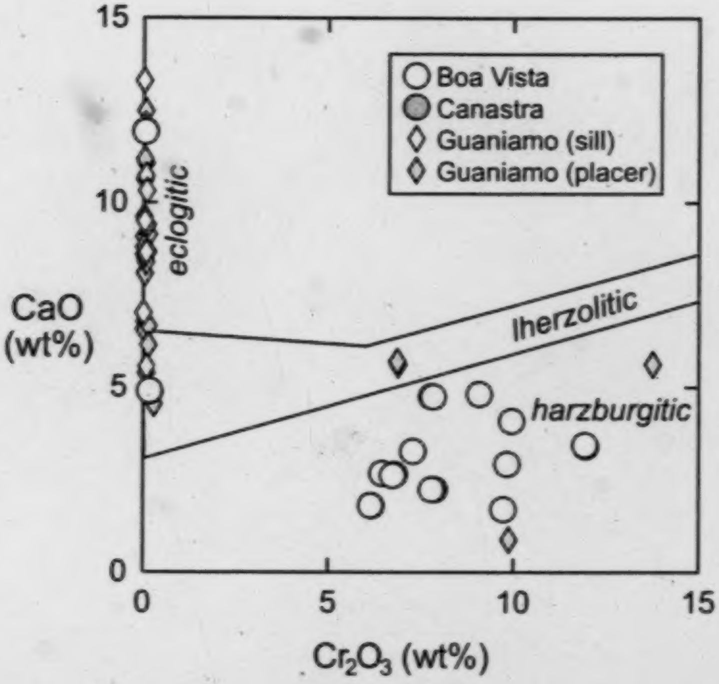

Figure 3-4: CaO versus Cr_2O_3 for garnet inclusions in diamonds from Boa Vista and Canastra. Compositional data for garnet inclusions in diamonds from kimberlitic sills as well as from placer deposits in the Guaniamo area, Venezuela (taken from Kaminsky *et al.*, 2000) are shown for comparison. The compositional field for lherzolitic garnets is taken from Sobolev *et al.* (1973).

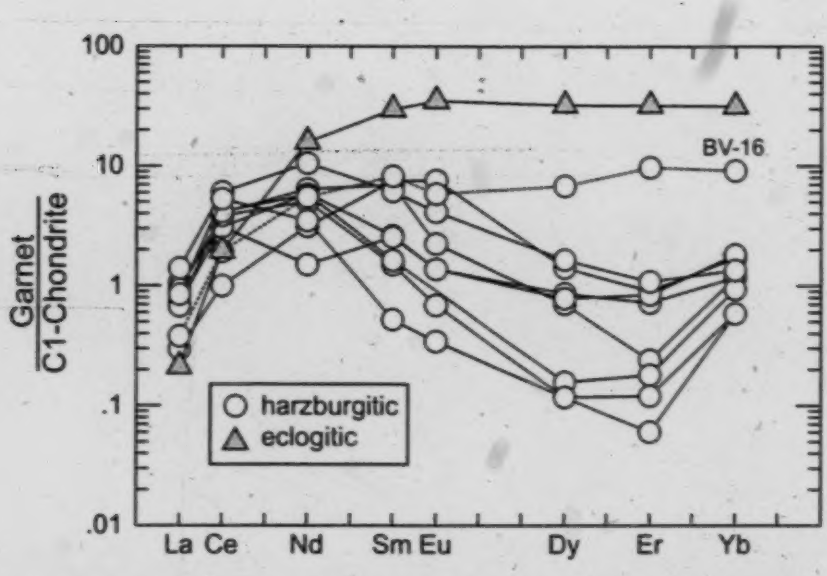

Figure 3-5: Rare earth element concentrations of garnet inclusions in diamonds from Boa Vista. Concentrations are normalized to C1-chondrite compositions after McDonough & Sun (1995).

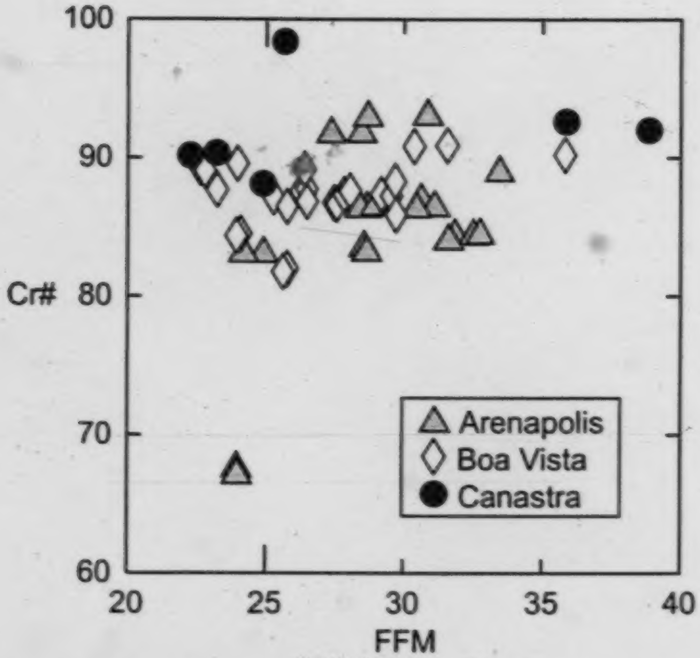

Figure 3-6: FFM (100*Fe^{2+}/Fe^{2+}+Mg) versus Cr# (100*Cr/Cr+Al) of magnesiochromite inclusions from Arenapolis, Boa Vista and Canastra diamonds. Fe^{3+} concentrations were calculated after Droop (1987).

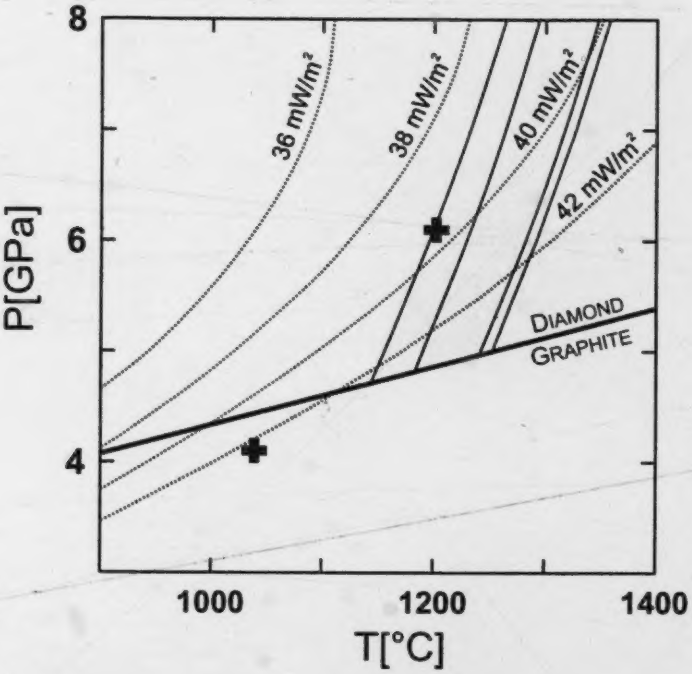

Figure 3-7: Pressure and temperature conditions calculated for non-touching inclusion pairs from Boa Vista. *Crosses*: results for garnet-orthopyroxene after Brey & Köhler (1990) and Harley (1984). *Grey field*: Range of results for garnet-olivine after O'Neill & Wood (1979); results for separate mineral pairs are marked as *solid lines*. The dotted lines mark conductive geotherms for various surface heat flow values, calculated after Pollack & Chapman (1977). The graphite-diamond phase boundary is after Kennedy & Kennedy (1976).

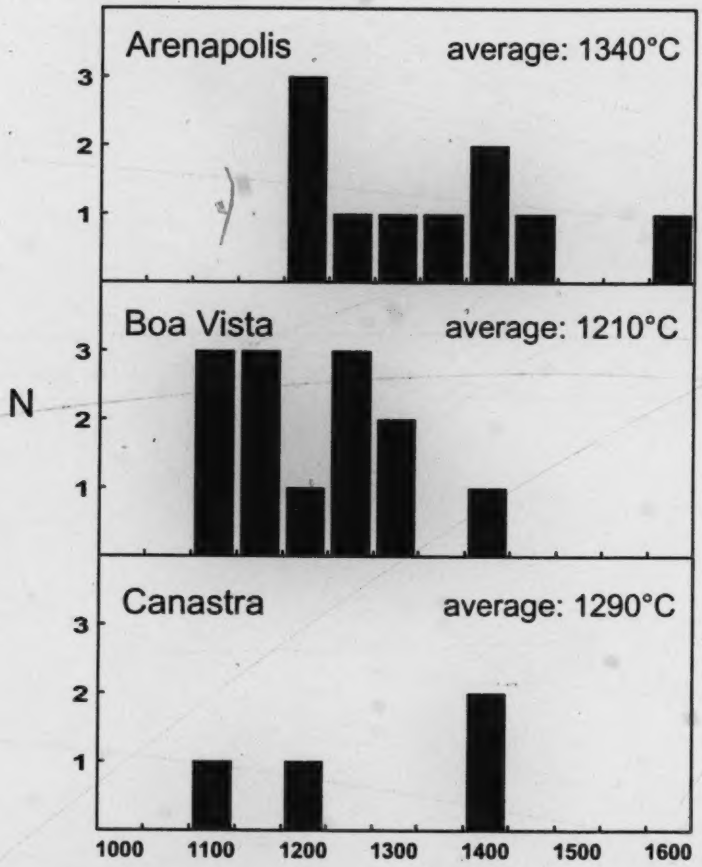

Figure 3-8: Histograms showing temperature estimates (based on empirical results of Ryan et al., 1996) determined for magnesiochromite inclusions in diamonds from Arenapolis, Boa Vista and Canastra. The data represent temperature averages for single diamonds.

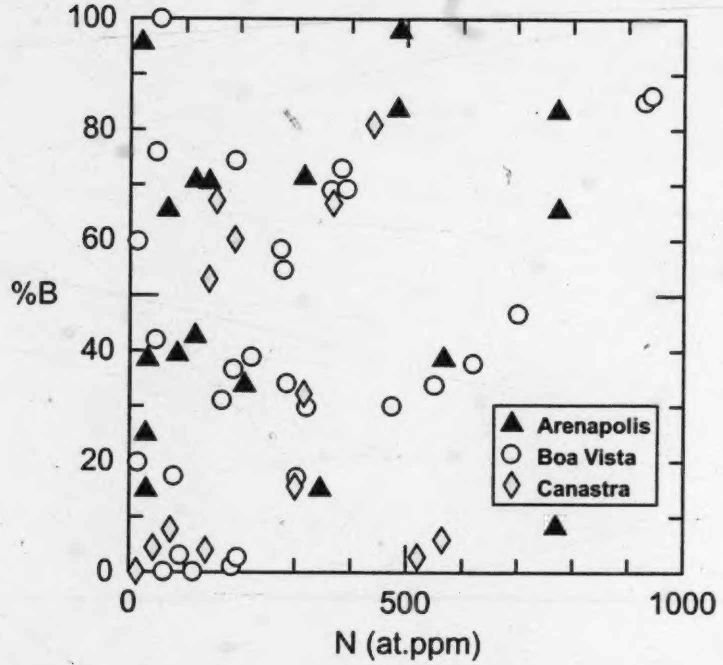

Figure 3-9: Aggregation state (given as percentage of higher aggregated B-center relative to the A-center) versus nitrogen concentration (in atomic ppm) of Type I diamonds from Brazil. Note that two diamonds from Boa Vista with a nitrogen contents of 1392 and 1856 at.ppm are not shown in the diagram.

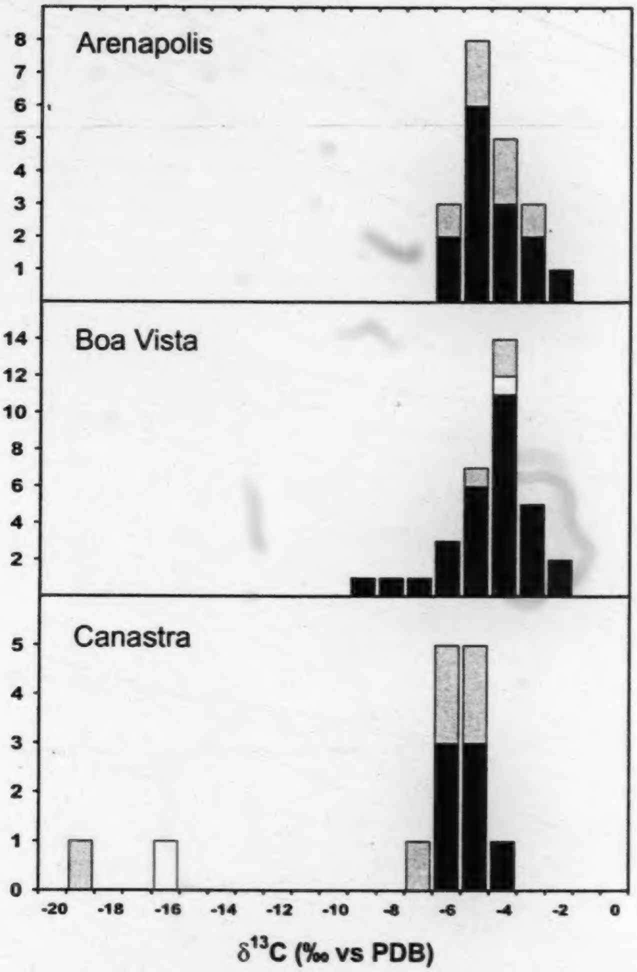

Figure 3-10: Carbon isotopic composition of diamonds from Arenapolis, Boa Vista and Canastra. *Black*: peridotitic, *white*: eclogitic, *grey*: unknown

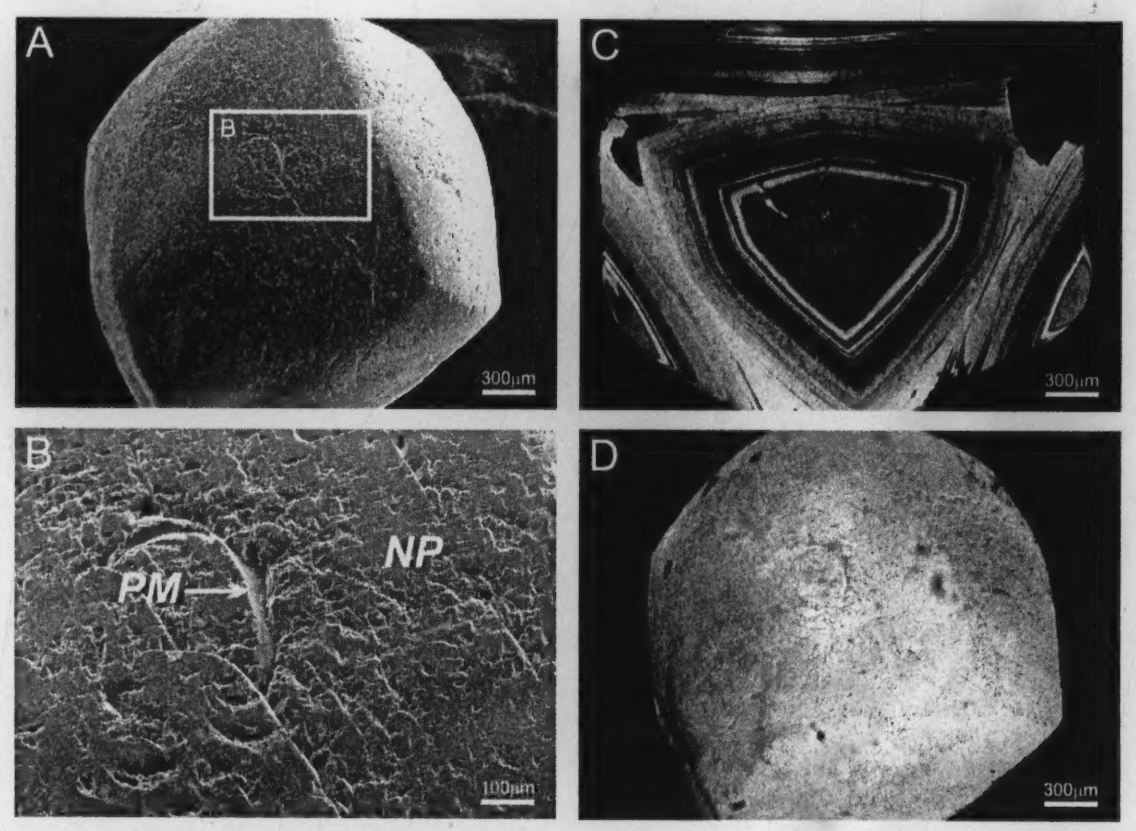

Plate 3-1: [A] SEI overview image of the surface of diamond AR-09 (Arenapolis) [B] Close-up of the surface of diamond AR-09 showing typical abrasion textures including percussion marks (*PM*) and network patterns (*NP*). [C] CL image of diamond AR-01, showing oscillatory growth zoning parallel to the octahedral faces. [D] CL image of unzoned diamond AR-09.

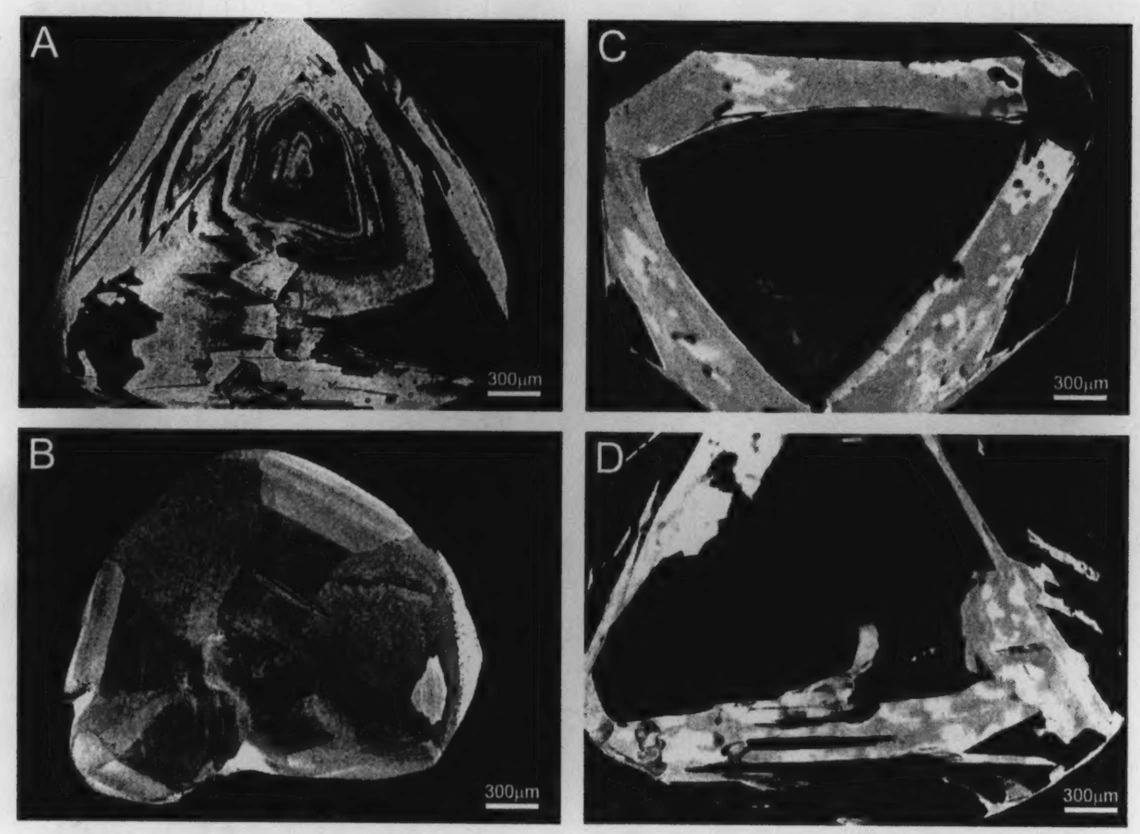
A
B
C
D
300μm
300μm
300μm
300μm

Plate 3-2: CL images of diamonds from Arenapolis, Boa Vista and Canastra, showing typical zoning patterns. [A] Irregular growth zoning of diamond AR-14. [B] Sector zoning of diamond CA-11. [C],[D] Low nitrogen outer octahedral layer of diamonds BV-03 and BV-05.

CHAPTER 4

Diamonds from Jagersfontein (South Africa): Messengers from the sublithospheric mantle

The content of this chapter is in preparation to be submitted for publication in *Contributions to Mineralogy and Petrology* as:
Tappert, R., Stachel, T., Harris, J.W., Muehlenbachs, K., Ludwig, T., Brey, G.P.: Diamonds from Jagersfontein (South Africa): Messengers from the sublithospheric mantle.

4.1 Introduction

Studies of mineral inclusions in diamonds have shown that the vast majority of diamonds form in the deep seated keels of the lithosphere beneath ancient cratonic crust at depths of 150-200 km (e.g. Boyd and Gurney, 1986; Meyer, 1987).

Mineral inclusions in a very small portion of diamonds indicate a much deeper, sublithospheric origin, i.e. within the asthenosphere, the transition zone and the lower mantle (Scott Smith et al., 1984; Moore and Gurney, 1985 and 1989; Harte and Harris, 1994; Harte et al., 1999; Stachel et al., 2000b). The composition of mineral inclusion in diamonds from the asthenosphere and transition zone is almost exclusively eclogitic, whereas lower mantle diamonds, like lithospheric diamonds, are dominated by inclusions that are consistent with a peridotitic bulk composition. The observation of eclogite-dominated asthenospheric and transition zone diamonds is not consistent with the concept of an overall peridotitic mantle and was used to argue for the presence of an eclogitic layer in Earth's mantle, at depths between 200 and 410 km (Gasparik, 2002). It was also suggested that these eclogitic inclusions represent precipitations of alkaline basalts or primitive ocean island basalts at great depths (Moore et al., 1991) or that they are remnants of subducted oceanic crust (Stachel et al., 2000a).

Chapter 4

In this paper evidence for a crustal derivation of asthenospheric and transition zone diamonds from the Jagersfontein kimberlite in South Africa will be presented. It will also be shown that the diamonds formed in subducting oceanic crust within the sublithospheric mantle by direct conversion from graphite of biogenic origin into diamond.

The Jagersfontein kimberlite is located ~150 km southeast of Kimberley in South Africa (Fig. 4-1). It is part of a small kimberlite cluster, which intruded Archean basement gneisses and schists, the Neoarchean Ventersdorp Supergroup and the Jurassic Karoo sequence (Wagner, 1914). Previous research established the presence of inclusions of garnet with a majorite component in diamonds from Jagersfontein (Tsai et al., 1979; Deines et al., 1991).

Majoritic garnet is the only high pressure mineral found as an inclusion in diamonds that provides evidence for an origin within the asthenosphere or transition zone (Stachel, 2001). The results of high pressure experiments (Ringwood, 1967; Ringwood and Major, 1971; Akaogi and Akimoto, 1977) were used to show that majoritic garnet forms as the result of increasing solubility of pyroxene in garnet at high pressures. The initiation of pyroxene dissolution in garnet starts at ~250 km and, for a pyrolitic bulk composition, is completed at a depth of ~450 km (Irifune, 1987).

Majoritic garnet, although rare, has been identified as inclusion in diamonds from a number of deposits on almost all cratons worldwide, but in most deposits it was only recognized in one or two diamonds. Besides Jagersfontein, higher abundances of majoritic garnets were found at Monastery, South Africa, (Moore and Gurney, 1989) the Juina-São Luiz area, Brazil, (Wilding, 1990; Harte, 1992; Hutchison 1997; Kaminsky et al., 2001) and Kankan, Guinea, (Stachel et al., 2000a). Most of the majoritic garnets are eclogitic, with chromium contents of <1.0 wt% Cr_2O_3 and Mg-numbers <80. To date, peridotitic garnets with a majorite component are exceptions and have only been identified at few localities (Stachel et al. 2001 and references therein; Pokhilenko et al., 2004)

For this study, 122 diamonds that visually appeared to contain inclusions were selected from a total of >4500 carats. Ninety-eight of these diamonds contained syngenetic inclusions (Tab. 4-1); ten of these contained inclusions that were exposed to the diamond surface and were therefore only used to determine the paragenetic association of the host diamond. Twenty-four diamonds, after breakage, were either inclusion-free (excluding graphite flakes) or contained secondary, epigenetic phases of unknown origin.

Morphological characteristics of the diamonds (including weight, crystal shape, color and presence of visible signs of deformation) are summarized in Appendix D: Table 1.

4.2 Sample preparation and analytical techniques

The inclusions were released by crushing of the host diamonds, separately mounted in brass rings and then polished. Major elements were determined with a JEOL JXA-8900RL electron microprobe at the University of Alberta. The measurements were made using a 20 kV acceleration voltage and 20 nA probe current, with a detection limit for oxide species of ~100 ppm (except Na_2O: 200 ppm). Accuracy and precision were tested on secondary standards and are within ~1.0% relative for the major elements. The complete set of microprobe analyses for the mineral inclusions analyzed in this study are given in Appendix D: Table D1.

Rare earth elements (REE) were analyzed using the CAMECA IMS3f ionprobe at the Universität Heidelberg. The primary beam was a 14.5keV O^- ion beam with a current of 20 nA and a spot size of ~25 μm. The mass resolution (m/Δm) was set to 370 and the energy window was set to 105 ± 25 eV (energy filtering) in order to minimize matrix effects and molecular interferences. Data were collected at mass 30 (^{30}Si) and from mass 138 to 176. The integration time for ^{30}Si was 2 s and for the REE typically 8 s. Six measurement cycles were averaged.

The major problem in analyzing REE with SIMS is molecular interference. Whereas complex (>2 atoms) molecular ions are suppressed sufficiently by energy filtering, the REE oxides are still present in the mass spectrum. Typical element to oxide ratios vary between 0.05 and 0.2. The deconvolution method of Zinner and Crozaz (1986) has been chosen to correct the acquired REE spectrum for REE oxides, but instead of solving the linear system of equations directly, it has been solved by numerical optimization. This process involves synthesizing a spectrum that matches the acquired mass spectrum as closely as possible. The optimization starts with estimated values for REE count rates and element to oxide ratios and minimizes the sum of the squared errors by varying the count rates and the element to oxide ratios. The advantage of this method lies in the fact that the element to oxide ratios can be limited to reasonable values. This helps to overcome the numerical problems for the elements Yb, Lu and Gd. The element/oxide ratios were limited to a range of 0.05 to 0.2 (0.05 to 0.1 for Gd). The optimization yields a set of REE count rates and REE/oxide ratios that can be used to calculate relative ion yields or concentrations. Exactly the same method and the same limits for the REE/oxide ratios were applied to the standard and all unknown samples. Each analysis was repeated six times on the same spot and each of the six spectra was deconvoluted separately. The resulting REE count rates were then averaged and the relative standard deviation (1 RSD) calculated. The standard deviation reflects in this case not only the precision of the acquired raw data but also the numerical (in-) stability of the deconvolution process. Values for the uncertainties for each sample are given in Tables 4-4 and 4-5.

The NIST SRM610 glass was used as a standard to determine the relative ion yields (values for REE concentrations are taken from Pearce et al., 1997). Two well characterized garnet megacrysts (PN1, PN2) were analyzed as a further accuracy test. Table 4-2 shows the results of these analyses and SIMS, INAA and LA-ICP-MS data of other laboratories. Except for very low La and high Ce using INAA, all three techniques and all laboratories are in satisfactory agreement.

The carbon isotope composition of each diamond was determined with a Finnigan MAT 252 gas flow mass spectrometer at the University of Alberta, after combusting ~1 mg of inclusion free diamond fragments. The fragments were combusted together with ~1g CuO as an oxygen source in a sealed and evacuated quartz tube at 1000°C for ~12 hours. The results are given with respect to the V-PDB standard (Coplen et al., 1983). Instrumental precision and accuracy is in the order of ± 0.02‰. The replication of analyses of selected samples showed a variability within

0.2‰, which may be related to the combustion/extraction process and/or to isotopic heterogeneities of the diamond.

The concentration and aggregation state of nitrogen impurities in the diamonds was determined from inclusion free, transparent fragments by Fourier transform infrared (FTIR) spectroscopy using a Thermo Nicolet Nexus 470 FT-IR Spectrometer with IR microscope at the University of Alberta. The spot size was set to 50 x 50μm. The detection limits are dependent on the quality of the fragments, but are generally in the range 10-20 ppm. The relative errors for concentration and aggregation state for each measurement are 10-20%.

4.3 Results

4.3.1 Lithospheric inclusion suite

Based on the composition of their inclusions ~34% of the diamonds from Jagersfontein belong to the peridotitic suite, ~47% are eclogitic (non majoritic garnet-bearing) and a small group (6%) is websteritic. The samples of this study, however, may not be representative because garnet-bearing diamonds were sampled preferentially.

The *peridotitic* diamonds contain olivine, Cr-pyrope garnet, orthopyroxene and Mg-chromite in order of decreasing abundance (Tab. 4-1). Olivines have Mg-numbers (100*Mg/(Mg+Fe)) between 92.8 and 94.9 (mode at 94) and a maximum CaO content of 0.05 wt% (Tab. 4-3). Figure 4-2 shows that all peridotitic garnets from Jagersfontein fall into the subcalcic, harzburgitic field (see also Tab. 4-4). The Mg-numbers of orthopyroxene inclusions are in the range 94.8-97.0.

The chondrite normalized REE (REE_N) patterns of three peridotitic garnets have a sinusoidal shape with a pronounced hump at Pr or Nd and troughs at Ho-Yb (Fig. 4-3). Sinusoidal REE_N patterns are a prominent feature observed among the majority of low Ca, harzburgitic garnet inclusions not only from the Kaapvaal craton but also from other deposits worldwide (Stachel et al., 2004).

The garnets of the *eclogitic* suite have a wide compositional range with calcium between 0.22 and 1.07 cations per formula unit (pfu: based on 12 oxygen) and Mg numbers of 50-75 (Tab. 4-3 and 4-4). Clinopyroxenes range from jadeite-rich omphacite to jadeite-poor diopside (Na: 0.03-0.34; Al: 0.04-0.42; Mg: 0.55-1.18; Ca: 0.23-0.76 cations for 6 oxygen). Less common constituents of the eclogitic suite are corundum and SiO_2 inclusions, which were found in association with garnet and clinopyroxene (Tab.4-1).

Websteritic inclusions are transitional in composition between eclogitic and peridotitic. Although a compositional range for websteritic garnets in diamonds has been defined by Deines et al. (1993) for samples from Orapa, Botswana, it is not generally applicable, because it failed to correctly assign parageneses for inclusions in diamonds from Venetia, South Africa (Aulbach et al., 1999). In the present case inclusions were defined as websteritic if almandine-pyrope garnet coexisted with orthopyroxene (Appendix D: Figs.1 and 2). These garnets are distinct from peridotitic garnets by lower Mg-numbers (Mg#<80) and from eclogitic garnets by higher chromium contents of 1-5 wt% Cr_2O_3 (Tab. 4-4).

The eclogitic garnet inclusions show two distinct REE_N patterns. The first and most common REE_N pattern is characterized by a strong increase from the light REE_N (subchondritic to chondritic La) towards the middle REE_N and a continuous moderate increase towards the heavy REE_N (~20 to 80 times chondritic Lu) (Fig. 4-4). The websteritic garnet that is part of the multiphase inclusion recovered from diamond JF-122 has a REE_N pattern that is indistinguishable from this first group of eclogitic garnet inclusions (Fig. 4-5 and Appendix D: Fig.1).

The two most calcium-rich eclogitic garnets (13.0-13.5 wt% CaO) recovered from diamonds JF-59 and JF-76 exhibit a second style of REE_N pattern, which is characterized by flat, ~10 times chondritic middle (Sm-Ho) and heavy REE_N. Both garnets show small positive Eu-anomalies, with Eu*/Eu >1.3 (Fig. 4-5).

Eclogitic clinopyroxene inclusions are characterized by flat or slightly convex REE_N patterns, with maxima at Nd or Sm (Fig. 4-6). Two clinopyroxenes show small positive Eu-anomalies. The single websteritic clinopyroxene inclusion, which is part of the multiphase inclusion of diamond JF-122, shows the lowest REE concentrations (Fig. 4-6 and Appendix D: Fig.1).

Equilibration temperatures and pressures of the lithospheric diamonds were calculated from coexisting mineral inclusion pairs. The peridotitic diamond suite is represented by only one touching inclusion assemblage of garnet and orthopyroxene and Mg-chromite. The calculated temperature and pressure (Harley, 1984; Brey and Köhler, 1990) of 1080°C and 5.5 GPa indicate equilibration of the diamond on a geothermal gradient corresponding to ~38 mW/m^2 surface heat flow (Pollack and Chapman, 1977). Two touching inclusion pairs of websteritic garnet, orthopyroxene and clinopyroxene equilibrated on a similar geothermal gradient, but at generally higher pressures (1170°C-6.6 GPa; 1230°C-7.1 GPa). The two non-touching websteritic garnet-orthopyroxene pairs equilibrated at 1240°C-5.5 GPa and 1430°C - 7.1 GPa respectively. For an assumed pressure of 5 GPa, three touching and two non-touching pairs of garnet and clinopyroxene gave temperatures in the range 1100-1220°C (calculated after Krogh, 1985; Fig. 4-7).

4.3.2 Sublithospheric inclusion suite

Thirteen diamonds contained garnets with a majorite component ranging from 3.05 (used here as minimum value for a significant majorite component) to a maximum of 3.54 Si per formula unit (pfu) (Fig. 4-8). On the basis of experimental data from Irifune (1987), the two garnets with the highest majorite component reflect a depth of origin of >500 km. More conservative depth estimates, based on the work of Gasparik (2002), still place the most majoritic garnet below the 410 km boundary, into the transition zone.

The majoritic garnets belong, with one exception, to the eclogitic suite, with <1.0 wt% Cr_2O_3 (Tab. 4-5). The exception is a websteritic garnet from diamond JF-43, with a majorite component corresponding to 3.16 Si pfu. It contains ~3.5 wt% Cr_2O_3 with an Mg# = 75 and occurs together with a non-majoritic garnet in the same diamond (Tab. 4-4). The calcium content of the majoritic garnets is generally in the range 3.9-8.0 wt% CaO, with the exception of one high-Ca garnet (11.1 wt% CaO) (Tab. 4-5). Titanium ranges from 0.09 to 0.54 wt% TiO_2. Magnesium (13.4-22.0 wt%

MgO) and sodium (0.12-0.65 wt% Na_2O) generally show a positive correlation with the silicon content.

In general, the shape of the REE_N pattern is similar for all majoritic garnets and also similar to the non-majoritic eclogitic garnets, with steeply increasing light to middle REE and flatter middle to heavy REE with Lu contents ranging from 10 to >100 times chondritic (Fig. 4-9). The lowest heavy REE abundances were found in the only websteritic garnet. However, unlike the lithospheric garnets, all majoritic garnet inclusions at Jagersfontein show a significant negative Eu-anomaly (Fig. 4-9), with Eu*/Eu values between 0.51 and 0.82.

Comparison of the observed REE compositions with available REE patterns for majoritic garnets from other sources (Fig. 4-9) shows that the patterns from Jagersfontein broadly resemble those found at Monastery (Moore et al., 1991), except for the HREE which generally extend to higher concentrations at Jagersfontein. The compositions of majoritic garnets from the Juina-São Luiz area (Harte, 1992; Kaminsky et al., 2001) are characterized by slightly steeper slopes from LREE to MREE. Majoritic garnets from Kankan (Stachel et al., 2000a) have higher, 10 to ~100 time chondritic, LREE concentrations and flat MREE and HREE. Kankan is the only diamond source for which a Eu-anomaly in a majoritic garnet inclusion has been previously reported by Stachel et al. (2000a).

4.3.3 Chemical and isotopic characteristics of the host diamonds

Chemical and isotopic information from the host diamond were obtained by determining the contents and the aggregation states of nitrogen impurities and the carbon isotope composition (Appendix D: Table 1).

Nitrogen contents of Jagersfontein diamonds range from below the detection limit (Type II diamonds) to a maximum of ~1200 ppm for a diamond of unknown paragenesis (Fig. 4-10). Peridotitic diamonds are restricted to maximum nitrogen contents of ~500 ppm, whereas eclogitic diamonds have nitrogen in the range <10 to ~700 ppm, with one at 1027 ppm. The aggregation state of nitrogen impurities of the lithospheric diamonds is variable and ranges from low aggregation levels, with nitrogen mainly in A-centers (Type IaA) to highly aggregated nitrogen (Type IaB). However, the majority of peridotitic (88%) and eclogitic diamonds (63%) have low aggregation states of <50% B-centers (Fig. 4-10).

The sublithospheric diamonds are either nitrogen free Type II diamonds (46%) or have low contents of nitrogen (< 60 ppm) in generally highly aggregated states (Type IaB). Lower nitrogen aggregation levels (<90% B-centers) were measured in four sublithospheric diamonds.

The carbon isotope composition for Jagersfontein diamonds ranges from -1 to -24 ‰ $\delta^{13}C$ relative to the V-PDB standard (Fig. 4-11) and correlates with the chemical environment of the source. Peridotitic diamonds have a restricted range in $\delta^{13}C$ from -1 to -8 ‰ with a mean of -4.8 ‰ (Fig. 4-11A), similar to peridotitic diamonds worldwide and the range observed for mantle-derived carbon (Cartigny et al., 2001). Eclogitic diamonds of lithospheric origin cover almost the entire range observed at Jagersfontein, but have a pronounced bimodal distribution (Fig. 4-11B). The group of diamonds with heavier isotopic compositions, which encompasses 57% of the eclogitic diamond population, ranges from -1 to -9 ‰ with a mean of -4.7 ‰. The isotopically lighter diamonds range from -13 to -24 ‰ with a mean of -18 ‰. This broad range and the bimodal distribution of carbon isotopes of eclogitic diamonds is a common feature found at diamond deposits worldwide (Kirkley et al., 1991).

Diamonds with majoritic garnet inclusions from Jagersfontein have a restricted carbon isotope range (Fig. 4-11C), between -17 and -24 ‰ and a mean of -19.9 ‰, which is in good agreement with previous observations (Deines et al., 1991) and demonstrates that these diamonds are isotopically distinct from the eclogitic and websteritic diamond population that formed in the lithosphere (Fig. 4-11C).

4.4 Discussion

4.4.1 Major and trace element compositions

The major element composition of peridotitic inclusions, with overall high Mg-numbers and low Ca contents for olivine, garnet and orthopyroxene, indicates a strongly depleted peridotitic source. This is in accordance with results from other diamond deposits on the Kaapvaal craton, summarized by Stachel et al. (2003), which show modes for the Mg-numbers of olivine at 94-95 and for orthopyroxene at 95-96. It demonstrates that the depleted character of the peridotitic source is a distinctive feature of lithospheric diamonds from the Kaapvaal craton.

Major element compositions of the lithospheric suite of eclogitic and websteritic inclusions from Jagersfontein diamonds resemble other deposits from the Kaapvaal craton and worldwide (e.g. Gurney et al., 1984; Meyer, 1987). In addition, the results of the P-T estimates for touching and non-touching websteritic and eclogitic inclusions assemblages in diamonds from Jagersfontein overlap with results for lithospheric diamonds from other deposits on the Kaapvaal craton (Stachel et al. 2003), with the exception of one high temperature, non-touching garnet-orthopyroxene pair (Fig.4-7). It is, however, interesting to note that the touching websteritic inclusion pairs are consistent with equilibration on a lower geothermal gradient of ~38 mW/m^2 surface heat flow compared to the geothermal gradient of 42 mW/m^2 for non-touching pairs (Fig.4-7). Similar observations have been made by Phillips and Harris (1995) on inclusions assemblages from the DeBeers pool mines and have been interpreted as being the result of re-equilibration of the touching inclusions to lower temperatures after diamond formation.

The occurrence of Eu-anomalies in garnet inclusions in diamonds is rare, but has been described from Kankan in Guinea (Stachel et al., 2000a), Venetia in South Africa (Aulbach et al., 2002), and from Namibia (Stachel et al., 2004).

Europium is the only REE that naturally occurs in divalent (Eu^{2+}) and trivalent (Eu^{3+}) oxidation state and therefore it can be separated from the rest of the exclusively trivalent REE (Goldschmidt, 1958). Under crustal conditions plagioclase is the only common mineral in mafic environments that takes up sufficient amounts of Eu^{2+} to produce significant anomalies (Philpotts and Schnetzler, 1968). No high pressure mineral phase from the Earth's mantle is known that would preferably take up Eu^{2+}. Therefore, fractionation or accumulation of plagioclase in silicate melts under crustal conditions is the only probable way to create Eu-anomalies and, accordingly, the appearance of Eu-anomalies in mantle derived material provides evidence for a crustal origin.

The positive Eu-anomalies observed in the high-Ca eclogitic garnet inclusions from Jagersfontein thus indicate that diamond formation took place in a crustal-derived protolith that experienced accumulation of Ca-rich plagioclase before it transformed into eclogite. This hypothesis is also supported by the high calcium contents of these garnet inclusions.

Majoritic garnet inclusions in diamonds from Jagersfontein are characterized by generally more magnesian compositions compared to majoritic garnet inclusions from other diamond deposits worldwide (Fig.4-12). The positive correlation between the magnesium and the silicon content of the majoritic garnets from Jagersfontein indicates a coupled substitution of Si^{4+} and Mg^{2+} for 2 Al^{3+}, which is in accordance with an increase of the majorite component. From Figure 4-12, however, it becomes apparent, that only majoritic garnets from Jagersfontein consistently follow this expected trend. Majoritic garnets inclusions from Monastery, Kankan, Juina-São Luiz and the Buffalo Head Hills are characterized by the presence of a large group of more Ca-rich (>0.75 Ca pfu) majoritic garnets. Within the group of Ca-rich majoritic garnets calcium strongly decreases with increasing silicon contents, i.e. increasing majorite component (Fig 4-12). The decrease of the calcium content, which continues to a maximum majorite component of ~3.4 Si (pfu), shows a negative correlation with the magnesium content. This is particularly prominent for samples from Monastery and Juina-São Luiz, where a sufficient number of data is available (Fig 4-12). The decrease of calcium is also accompanied by a decrease of titanium at increasing majorite component. The calcium decrease could either mark a drop of the solubility of calcium in garnet with increasing majorite component, or it could be caused by a change in the source rock composition with increasing majorite component (and depths). Experimental data from Irifune (1987) show an increase of calcium in garnet at pressures >10 GPa, after the exhaustion of orthopyroxene in the source (Fig. 4-12). This indicates that a drop in the solubility of calcium in garnet at high pressures does not occur, but rather suggests increasing depletion of calcium in the source of the Ca-rich majoritic garnets with increasing depth. The most likely reason for the calcium depletion is progressive "melting" of the majoritic garnet source during subduction to pressures of ~15 GPa (>400 km). Progressive "melting" of the source is also supported by the decrease of the titanium contents in garnet with increasing majorite component. At the pressure range of majorite stability the solvus between hydrous fluids and silicate melts ceases to exist. Progressive melting thus may relate to continued slab dehydration beyond the critical endpoint (Bureau and Keppler, 1999; Wyllie and Ryabchikov, 2000).

The absence of a Ca-depletion trend for the majoritic garnet inclusions from Jagersfontein and a small group of majoritic garnets from Monastery, Juina-São Luiz and Kankan is consistent with their overall more magnesian, thereby more refractory composition. The depleted character of the source of these majoritic garnets may be the result of an earlier melt depletion event, at lower pressures.

Negative Eu-anomalies are commonly found in higher sections of an oceanic sequence comprising extrusive basaltic rocks (Kay et al., 1970). The websteritic garnet inclusions from diamond JF-43 are probably derived from the same source, because they also show negative Eu-anomaly and a carbon isotope composition that is in accordance with the other sublithospheric diamonds. However, their higher chromium contents indicate that the crustal source was not homogeneous. Accumulation of Cr-spinel in a basaltic protolith can explain the elevated chromium contents in the websteritic source. Alternatively, the websteritic source may be the result of slab-derived melts that have reacted with surrounding mantle peridotite, in which case the trace element characteristics are inherited from the melt source (Aulbach et al., 2002).

The occurrence of non-majoritic garnet together with a majoritic garnet in a single websteritic diamond may indicate that diamond formation, at least in some cases, took place in multiple episodes.

4.4.2 Carbon Isotopes

The majoritic garnet-bearing diamonds have not only the most negative carbon isotope values among the Jagersfontein diamonds, but they also represent the isotopically lightest sublithospheric diamonds worldwide (c.f. Stachel et al., 2002). The few available carbon isotope analyses of diamonds containing majoritic garnet from other deposits, primarily the Juina-São Luiz area (Wilding, 1990; Hutchison et al., 1999) and Kankan (Stachel et al., 2002) and single analyses from Premier (South Africa) (Deines et al., 1984), DO-27 (Canada) (Davies et al., 1999) and Orapa (Bostwana) (Deines et al., 1993) are in the range 0 to -14 ‰.

Each deposit with multiple analyses displays a relatively narrow range of carbon isotopes compositions of about 7 ‰. Each deposit is, however, distinct in terms of its isotopic composition, with Kankan having the highest (+0.9 to -3.1‰), Juina-São Luiz intermediate (-4.6 to -11.4‰) and Jagersfontein the lowest $\delta^{13}C$ values (-17.2 to -23.6‰) (Fig. 4-11C). This is in stark contrast to the distribution observed for their lithospheric equivalents and indicates that the carbon source of asthenospheric and transition zone diamonds is distinct from the bulk of lithospheric diamonds. In addition, it shows that the carbon sources of the deep diamonds have not been homogenized.

The origin of the isotopically light carbon within the Earth's mantle and its close relation to eclogitic environments is still a matter of debate. Different models for its origin have been proposed, including fractionation of various carbon species during reduction or oxidation processes (Galimov et al., 1989), the loss of CO_2 from an ascending melt (Javoy et al., 1978; Cartigny et al., 2001), the existence of high-temperature fractionation processes (Deines, 2001) or it has been attributed to heterogeneous carbon sources in the mantle (Boyd et al., 1987; Mattey, 1987). An alternative model is based on the observation that carbon derived from organic matter is enriched in ^{12}C and consequently supports the idea that organic material from subducted sediments, which was introduced into the mantle, represents the source of the isotopically light diamonds (Milledge et al., 1983). The presence of recycled crustal material in the lithospheric mantle is supported by the oxygen isotope compositions of eclogite xenoliths (MacGregor and Manton, 1986; Deines et al., 1991; Jacob et al., 1994) and eclogitic inclusions in diamonds (Schulze et al., 2003 and 2004). In both cases, the isotopic compositions deviate from the typical mantle values and suggest a derivation from subducted, hydrothermally altered seafloor (Muehlenbachs and Clayton, 1976). Further support comes from the sulfur isotope composition of sulfide inclusions in diamonds, which shows evidence of mass independent sulfur fractionation and thereby indicates that the sulfur was originally derived from the Earth's atmosphere (Farquhar et al., 2002).

A concern with such a model is the scarcity of diamonds that have carbon isotopic compositions similar to carbonates, (~ 0 ‰ $\delta^{13}C$) because carbonates are generally expected to be associated with organic matter in oceanic sediments. Numerical modeling (Deines, 2001) has shown that mixing of carbon from carbonates and organic carbon would produce isotopic characteristic that are very different from the observed distribution for eclogitic diamonds. However, these mixing models are based on generalized ratios between carbonates and organic matter, averaging their proportions found on the Earth's surface. This is viable for a worldwide carbon cycle model, but does not account for potential heterogeneities of carbon sources. Oceanic sediments can in reality have significantly different ratios of carbonate to organic carbon, depending on their geographical setting and depositional environment. Pelagic sediments that were deposited close to the poles are virtually free of carbonates, whereas sediments that formed closer to the equator have generally higher carbonate contents (Jenkyns, 1986). This results in significant variability in the carbon isotope composition of sediments that form part of subducting slabs, which should be reflected by the isotope composition of the diamonds that were formed within these slabs. "Shallow", lithospheric diamonds of the eclogite suite from deposits worldwide generally have broad isotope ranges and typically show bimodal distributions. Sublithospheric, majoritic garnet-bearing diamonds, however, are distinct from "shallow" eclogitic diamonds, by having rather restricted isotopic ranges of ~7‰ (see above) and values that are distinctive for each deposit (Fig. 4-11C). Narrow ranges of carbon isotope values of single deposits compared to the large variability between deposits suggest that sublithospheric diamonds reflect the primary composition of their carbon source, which most likely is linked to the composition of the subducted sedimentary sequences. In such a scenario the exceptionally low $\delta^{13}C$ values of the Jagersfontein diamonds would represent sediments that were dominated by organic matter, whereas the less negative values of +0.9 to -3.1‰ found in majoritic garnet-bearing diamonds from Kankan (Stachel et al., 2002) would represent a carbonate-dominated source.

Organic matter in oceanic sequences can not only occur as carbon-rich sediments, but also in form of microbes that directly inhabit ocean floor basalts. Remnants of such microbial activity with corresponding low carbon isotope values were not only found in modern oceanic basalts (Thorseth et al., 1995; Torsvik et al., 1998), but also in Archean pillow lavas of the Barberton greenstone belt, South Africa (Furnes et al., 2004).

A low probability of a survival of carbon in the form of organic matter to sublithospheric depths without converting into diamond was raised as an argument against an organic source of the carbon of deep diamonds (Stachel et al., 2002). However, studies of the alteration of organic matter indicate that at increasing temperatures and pressures, for example during subduction, organic matter will gradually purify and convert to graphite (Gorokhov et al., 1973). Graphite can survive metastably at pressure and temperature conditions well within the diamond stability field without converting to diamond. Synthesis of diamond by direct conversion from graphite has been successfully performed at pressures similar to expected asthenospheric and transition zone conditions to overcome the kinetic barrier (e.g. DeCarli and Jamieson, 1961; Bundy, 1962; Irifune et al., 2003). These experiments, however, which were either performed at very high temperatures (>2000°C) and/or for very short times (shock experiments), produced generally polycrystalline diamond aggregates. Larger single diamond crystals as observed in nature may be the result of recrystallization of such polycrystalline diamond aggregates.

Sublithospheric diamonds from Jagersfontein are not only distinct from the lithospheric diamond suite in their stable carbon isotope composition, but also in their nitrogen characteristics. Lithospheric diamonds from Jagersfontein have a wide range of nitrogen concentrations and aggregation states which resembles those of lithospheric diamonds from other deposits worldwide (Cartigny et al., 2001). Sublithospheric diamonds from Jagersfontein, in contrast, are characterized by generally low nitrogen concentrations or the absence of detectable nitrogen, which is in accordance with results from sublithospheric diamonds from other deposits (Stachel et al., 2002). Low nitrogen concentrations seem to contradict a formation of these diamonds from carbon of organic origin, because organic matter is generally nitrogen-rich. Studies on gases released by arc volcanism, however, have shown that nitrogen is efficiently removed from subducting slabs in the early stages of the subduction (Fischer et al., 2002). The low nitrogen concentration of sublithospheric diamonds, therefore, may be the result of nitrogen loss during a subduction process.

The "low" nitrogen aggregation states (<80% B-centers) found in four of the majoritic garnet-bearing diamonds may be the result of late stage diamond overgrowths.

4.4.3 Age and geological framework for the formation of the sublithospheric diamonds

Attempts in determining the age of diamond formation in the lithosphere have been made by a number of workers and are generally based on radiogenic isotopic systematics of mineral inclusions (see Pearson and Shirey, 1999 for review) or on the nitrogen aggregation characteristics of the host diamonds (Evans and Harris, 1989). For sublithospheric diamonds it is more difficult to estimate the age of their formation, because of a restricted mineralogical variability of the inclusion assemblages, which generally lack datable minerals, and also because of the low contents or complete absence of nitrogen in the host diamonds. The presence of majoritic garnet inclusions in diamonds from Jagersfontein itself, however, can be used to constrain the timing of the subduction event in which the host diamonds formed.

Because the stability of majoritic garnet in the mantle is restricted to the asthenosphere and the transition zone, its presence as inclusion in diamonds indicates that the host diamonds were transported to the Earth's surface very rapidly. Long time storage and re-equilibration at shallower depths in the mantle would result in the exsolution of the pyroxene component in the majoritic garnet inclusions. The occurrence of unexsolved majoritic garnet-bearing inclusions, therefore, indicates that the source in which the diamond grew was present in the asthenosphere/transition zone at the time of the kimberlite emplacement, in case of Jagersfontein in the Late Cretaceous (86 Ma). Furthermore, the uniform major and trace element composition of the majoritic garnet inclusions together with the uniform carbon isotope composition of their host diamonds provides evidence that the entire sublithospheric diamond suite formed in the same geochemical environment, therefore most likely during the same subduction event. This subduction event probably is related to the youngest orogenic event that affected the immediate vicinity of the Kaapvaal craton prior to the kimberlite emplacement: the formation of the Cape Fold Belt during the Early Mesozoic (Fig. 4-13).

The Kaapvaal craton in the Early Mesozoic was part of the amalgamated continent Gondwanaland. The formation of the Cape Fold Belt was the result of northwestward directed subduction of oceanic lithosphere under southern Gondwanaland (Lock, 1980). The location of the Cape Fold Belt has been interpreted as marking the region under which the subduction zone steepened (Fig. 4-13), thereby separating the subducting slab from the overlying continental plate (Lock, 1980). The separation of the subducting plate from the overlying Gondwanaland lithosphere and the continuation of the subduction into the deeper Earth's mantle may have ultimately resulted in the formation of a megalith at the boundary between transition zone and lower mantle (Ringwood,1991), located beneath the Kaapvaal craton at the time of the kimberlite emplacement in the Late Cretaceous (Fig.4-13). The presence of a megalith beneath the Kaapvaal craton in the Cretaceous has previously been proposed by Helmstaedt and Gurney (1997) who suggested that kimberlite magmatism and enriched geochemical signatures in South African kimberlites are related to the presence of such a megalith.

4.5 Conclusions

The data presented here give insights into large-scale processes that occur within the Earth's mantle. The observed Eu-anomalies of the majoritic garnet inclusions provide direct evidence for a subduction-related origin of their diamond source, which can be traced through the asthenosphere into the transition zone. The deep diamonds from Jagersfontein are exceptional compared to similar occurrences worldwide by showing both, a consistent crustal signature of their inclusions, and a isotopically light carbon signature. The correlation of inclusion composition and isotopic composition of the diamond host demonstrates that deep diamonds form in a principally different way than lithospheric diamonds. Deep diamonds seem to preserve the original isotopic signature of their source, most likely as a result of formation from graphite, whereas crystallization of lithospheric diamonds involves fluid processes that either mask the original isotopic compositions of the carbon source or that involve primordial carbon.

The isotopically light carbon of the sublithospheric diamonds in combination with negative Eu-anomalies of all majoritic garnet inclusions is consistent with a derivation from higher sections of an oceanic sequence comprising extrusive basaltic rocks. These oceanic basalts were probably closely associated with organic carbon-rich sediments or, alternatively, organic matter in the form of microbial cultures penetrating the basaltic rocks. During subduction the basaltic rocks may have experienced partial melting, resulting in a more depleted character of the source of the sublithospheric diamonds from Jagersfontein compared to other deposits.

The sublithospheric diamonds from Jagersfontein may have formed during a young (Mesozoic) subduction event, which also, ultimately, caused the Cretaceous kimberlite magmatism on the Kaapvaal craton.

Bibliography

Akaogi, M. and Akimoto, S., 1977. Pyroxene-garnet solid-solution equilibria in the systems $Mg_4Si_4O_{12}$-$Mg_3Al_2Si_3O_{12}$ and $Fe_4Si_4O_{12}$-$Fe_3Al_2Si_3O_{12}$ at high pressures and temperatures. Physics of the Earth and Planetary Interiors, 15: 90-106.

Aulbach, S., Stachel, T., Viljoen, K.S., Brey, G.P. and Harris, J.W., 2002. Eclogitic and websteritic diamond sources beneath the Limpopo Belt - is slab-melting the link? Contributions to Mineralogy and Petrology, 143: 56-70.

Boyd, F.R. and Gurney, J.J., 1986. Diamonds and the African lithosphere. Science, 232: 472-477.

Boyd, S.R. et al., 1987. Multiple growth events during diamond genesis: an integrated study of carbon and nitrogen isotopes and nitrogen aggregation state in coated stones. Earth and Planetary Science Letters, 86: 341-353.

Brey, G.P. and Köhler, T., 1990. Geothermobarometry in four-phase lherzolites II. New thermobarometers, and practical assessment of existing thermobarometers. Journal of Petrology, 31: 1353-1378.

Brey, G.P., Köhler, T. and Nickel, K.G., 1990. Geothermobarometry in four-phase lherzolites I. Experimental results from 10 to 60 kb. Journal of Petrology, 31: 1313-1352.

Bundy, F.P., 1962. Direct conversion of graphite to diamond in static pressure apparatus. Science, 137: 1057-1058.

Bureau, H. and Keppler, H., 1999. Complete miscibility between silicate melts and hydrous fluids in the upper mantle: experimental evidence and geochemical implications. Earth and Planetary Science Letters, 165: 187-196.

Canil, D., Schulze, D.J., Hall, D., Hearn Jr., B.C. and Milliken, S.M., 2003. Lithospheric roots beneath western Laurentia: the geochemical signal in mantle garnets. Canadian Journal of Earth Sciences, 40: 1027-1051.

Cartigny, P., Harris, J.W. and Javoy, M., 2001. Diamond genesis, mantle fractionations and mantle nitrogen content: a study of $\delta^{13}C$-N concentrations in diamonds. Earth and Planetary Science Letters, 185: 85-98.

Coplen, T.B., Kendall, C. and Hopple, J., 1983. Comparison of stable isotope reference samples. Nature, 302: 236-238

Davies, R.M. et al., 1999. Diamonds from the deep: pipe DO-27, Slave Craton, Canada. In: J.J. Gurney, J.L. Gurney, M.D. Pascoe and S.H. Richardson (Editors), The J.B. Dawson Volume, Proceedings of the VIIth International Kimberlite Conference. Red Roof Design, Capetown, pp. 148-155.

Davies, R.M., Griffin, W.L., O'Reilly, S.Y. and McCandless, T.E., 2004. Inclusions in diamonds from the K14 and K10 kimberlites, Buffalo Head Hills, Alberta, Canada: diamond growth in a plume? Lithos, 77: 99-111.

DeCarli, P.S. and Jamieson, J.C., 1961. Formation of diamond by explosive shock. Science, 133(3467): 1821-1822.

De Wit, M.J. et al., 1992. Formation of an Archean continent. Nature, 357: 553-562.

Deines, P., 2001. The carbon isotope geochemistry of mantle xenoliths. Earth-Science Reviews, 58: 247-278.

Deines, P., Gurney, J. and Harris, J., 1984. Associated chemical and carbon isotopic composition variations in diamonds from Finsch and Premier kimberlite, South Africa. Geochimica et Cosmochimica Acta, 51: 1227-1243.

Deines, P., Harris, J.W. and Gurney, J.J., 1991. The carbon isotopic composition and nitrogen content of lithospheric and asthenospheric diamonds from the Jagersfontein and Koffiefontein kimberlite, South Africa. Geochimica et Cosmochimica Acta, 55: 2615-2625.

Deines, P., Harris, J.W. and Gurney, J.J., 1993. Depth-related carbon-isotope and nitrogen concentration variability in the mantle below the Orapa kimberlite, Botswana, Africa. Geochimica et Cosmochimica Acta, 57(12): 2781-2796.

Deines, P., Harris, J.W., Robinson, D.N., Gurney, J.J. and Shee, S.R., 1991. Carbon and oxygen isotope variations in diamond and graphite eclogites from Orapa, Botswana, and the nitrogen-content of their diamonds. Geochimica et Cosmochimica Acta, 55(2): 515-524.

Chapter 4

Evans, T. and Harris, J.W., 1989. Nitrogen aggregation, inclusion equilibration temperatures and the age of diamonds. In: J. Ross et al. (Editors), Kimberlites and related rocks. GSA Spec Publ 14. Blackwell, Carlton, pp. 1001-1006.

Farquhar, J. et al., 2002. Mass-independent sulfur of inclusions in diamond and sulfur recycling on early Earth. Science, 298: 2369-2372.

Fischer, T.P., Hilton, D.R., Zimmer, M.M., Shaw, A.M., Sharp, Z.D., and Walker, J.A., 2002. Subduction and recycling of nitrogen along the Central American margin: Science, 297, 1154–1157

Furnes, H., Banerjee, N.R., Muehlenbachs, K., Staudigel, H. and De Wit, M., 2004. Early life recorded in Archean pillow lavas. Science, 304: 580-581.

Galimov, E.M., Solov'yeva, L.V. and Belomestnykh, A.V., 1989. Carbon-isotope composition of metasomatized mantle rocks. Geochemistry International, 26: 38-43.

Gasparik, T., 2002. Experimental investigation of the origin of majoritic garnet inclusions in diamonds. Physics and Chemistry of Minerals, 29: 170-180.

Goldschmidt, V.M., 1958. Geochemistry. Oxford University Press, London, 730 pp.

Gorokhov, S.S., Petrova, N.I. and Kovalenko, V.S., 1973. Experimental study of the alteration of biogenic carbon at high temperatures and pressures. Doklady Akademii Nauk SSSR, 209: 194-196.

Gurney, J.J., Harris, J.W. and Rickard, R.S., 1984. Silicate and oxide inclusions in diamonds from the Orapa Mine, Botswana. In: J. Kornprobst (Editor), Kimberlites II: the mantle and crust-mantle relationships. Elsevier, Amsterdam, pp. 1-9.

Harley, S., 1984. An experimental study of the partitioning of iron and magnesium between garnet and orthopyroxene. Contributions to Mineralogy and Petrology, 86: 359-373.

Harte, B., 1992. Trace element characteristics of deep-seated eclogite parageneses - an ion microprobe study of inclusions in diamonds, V.M. Goldschmidt Conference. The Geochemical Society, Reston, Virginia, pp. A-48.

Harte, B. and Harris, J.W., 1994. Lower mantle associations preserved in diamonds. Mineralogial Magazine, 58A: 384-385.

Harte, B., Harris, J.W., Hutchison, M.T., Watt, G.R. and Wilding, M.C., 1999. Lower mantle mineral associations in diamonds from São Luiz, Brazil. In: Y. Fei, C.M. Bertka and B.O. Mysen (Editors), Mantle Petrology: Field Observations and High Pressure Experimentation: A tribute to Francis R. (Joe) Boyd. Special Publication. The Geochemical Society, Houston, pp. 125-153.

Helmstaedt, H.H. and Gurney, J.J., 1997. Geodynamic controls of kimberlites - what are the roles of hotspot and plate tectonics? In: N.V. Sobolev and R.H. Mitchell (Editors), 6th International Kimberlite Conference Volume 2, Diamonds: Characterization, Genesis and Exploration. Russian Geology and Geophysics, 38. Allerton Press, New York, pp. 394-404.

Hutchison, M.T., 1997. Constitution of the deep transition zone and lower mantle shown by diamonds and their inclusions. PhD Thesis, University of Edinburgh, 306 pp.

Hutchison, M.T., Cartigny, P. and Harris, J.W., 1999. Carbon and nitrogen composition and physical characteristics of transition zone and lower mantle diamonds from São Luiz, Brazil. In: J.J. Gurney, J.L. Gurney, M.D. Pascoe and S.H. Richardson (Editors), The J.B. Dawson Volume, Proceedings of the VIIth International Kimberlite Conference. Red Roof Design, Capetown, pp. 372-382.

Irifune, T., 1987. An experimental investigation of the pyroxene-garnet transformation in a pyrolite composition and its bearing on the constitution of the mantle. Physics of the Earth and Planetary Interiors, 45: 324-336.

Irifune, T., Kurio, A., Sakamoto, S., Inoue, T. and Sumiya, H., 2003. Ultrahard polycrystalline diamond from graphite. Nature, 421(6): 599-600.

Jacob, D., Jagoutz, E., Lowry, D., Mattey, D. and Kudrjavtseva, G., 1994. Diamondiferous eclogites from Siberia - Remnants of Archean oceanic crust. Geochimica et Cosmochimica Acta, 58(23): 5191-5207.

Javoy, M., Pineau, F. and Iiyama, I., 1978. Experimental determination of the isotopic fractionation between gaseous CO_2 and carbon dissolved in tholeiitic magma. Contributions to Mineralogy and Petrology, 67: 35-39.

Jenkyns, H.C., 1986. Pelagic environments. In: H.G. Reading (Editor), Sedimentary environments and facies. Blackswell, Oxford, pp. 343-397.

Kaminsky, F.V. et al., 2001. Superdeep diamonds from the Juina area, Mato Grosso State, Brazil. Contributions to Mineralogy and Petrology, 140: 734-753.

Kay, R., Hubbard, N.J. and Gast, P.W., 1970. Chemical characteristics and origin of oceanic ridge volcanic rocks. Journal of Geophysical Research, 75: 1585-1613.

Kennedy, C. and Kennedy, G., 1976. The equilibrium boundary between graphite and diamond. Journal of Geophysical Research, 81: 2467-2470.

Kirkley, M.B., Gurney, J.J., Otter, M.L., Hill, S.J. and Daniels, L.R., 1991. The Application of C isotope measurements to the identification of the sources of C in diamonds - a review. Applied Geochemistry, 6(5): 477-494.

Krogh, E., 1988. The garnet-clinopyroxene-iron-magnesium geothermometer - a reinterpretation of existing experimental data. Contributions to Mineralogy and Petrology, 99: 44-48.

Lock, B.E., 1980. Flate-plate subduction and the Cape Fold Belt of South Africa. Geology, 8: 35-39.

Mattey, D.P., 1987. Carbon isotopes in the mantle. Terra Cognita, 7: 31-37.

MacGregor, I.D. and Manton, W.I., 1986. Roberts Victor eclogites: ancient oceanic crust. Journal of Geophysical Research, 91: 14063-14079.

McDonough, W. and Sun, S.S., 1995. The composition of the Earth. Chemical Geology, 120: 223-253.

Meyer, H.O.A., 1987. Inclusions in diamond. In: P.H. Nixon (Editor), Mantle xenoliths. John Wiley & Sons, Chichester, pp. 501--522.

Milledge, H.J. et al., 1983. Carbon isotopic variations in spectral type II diamonds. Nature, 303: 791-792.

Moore, R.O. and Gurney, J.J., 1985. Pyroxene solid solution in garnets included in diamonds. Nature, 318: 553-555.

Moore, R.O. and Gurney, J.J., 1989. Mineral inclusions in diamond from Monastery kimberlite, South Africa. In: J. Ross et al. (Editors), Kimberlites and related rocks. GSA Special Publication 14. Blackwell, Carlton, pp. 1029-1041.

Moore, R.O., Gurney, J.J., Griffin, W.L. and Shimizu, N., 1991. Ultra-high pressure garnet inclusions in Monastery diamonds – Trace element abundance patterns and conditions of origin. European Journal of Mineralogy, 3(2): 213-230.

Muehlenbachs, K. and Clayton, R.N., 1976. Oxygen isotope composition of the oceanic crust and its bearing on seawater. Journal of Geophysical Research, 81: 4365-4369.

Pearce, N.J.G. et al., 1997. A compilation of new and published major and trace element data for NIST SRM 610 and NIST SRM 612 glass reference materials. The Journal of Geostandards and Geoanalysis, 21: 115-144.

Pearson, D.G. and Shirey, S.B., 1999. Isotopic dating of diamonds. In: J. Ruiz and D.D. Lambert (Editors), Applications of radiogenic isotopes to ore deposit research. Economic Geology special publication : SEG Reviews in Economic Geology., pp. 143-171.

Philpotts, J.A. and Schnetzler, C.C., 1968. Europium anomalies and the genesis of basalts. Chemical Geology, 3: 5-13.

Pokhilenko, N.P., Sobolev, N.P., Reutsky, V.N., Hall, A.E. and Taylor, L.A., 2004. Crystalline inclusions and C isotope ratios in diamonds from the Snap Lake/King Lake kimberlite dyke system: evidence of ultradeep and enriched lithospheric mantle. Lithos, 77: 57-67

Pollack, H.N. and Chapman, D.S., 1977. On the regional variation of heat flow, geotherms, and lithospheric thickness. Tectonophysics, 38: 279-296.

Ringwood, A.E., 1967. The pyroxene garnet transformation in the earth's mantle. Earth and Planetary Science Letters, 2: 255-263.

Ringwood, A.E. and Major, A., 1971. Synthesis of majorite and other high pressure garnets and perovskites. Earth and Planetary Science Letters, 12: 411-418.

Schulze, D.J., Harte, B., Valley, J.W., Brenan, J.M. and Channer, D.M.D., 2003. Extreme crustal oxygen isotope signatures preserved in coesite in diamond. Nature, 423: 68-70.

Schulze, D.J., Harte, B., Valley, J.W. and Channer, D.M.D., 2004. Evidence of subduction and crust-mantle mixing from a single diamond. Lithos, 77: 349-358.

Scott Smith, B.H., Danchin, R.V., Harris, J.W. and Stracke, K.J., 1984. Kimberlites near Orroroo, South Australia. In: J. Kornprobst (Editor), Kimberlites I: Kimberlites and related rocks. Elsevier, Amsterdam, pp. 121-142.

Sobolev, N.V., Lavrentev, Y.G., Pokhilenko, N.P. and Usova, L.V., 1973. Chrome-rich garnets from the kimberlites of Yakutia and their paragenesis. Contributions to Mineralogy and Petrology, 40: 39-52.

Stachel, T., 2001. Diamonds from the asthenosphere and the transition zone. European Journal of Mineralogy, 13: 883-892.

Stachel, T. et al., 2004. The trace element composition of silicate inclusions in diamonds: a review. Lithos, 77: 1-19.

Stachel, T., Brey, G.P. and Harris, J.W., 2000a. Kankan diamonds (Guinea) I: from the lithosphere down to the transition zone. Contributions to Mineralogy and Petrology, 140: 1-15.

Stachel, T., Harris, J.W., Aulbach, S. and Deines, P., 2002. Kankan diamonds (Guinea) III: $\delta^{13}C$ and nitrogen characteristics of deep diamonds. Contributions to Mineralogy and Petrology, 142: 465-475.

Stachel, T., Harris, J.W., Brey, G.P. and Joswig, W., 2000b. Kankan diamonds (Guinea) II: lower mantle inclusion parageneses. Contributions to Mineralogy and Petrology, 140: 16-27.

Stachel, T., Harris, J.W., Tappert, R. and Brey, G.P., 2003. Peridotitic inclusions in diamonds from the Slave and the Kaapvaal cratons - similarities and differences based on a preliminary data set. Lithos, 71: 489-503.

Thorseth, I.H., Torsvik, T., Furnes, H. and Muehlenbachs, K., 1995. Microbes play an important role in the alteration of oceanic crust. Chemical Geology, 126: 137-146.

Torsvik, T., Furnes, H., Muehlenbachs, K., Thorseth, I.H. and Tumyr, O., 1998. Evidence for microbial activity at the glass-alteration interface in oceanic basalts. Earth and Planetary Science Letters, 162: 165-176.

Tsai, H.M., Meyer, H.O.A., Moreau, J. and Milledge, H.J., 1979. Mineral inclusions in diamonds: Premier, Jagersfontein and Finsch kimberlites, South Africa, and Williamson mine, Tanzania. In: F.R. Boyd and H.O.A. Meyer (Editors), Kimberlites, diatremes, and diamonds: Their geology, petrology, and geochemistry. American Geophysical Union, Washington, DC., pp. 400.

Wagner, P.A., 1914. The diamond fields of southern Africa. Transvaal Leader, Johannesburg, 347 pp.

Wilding, M.C., 1990. PhD thesis, University of Edinburgh, 281 pp.

Wyllie, P.J. and Ryabchikov, I.D., 2000. Volatile components, magmas, and critical fluids in upwelling mantle. Journal of Petrology, 41, 1195-1206.

Zinner, E.K. and Crozaz, G., 1986. A method for the quantitative measurement of rare earth elements in the ion microprobe. International Journal of Mass Spectrometry and Ion Processes, 69: 17-38.

Table 4-1: Abundance of inclusions in diamonds from Jagersfontein.

Paragenesis	Inclusion phase	No. of diamonds
Peridotitic	ol	10
	gt	8
	gt (ex)	1
	opx	6
	chr	6
	chr (ex)	1
	gt, gt-opx-chr	1
Eclogitic	cpx	19
	cpx (ex)	1
	gt	11
	gt (ex)	7
	gt, cpx	2
	gt-cpx	2
	cpx, gt-cpx	1
	cpx, SiO_2	1
	gt, cor	1
	gt-cpx-SiO_2	1
Websteritic	opx	2
	gt, opx	2
	gt-opx-cpx	2
Sublithospheric	majoritic gt	12
	majoritic gt, gt	1
Unknown/Epigenetic		24

Abbreviations "Assemblage":

ol: olivine, gt: garnet, *cpx*: clinopyroxene, *chr*: chromite

opx: orthopyroxene, cor: corundum, (ex): surface exposed

comma: non-touching pair with..., *dash*: touching pair with...

Table 4-2: Comparison of REE concentrations of PN-garnet megacrysts determined by secondary ion mass spectrometry methods used in this study with independent results.

	PN1-Garnet Megacryst					PN2-Garnet Megacryst					
Method	INAA[a]	SIMS[b]	SIMS[b]	SIMS[b]	SIMS[b]	INAA[a]	SIMS[b]	SIMS[b]	SIMS[b]	LA-ICP-MS[c]	SIMS[b]
Laboratory	Mainz[1]	Pavia[2]	Edinburgh[3]	Woods Hole[4]	this study	Mainz[1]	Pavia[2]	Edinburgh[3]	Woods Hole[4]	Victoria[5]	this study
La [ppm]	0.04	0.02	0.02	0.04	0.02	0.03	0.02	0.02	0.03	0.01	0.02
Ce [ppm]	0.60	0.18	0.21	0.28	0.18	<0.40	0.19	0.21	0.25	0.20	0.14
Pr [ppm]			0.08		0.07			0.08		0.09	0.09
Nd [ppm]	1.50	0.97	0.97	1.03	0.89	1.50	0.95	1.03	1.05	1.05	0.91
Sm [ppm]	1.12	1.34	1.12	1.21	1.05	1.23	1.32	1.33	1.23	1.40	1.10
Eu [ppm]	0.67	0.79	0.70	0.68	0.64	0.75	0.81	0.83	0.76	0.89	0.67
Gd [ppm]	3.40	4.04	3.62		3.21	3.60	3.89	4.04		4.06	3.23
Tb [ppm]	1.02		1.00		0.95	1.03		1.06		1.08	0.87
Dy [ppm]	8.56	8.91	8.70	7.87	7.93	9.98	8.76	9.73	7.62	9.08	7.94
Ho [ppm]	2.20		2.40		2.16	2.20		2.44		2.13	2.04
Er [ppm]	7.90	7.31	8.37	6.75	7.04	6.80	6.59	8.32	6.24	6.32	6.13
Tm [ppm]	1.23				1.12	0.99				0.82	0.83
Yb [ppm]	8.38	8.72	9.25	7.57	8.58	6.20	6.59	8.55	6.09	4.73	6.56
Lu [ppm]	1.26		1.52		1.26	0.91		1.45		0.62	0.75

[1] Max-Planck Institut, Mainz, Germany (Brey and Spettel, unpubl.)

[2] University of Pavia, Pavia, Italy (Ottolini, unpubl.)

[3] Edinburgh University, Edinburgh, U.K. (Stachel, unpubl.)

[4] Woods Hole Oceanographic Institutions, Woods Hole, MA, USA (Shimizu and Banas, unpubl.)

[5] University of Victoria, Victoria, Canada. Data taken from Canil et al. (2003)

[a] Instrumental Neutron Activation analysis

[b] Secondary Ion Mass Spectrometry

[c] Laser-Ablation-Inductively Coupled Plasma-Mass Spectrometry

Table 4-3: Composition of selected silicate inclusions in lithospheric diamonds from Jagersfontein. Major element composition (EPMA-analysis) are given as wt%

Mineral	Olivine	Olivine	Opx (-gt-chr)	Opx	Opx	Garnet	Garnet	Garnet (-cpx)	Garnet	Garnet
Comment	JF-02	JF-88	JF-35	JF-17	JF-97	JF-57	JF-114	JF-34	JF-51	JF-51
Assemblage	ol	ol	gt, gt-opx-chr	opx	2opx	gt	gt	gt-cpx	2gt	2gt
Paragenesis	peridotitic	peridotitic	peridotitic	peridotitic	peridotitic	peridotitic	peridotitic	eclogitic	eclogitic	eclogitic
P_2O_5	0.02	≤ 0.01	≤ 0.01	≤ 0.01	≤ 0.01	0.03	≤ 0.01	≤ 0.01	0.03	≤ 0.01
SiO_2	40.8	41.4	58.1	58.1	58.1	42.1	42.0	41.2	41.1	40.9
TiO_2	0.02	≤ 0.01	0.02	0.02	≤ 0.01	0.06	0.04	0.97	0.14	0.22
Al_2O_3	0.05	0.03	0.57	0.54	0.63	18.6	18.3	19.6	22.0	22.1
Cr_2O_3	0.09	0.03	0.45	0.46	0.55	6.85	7.10	0.56	0.05	0.08
FeO	7.00	5.66	2.94	3.41	2.08	5.19	6.04	15.0	15.3	14.7
MnO	0.09	0.07	0.06	0.07	0.05	0.26	0.28	0.35	0.38	0.40
NiO	0.34	0.35	0.15	0.12	0.12	≤ 0.01	≤ 0.01	≤ 0.01	≤ 0.01	≤ 0.01
MgO	50.7	52.3	36.6	36.0	37.5	25.2	23.3	17.1	15.0	15.3
CaO	0.05	0.02	0.10	0.45	0.06	0.73	2.57	5.48	5.97	6.12
Na_2O	0.04	0.03	0.03	0.06	0.04	0.02	0.02	0.04	0.22	0.08
K_2O	≤ 0.01	≤ 0.01	≤ 0.01	≤ 0.01	0.02	≤ 0.01	≤ 0.01	≤ 0.01	≤ 0.01	≤ 0.01
Total	99.1	99.9	99.1	99.2	99.2	99.0	99.7	100.2	100.2	99.9

Mineral	Garnet	Cpx (-gt)	Cpx	Cpx	Cpx	Garnet	Opx	Garnet (-opx-cpx)	Cpx (-gt-opx)	Opx (-gt-cpx)
Comment	JF-61	JF-34	JF-19	JF-26	JF-80	JF-49	JF-49	JF-54	JF-54	JF-54
Assemblage	gt	gt-cpx	cpx, SiO_2	cpx	cpx	gt, opx	gt, opx	gt-opx-cpx	gt-opx-cpx	gt-opx-cpx
Paragenesis	eclogitic	eclogitic	eclogitic	eclogitic	eclogitic	websteritic	websteritic	websteritic	websteritic	websteritic
P_2O_5	0.02	≤ 0.01	≤ 0.01	0.03	≤ 0.01	≤ 0.01	≤ 0.01	0.03	≤ 0.01	≤ 0.01
SiO_2	39.5	54.3	54.3	54.6	54.1	42.2	56.3	41.4	54.6	56.4
TiO_2	0.41	0.14	0.11	0.26	0.22	0.47	0.07	0.56	0.08	0.06
Al_2O_3	21.9	0.78	1.75	2.11	2.26	20.52	0.91	19.14	0.90	0.55
Cr_2O_3	0.07	0.04	0.05	0.03	0.03	1.84	0.16	1.38	0.17	0.06
FeO	21.0	8.07	7.13	5.58	10.55	12.56	10.62	15.50	7.45	11.36
MnO	0.60	0.15	0.18	0.10	0.14	0.30	0.16	0.37	0.17	0.18
NiO	≤ 0.01	≤ 0.01	≤ 0.01	≤ 0.01	0.05	≤ 0.01	0.05	≤ 0.01	0.02	0.03
MgO	12.4	20.9	19.0	16.0	13.8	18.8	30.0	17.2	18.9	31.0
CaO	4.65	13.9	15.0	19.3	16.84	3.78	1.24	5.19	16.76	1.17
Na_2O	0.16	0.34	0.72	1.06	1.81	0.05	0.09	0.05	0.68	0.13
K_2O	≤ 0.01	0.03	0.02	0.12	0.03	0.02	≤ 0.01	≤ 0.01	≤ 0.01	≤ 0.01
Total	100.7	98.6	98.2	99.2	99.9	100.6	99.6	100.8	99.8	100.9

Table 4-4: Major and trace element composition of lithospheric inclusions in diamonds from Jagersfontein. Major element composition (EPMA-analysis) are given as wt%. For the REE the standard deviations (1σ) are given.

Mineral	Garnet (-opx-chr)	Garnet	Garnet	Cpx	Garnet (-cpx)	Cpx (-gt)	Garnet (-cpx)	Cpx (-gt)	Garnet	Garnet
Sample	JF-35	JF-36	JF-62	JF-04	JF-04	JF-04	JF-20	JF-20	JF-43	JF-52
Assemblage	gt, gt-opx-chr	gt	gt	cpx,gt-cpx	cpx, gt-cpx	cpx, gt-cpx	gt-cpx	gt-cpx	maj, gt	gt
Paragenesis	peridotitic	peridotitic	peridotitic	eclogitic	eclogitic	eclogitic	eclogitic	eclogitic	deep-websteritic	eclogitic
P_2O_5	0.03	0.02	≤ 0.01	0.03	0.05	0.02	0.02	0.02	0.02	0.14
SiO_2	42.3	41.6	40.7	53.3	39.5	53.5	41.1	55.0	42.0	39.6
TiO_2	0.01	0.03	0.02	0.67	0.97	0.66	0.27	0.27	0.40	1.3
Al_2O_3	17.8	11.2	19.2	8.25	21.1	8.29	22.3	5.73	19.8	19.5
Cr_2O_3	8.63	17.8	5.83	0.03	0.04	0.02	0.17	0.15	3.61	0.08
FeO	4.84	5.64	7.02	7.49	18.0	7.61	16.1	8.38	11.0	18.1
MnO	0.21	0.29	0.31	0.09	0.37	0.10	0.3	0.14	0.34	0.34
NiO	≤ 0.01	≤ 0.01	≤ 0.01	0.03	≤ 0.01	0.03	≤ 0.01	0.07	≤ 0.01	≤ 0.01
MgO	24.9	24.0	22.5	9.9	10.8	9.94	16.8	15.2	20.0	15.1
CaO	1.28	1.25	3.24	13.9	8.6	13.9	2.91	10.5	3.14	4.1
Na_2O	0.03	0.04	0.03	4.38	0.25	4.47	0.12	3.50	0.03	0.23
K_2O	≤ 0.01	≤ 0.01	≤ 0.01	0.16	≤ 0.01	0.14	≤ 0.01	0.13	≤ 0.01	≤ 0.01
Total	99.9	101.8	98.7	98.3	99.7	98.7	100.0	99.1	100.4	98.6
La [ppm]	0.08 (0.02)	0.94 (0.06)	0.17 (0.03)	1.76 (0.18)	0.10 (0.04)	1.57 (0.09)	0.01 (0.01)	0.64 (0.11)	0.01 (0.01)	0.24 (0.04)
Ce [ppm]	1.03 (0.16)	12.3 (0.29)	1.28 (0.15)	5.30 (0.17)	0.86 (0.11)	4.63 (0.16)	0.07 (0.03)	2.36 (0.15)	0.15 (0.05)	1.34 (0.12)
Pr [ppm]	0.27 (0.07)	3.34 (0.38)	0.32 (0.09)	0.89 (0.14)	0.31 (0.03)	0.81 (0.07)	0.06 (0.04)	0.62 (0.07)	0.06 (0.02)	0.35 (0.05)
Nd [ppm]	1.88 (0.27)	18.7 (0.55)	1.57 (0.15)	4.80 (0.25)	2.83 (0.22)	4.52 (0.27)	0.72 (0.10)	4.75 (0.29)	0.66 (0.09)	3.20 (0.27)
Sm [ppm]	0.44 (0.09)	2.84 (0.25)	0.25 (0.04)	1.42 (0.13)	2.02 (0.17)	1.22 (0.18)	0.86 (0.13)	1.79 (0.23)	0.43 (0.13)	1.79 (0.13)
Eu [ppm]	0.11 (0.03)	0.63 (0.07)	0.07 (0.01)	0.42 (0.07)	1.02 (0.11)	0.43 (0.07)	0.45 (0.08)	0.67 (0.08)	0.16 (0.07)	0.88 (0.04)
Gd [ppm]	0.34 (0.11)	1.12 (0.48)	0.07 (0.07)	1.00 (0.15)	4.02 (0.27)	0.95 (0.20)	1.80 (0.13)	1.75 (0.18)	0.90 (0.17)	3.59 (0.18)
Tb [ppm]	0.07 (0.05)	0.10 (0.10)	0.02 (0.02)	0.14 (0.07)	0.94 (0.10)	0.16 (0.03)	0.41 (0.12)	0.28 (0.06)	0.23 (0.07)	0.76 (0.09)
Dy [ppm]	0.42 (0.07)	0.35 (0.15)	0.20 (0.06)	0.86 (0.13)	7.61 (0.35)	0.79 (0.17)	3.72 (0.29)	2.13 (0.23)	2.03 (0.12)	6.57 (0.21)
Ho [ppm]	0.06 (0.05)	0.05 (0.04)	0.04 (0.02)	0.19 (0.07)	1.86 (0.24)	0.12 (0.03)	0.92 (0.10)	0.47 (0.08)	0.55 (0.08)	1.55 (0.10)
Er [ppm]	0.17 (0.06)	0.09 (0.09)	0.12 (0.03)	0.29 (0.13)	6.15 (0.28)	0.26 (0.13)	3.23 (0.22)	1.38 (0.18)	2.11 (0.18)	5.10 (0.23)
Tm [ppm]	0.03 (0.03)	0.01 (0.01)	0.02 (0.01)	0.05 (0.05)	0.90 (0.14)	0.03 (0.03)	0.48 (0.10)	0.21 (0.06)	0.35 (0.09)	0.70 (0.14)
Yb [ppm]	0.26 (0.10)	0.13 (0.07)	0.17 (0.03)	0.32 (0.06)	6.80 (0.38)	0.29 (0.07)	4.25 (0.30)	1.82 (0.14)	3.00 (0.22)	5.96 (0.42)
Lu [ppm]	0.05 (0.04)	0.03 (0.03)	0.05 (0.02)	0.04 (0.03)	1.07 (0.11)	0.03 (0.03)	0.63 (0.14)	0.26 (0.06)	0.44 (0.07)	0.90 (0.12)

Table 4-4 continued

Mineral	Garnet	Cpx	Garnet (-cpx-SiO$_2$)	Garnet	Garnet	Cpx	Garnet	Garnet (-cpx-opx)	Cpx (-gt-opx)	Opx (-gt-cpx)
Sample	JF-53	JF-53	JF-56	JF-59	JF-67	JF-67	JF-76	JF-122	JF-122	JF-122
Assemblage	gt, cpx	gt, cpx	gt-cpx-SiO$_2$	gt, corundum	gt, cpx	gt, cpx	gt	gt-opx-cpx	gt-opx-cpx	gt-opx-cpx
Paragenesis	eclogitic	eclogitic	eclogitic	eclogitic	eclogitic	eclogitic	eclogitic	websteritic	websteritic	websteritic
P_2O_5	0.02	0.02	0.03	≤ 0.01	0.02	≤ 0.01	0.03	0.03	≤ 0.01	≤ 0.01
SiO_2	40.1	55.7	40.2	40.4	41.1	54.4	40.4	41.2	54.0	55.3
TiO_2	0.25	0.36	0.33	0.22	0.39	0.37	0.25	0.35	0.05	0.04
Al_2O_3	22.5	9.44	22.2	23.0	22.3	6.74	22.8	19.7	1.01	0.57
Cr_2O_3	0.04	0.05	0.16	0.04	0.12	0.14	0.05	1.24	0.17	0.06
FeO	20.4	7.46	21.1	14.1	17.7	8.73	14.8	15.7	7.84	11.75
MnO	0.49	0.14	0.49	0.23	0.33	0.15	0.26	0.38	0.18	0.18
NiO	≤ 0.01	0.02	≤ 0.01	≤ 0.01	≤ 0.01	0.05	≤ 0.01	≤ 0.01	≤ 0.01	0.02
MgO	14.1	10.2	11.9	10.0	16.4	13.5	9.1	17.1	18.4	30.3
CaO	3.11	9.85	5.26	12.98	2.87	9.66	13.48	4.75	15.9	1.15
Na_2O	0.15	6.07	≤ 0.02	0.16	0.15	4.28	0.14	0.04	0.82	0.13
K_2O	≤ 0.01	0.09	≤ 0.01	≤ 0.01	≤ 0.01	0.19	≤ 0.01	≤ 0.01	≤ 0.01	≤ 0.01
Total	101.1	99.4	101.7	101.1	101.5	98.3	101.3	100.5	98.5	99.5
La [ppm]	0.02 (0.01)	1.12 (0.09)	0.01 (0.01)	0.24 (0.04)	0.02 (0.02)	1.71 (0.06)	0.05 (0.03)	0.01 (0.01)	0.22 (0.04)	0.00 (0.00)
Ce [ppm]	0.15 (0.02)	4.69 (0.13)	0.21 (0.07)	0.44 (0.11)	0.19 (0.08)	5.50 (0.37)	0.67 (0.08)	0.19 (0.04)	1.55 (0.16)	0.02 (0.02)
Pr [ppm]	0.06 (0.02)	0.86 (0.08)	0.10 (0.02)	0.08 (0.01)	0.09 (0.04)	1.31 (0.10)	0.38 (0.08)	0.11 (0.05)	0.38 (0.08)	0.00 (0.00)
Nd [ppm]	0.76 (0.07)	5.09 (0.25)	1.27 (0.14)	0.50 (0.14)	1.30 (0.10)	10.6 (0.49)	4.30 (0.25)	1.13 (0.12)	2.14 (0.19)	0.04 (0.02)
Sm [ppm]	0.79 (0.13)	1.49 (0.07)	1.31 (0.07)	0.53 (0.09)	1.51 (0.09)	3.69 (0.17)	2.33 (0.26)	0.95 (0.20)	0.64 (0.13)	0.03 (0.01)
Eu [ppm]	0.60 (0.08)	0.61 (0.07)	0.65 (0.06)	0.47 (0.08)	0.72 (0.05)	1.10 (0.12)	1.18 (0.10)	0.47 (0.16)	0.21 (0.08)	0.00 (0.00)
Gd [ppm]	2.38 (0.19)	1.29 (0.29)	3.26 (0.22)	1.79 (0.18)	3.21 (0.28)	2.25 (0.50)	3.18 (0.31)	2.33 (0.33)	0.57 (0.13)	0.02 (0.02)
Tb [ppm]	0.74 (0.09)	0.22 (0.07)	0.80 (0.11)	0.46 (0.14)	0.77 (0.08)	0.30 (0.06)	0.50 (0.15)	0.66 (0.10)	0.09 (0.06)	0.00 (0.00)
Dy [ppm]	6.89 (0.29)	1.50 (0.19)	7.21 (0.24)	3.13 (0.19)	5.47 (0.20)	1.73 (0.18)	3.40 (0.26)	6.15 (0.35)	0.56 (0.08)	0.03 (0.02)
Ho [ppm]	2.20 (0.17)	0.31 (0.06)	1.80 (0.16)	0.70 (0.11)	1.34 (0.08)	0.30 (0.06)	0.76 (0.11)	1.75 (0.17)	0.11 (0.05)	0.00 (0.00)
Er [ppm]	7.98 (0.20)	0.77 (0.11)	5.58 (0.56)	1.89 (0.22)	4.47 (0.24)	0.56 (0.09)	1.97 (0.26)	5.97 (0.57)	0.26 (0.13)	0.02 (0.01)
Tm [ppm]	1.27 (0.10)	0.07 (0.05)	0.81 (0.08)	0.26 (0.11)	0.69 (0.15)	0.03 (0.03)	0.24 (0.09)	0.97 (0.06)	0.05 (0.05)	0.01 (0.01)
Yb [ppm]	11.6 (0.47)	0.54 (0.16)	6.65 (0.49)	1.75 (0.33)	5.61 (0.58)	0.47 (0.12)	2.04 (0.34)	7.94 (0.41)	0.22 (0.13)	0.02 (0.02)
Lu [ppm]	1.75 (0.22)	0.06 (0.05)	0.85 (0.19)	0.20 (0.10)	0.93 (0.17)	0.03 (0.03)	0.26 (0.16)	1.34 (0.25)	0.01 (0.01)	0.00 (0.00)

7

Table 4-5: Major and trace element composition of majoritic garnet inclusions in diamonds from Jagersfontein. Major element composition (EPMA-analysis) are given as wt%. For the REE the standard deviations (1σ) are given.

Mineral	Maj. garnet	Maj. garnet	Maj. garnet	Maj. garnet	Maj. garnet	Maj. garnet	Maj. garnet	Maj. garnet	Maj. garnet	Maj. garnet	Maj. garnet	Maj. garnet
Comment	av. (n=2)			av. (n=2)			av. (n=2)			av. (n=2)	av. (n=2)	
Sample	JF-01	JF-09	JF-22	JF-37	JF-39	JF-42	JF-43	JF-44	JF-48	JF-55	JF-58	JF-84
Assemblage	2maj	maj	maj	2maj	maj	maj	maj, gt	maj	maj	2maj	maj	maj
Paragenesis	eclogitic	eclogitic	eclogitic	eclogitic	eclogitic	eclogitic	websteritic	eclogitic	eclogitic	eclogitic	eclogitic	eclogitic
P_2O_5	0.02	0.02	0.09	0.02	0.03	≤ 0.01	0.02	0.02	0.02	0.03	0.03	0.02
SiO_2	42.6	42.4	48.7	42.4	45.2	43.4	43.2	44.1	41.8	48.0	43.5	44.3
TiO_2	0.14	0.09	0.50	0.18	0.31	0.54	0.53	0.32	0.19	0.36	0.28	0.41
Al_2O_3	20.0	21.0	9.65	20.7	15.0	17.4	16.1	17.9	21.6	12.1	18.3	17.3
Cr_2O_3	0.24	0.08	0.22	0.13	0.24	0.03	3.47	0.31	0.11	0.36	0.18	0.30
FeO	12.6	14.1	11.7	12.9	10.8	12.9	11.7	11.8	13.8	9.3	14.7	11.7
MnO	0.42	0.40	0.36	0.38	0.24	0.36	0.39	0.30	0.40	0.25	0.41	0.31
NiO	≤ 0.01	≤ 0.01	≤ 0.01	≤ 0.01	≤ 0.01	0.02	≤ 0.01	≤ 0.01	≤ 0.01	0.02	0.02	≤ 0.01
MgO	17.6	16.2	21.7	16.9	20.3	13.4	20.0	17.7	16.2	22.0	18.3	18.8
CaO	6.14	6.11	5.73	6.43	5.67	11.16	3.89	7.97	5.89	7.33	4.62	6.36
Na_2O	0.15	0.20	0.65	0.14	0.37	0.54	0.12	0.18	0.13	0.43	0.27	0.30
K_2O	≤ 0.01	≤ 0.01	≤ 0.01	≤ 0.01	≤ 0.01	0.02	≤ 0.01	≤ 0.01	≤ 0.01	0.02	≤ 0.01	≤ 0.01
Total	99.8	100.6	99.4	100.1	98.1	99.7	99.4	100.6	100.1	100.2	100.5	99.7
La [ppm]	0.01 (0.01)	0.00 (0.00)	0.00 (0.00)	0.02 (0.02)	0.06 (0.02)	0.06 (0.03)	0.01 (0.01)	0.01 (0.01)	0.01 (0.01)	0.01 (0.01)	0.02 (0.02)	0.05 (0.02)
Ce [ppm]	0.10 (0.06)	0.09 (0.04)	0.10 (0.04)	0.12 (0.06)	0.35 (0.07)	0.86 (0.09)	0.02 (0.02)	0.12 (0.05)	0.03 (0.03)	0.14 (0.07)	0.21 (0.07)	0.23 (0.05)
Pr [ppm]	0.05 (0.03)	0.02 (0.02)	0.10 (0.04)	0.08 (0.04)	0.08 (0.02)	0.45 (0.05)	0.02 (0.02)	0.05 (0.02)	0.02 (0.02)	0.08 (0.05)	0.12 (0.04)	0.10 (0.02)
Nd [ppm]	0.72 (0.10)	0.39 (0.07)	1.04 (0.19)	0.81 (0.11)	0.76 (0.16)	4.05 (0.31)	0.21 (0.04)	0.64 (0.08)	0.42 (0.06)	0.96 (0.14)	1.54 (0.18)	1.15 (0.13)
Sm [ppm]	0.84 (0.11)	0.38 (0.05)	1.33 (0.19)	1.74 (0.23)	0.55 (0.15)	2.17 (0.15)	0.24 (0.06)	0.56 (0.12)	0.83 (0.17)	0.81 (0.15)	2.22 (0.27)	1.42 (0.08)
Eu [ppm]	0.39 (0.06)	0.09 (0.03)	0.37 (0.06)	0.68 (0.10)	0.19 (0.03)	0.72 (0.09)	0.09 (0.03)	0.26 (0.05)	0.37 (0.10)	0.29 (0.06)	0.82 (0.18)	0.55 (0.07)
Gd [ppm]	3.86 (0.37)	0.74 (0.10)	2.61 (0.13)	5.20 (0.35)	1.31 (0.18)	5.06 (0.25)	0.52 (0.10)	1.53 (0.16)	3.54 (0.20)	1.55 (0.15)	5.33 (0.34)	2.85 (0.23)
Tb [ppm]	1.21 (0.11)	0.21 (0.05)	0.67 (0.05)	1.35 (0.12)	0.36 (0.06)	1.34 (0.11)	0.16 (0.07)	0.45 (0.11)	0.99 (0.10)	0.39 (0.10)	1.32 (0.23)	0.74 (0.08)
Dy [ppm]	12.6 (0.53)	2.09 (0.17)	6.28 (0.28)	12.1 (0.47)	3.19 (0.18)	11.8 (0.55)	1.23 (0.13)	5.30 (0.25)	9.13 (0.36)	3.17 (0.38)	11.55 (0.49)	5.23 (0.40)
Ho [ppm]	3.22 (0.21)	0.62 (0.07)	1.71 (0.17)	3.39 (0.18)	0.81 (0.06)	3.37 (0.23)	0.33 (0.07)	1.66 (0.27)	2.31 (0.23)	0.82 (0.12)	3.25 (0.36)	1.35 (0.10)
Er [ppm]	11.0 (0.57)	2.38 (0.16)	6.25 (0.34)	12.1 (0.41)	3.37 (0.05)	11.1 (0.36)	1.16 (0.13)	6.97 (0.66)	8.11 (0.37)	2.38 (0.29)	11.92 (0.74)	5.14 (0.25)
Tm [ppm]	1.65 (0.24)	0.46 (0.07)	1.12 (0.13)	2.05 (0.22)	0.53 (0.07)	1.80 (0.18)	0.20 (0.05)	1.28 (0.14)	1.26 (0.16)	0.39 (0.10)	1.94 (0.18)	0.80 (0.09)
Yb [ppm]	12.4 (0.89)	3.94 (0.34)	8.41 (0.50)	16.0 (0.44)	4.60 (0.41)	13.5 (0.87)	1.80 (0.21)	10.7 (0.83)	9.85 (0.56)	2.95 (0.23)	16.6 (0.46)	7.29 (0.43)
Lu [ppm]	1.78 (0.20)	0.74 (0.12)	1.22 (0.14)	2.41 (0.40)	0.70 (0.15)	1.92 (0.20)	0.28 (0.11)	1.87 (0.18)	1.54 (0.19)	0.38 (0.10)	2.50 (0.33)	1.12 (0.16)

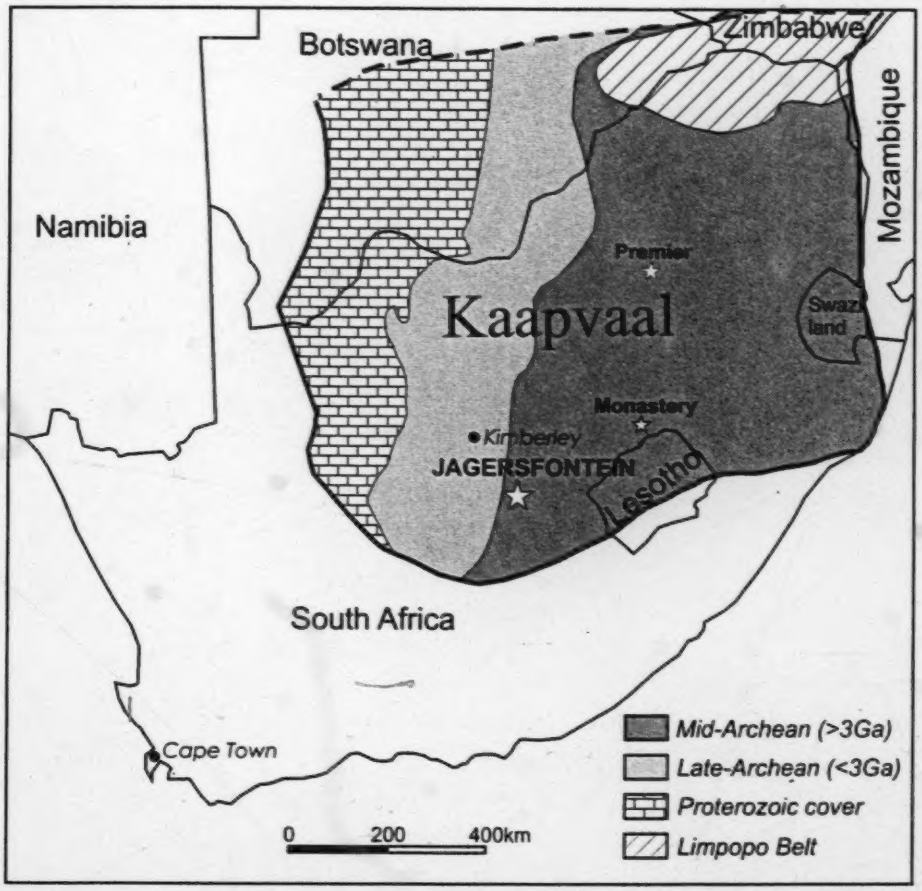
Botswana
Zimbabwe
Mozambique
Namibia
Premier
Kaapvaal
Swaziland
Monastery
Kimberley
JAGERSFONTEIN
Lesotho
South Africa
Cape Town
0
200
400km
Mid-Archean (>3Ga)
Late-Archean (<3Ga)
Proterozoic cover
Limpopo Belt

Figure 4-1: Location of the Jagersfontein kimberlite and other diamond deposits on the Kaapvaal cratonic block (Monastery, Premier) from which majoritic garnet inclusions in diamonds have been described. Geological map modified after De Wit et al. (1992)

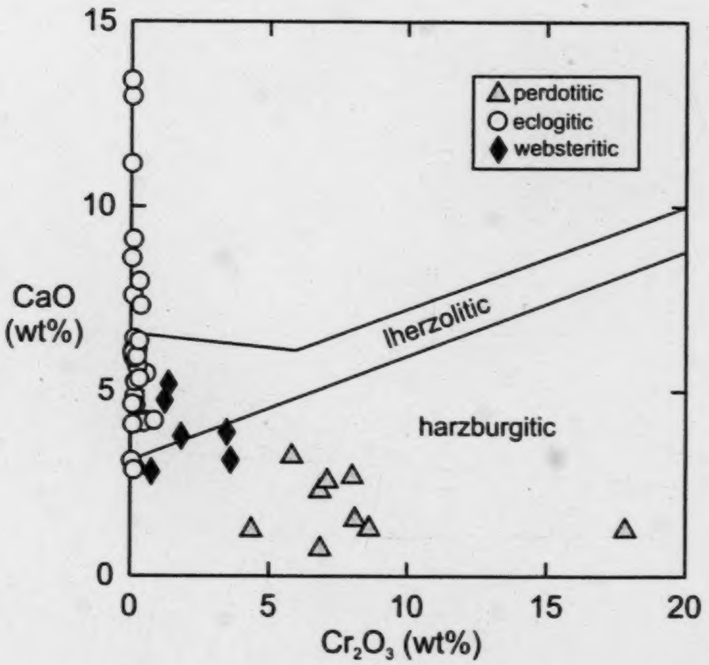

Figure 4-2: The composition of CaO versus Cr_2O_3 of garnet inclusions in diamonds from Jagersfontein. Note that eclogitic and websteritic garnet inclusions have Mg-numbers of <80, whereas the Mg-number of peridotitic garnets is >80. The compositional field for lherzolitic garnets after Sobolev *et al.* (1973).

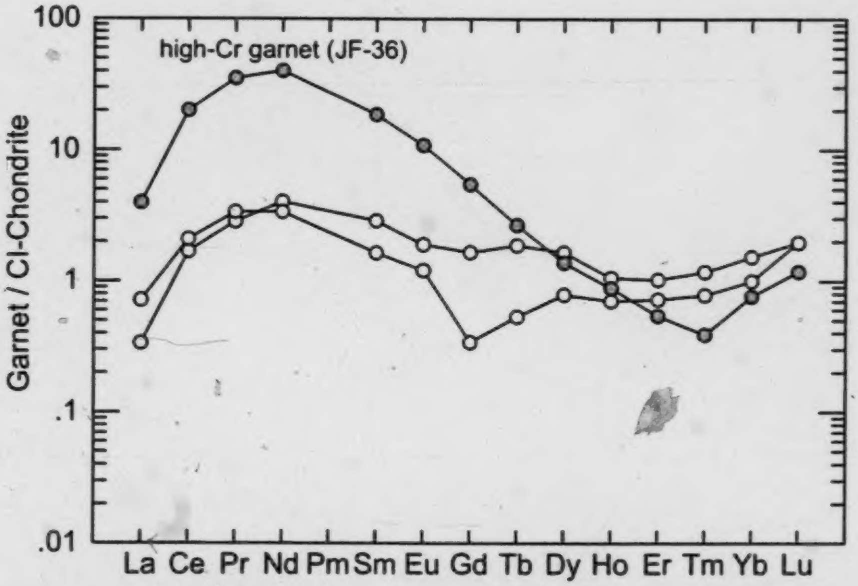

Figure 4-3: Rare earth element composition of peridotitic garnet inclusions from Jagersfontein diamonds. Normalized to chondrite composition (McDonough & Sun, 1995)

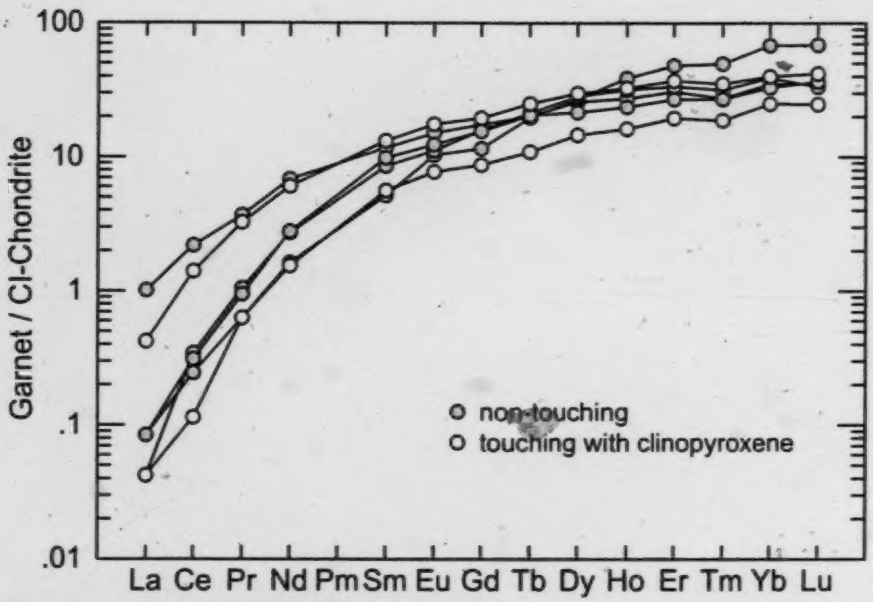

Figure 4-4: Chondrite normalized rare earth element composition of eclogitic garnet inclusions in diamonds from Jagersfontein.

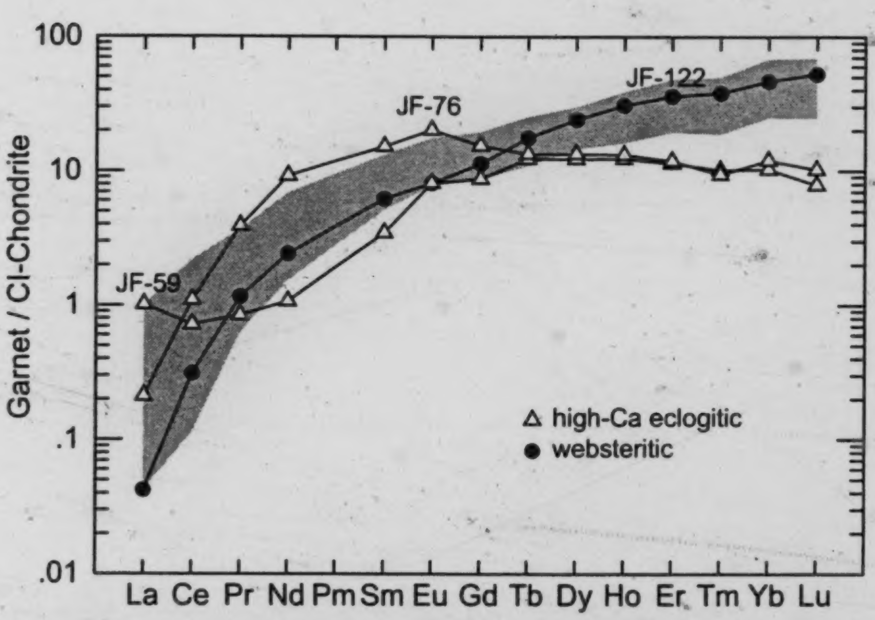

Figure 4-5: Chondrite normalized rare earth element composition of websteritic and high-calcium (>13 wt% CaO) eclogitic garnet inclusions in diamonds from Jagersfontein. The *shaded area* marks the compositional field of eclogitic garnet inclusions with lower calcium contents (Fig. 4-4). The websteritic garnet inclusion from diamond JF-43 was found in association with a majoritic garnet.

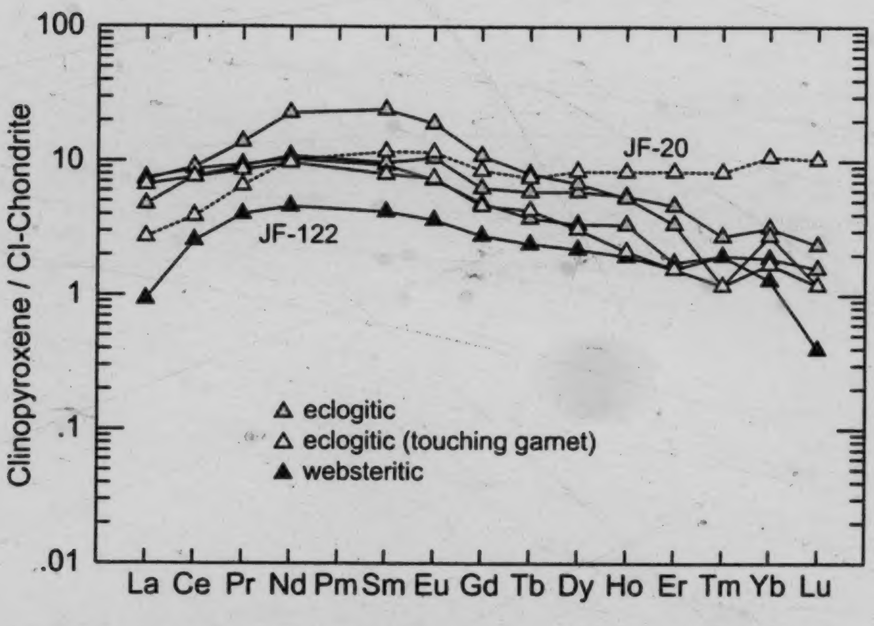

Figure 4-6: Chondrite normalized rare earth element composition of clinopyroxene inclusions in diamonds from Jagersfontein.

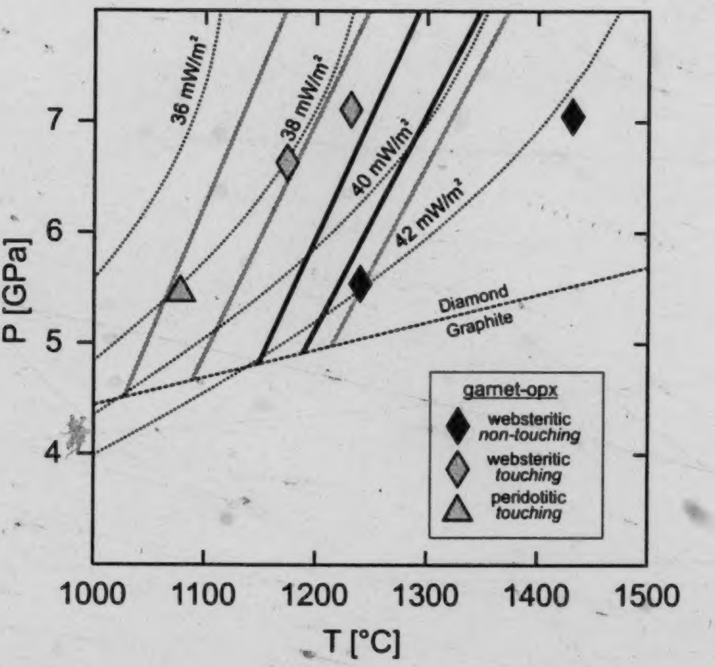

Figure 4-7: Results of geothermobarometric calculations for garnet-opx inclusion pairs from Jagersfontein diamonds (*diamond symbol and triangle*) calculated after Harley (1984) and Brey & Köhler (1990). The *bold lines* represents the range of temperatures at given pressures calculated for touching (*grey*) and non-touching (*black*) eclogitic garnet-clinopyroxene pairs (Krogh, 1988) recovered from Jagersfontein diamonds. The dotted lines indicate conductive geotherms for various surface heat flow values calculated after Pollack & Chapman (1977). Graphite-diamond phase boundary from Kennedy & Kennedy (1976).

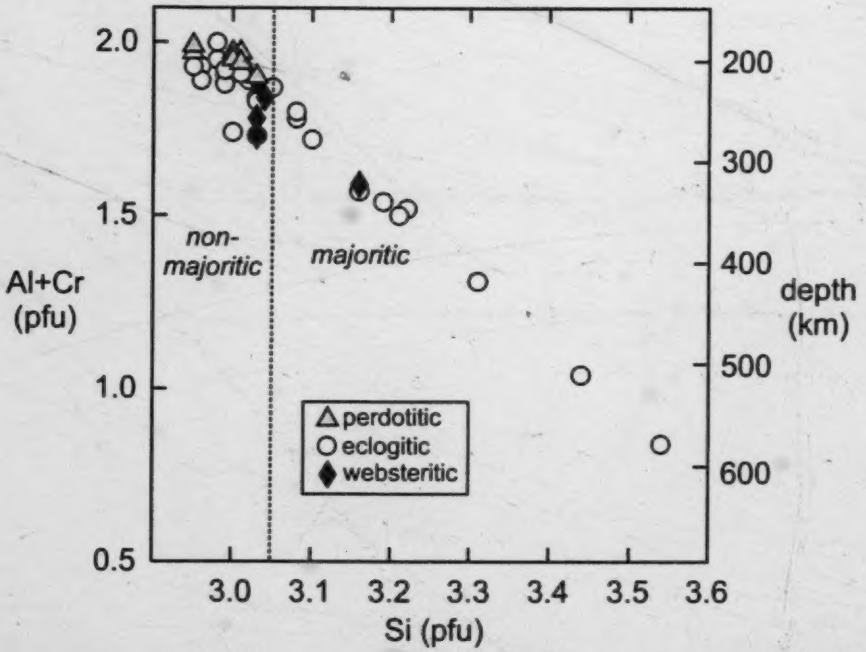

Figure 4-8: Al+Cr versus Si (per formula unit) of garnet inclusions from Jagersfontein diamonds. The majorite component is described in terms of silicon excess which represents the extent of pyroxene solution in the garnet structure, with non-majoritic garnets having silicon contents of 3.0 Si per formula unit (pfu) and pure end-member majorite having 4.0 Si pfu. The *dashed line* at 3.05 Si per formula unit (pfu) marks our cut-off line for a significant majorite component. Estimates for the depth of origin (right axis) are based on experimental data from Irifune (1987).

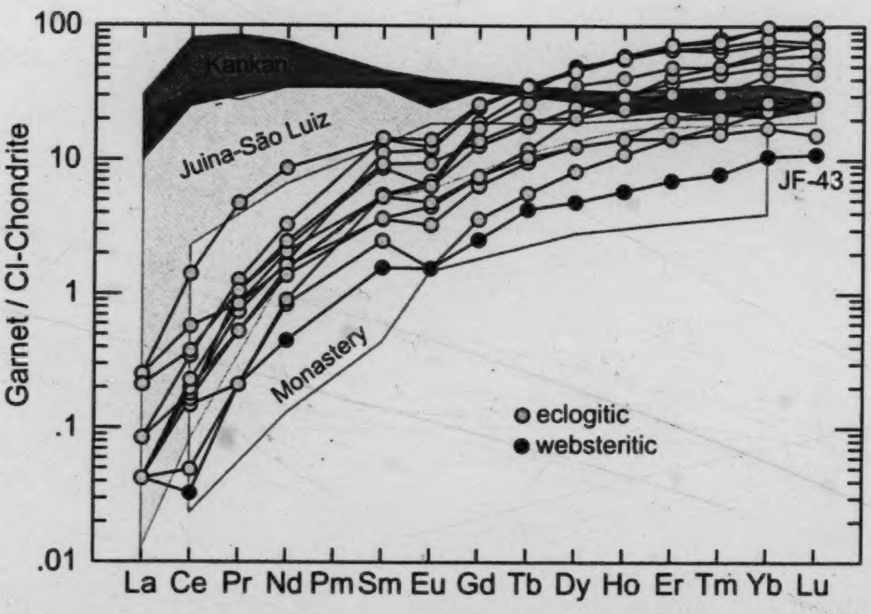

Figure 4-9: Chondrite normalized rare earth element composition of majoritic garnet inclusions in diamonds from Jagersfontein. The compositional fields for majoritic garnet inclusions in diamonds from Kankan, Guinea (Stachel et al., 2000a), the Juina-São Luiz area, Brazil (Wilding, 1990; Hutchison et al., 1997; Harte et al. 1999; Kaminsky et al. 2001), and Monastery, South Africa (Moore et al. 1990) are show for comparison.

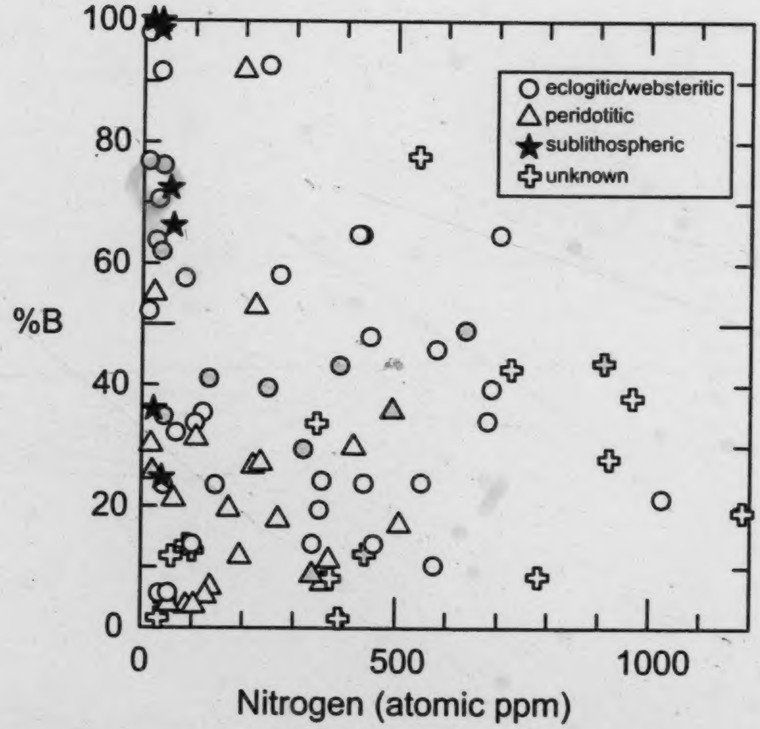

Figure 4-10: Aggregation level (percentage of higher aggregated B-center relative to the A-center) versus nitrogen concentration (atomic ppm) in Jagersfontein diamonds. *Grey symbols* mark diamonds that show evidence for plastic deformation (e.g. deformation lines, brown body color).

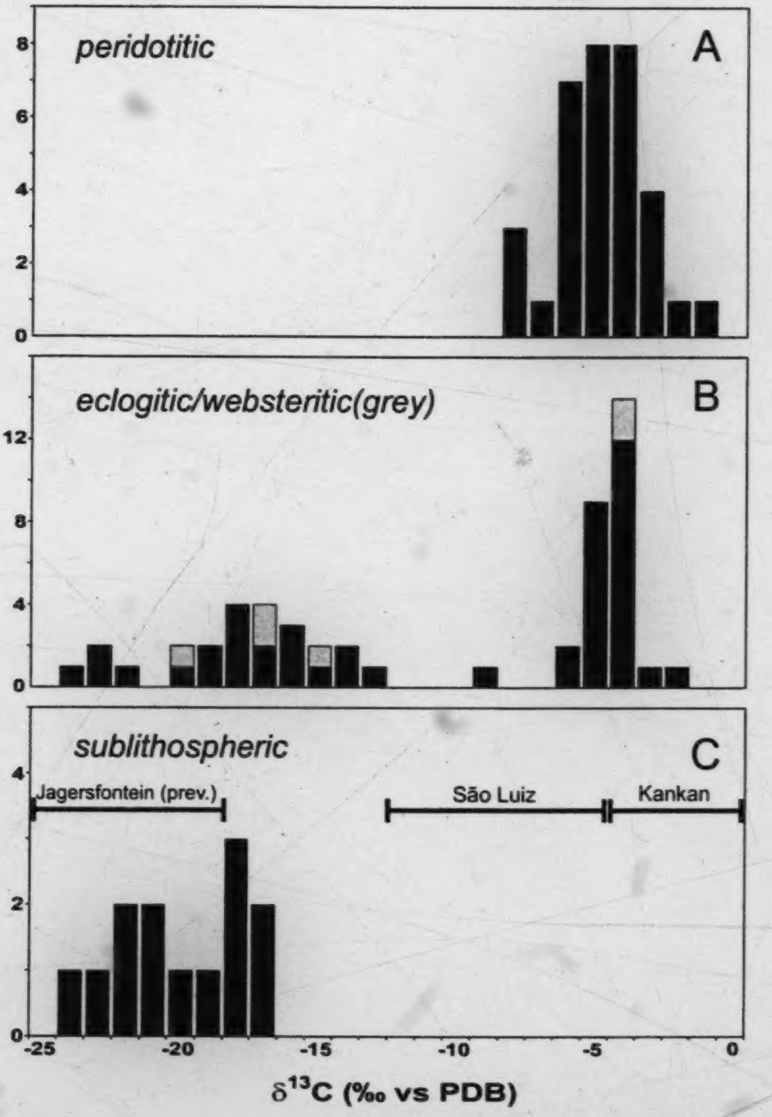

Figure 4-11: Carbon isotopic composition of (A) peridotitic, (B) eclogitic and websteritic, (C) majoritic garnet-bearing, sublithospheric diamonds from Jagersfontein. The *black bars* show the range of isotopic compositions of majoritic garnet bearing diamonds from Kankan (Stachel et al. 2002), São Luiz (Wilding, 1990; Hutchison et al., 1999) and previous results from Jagersfontein (Deines et al., 1991).

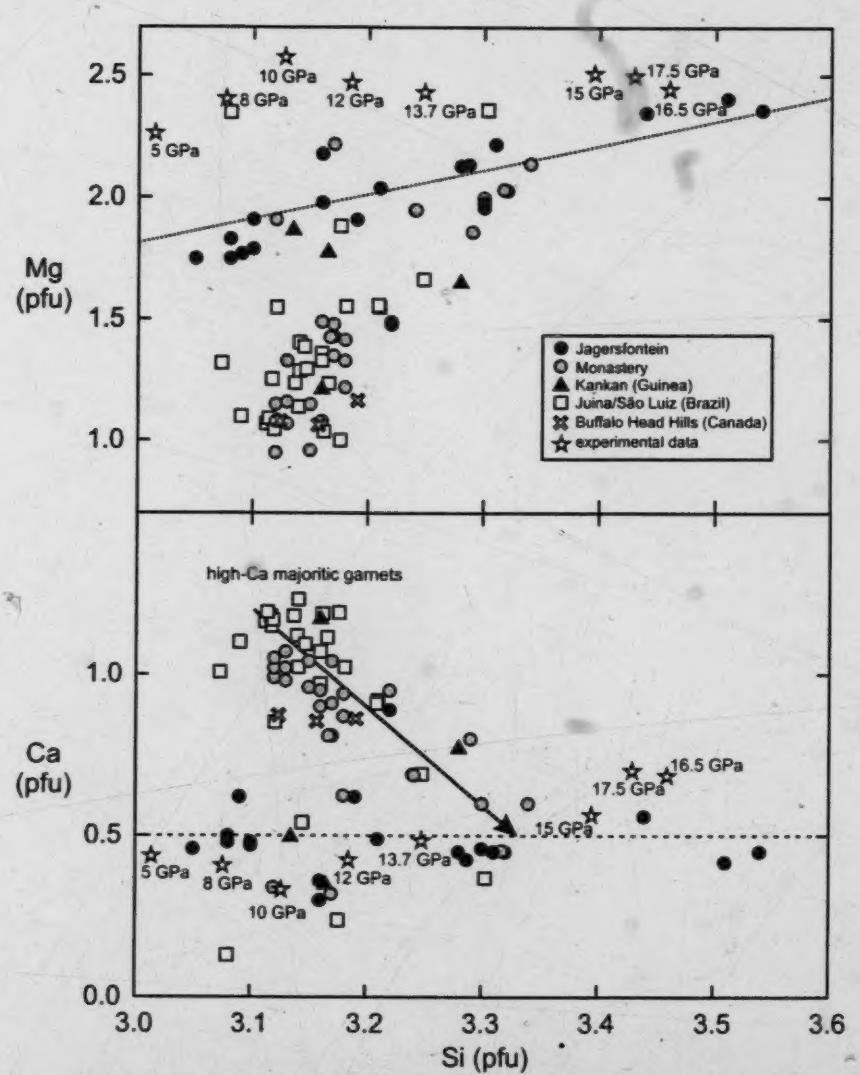

Figure 4-12: Composition of majoritic garnet inclusions in diamonds from Jagersfontein (calculated for 12 oxygen) and comparison with available data for majoritic garnet inclusions (eclogitic only) in diamonds from other deposits worldwide. Also shown is the composition of majoritic garnets synthesized in high pressure experiments (pressures given) by Irifune (1987). The *dotted line* indicates the expected slope for the coupled substitution of Si and Mg for 2 Al in majoritic garnet. The *dashed line* marks the average Ca content of majoritic garnet inclusions in Jagersfontein diamonds. The arrow indicates the proposed melt depletion trend (see text). Compositional data from Jagersfontein: Tsai et al. (1979), Deines et al. (1991), this study; Monastery: Moore et al. (1989), Moore and Gurney (1991); Kankan: Stachel et al. (2000b); São Luiz: Wilding (1990), Harte (1992), Hutchison (1997), Kaminsky et al. (2001); Buffalo Head Hills: Davies et al. (2004).

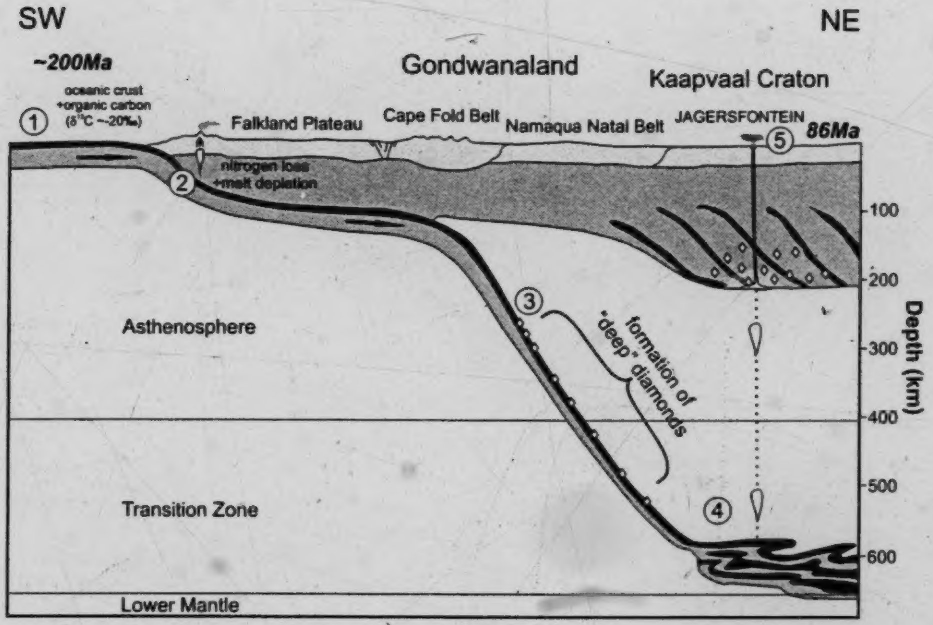
SW
NE
~200Ma
Gondwanaland
Kaapvaal Craton
①
oceanic crust
+organic carbon
(δ13C ~-20‰)
Falkland Plateau
Cape Fold Belt
Namaqua Natal Belt
JAGERSFONTEIN
⑤
86Ma
②
nitrogen loss
+melt depletion
100
200
③
formation of "deep" diamonds
Asthenosphere
300
400
Depth (km)
500
Transition Zone
④
600
Lower Mantle

Figure 4-13: Cross section of southwestern Gondwanaland from ~200 to 86 Ma, illustrating the processes that may have led to the formation of the "deep", sublithospheric diamonds. 1: Deposition of biogenic carbon-rich sediments on oceanic crust. 2: Subduction of the oceanic plate beneath southern Gondwanaland, leading to the conversion of organic carbon to graphite and contemporaneous nitrogen release. Partial melting of the subducting slab. 3: Continuation of subduction into the deeper asthenosphere and onset of the formation of majoritic garnet-bearing diamonds. 4: Formation of a megalith beneath the Kaapvaal craton from which melts (containig the "deep" diamonds) ascend to the base of the lithosphere and the Earth's surface. 5: Kimberlite emplacement.

CHAPTER 5

Subducting oceanic crust: The source of deep diamonds

The content of this chapter, in modified form, has been accepted for publication in *Geology* as:

Tappert, R., Stachel, T., Harris, J.W., Muehlenbachs, K., Ludwig, T., Brey, G.P.: Subducting oceanic crust: The source of deep diamonds

5.1 Introduction

At depths exceeding 250 km, pyroxene in Earth's mantle begins to dissolve into garnet, creating a majorite component that is chemically characterized by an excess of silicon (>3.0 Si per formula unit) (Ringwood, 1967; Akaogi and Akimoto, 1977; Irifune, 1987). Rare inclusions of majoritic garnet have been observed in diamonds from a number of mines, indicating that these diamonds formed much deeper than most other diamonds. Contrary to the expected composition of the deep mantle, majoritic garnet inclusions are rarely peridotitic and almost exclusively eclogitic in paragenesis (Stachel, 2001), indicating a basaltic source composition. The nature of this basaltic source in the sublithospheric mantle is controversial. It has been interpreted as being a discrete, 200-km-thick eclogitic layer within Earth's upper mantle (Gasparik, 2002); as precipitations from alkaline melts like kimberlites or ocean island basalts at great depths (Moore et al., 1991); and as subducted oceanic crust (Ringwood, 1991; Stachel et al., 2000). Each model has far-reaching implications for the dynamics of Earth's mantle.

To resolve the origin of the deep, majorite-bearing diamonds, a study on diamonds from the Jagersfontein kimberlite, South Africa, has been carried out which combined the precise determination of rare earth element (REE) concentrations of majoritic garnet inclusions with the carbon isotopic composition of their diamond hosts.

5.2 Methods

The measurements of the REE concentrations were performed on a Cameca ims-3f ion probe at the Universität Heidelberg. The primary beam was a 14.5 keV oxygen ion beam with a current of 20 nA and a lateral resolution of ~25 μm. Isotopes in the mass range from ^{138}La to ^{176}Lu were analyzed at a mass resolution (m/Δm) of 370. An energy window was set to 105 ± 25eV (energy filtering) in order to minimize molecular interferences. The acquired spectra were deconvoluted to separate the REE atomic ions from interfering REE oxides. The NIST SRM610 glass was used as primary standard, and additional analyses of well-characterized garnet megacrysts (PN-1 and -2) were performed to assure accuracy.

The carbon stable isotope composition of the diamonds was determined with a Finnigan MAT 252 mass spectrometer at the University of Alberta after combusting ~1 mg of inclusion free diamond cleavage chips at 1000 °C for ~12 h. The data are reported in the usual delta notation with respect to the Peedee belemnite standard.

5.3 Results

Including previous work (Deines et al., 1991), garnet inclusions in diamonds from the Jagersfontein kimberlite show the largest range in the majorite component observed to date. By using 3.05 Si atoms per formula unit (pfu) as a minimum value for a majorite component, majoritic garnets have been recovered from 12 diamonds, ranging up to 3.54 silicon pfu (Fig. 1). These compositions correspond to depths of ~250 to ≥500 km according to the experiments of Irifune (1987) (Fig. 1). The REE composition of the majoritic garnets is characterized by subchondritic to chondritic light REE and 10–100 times chondritic heavy REE (Fig. 2). More importantly, all majoritic garnets show pronounced negative Eu anomalies (Eu/Eu* 0.51–0.82), unlike all nonmajoritic garnets from the same kimberlite.

The host diamonds of the majoritic garnets have carbon isotope compositions ($\delta^{13}C$) that fall into a narrow range between –17 and –24‰ (Fig. 3A). This coincides with the range of five previous analyses from Jagersfontein (Deines et al., 1991) (Fig. 3A). Majoritic garnet-bearing diamonds from São Luiz, Brazil (Wilding, 1990;

Hutchison et al., 1999; Kaminsky et al., 2001), and Kankan, Guinea (Stachel et al., 2002), are isotopically heavier (less negative values of $\delta^{13}C$) than the Jagersfontein samples but also show narrow ranges in $\delta^{13}C$ (Fig. 3A). In contrast to the diamonds that contain majoritic garnet, the lithospheric diamonds from Jagersfontein that belong to the eclogite suite show a broad isotopic range with a bimodal $\delta^{13}C$ distribution (Fig. 3B). Such ranges and distributions are characteristic for the eclogitic diamond population of many other deposits worldwide (Kirkley et al., 1991). The pronounced difference in the isotopic composition of deep, majoritic garnet-bearing diamonds and diamonds from the shallower lithosphere indicates distinct carbon sources and/or distinct fractionation mechanisms.

5.4 Discussion

It is generally accepted that negative Eu anomalies are caused by the fractionation of feldspar (Philpotts and Schnetzler, 1968; Kay et al., 1970). Because feldspar is not stable at pressures above ~2 GPa, Eu anomalies provide evidence for a low pressure (i.e., crustal) origin of the source of the majoritic garnets. Negative Eu anomalies are commonly found in midocean ridge basalts in the upper portion of typical oceanic crust. The negative Eu anomalies in the majoritic garnet inclusions therefore establish a link between the deep diamond sources and shallow basaltic precursors. In the framework of plate tectonics, basaltic oceanic crust is recycled back into Earth's mantle through the process of subduction.

Because diamonds with $\delta^{13}C$ below -10‰ fall into the compositional range of organic matter (Schidlowski et al., 1983) (Fig. 3C), it has been proposed that isotopically light diamonds form directly from subducted organic carbon (Kirkley et al., 1991; McCandless and Gurney, 1997). Cartigny et al. (1998), on the other hand, used the nitrogen isotopic composition of diamonds to show that there is no link between diamonds and subducted organic carbon. Rather, it was suggested that the isotopically light carbon in Earth's mantle is the result of fractionation processes (Galimov, 1991; Cartigny et al., 1998; Deines, 2002). These conclusions, however, are made solely on the basis of lithospheric diamonds and cannot be applied to sublithospheric diamonds, for which nitrogen isotopic data are not available. The lack of such data is mainly the result of exclusively low nitrogen abundances or the complete absence of detectable nitrogen in majoritic garnet-bearing diamonds, as previously shown for diamonds from Jagersfontein (Deines et al., 1991), São Luiz (Hutchison et al., 1999), and Kankan (Stachel et al., 2002). The absence of nitrogen in these deep diamonds is most likely the result of efficient removal of nitrogen from slabs, which has been shown to occur in the early stages of the subduction process; nitrogen is thereby cycled back into the atmosphere by arc volcanism (Fischer et al., 2002).

The distinctively narrow carbon isotope ranges (Fig. 3A) combined with the large depth range of majoritic garnet-bearing diamonds (Fig. 1) shows that isotopic fractionation cannot be responsible for the isotopically light composition of sublithospheric diamonds. In the case of Jagersfontein, negative Eu anomalies in all majoritic garnet inclusions, coupled with an exclusively light carbon isotopic composition of the host diamonds (Fig. 3A), suggest that the deep diamonds are derived from crustal organic matter. This organic matter may have been derived from intercalated sediments within the subducted slab or from in situ microbial activity, which has been shown to penetrate oceanic rocks (Furnes et al., 2004).

If all majoritic garnet-bearing diamonds at Jagersfontein, São Luiz, and Kankan formed from subducted carbon, variations between different deposits are still to be expected because oceanic crust varies in its proportions of carbonate ($\delta^{13}C$ of ~0‰; see Schidlowski et al., 1983) to organic matter (40 to −10‰) depending on depositional environment and geographic setting (Jenkyns, 1986). Such compositional variability is reflected in the carbon isotopic composition of majoritic garnet-bearing diamonds worldwide, with Kankan (Stachel et al., 2002) possibly reflecting a carbonate-rich end member. The contrast of $\delta^{13}C$ values between the different diamond deposits also shows that the subducted carbon reservoirs have not homogenized.

The formation of majoritic garnet-bearing diamonds directly from subducted organic matter is problematic because they form deep within the diamond stability field, rather than at ~120 km, which is the depth at which a subducting slab enters the diamond stability field (Green and Falloon, 1998). However, high-pressure experiments on diamond synthesis (Irifune et al., 2003) show that metastable graphite persists to very high pressures (12–25 GPa, equivalent to ~350–700 km) before converting to diamond. This suggests that these very deep diamonds might form directly from graphite, whereas their lithospheric counterparts may form from CHO fluids (Deines, 2002).

5.5 Conclusion

The results presented here support a model in which the eclogitic paragenesis of majoritic garnet inclusions is related to diamond formation in subducting slabs over an extended depths range (~250 to >500 km) rather than in an isolated eclogitic layer within Earth's upper mantle. Inclusions in such ultradeep diamonds document the subduction process of slabs as they descend through the asthenosphere and transition zone. The major- and trace-element patterns of these inclusions establish boundary conditions for the compositional changes that occur during slab dehydration and melting. The presence of uniform (unexsolved) majoritic garnet inclusions in diamonds from Jagersfontein also shows that ancient slab material was present in the transition zone at the time of kimberlite emplacement (86 Ma). From there, the diamonds were entrained into a rapidly ascending kimberlite; otherwise, exsolution of pyroxene from the majoritic garnets would have occurred.

The compositional and isotopic variability of majoritic garnet-bearing diamonds worldwide indicates that subduction carries compositionally heterogeneous material into the deep mantle and that recycling of such heterogeneous material back into the mantle creates chemically distinct domains that do not equilibrate with time.

Bibliography

Akaogi, M., and Akimoto, S., 1977, Pyroxene-garnet solid-solution equilibria in the systems $Mg_4Si_4O_{12}$-$Mg_3Al_2Si_3O_{12}$ and $Fe_4Si_4O_{12}$-$Fe_3Al_2Si_3O_{12}$ at high pressures and temperatures: Physics of the Earth and Planetary Interiors, v. 15, p. 90–106.

Cartigny, P., Harris, J.W., and Javoy, M., 1998, Eclogitic diamond formation at Jwaneng: No room for a recycled component: Science, v. 280, p. 1421–1424.

Deines, P., 2002, The carbon isotope geochemistry of mantle xenoliths: Earth Science Reviews, v. 58, p. 247–278.

Deines, P., Harris, J.W., and Gurney, J.J., 1991, The carbon isotopic composition and nitrogen content of lithospheric and asthenospheric diamonds from the Jagersfontein and Koffiefontein kimberlite, South Africa: Geochimica et Cosmochimica Acta, v. 55, p. 2615–2625.

Fischer, T.P., Hilton, D.R., Zimmer, M.M., Shaw, A.M., Sharp, Z.D., and Walker, J.A., 2002, Subduction and recycling of nitrogen along the Central American margin: Science, v. 297, p. 1154–1157.

Furnes, H., Banerjee, N.R., Muehlenbachs, K., Staudigel, H., and de Wit, M., 2004, Early life recorded in Archean pillow lavas: Science, v. 304, p. 578–581.

Galimov, E.M., 1991, Isotope fractionation related to kimberlite magmatism and diamond formation: Geochimica et Cosmochimica Acta, v. 55, p. 1697–1708.

Gasparik, T., 2002, Experimental investigation of the origin of majoritic garnet inclusions in diamonds: Physics and Chemistry of Minerals, v. 29, p. 170–180.

Green, D.H., and Falloon, T.J., 1998, Pyrolite: A Ringwood concept and its current expression, *in* Jackson, I., ed., The Earth's mantle: Cambridge, Cambridge University Press, p. 311–378.

Hutchison, M.T., Cartigny, P., and Harris, J.W., 1999, Carbon and nitrogen composition and physical characteristics of transition zone and lower mantle diamonds from São Luiz, Brazil, *in* Gurney, J.J., et al., eds., The J.B. Dawson Volume: Proceedings of the 7th International Kimberlite Conference: Capetown, Red Roof Design, p. 372–382.

Irifune, T., 1987, An experimental investigation of the pyroxene-garnet transformation in a pyrolite composition and its bearing on the constitution of the mantle: Physics of the Earth and Planetary Interiors, v. 45, p. 324–336.

Irifune, T., Kurio, A., Sakamoto, S., Inoue, T., and Sumiya, H., 2003, Ultrahard polycrystalline diamond from graphite: Nature, v. 421, p. 599–600.

Jenkyns, H.C., 1986, Pelagic environments, *in* Reading, H.G., ed., Sedimentary environments and facies: Oxford, Blackwell, p. 343397.

Kaminsky, F.V., Zakharchenko, O.D., Davies, R.M., Griffin, W.L., Khachatryan-Blinova, G.K., and Shiryaev, A.A., 2001, Superdeep diamonds from the Juina area, Mato Grosso State, Brazil: Contributions to Mineralogy and Petrology, v. 140, p. 734753.

Kay, R., Hubbard, N.J., and Gast, P.W., 1970, Chemical characteristics and origin of oceanic ridge volcanic rocks: Journal of Geophysical Research, v. 75, p. 1585–1613.

Kirkley, M.B., Gurney, J.J., Otter, M.L., Hill, S.J., and Daniels, L.R., 1991, The application of C isotope measurements to the identification of the sources of C in diamondsA-review: Applied Geochemistry, v. 6, p. 477494.

McCandless, T.E., and Gurney, J.J., 1997, Diamond eclogites: Comparison with carbonaceous chondrites, carbonaceous shales, and microbial carbon-enriched MORB, *in* Sobolev, N.V., and Mitchell, R.H., eds., 6th International Kimberlite Conference, Volume 2: Diamonds: Characterization, genesis and exploration, Russian geology and geophysics: New York, Allerton Press, v. 38, p. 394404.

Moore, R.O., Gurney, J.J., Griffin, W.L., and Shimizu, N., 1991, Ultra-high pressure garnet inclusions in Monastery diamondsTrace-element abundance patterns and conditions of origin: European Journal of Mineralogy, v. 3, p. 213230.

Philpotts, J.A., and Schnetzler, C.C., 1968, Europium anomalies and the genesis of basalt: Chemical Geology, v. 3, p. 513.

Ringwood, A.E., 1967, The pyroxene garnet transformation in the earth's mantle: Earth and Planetary Science Letters, v. 2, p. 255263.

Ringwood, A.E., 1991, Phase transformations and their bearing on the constitution and dynamics of the mantle: Geochimica et Cosmochimica Acta, v. 55, no. 8, p. 20832110.

Schidlowski, J.M., Hayes, J.M., and Kaplan, I.R., 1983, Isotopic inferences of ancient biochemistries: Carbon, sulfur, hydrogen, and nitrogen, *in* Schopf, J.W., ed., Earth's earliest biosphere: Princeton, Princeton University Press, p. 149186.

Chapter 5

Stachel, T., 2001, Diamonds from the asthenosphere and the transition zone: European Journal of Mineralogy, v. 13, p. 883892.

Stachel, T., Brey, G.P., and Harris, J.W., 2000, Kankan diamonds (Guinea) I: From the lithosphere down to the transition zone: Contributions to Mineralogy and Petrology, v. 140, p. 1-15.

Stachel, T., Harris, J.W., Aulbach, S., and Deines, P., 2002, Kankan diamonds (Guinea) III: $\delta^{13}C$ and nitrogen characteristics of deep diamonds: Contributions to Mineralogy and Petrology, v. 142, p. 465475.

Wilding, M.C., 1990, [untitled PhD thesis] University of Edinburgh, 281 p.

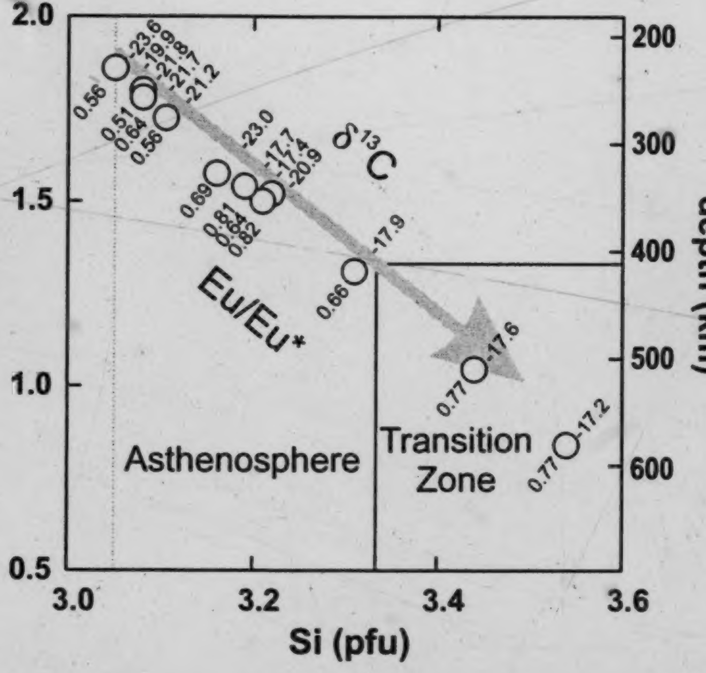

Figure 5-1: Atomic proportions of Al+Cr versus Si (per formula unit (pfu) at [O]=12) of majoritic garnet inclusions in diamonds from the Jagersfontein kimberlite (open circles). The arrow indicates the direction of increasing majorite component. Also given are values for the Eu-anomalies (Eu/Eu*) of the majoritic garnet inclusions and the carbon isotope composition (δ^{13}C vs. PDB) of the host diamonds. Approximate depth estimates are based on experimental results carried out at 1200°C (Irifune, 1987). The dashed line marks our cut-off value (3.05 Si) for a significant majorite component.

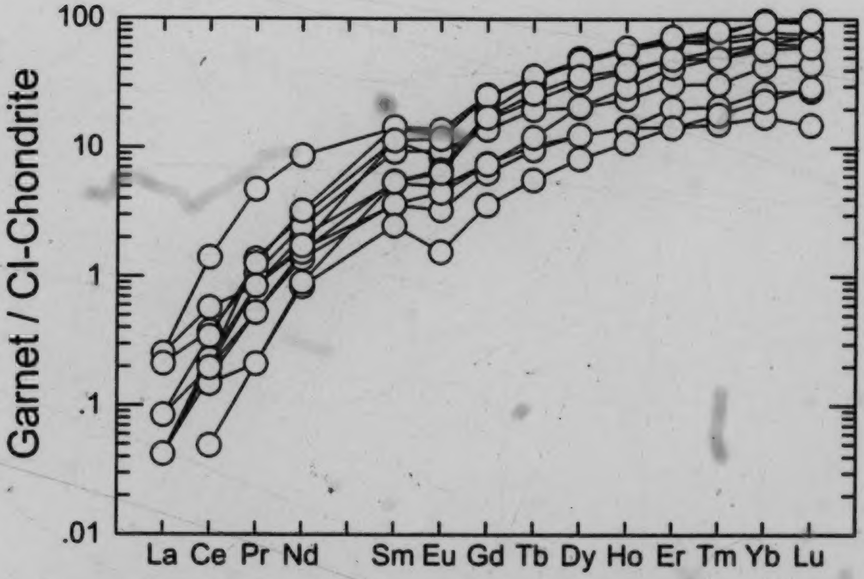

Figure 5-2: Chondrite normalized rare earth element composition of majoritic garnet inclusions in Jagersfontein diamonds.

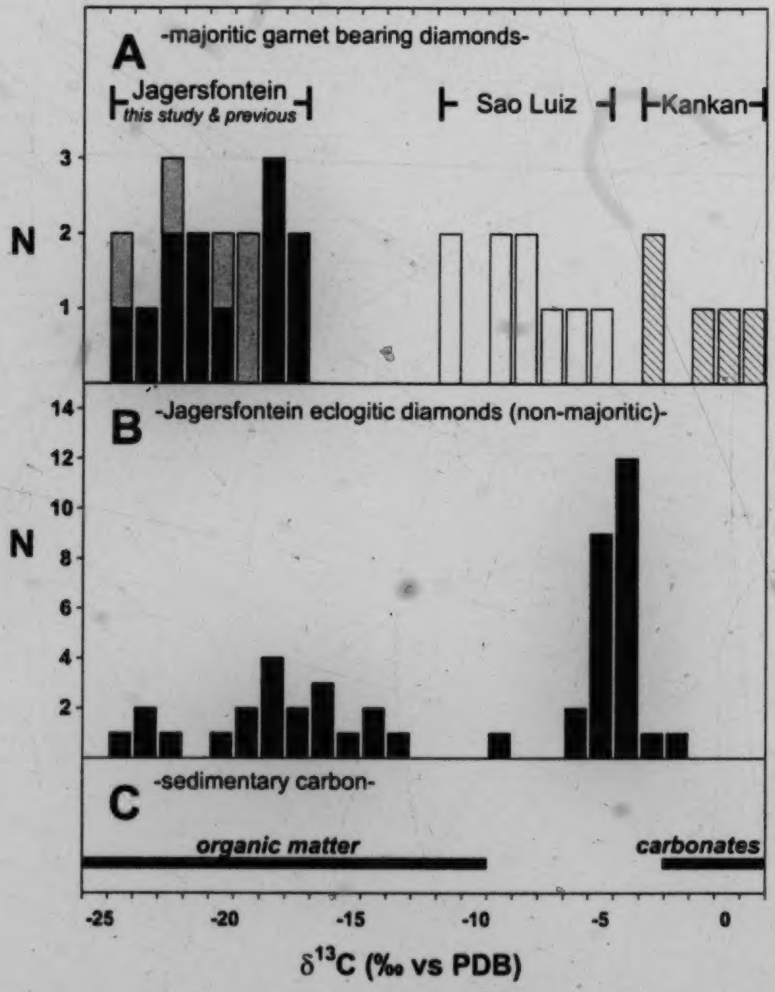

Figure 5-3: [A] Carbon isotope composition ($\delta^{13}C$) of eclogitic diamonds with majoritic garnet inclusions from the Jagersfontein kimberlite. Black: this study, grey: previous results (Deines et al., 1991). The distribution of $\delta^{13}C$-results of diamonds with majoritic garnet inclusions from Sao Luiz, Brazil (Wilding, 1990; Hutchison et al., 1999; Kaminsky et al., 2001) and Kankan, Guinea (Stachel et al., 2002) are shown for comparison. [B] Carbon isotope composition of eclogitic diamonds from Jagersfontein that formed in the lithosphere. [C] Isotopic ranges of carbon within various sedimentary source rocks (Schidlowski et al., 1983).

CHAPTER 6

General Discussion and Conclusions

The previous chapters contain the detailed descriptions of the results of the study of diamonds and their mineral inclusions from a variety of diamond deposits worldwide, representing very different geological settings. Not only are the studied diamonds derived from geographically distinct regions, but they also were formed in different chemical environments and at different depths in the Earth's mantle, ranging from the subcratonic lithospheric upper mantle (>150 km) through the asthenosphere and the transition zone (>410 km) to the lower mantle (>660 km).

Because of the diversity of sources of the diamonds, it is possible to draw general conclusions on the composition and the evolution of the Earth's mantle and on processes of diamond formation in different parts of the mantle.

6.1 Diamond formation in the lithospheric mantle

The results from the lithospheric diamonds of the Panda kimberlite show that the Earth's mantle underneath the central Slave Province is not as chemically unusual as a previous study on diamond inclusions from this region by Davies et al. (1999) suggested. The samples from the Panda kimberlite indicate that diamond formation took place in an overall moderately depleted peridotitic environment with a minor eclogitic component, which is in general accordance with results from xenoliths from this region (Griffin et al., 1999).The results indicate that during diamond formation the lithospheric mantle underneath the central Slave Province was not as depleted as other cratons, for example the Kaapvaal craton (see Stachel et al., 2003 and references therein) or the Siberian craton (e.g. Sobolev, 1977; Griffin et al., 1993).

The relatively fertile character of the deep (>150 km) subcratonic lithospheric mantle underneath the central Slave Province has been interpreted as being the result of the emplacement of an ascending plume head (Griffin et al., 1999). The results from the Panda diamonds do not support such an interpretation, in that high-pressure melting can not provide an explanation for the observed high chromium contents in peridotitic garnets inclusions in diamonds (see discussion in Stachel et al., 2003).

The results show that diamond formation took place in a geothermal regime with a thermal gradient higher (around 40 mW/m^2) than the steady state geotherm underneath the central Slave of around 37 mW/m^2 surface heat flow. This observation is consistent with results of similar studies from other cratons and indicates that diamond formation is generally linked to a geothermal gradient of 40-42 mW/m^2.

Combined with nitrogen data and the age constraints from sulfide inclusions by Westerlund et al. (2003), which indicate an Archean age of at least some of the Panda diamonds, it becomes apparent that the higher geothermal gradient during diamond formation was a transient feature and ambient temperatures dropped by ~100-150°C soon after diamond formation. The comparison with xenolith data from the central Slave (e.g. Menzies et al., 2003) indicates that such brief heating and cooling events of the deeper lithosphere may have happened repeatedly with clear evidence for a heating pulse prior to the kimberlite emplacement in the late Cretaceous/Early Tertiary. Such short time heating events are most likely related to small-scale magmatic intrusions rather than to the emplacement of large plumes.

The results from the Panda diamonds also indicate that the suite of lower mantle inclusions, which was used as an argument for an plume origin of the deep lithosphere, is not as common as previously suggested (Davies et al., 1999; Griffin et al., 1999) and that many of the inclusion assemblages that were interpreted as being derived from the lower mantle may actually have formed in the upper mantle.

The mineral inclusions recovered from placer diamonds from Brazil (Arenapolis, Boa Vista, Canastra) indicate that over large distances the majority of these placer diamonds formed in a depleted peridotitic environment that contained, similar to the source of the Panda diamonds, only a minor eclogitic component. This conclusion is consistent with results of a preliminary study on Brazilian diamonds by Meyer and Svisero (1975) and to the majority of diamond sources worldwide, but in contrast to the results of the few detailed studies on diamonds from the Juina-São Luiz area in Brazil (Harte et al., 1999; Hutchison, 1997; Kaminsky et al., 2001) and from adjacent Venezuela (Sobolev et al., 1998; Kaminsky et al., 2000). The latter studies indicate that diamonds formed in a predominantly eclogitic environment and, in the case of Juina-São Luiz, reveal a high proportion of sublithospheric diamonds. Sublithospheric diamonds have not been found in any of the studied Brazilian placer deposits and together with the low abundance of eclogitic diamonds this indicates that the mantle sources of the Juina-São Luiz and Guaniamo diamonds are rather unusual and probably geographically restricted.

The common occurrence of sinusoidal $\mathrm{REE_N}$ patterns in peridotitic garnet inclusion from Boa Vista and many other deposits worldwide (e.g. Shimizu and Richardson, 1987; Stachel and Harris, 1997; Stachel et al., 1998 and the review in Stachel et al., 2004) suggests that the peridotitic portion of the subcratonic lithospheric mantle underneath Brazil and many other cratons has a long history of depletion and subsequent re-enrichment. The degree of depletion and re-enrichment, however, may vary from one craton to another or even on a smaller scale.

Similar styles of depletion and re-enrichment are also preserved in the peridotitic inclusion suite of diamonds from the Jagersfontein kimberlite. The peridotitic sources at Jagersfontein show even higher degrees of depletion than at Panda and in Brazil. Such strongly depleted peridotitic diamond sources are consistent with observations from other diamond deposits on the Kaapvaal craton.

Unlike at Panda and in Brazil, lithospheric diamond sources at Jagersfontein are predominantly eclogitic, which is consistent with previous observations (Tsai et al., 1979; Deines et al., 1991). The presence of positive Eu-anomalies in eclogitic garnet inclusions from Jagersfontein indicates that subducted oceanic crust has been incorporated into the lithospheric mantle beneath the Kaapvaal and represents a major component of the Jagersfontein diamond source.

6.2 Diamond formation in the sublithospheric mantle

The diamond suite from Jagersfontein is characterized by a high abundance (~10 %) of diamonds with inclusions of majoritic garnets. The presence of majoritic garnets as inclusions in diamonds indicates an origin at depths beneath the subcratonic lithosphere, well within the asthenosphere and transition zone (Ringwood, 1967; Akaogi and Akimoto, 1977; Moore and Gurney, 1985; Irifune, 1987). The composition of the majoritic garnet inclusions and their host diamonds shows that formation processes of majoritic garnet-bearing diamonds are very distinct from diamonds that formed in the shallower lithosphere. The presence of negative Eu-anomalies in all majoritic garnet inclusions shows that the diamonds formed during the subduction of oceanic crust. Furthermore, a narrow range of isotopically light carbon compositions of the host diamonds, which mirrors previous results from Jagersfontein (Deines et al., 1991), indicates that these diamonds, unlike their lithospheric counterparts, preserve the original isotopic composition of their source, which in case of the Jagersfontein most likely is subducted organic matter. The comparison with samples from other deposits shows that many majoritic garnet-bearing diamonds probably have formed during subduction processes. The variability of isotopic compositions of the diamonds between different deposits is thereby only controlled by the primary composition of the subducted carbon source. The main mechanism responsible for the formation of majoritic garnet-bearing diamonds may be the direct conversion from graphite, which due to sluggish kinetics can occur deep in the diamond stability field.

The results from the Jagersfontein diamonds show that previous models for the formation of majoritic garnet-bearing diamonds, which suggested the presence of eclogitic layers in the Earth's mantle (Gasparik, 1997) or melt precipitations at great depths (Moore et al., 1991; Haggerty, 1999), have to be revised.

Bibliography

Akaogi, M. and Akimoto, S., 1977. Pyroxene-garnet solid-solution equilibria in the systems $Mg_4Si_4O_{12}$-$Mg_3Al_2Si_3O_{12}$ and $Fe_4Si_4O_{12}$-$Fe_3Al_2Si_3O_{12}$ at high pressures and temperatures. Physics of the Earth and Planetary Interiors, 15: 90-106.

Davies, R.M. et al., 1999. Diamonds from the deep: pipe DO-27, Slave Craton, Canada. In: J.J. Gurney, J.L. Gurney, M.D. Pascoe and S.H. Richardson (Editors), The J.B. Dawson Volume, Proceedings of the VIIth International Kimberlite Conference. Red Roof Design, Capetown, pp. 148-155.

Deines, P., Harris, J.W. and Gurney, J.J., 1991. The carbon isotopic composition and nitrogen content of lithospheric and asthenospheric diamonds from the Jagersfontein and Koffiefontein kimberlite, South Africa. Geochimica et Cosmochimica Acta, 55: 2615-2625.

Gasparik, T., 1997. A model for the layered upper mantle. Physics of the Earth and Planetary Interiors, 100(1-4): 197-212.

Griffin, W.L. et al., 1999. Layered mantle lithosphere in the Lac de Gras area, Slave Craton: Composition, structure and origin. Journal of Petrology, 40(5): 705-727.

Griffin, W.L. et al., 1993. Trace-Elements in garnets and chromites - Diamond formation in the Siberian lithosphere. Lithos, 29(3-4): 235-256.

Haggerty, S.E., 1999. Earth and planetary sciences - A diamond trilogy: Superplumes, supercontinents, and supernovae. Science, 285(5429): 851-860.

Harte, B., Harris, J.W., Hutchison, M.T., Watt, G.R. and Wilding, M.C., 1999. Lower mantle mineral associations in diamonds from São Luiz, Brazil. In: Y. Fei, C.M. Bertka and B.O. Mysen (Editors), Mantle Petrology: Field Observations and High Pressure Experimentation: A tribute to [illegible]ancis R. (Joe) Boyd. Special Publication. The Geochemical Society, Houston, pp. 125-153.

Hutchison, M.T., 1997. Constitution of the deep transition zone and lower mantle shown by diamonds and their inclusions. PhD Thesis, University of Edinburgh, 340, 306 pp.

Irifune, T., 1987. An experimental investigation of the pyroxene-garnet transformation in a pyrolite composition and its bearing on the constitution of the mantle. Physics of the Earth and Planetary Interiors, 45: 324-336.

Kaminsky, F.V. et al., 2001. Superdeep diamonds from the Juina area, Mato Grosso State, Brazil. Contributions to Mineralogy and Petrology, 140: 734-753.

Kaminsky, F.V., Zakharchenko, O.D., Griffin, W.L., Channer, D.M.D. and Khachatryan-Blinova, G.K., 2000. Diamond from the Guaniamo area, Venezuela. The Canadian Mineralogist, 38: 1347-1370.

Menzies, A.H. et al., 2003. Peridotitic mantle xenoliths from kimberlites on the Ekati diamond mine property, NWT, Canada, 8th International Kimberlite Conference, Extended Abstract, Victoria, Canada.

Meyer, H. and Svisero, D., 1975. Mineral inclusions in Brazilian diamonds. Physics and Chemistry of the Earth, 9: 785-795.

Moore, R.O. and Gurney, J.J., 1985. Pyroxene solid solution in garnets included in diamonds. Nature, 318: 553-555.

Moore, R.O., Gurney, J.J., Griffin, W.L. and Shimizu, N., 1991. Ultra-high pressure garnet inclusions in Monastery diamonds - Trace-element abundance patterns and conditions of origin. European Journal of Mineralogy, 3(2): 213-230.

Ringwood, A.E., 1967. The pyroxene garnet transformation in the earth's mantle. Earth and Planetary Science Letters, 2: 255-263.

Shimizu, N. and Richardson, S.H., 1987. Trace-element abundance patterns of garnet inclusions in peridotite-suite diamonds. Geochimica et Cosmochimica Acta, 51(3): 755-758.

Sobolev, N.V., 1977. Deep-seated inclusions in kimberlites and the problem of the composition of the upper mantle. (Translated from the Russian edition, 1974). AGU, Washington, 279 pp.

Sobolev, N.V., Yefimova, E.S., Channer, D.M.D., Anderson, P.F.N. and Barron, K.M., 1998. Unusual upper mantle beneath Guaniamo, Guyana shield, Venezuela: Evidence from diamond inclusions. Geology, 26(11): 971-974.

Stachel, T. et al., 2004. The trace element composition of silicate inclusions in diamonds: a review. Lithos, 77: 1-19.

Stachel, T. and Harris, J.W., 1997. Diamond precipitation and mantle metasomatism - evidence from the trace element chemistry of silicate inclusions in diamonds from Akwatia, Ghana. Contributions to Mineralogy and Petrology, 129(2-3): 143-154.

Stachel, T., Harris, J.W., Tappert, R. and Brey, G.P., 2003. Peridotitic inclusions in diamonds from the Slave and the Kaapvaal cratons - similarities and differences based on a preliminary data set. Lithos, 71: 489-503.

Stachel, T., Viljoen, K.S., Brey, G. and Harris, J.W., 1998. Metasomatic processes in lherzolitic and harzburgitic domains of diamondiferous lithospheric mantle: REE in garnets from xenoliths and inclusions in diamonds. Earth and Planetary Science Letters, 159(1-2): 1-12.

Tsai, H.M., Meyer, H.O.A., Moreau, J. and Milledge, H.J., 1979. Mineral inclusions in diamonds: Premier, Jagersfontein and Finsch kimberlites, South Africa, and Williamson mine, Tanzania. In: F.R. Boyd and H.O.A. Meyer (Editors), Kimberlites, Diatremes and Diamonds.

Westerlund, K.J., Shirey, S.B., Richardson, S.H., Gurney, J.J. and Harris, J.W., 2003. Re-Os systematics of diamond inclusion sulfides from the Panda kimberlite, Slave craton, VIIIth International Kimberlite Conference, Extended Abstracts, Victoria, Canada.

APPENDIX A: METHODOLOGY

Appendix A

DIAMOND CRUSHING AND POLISHING

After detailed microscopic examination of the diamond samples and description of morphological features, the diamonds were crushed using a hardened steel piston crusher (Figure A1).

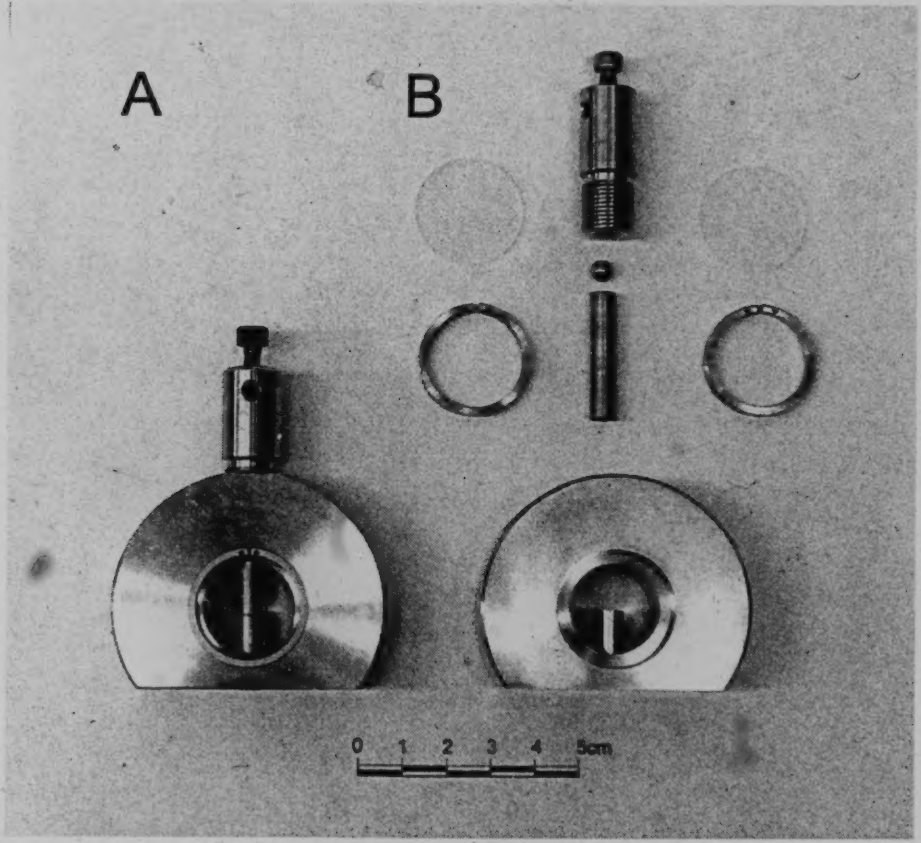

Figure A1: Piston crusher (A) assembled (B) partially disassembled

After crushing inclusions were recovered from the diamond fragments and separately mounted in ~5 mm long brass rings (outer diameter 6 mm) using Araldite epoxy resin. After hardening of the resin the sample surfaces were polished using Al_2O_3 and diamond abrasives.

Appendix A

Electron-Probe Microanalysis (EPMA)

General

Concentrations of major- and abundant trace-elements for the mineral inclusions in diamonds have been quantitatively determined by electron microprobe (EPMA) techniques. Electron microprobes were also used for secondary electron, backscattered electron and cathodoluminescence imagery.

JEOL JXA-8900 Superprobes at the following facilities have been used:

1.) Department of Earth and Atmospheric Sciences, University of Alberta, Edmonton, Canada

2.) Institut für Mineralogie, J.W.Goethe Universität, Frankfurt/Main, Germany

The electron microprobes were equipped with:

- -Five wavelength dispersive spectrometers (WDS) with TAP, PET, PETH and LIFH crystals.
- -Energy dispersive spectrometer (EDS)
- -Backscattered electron (BSE) detector
- -Secondary electron (SE) detector
- -Cathodoluminescence (CL) detector

Sample preparation

-Each polished sample was cleaned for ~5 minutes in an ultrasonic bath using purified ethanol.

-To attain electrical conductivity the samples were coated with carbon by combusting graphite rods in a high vacuum chamber.

Analytical Settings

All analyses have been performed at 20 kV acceleration voltage to sufficiently excite elements with excitation potentials of up to ~8 keV and a probe current of 20 nA. The probe diameter was set to 2 μm, resulting in a spatial resolution (excited volume) of ~5-6 μm. For quantitative analyses the wavelength dispersive spectrometers (WDS) were used.

The spectrometer settings are summarized in Table A1, showing
-the x-ray line
-the detector crystal
-the position of the background measurements relative to the peak position
-the background and peak counting times
-the measurement mode
-the secondary standards for each microprobe facility (synthetic standards in italics)

Detector settings:

The PHA gain and the high voltage (1650-1750 V) of the detector were optimized so that individual counting events for analyzed elements corresponded to a drop in the high voltage of 4 V. For all lighter elements up to Ti, the PHA gain was set to accept counts between 1.2-6 V in order to reduce background and to avoid overlaps through higher order Bragg reflexes.

Three to four analytical points were averaged to ensure detection limits of 100 ppm or better for all oxide-species except Na_2O (ca. 200 ppm). Analytical accuracy and precision was tested using secondary standards (Table A1) and was shown to be better than 1% (relative) for major elements.

Appendix A

Table A1: Settings for the quantitative analysis of major and trace elements using wave length dispersive spectrometers

Element	X-ray	Crystal	Backgr. Pos. (mm)		Count Time (sec)		PHA	Standards	
			lower	upper	peak	backgr.	Mode	Edmonton	Frankfurt
Na	Kα	TAP	n.d.	3.0	30	15	Differential	Albite	Albite
Mg	Kα	TAP	n.d.	3.0	30	15	Differential	Forsterite	Forsterite
Al	Kα	TAP	n.d.	2.0	40	20	Differential	Pyrope	Kyanite
Si	Kα	TAP	n.d.	2.0	30	15	Differential	Diopside	Wollastonite
P	Kα	PET	1.8	1.5	40	20	Differential	Apatite	$KTiOPO_4$
S	Kα	PET	1.7	1.7	30	15	Differential	Pyrite	Pyrite
K	Kα	PET	1.7	1.7	40	20	Differential	Orthoclase	$KTiOPO_4$
Ca	Kα	PET	2.0	2.0	40	20	Differential	Diopside	Wollastonite
Ti	Kα	PET	2.0	2.0	50	25	Differential	Rutile	$MnTiO_3$
V	Kα	LIFH	3.0	3.0	30	15	Integral	*V-Metal*	*V-Metal*
Cr	Kα	PET	2.0	2.0	40	20	Integral	Chromite	Cr_2O_3
Mn	Kα	LIFH	n.d.	1.5	30	15	Integral	Mn_2O_3	$MnTiO_3$
Fe	Kα	LIFH	2.6	1.5	30	15	Integral	Fayalite	Fayalite
Co	Kα	LIFH	0.0	1.5	40	20	Integral	*Co-Metal*	*Co-Metal*
Ni	Kα	LIFH	1.5	1.5	50	25	Integral	*Ni-Metal*	*NiO*
Cu	Kα	LIFH	1.5	1.5	40	20	Integral	*Cu-Metal*	*Cu-Metal*
Zn	Kα	LIFH	1.5	1.5	40/100*	20/100*	Integral	Sphalerite	*ZnO*

*Longer count times for Zn in spinel

Appendix A

SECONDARY ION MASS SPECTROMETRY (SIMS)

The concentrations of REE and other trace elements (Ti, Y, Zr, Sr,) have been determined for selected garnet and pyroxene samples using Secondary Ion Mass Spectrometry (SIMS).

CAMECA IMS-3f ion microprobes at the following facilities have been used:
1.) Clark Laboratories, Woods Hole Oceanographic Institutions, Massachusetts, USA; operated by: Dr. Nobumichi Shimizu
2.) Institut für Mineralogie, Ruprecht-Karls Universität, Heidelberg, Germany; operated by: Thomas Ludwig

The general approach for the analyses was the same at both facilities. A beam of negatively charged oxygen ions was focused onto the cleaned and gold-coated (electrical conductivity) sample surface. The resulting secondary ions were accelerated into the mass spectrometer, separated according to their mass and counted by a detector. Different analytical settings and the data correction procedures were applied by the operators.

Woods Hole:

The primary beam size at Woods Hole was set to a diameter of ~30 µm for the REE analyses and to ~5 µm other trace elements (Ti, Y, Zr, Sr,). To suppress molecular interferences, an energy offset of -60V for the REE and -90 V for the remaining trace elements was applied (Shimizu and Hart, 1982). Trace element concentrations were calculated using empirical relationships between concentration and secondary ion yields in well-characterized standards (working curves) and by normalization to silicon as an internal standard. The analytical uncertainties are in the order of 10-30 % (relative) for the REE and 5-15 % for the other trace elements.

Heidelberg (taken from Chapter 4):

At Heidelberg the primary beam was a 14.5keV O- ion beam with a current of 20 nA and a spot size of ~25 µm. The mass resolution (m/Δm) was set to 370 (10%)

and the energy window was set to 105 ± 25 eV (energy filtering) in order to minimize matrix effects and molecular interferences. Data were collected at mass 30 (^{30}Si) and from mass 138 to 176. The integration time for ^{30}Si was 2 s and for the REE typically 8 s. Interferences of complex (>2 atoms) molecular ions were suppressed by energy filtering. To correct the spectra for interferences of REE oxides, which are typically present in element to oxide ratios between 0.05 and 0.2, the deconvolution method of (Zinner and Crozaz, 1986) was chosen. However, instead of solving the linear system of equations directly, it was solved by numerical optimization (Ludwig, unpublished). This process involves synthesizing a spectrum that matches the acquired mass spectrum as closely as possible. The optimization starts with estimated values for REE count rates and element to oxide ratios and minimizes the sum of the squared errors by varying the count rates and the element to oxide ratios. The advantage of this method lies in the fact that the element to oxide ratios can be limited to reasonable values. This helps to overcome the numerical problems for the elements Yb, Lu and Gd. The element/oxide ratios were limited to a range of 0.05 to 0.2 (Gd 0.05 to 0.1). The optimization yields a set of REE count rates and REE/oxide ratios that can be used to calculate relative ion yields or concentrations. Exactly the same method and the same limits for the REE/oxide ratios were applied for the standard and all unknown samples. Each analysis was repeated six times on the same spot and each of the six spectra was deconvoluted separately. The resulting REE count rates were then averaged and the relative standard deviation (1 RSD) calculated. The standard deviation reflects in this case not only the precision of the acquired raw data but also the numerical (in-) stability of the deconvolution process.

NIST SRM610 glass was used as standard to determine the relative ion yields (values for REE concentrations are taken from (Pearce et al., 1997). Two well characterized garnet megacrysts (PN1, PN2) were also analyzed as further accuracy test.

Appendix A

FOURIER TRANSFORM INFRARED (FTIR) SPECTROSCOPY

The concentration of nitrogen impurities in diamond samples as well as the aggregation state of the nitrogen has been determined using Fourier Transform Infrared (FTIR) Spectrometry.

The measurements have been performed at the University of Alberta using a Thermo Nicolet Nexus 470 FT-IR spectrometer equipped with a Nicolet Continuum IR microscope.

Measurements were collected in transmission mode, using an EverGlo™ light source and a DTGS detector with KBr window. Absorption was calculated (1-A=T). The spot size/aperture size was set to 50 x 50 μm. 200 spectra were collected for each analysis in the range of 650-4000 cm^{-1} at a spectral resolution of 2 cm^{-1}. The instrument was purged with H_2O and CO_X free air; background measurements were taken in regular intervals.

The measurements have been carried out on inclusion free, transparent diamond cleavage chips, which were separately placed onto a sample holder and adjusted under the microscope. During the measurements the sample was purged in purified air.

In order to determine the nitrogen contents and aggregation states quantitatively the spectra of the diamond samples were, after the correction for background and baseline, normalized to a thickness of 1 cm and the resulting spectra deconvoluted.

The normalization was accomplished by measuring the absorption spectrum of a nitrogen free (Type II) diamond plate. After baseline correction the absorbance at 1995 cm^{-1} was determined and normalized to 11.94 (the experimentally determined intrinsic absorbance in diamond), giving the conversion factor for the normalization of the unknown sample.

The spectra of the Type II diamond plate was in a subsequent step subtracted from the baseline corrected spectra of the unknown sample and the remaining absorption spectra (mainly nitrogen) normalized using the given conversion factor.

Appendix A

In order to determine absorption coefficients for the A- and B-centers, the normalized absorption spectra in the range 900-1500 cm^{-1} were deconvoluted using the program *abdfit*, developed by David Fisher (DTC, Maidenhead).

The deconvolution program separates the spectrum into A-, B- and D-component and calculates the absorption coefficient for each component.

To obtain concentrations of nitrogen in A- and B-centers, the absorption coefficients were multiplied with experimentally derived conversion factors (Boyd et al., 1994; Boyd et al., 1995).

Applications: Measuring nitrogen in Diamond

Nitrogen is the most common impurity in diamonds and can reach concentrations of >1000 ppm. Optical absorption measurements show that nitrogen in almost all natural diamonds is present in several different aggregation states. Based on the absence or presence of nitrogen and its aggregation state, diamonds are classified as following:

Type I: Diamonds with detectable nitrogen content; subdivided into:
  Type Ia: Diamonds that contain aggregated nitrogen (A-, B-, N3-centers, platelets; see below); subdivided into:
    Type IaA: Diamonds with nitrogen mainly ($\leq$ 90%) in A-centers
    Type IaB: Diamonds with nitrogen mainly ($\leq$ 90%) in B-centers
    Type IaAB: Diamonds with nitrogen in A- and B-centers
  Type Ib: Diamonds with single substitutional nitrogen
Type II: Diamonds with very low or non-detectable nitrogen
  Type IIa: Nitrogen free diamonds
  Type IIb: Diamonds with boron as main impurity

It was suggested by Evans (1976) that nitrogen is incorporated into the diamond lattice as dispersed, single substitutional atoms. During the long residence times at high temperatures in the Earth's mantle, the single nitrogen atoms slowly migrate in the diamond and form more complex types of nitrogen aggregates (Evans, 1992). Although single atomic nitrogen is present in natural diamonds, its concentrations are too low to be detected by optical absorption measurements.

In Type IaA diamonds nitrogen is present mainly in A-centers, which are considered to be two nitrogen atoms on adjacent lattice sites (Davies, 1976). Type IaB diamonds contain nitrogen that is present almost exclusively in B-centers, which consist of four nitrogen atoms and one vacancy (Evans, 1992 and references therein). Diamonds that contain nitrogen as A- and B-centers are classified as Type IaAB. Examples of absorption spectra of Type IaA, IaB and IaAB diamonds are shown in Figure A2.

Further aggregation states of nitrogen which can be found in natural Type Ia diamonds, but which were not quantitatively determined for this study, include N3-centers and platelets. N3-centers (not IR-active) are considered to consist of three nitrogen atoms and one vacancy; platelets are planar defects, which range in size from ~10 nm to few micrometers (Evans et al., 1981).

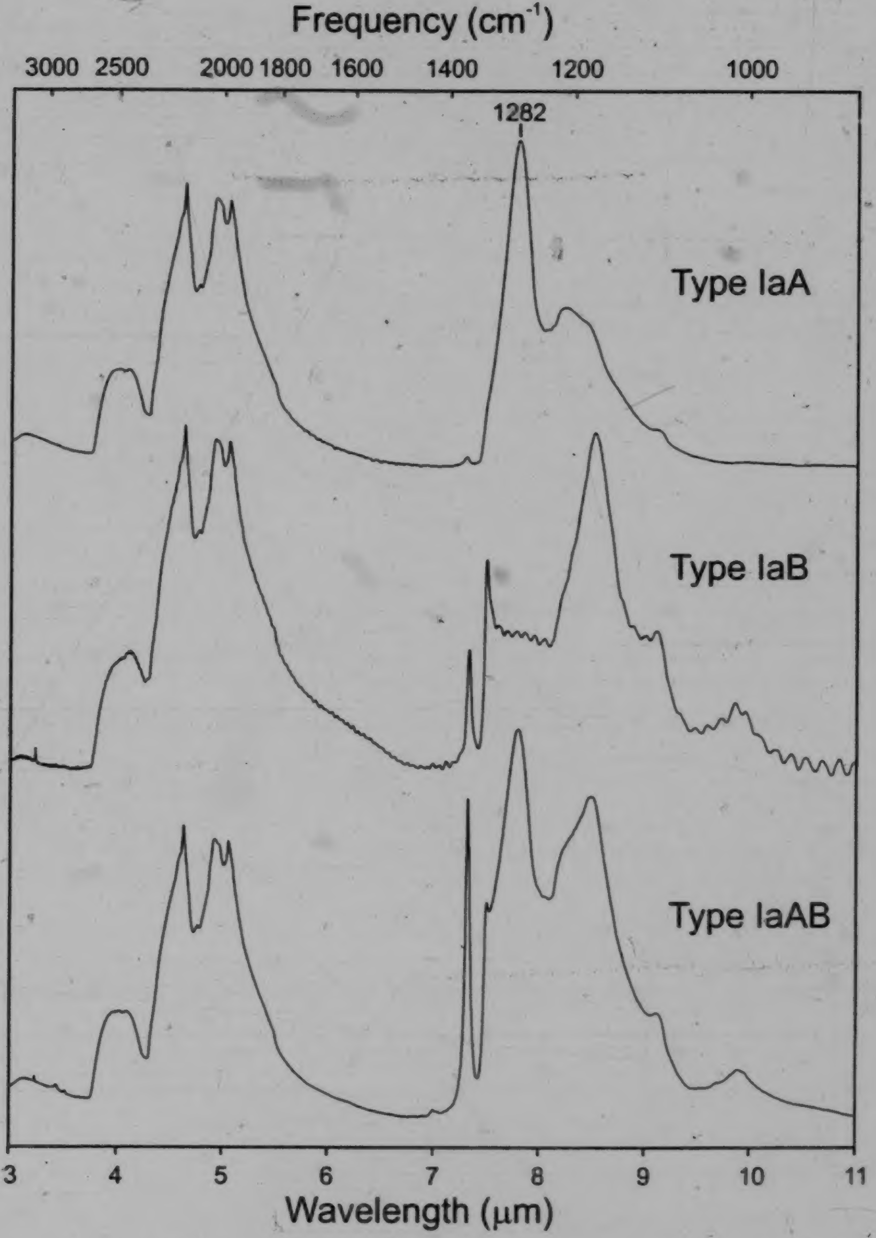

Figure A2: Examples of infrared spectra of Type IaA, Type IaB and Type IaAB diamonds. The spectra were collected from diamonds JF-100 (IaA), AR-20 (IaB) and JF-20 (IaAB).

Appendix A

CARBON STABLE ISOTOPE ANALYSIS

The stable carbon isotope composition of diamonds has been analyzed at the Stable Isotope Laboratory at the University of Alberta in coöperation with Dr. Karlis Muehlenbachs.

The diamond samples were converted into CO_2 gas in sealed and evacuated quartz glass tubes. The resulting CO_2 gas was extracted and the isotopic composition measured at a Finnigan MAT 252 gas flow mass spectrometer. Instrumental precision and accuracy is in the order of ± 0.02 ‰. The replication of analyses of different aliquots of selected samples showed a variability within 0.2‰, which may be related to the combustion/extraction process or to isotopic heterogeneities of the diamond.

Sample preparation

1-2 milligrams of inclusion free, transparent diamond cleavage chips were filled into a ~25 cm long quartz glass tube (outer diameter 6 mm), that was sealed on one end. 1-2 grams of CuO (99.95% pure), as oxygen source, were added to the diamond sample.

The quartz tube with diamond sample and CuO was evacuated for several hours and afterwards by using a blow torch removed (cut) from the vacuum line and simultaneously sealed.

In order to convert the diamond sample into CO_2 gas, the filled and evacuated quartz tube was heated for at least 12 hours at ~1000°C and afterwards slowly cooled (over at least 2 hours).

The sample gas was extracted under vacuum (after breaking the quartz tube) using nitrogen traps and a mixture of dry ice and ethanol to remove water impurities. During the extraction the sample gas volume was measured to assure complete combustion of the diamond sample.

The extracted sample gas was transferred into glass sample tubes for subsequent measurements with the gas flow mass spectrometer.

Appendix A

Bibliography:

Boyd, S.R., Kiflawi, I. and Woods, G.S., 1994. The relationship between infrared absorption and the A defect concentration in diamond. Philosophical Magazine B, 69: 1149-1153.

Boyd, S.R., Kiflawi, I. and Woods, G.S., 1995. Infrared absorption by the B nitrogen aggregate in diamond. Philosophical Magazine B, 72: 351-361.

Davies, G., 1976. The A nitrogen aggregate in diamond - its symmetry and possible structure. Journal of Physics, C 9: 537-542.

Evans, T., 1976. Diamonds. Contemporary Physics, 17(1): 45-70.

Evans, T., 1992. Aggregation of nitrogen in diamonds. In: J.E. Field (Editor), The properties of natural and synthetic diamond. Academic Press, pp. 259-290.

Evans, T., Qi, Z. and Maguire, J., 1981. The stages of nitrogen aggregation in diamond. Journal of Physics, C14: 379-384.

Pearce, N.J.G. et al., 1997. A compilation of new and published major and trace element data for NIST SRM 610 and NIST SRM 612 glass reference materials. The Journal of Geostandards and Geoanalysis, 21: 115-144.

Shimizu, N. and Hart, S.R., 1982. Applications of the ion microprobe to geochemistry and cosmochemistry. Annual Review of Earth and Planetary Sciences, 10: 483-526.

Zinner, E.K. and Crozaz, G., 1986. A method for the quantitative measurement of rare earth elements in the ion microprobe. International Journal of Mass Spectrometry and Ion Processes, 69: 17-38.

APPENDIX B: PANDA

Table B1: Composition of silicate/oxide inclusions in diamonds from the Panda kimberlite (EPMA-analyses, given in wt%)

Sample	Mineral	Parag.	Assemblage	P_2O_5	SiO_2	TiO_2	Al_2O_3	Cr_2O_3	V_2O_3	FeO	MnO	NiO	MgO	CaO	ZnO	Na_2O	K_2O	Total
PA-01a	garnet	p	gt,gt-ol	0.01	41.9	0.03	15.8	10.2		6.27	0.31	0.02	21.6	4.11		0.00	0.00	100.2
PA-01b(I)*	garnet (-ol)	p	gt,gt-ol	0.01	41.3	0.02	16.3	10.5		6.37	0.31	0.01	20.8	4.67		0.31	0.00	100.5
PA-01b(II)*	olivine (-gt)	p	gt,gt-ol	0.00	41.1	0.00	0.01	0.12		6.87	0.09	0.39	50.7	0.03		0.23	0.00	99.6
PA-02a	garnet	p	gt	0.02	42.2	0.03	16.4	9.22		6.29	0.31	0.01	20.8	5.57		0.02	0.00	100.8
PA-03a*	garnet	p	gt	0.01	40.8	0.03	13.2	13.7		5.59	0.28	0.01	21.7	3.71		0.02	0.01	99.0
PA-04a	garnet	p	gt	0.02	41.9	0.04	18.0	7.61		5.98	0.29	0.01	22.4	3.15		0.02	0.00	99.5
PA-05a(I)*	garnet (-ol-opx)	p	gt-ol-opx	0.02	41.7	0.08	16.8	9.63		6.45	0.32	0.01	21.4	3.93		0.01	0.00	100.4
PA-05a(III)*	olivine (-gt-ol)	p	gt-ol-opx	0.00	41.1	0.01	0.0	0.21		7.08	0.10	0.40	50.4	0.04		0.01	0.00	99.4
PA-05a(III)*	opx (-gt-ol)	p	gt-ol-opx	0.00	57.9	0.02	0.40	0.34		4.13	0.10	0.11	35.6	0.34		0.01	0.00	98.9
PA-06a	garnet	p	gt	0.01	41.5	0.02	15.4	10.4		6.23	0.31	0.01	20.9	4.85		0.02	0.00	99.6
PA-07a	garnet	p	gt	0.02	41.7	0.08	15.9	9.53		6.31	0.31	0.02	21.3	4.61		0.02	0.00	99.8
PA-08a	garnet	p	2gt	0.02	41.4	0.04	15.3	10.0		6.29	0.30	0.01	20.6	5.18		0.02	0.00	99.2
PA-08b	garnet	p	2gt	0.02	42.1	0.05	15.8	10.0		6.30	0.30	0.02	21.0	5.17		0.10	0.00	100.8
PA-09a	garnet	p	gt	0.02	41.1	0.04	15.4	10.5		6.18	0.29	0.01	20.4	5.21		0.04	0.00	99.2
PA-10a	garnet	p	gt,ol	0.01	41.6	0.05	16.3	9.03		6.29	0.29	0.02	20.6	5.41		0.01	0.01	99.5
PA-10b	olivine	p	gt,ol	0.00	40.1	0.00	0.02	0.06		7.73	0.12	0.38	49.0	0.05		0.01	0.00	97.5
PA-11a	garnet	p	2gt	0.02	41.7	0.13	16.6	8.57		6.53	0.31	0.01	20.3	5.78		0.01	0.00	100.0
PA-11b	garnet	p	2gt	0.02	41.7	0.14	16.6	8.58		6.51	0.32	0.01	20.3	5.81		0.02	0.01	100.1
PA-12a	garnet	p	gt	0.01	42.2	0.01	16.0	10.8		5.81	0.29	0.01	22.3	3.81		0.01	0.00	101.1
PA-13a*	garnet	p	gt,chr	0.04	41.0	0.09	13.9	12.7		6.71	0.37	0.02	19.4	6.14		0.00	0.00	100.4
PA-13b	chromite	p	gt,chr	0.00	0.20	0.16	4.12	65.7	0.22	16.7	0.28	0.10	12.8	0.00	0.043	0.01	0.08	100.4
PA-14a	garnet	p	gt	0.02	42.0	0.07	16.5	8.87		6.16	0.30	0.01	21.4	4.38		0.01	0.00	99.7
PA-15a	garnet	p	gt	0.01	42.0	0.05	16.4	9.39		6.23	0.30	0.01	21.8	4.17		0.01	0.01	100.3
PA-16a	garnet	p	gt	0.01	41.5	0.02	14.7	11.1		6.35	0.31	0.01	21.0	4.74		0.01	0.00	99.8
PA-17a	garnet	p	gt	0.00	41.9	0.03	15.6	10.3		6.16	0.29	0.01	21.5	4.33		0.02	0.00	100.2
PA-18a	garnet	p	gt	0.02	41.1	0.02	14.9	11.1		6.74	0.35	0.01	20.4	4.90		0.01	0.00	99.6
PA-19a(I)*	garnet (-opx)	p	gt-opx,ol	0.05	41.8	0.07	16.8	9.08		6.04	0.29	0.01	20.5	5.96		0.01	0.00	100.6
PA-19a(II)*	opx (-gt)	p	gt-opx,ol	0.00	57.9	0.02	0.45	0.38		3.79	0.09	0.14	36.0	0.54		0.02	0.00	99.3
PA-19b	olivine	p	gt-opx,ol	0.01	40.9	0.00	0.02	0.05		7.19	0.11	0.35	50.7	0.04		0.01	0.00	99.3
PA-20a	garnet	p	gt,chr,chr-ol	0.01	42.2	0.02	14.3	12.6		6.19	0.33	0.01	22.5	3.14		0.28	0.00	101.5
PA-20b	chromite	p	gt,chr,chr-ol	0.01	0.17	0.03	4.99	66.1	0.24	15.2	0.26	0.10	13.5	0.00	0.040	0.01	0.00	100.6

* Data already published in Stachel *et al.* (2003)

Table B1 continued

Sample	Mineral	Parag.	Assemblage	P_2O_5	SiO_2	TiO_2	Al_2O_3	Cr_2O_3	V_2O_3	FeO	MnO	NiO	MgO	CaO	ZnO	Na_2O	K_2O	Total
PA-20c(I)	chromite (-ol)	p	gt,chr,chr-ol	0.00	0.17	0.02	5.07	65.9	0.25	15.3	0.27	0.09	13.6	0.00	0.046	0.02	0.00	100.7
PA-20c(II)	olivine (-chr)	p	gt,chr,chr-ol	0.01	41.1	0.01	0.01	0.10		6.58	0.09	0.36	50.9	0.01		0.02	0.00	99.2
PA-21a	garnet	p	gt,ol	0.01	40.9	0.05	14.0	11.6		6.40	0.33	0.01	20.6	4.71		0.01	0.00	98.5
PA-21b	olivine	p	gt,ol	0.01	41.0	0.01	0.02	0.04		7.42	0.11	0.37	50.5	0.03		0.02	0.00	99.5
PA-22a	garnet	p	gt,ol	0.01	42.1	0.01	16.1	9.34		6.23	0.29	0.02	21.1	5.14		0.02	0.00	100.3
PA-22b	olivine	p	gt,ol	0.00	40.9	0.01	0.02	0.04		7.58	0.11	0.38	50.2	0.05		0.03	0.01	99.3
PA-23a*	garnet	p	gt,ol	0.01	41.8	0.16	16.9	8.14		6.10	0.29	0.01	20.8	5.51		0.01	0.00	99.8
PA-23b*	olivine	p	gt,ol	0.00	40.9	0.00	0.03	0.07		7.44	0.11	0.34	50.1	0.05		0.02	0.00	99.0
PA-24a*	chromite	p	chr,chr(ex)	0.00	0.12	0.04	5.74	65.6	0.31	16.2	0.30	0.06	11.6	0.00	0.083	0.02	0.01	100.3
PA-25a	chromite	p	chr	0.00	0.19	0.09	4.89	66.1	0.20	15.4	0.27	0.10	13.4	0.00	0.042	0.01	0.00	100.6
PA-26a*	chromite	p	chr	0.01	0.10	0.10	7.25	63.9	0.25	15.0	0.25	0.10	13.7	0.00	0.050	0.01	0.00	100.8
PA-29a*	chromite	p	chr	0.00	0.09	0.22	7.20	63.7	0.24	14.9	0.25	0.10	13.8	0.01	0.046	0.04	0.00	100.6
PA-31b*	chromite	p	chr,chr(ex)	0.01	0.10	0.10	7.16	64.0	0.26	15.0	0.25	0.09	13.8	0.00	0.048	0.01	0.00	100.8
PA-32a	chromite	p	chr	0.00	0.10	0.11	7.12	64.0	0.27	15.2	0.26	0.10	13.8	0.00	0.055	0.01	0.00	101.0
PA-33a	chromite	p	chr	0.01	0.10	0.18	7.28	63.3	0.26	15.2	0.26	0.10	13.9	0.00	0.072	0.01	0.00	100.7
PA-34a	chromite	p	chr	0.00	0.10	0.12	6.92	63.9	0.25	15.3	0.26	0.10	13.5	0.00	0.063	0.01	0.00	100.5
PA-35a	chromite	p	chr	0.00	0.09	0.09	6.80	64.0	0.28	15.5	0.25	0.08	13.3	0.00	0.060	0.01	0.01	100.4
PA-36a	olivine	p	ol	0.00	40.9	0.00	0.02	0.05		7.52	0.11	0.36	50.1	0.04		0.02	0.00	99.1
PA-37a	olivine	p	ol	0.01	41.2	0.00	0.02	0.06		7.21	0.11	0.35	50.5	0.03		0.02	0.00	99.5
PA-38a	olivine	p	ol	0.00	40.3	0.00	0.01	0.04		6.47	0.09	0.38	49.7	0.02		0.03	0.00	97.0
PA-39a	olivine	l.m.?	fper,ol	0.01	40.9	0.01	0.02	0.03		5.90	0.09	0.22	50.8	0.03		0.01	0.00	98.1
PA-39b	fper	l.m.?	fper,ol	0.01	0.02	0.01	0.01	0.61		20.9	0.16	1.34	75.0	0.00		0.02	0.00	98.1
PA-40a*	olivine	p	ol	0.01	40.8	0.01	0.02	0.06		7.13	0.10	0.35	50.2	0.04		0.00	0.00	98.8
PA-40b*	garnet	p	gt,ol	0.03	42.4	0.13	16.3	8.59		5.95	0.28	0.01	20.7	5.79		0.03	0.00	100.2
PA-41b	olivine	p	ol	0.01	41.6	0.00	0.02	0.05		7.41	0.11	0.35	50.9	0.04		0.01	0.00	100.4
PA-42a*	olivine	p	ol	0.00	40.9	0.00	0.02	0.04		7.57	0.11	0.38	50.1	0.04		0.02	0.00	99.1
PA-42b*	garnet	p	gt,ol	0.01	42.1	0.03	15.0	10.7		6.61	0.34	0.01	20.6	5.21		0.02	0.00	100.7
PA-43a	olivine	p	ol	0.00	40.8	0.00	0.02	0.06		7.55	0.11	0.37	49.7	0.05		0.02	0.00	98.7
PA-45a	olivine	p	3ol	0.00	41.8	0.00	0.02	0.06		7.11	0.11	0.35	51.2	0.04		0.02	0.00	100.7
PA-45b	olivine	p	3ol	0.01	41.3	0.00	0.02	0.04		7.37	0.11	0.36	50.4	0.04		0.02	0.00	99.7
PA-45c	olivine	p	3ol	0.00	40.6	0.01	0.02	0.04		6.99	0.10	0.39	50.1	0.05		0.01	0.00	98.3

* Data already published in Stachel *et al.* (2003)

Table B1 continued

Sample	Mineral	Parag.	Assemblage	P_2O_5	SiO_2	TiO_2	Al_2O_3	Cr_2O_3	V_2O_3	FeO	MnO	NiO	MgO	CaO	ZnO	Na_2O	K_2O	Total
PA-46a	olivine	p	ol	0.00	40.9	0.01	0.01	0.04		7.40	0.10	0.39	50.2	0.03		0.01	0.00	99.1
PA-48a	olivine	p	ol	0.01	41.6	0.00	0.02	0.04		7.01	0.10	0.39	51.1	0.03		0.02	0.01	100.3
PA-49a	olivine	p	ol	0.00	40.8	0.00	0.02	0.05		7.11	0.10	0.37	50.0	0.04		0.02	0.00	98.6
PA-50a	fper	l.m.	2fper	0.00	0.02	0.00	0.07	0.75		21.4	0.23	1.35	75.3	0.00		0.02	0.00	99.1
PA-50b	fper	l.m.	2fper	0.00	0.03	0.00	0.07	0.74		21.4	0.24	1.34	75.2	0.00		0.07	0.02	99.1
PA-50c	CaSiPvk	l.m.	2fper,CaSiPvk	0.01	51.1	0.01	0.08	0.01		0.04	0.04	0.00	0.1	47.9		0.02	0.10	99.4
PA-51a	olivine	p	ol	0.00	40.6	0.00	0.01	0.03		7.82	0.11	0.43	49.7	0.03		0.02	0.00	98.8
PA-52a	olivine	p	2ol	0.00	40.6	0.00	0.02	0.05		7.54	0.11	0.35	49.6	0.04		0.01	0.00	98.3
PA-52b	olivine	p	2ol	0.00	40.4	0.00	0.01	0.05		7.47	0.10	0.36	49.5	0.04		0.01	0.00	98.0
PA-54a(I)	fper (-spinel)	l.m.?	fper-spin,fper-ol,ol		0.08	0.01	0.41	0.71		28.9	0.12	2.11	67.9	0.00		0.15	0.00	100.4
PA-54a(II)	spinel (-fper)	l.m.?	fper-spin,fper-ol,ol	0.00	0.40	0.10	57.4	8.47		9.10	0.07	0.23	23.8	0.00		0.00	0.00	99.6
PA-54b(I)	fper (-olivine)	l.m.?	fper-spin,fper-ol,ol	0.00	0.04	0.00	0.11	0.64		29.6	0.14	2.14	66.7	0.00		0.12	0.00	99.5
PA-54b(II)	olivine (-fper)	l.m.?	fper-spin,fper-ol,ol	0.01	40.8	0.00	0.05	0.02		4.61	0.06	0.20	51.5	0.09		0.02	0.00	97.4
PA-54c	olivine	l.m.?	fper-spin,fper-ol,ol	0.02	41.2	0.00	0.05	0.01		4.63	0.08	0.19	51.7	0.08		0.02	0.00	98.0
PA-55a	silica	l.m.?	silica,fper(lost)	0.01	99.5	0.01	0.05	0.01		0.01	0.01	0.00	0.01	0.01		0.00	0.00	99.6
PA-56a	olivine	p	ol	0.01	40.4	0.00	0.03	0.06		7.12	0.11	0.34	49.6	0.05		0.01	0.00	97.8
PA-57a	olivine	p	ol,sulf	0.00	40.7	0.00	0.01	0.03		7.57	0.11	0.33	49.8	0.02		0.02	0.00	98.6
PA-58a	garnet	p	gt	0.02	41.6	0.07	16.1	8.99		6.27	0.30	0.02	21.2	4.87		0.01	0.00	99.5
PA-65a	garnet	e	2gt	0.08	40.0	0.91	22.5	0.03		13.6	0.27	0.01	10.1	12.7		0.31	0.00	100.6
PA-65b	garnet	e	2gt	0.07	40.3	0.90	22.3	0.03		13.4	0.26	0.00	10.1	12.9		0.28	0.00	100.6
PA-66a(I)	cpx (-rutile)	e	cpx-rut,sulf	0.02	53.6	0.38	4.78	0.08		8.61	0.13	0.03	13.4	14.5		2.75	0.19	98.6
PA-66a(II)	rutile (-cpx)	e	cpx-rut,sulf	0.00	0.04	100.3	0.15	0.21		0.29	0.00	0.00	0.04	0.20		0.02	0.00	101.2
PA-79b	chromite	p	chr,sulf	0.00	0.12	0.07	6.75	65.1		15.3	0.26	0.08	12.5	0.00		0.01	0.00	100.2

Table B1 continued (Composition of minerals exposed to the surface of Panda diamonds)

Sample	Mineral	Parag.	Assemblage	P_2O_5	SiO_2	TiO_2	Al_2O_3	Cr_2O_3	V_2O_3	FeO	MnO	NiO	MgO	CaO	ZnO	Na_2O	K_2O	Total
PA-24b	chr(ex)	p	chr,chr(ex)	0.00	0.1	0.05	5.70	64.7	0.31	18.0	0.27	0.08	10.3	0.00	0.080	0.01	0.00	99.6
PA-27a	chr(ex)	p	chr	0.00	0.1	0.10	7.04	64.2	0.27	15.3	0.26	0.10	13.5	0.00	0.051	0.01	0.00	100.9
PA-28a	chr(ex)	p	chr	0.00	0.1	0.10	7.04	64.2	0.27	15.3	0.26	0.10	13.5	0.00	0.071	0.01	0.00	100.9
PA-30a	chr(ex)	p	chr	0.00	0.1	0.11	7.15	64.5	0.25	15.0	0.24	0.09	12.6	0.00	0.050	0.01	0.01	100.0
PA-31a	chr(ex)	p	chr,chr(ex)	0.00	0.1	0.10	6.23	64.8	0.26	16.1	0.29	0.09	12.7	0.01	0.062	0.03	0.00	100.9
PA-59a	cpx(ex)	p	cpx (ex)	0.02	54.5	0.07	1.53	1.22		2.52	0.11	0.06	17.3	19.8		1.32	0.07	98.5
PA-60a	cpx(ex)	p	cpx(ex),gt(ex)	0.01	54.0	0.04	1.36	1.72		2.47	0.11	0.06	17.2	19.5		1.33	0.11	97.9
PA-60b	gt(ex)	p	cpx(ex),gt(ex)	0.03	40.9	0.24	16.8	8.24		6.13	0.29	0.01	20.4	5.72		0.04	0.00	98.9
PA-61a	cpx(ex)	p	cpx (ex)	0.00	54.3	0.06	1.62	0.89		2.60	0.10	0.06	17.7	19.8		1.31	0.06	98.5
PA-62a	cpx(ex)	p	cpx (ex)	0.02	54.6	0.06	1.63	1.06		2.57	0.11	0.06	17.5	19.6		1.34	0.07	98.6
PA-63a	gt(ex)	e	gt(ex)	0.06	41.3	0.40	23.2	0.21		12.8	0.29	0.01	17.4	4.81		0.10	0.00	100.6
PA-64a	gt(ex)	e	gt(ex)	0.03	39.3	0.54	22.5	0.04		16.0	0.26	0.00	8.44	12.8		0.19	0.00	100.1
PA-67a	cpx(ex)	p	cpx (ex)	0.00	54.1	0.14	2.58	1.01		2.87	0.10	0.05	15.8	19.2		2.21	0.07	98.2
PA-68a	cpx(ex)	p	cpx (ex)	0.01	53.6	0.09	1.02	1.14		2.87	0.10	0.05	16.8	20.8		1.29	0.02	97.8
PA-69a	cpx(ex)	p	cpx (ex)	0.01	54.1	0.25	1.65	1.50		2.80	0.11	0.04	16.9	18.9		1.89	0.05	98.2
PA-70a	cpx(ex)	p	cpx (ex)	0.01	54.1	0.01	1.08	1.65		2.27	0.10	0.06	17.7	19.6		1.22	0.15	98.0
PA-71a	gt(ex)	e	sulf,gt(ex)	0.10	39.3	1.04	20.8	0.03		19.6	0.41	0.00	8.82	9.67		0.29	0.00	100.1
PA-71b	gt(ex)	e	sulf,gt(ex)	0.08	39.5	0.83	21.3	0.04		19.9	0.43	0.00	8.85	9.28		0.22	0.00	100.4
PA-73a	gt(ex)	e	gt(ex)	0.02	39.5	0.60	22.3	0.03		19.2	0.38	0.00	9.58	8.83		0.20	0.00	100.6
PA-74a	gt(ex)	e	gt(ex)	0.02	40.0	0.41	22.3	0.02		19.8	0.37	0.01	9.10	8.93		0.14	0.00	101.1

Table B2: Composition of sulfide inclusions in diamonds from the Panda kimberlite (EPMA-analyses, given in wt%)

Sample	Mineral	Paragenesis	Assemblage	S	Cr	Mn	Fe	Co	Ni	Cu	Zn	As	Total
PA-57c	sulfide	p	ol,sulf	36.6	0.10	0.01	39.9	0.48	20.7	1.29	0.00	0.00	99.0
PA-66b	sulfide	e	cpx-rut,sulf	37.7	0.00	0.00	56.0	0.32	3.26	1.88	0.01	0.01	99.2
PA-71c	sulfide	e	sulf,gt(ex)	37.9	0.00	0.00	54.9	0.41	2.94	2.35	0.01	0.00	98.5
PA-75a	sulfide	p	2sulf	36.7	0.08	0.01	42.0	0.49	18.8	0.89	0.01	0.00	99.0
PA-75b	sulfide	p	2sulf	36.6	0.08	0.00	41.8	0.48	18.9	0.78	0.00	0.00	98.7
PA-78a	sulfide	p	sulf	36.6	0.13	0.01	39.9	0.47	20.4	1.37	0.01	0.01	99.0
PA-79a	sulfide	p	chr,sulf	36.7	0.12	0.01	38.4	0.52	22.3	0.66	0.00	0.00	98.6
PA-80a	sulfide	p	2sulf	36.6	0.09	0.01	40.7	0.46	19.8	1.19	0.01	0.00	98.8
PA-80b	sulfide	p	2sulf	36.7	0.08	0.01	40.7	0.45	19.2	2.05	0.01	0.00	99.1
PA-81a	sulfide	p	sulf	37.0	0.16	0.01	40.3	0.51	20.2	0.66	0.02	0.00	98.8
PA-82a	sulfide	p	sulf	36.7	0.12	0.01	37.9	0.50	22.6	0.66	0.02	0.00	98.5
PA-83a	sulfide	p	sulf	36.8	0.13	0.01	38.6	0.49	21.5	1.86	0.01	0.00	99.3
PA-84a	sulfide	p	sulf	37.2	0.16	0.01	40.0	0.46	20.6	0.97	0.00	0.00	99.4
PA-85a	sulfide	p	2sulf	36.3	0.11	0.01	38.9	0.51	21.6	2.09	0.01	0.00	99.6
PA-85b	sulfide	p	2sulf	36.4	0.11	0.01	39.0	0.50	20.8	2.34	0.01	0.01	99.3
PA-87a	sulfide	p	2sulf	37.0	0.13	0.01	41.3	0.50	19.8	0.56	0.01	0.00	99.4
PA-87b	sulfide	p	2sulf	36.7	0.14	0.01	41.9	0.48	19.1	0.61	0.01	0.00	99.0
PA-88a	sulfide	p	sulf	37.0	0.17	0.01	39.1	0.47	21.5	0.59	0.00	0.01	98.9
PA-89a	sulfide	p	sulf	36.5	0.11	0.00	39.0	0.48	21.1	1.70	0.01	0.01	98.9
PA-90a	sulfide	p	sulf	36.9	0.11	0.01	38.7	0.52	22.5	0.65	0.00	0.00	99.4

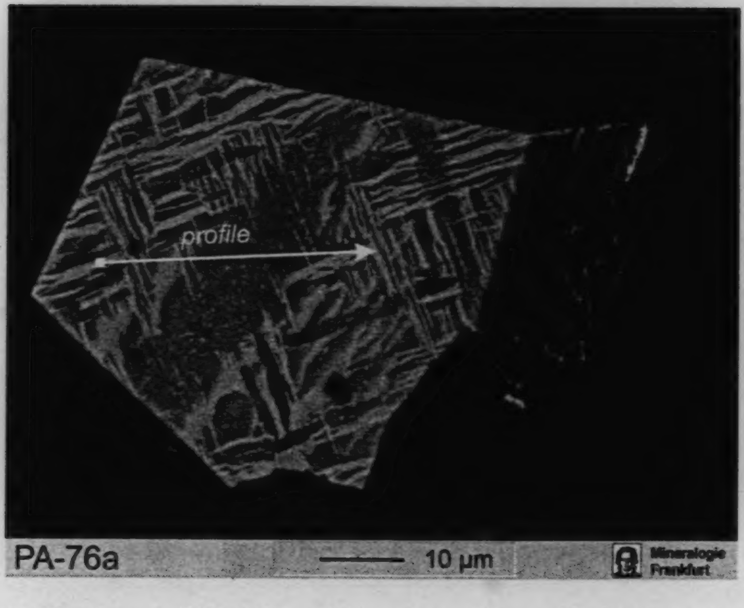

Figure B1: BSE-Image of the Cu-Fe sulfide recovered from diamond PA-76. The arrow indicates the position of the compositional profile-line (see Tab. B3, below).

Distance [µm]	S	Fe	Co	Ni	Cu	Ag	Pb	Bi	Total
0	30.5	22.5	0.06	0.54	42.6	0.04	0.26	0.10	96.6
2	30.4	24.3	0.08	0.57	40.9	0.02	0.22	0.11	96.6
4	32.0	25.8	0.10	0.50	38.7	0.05	0.13	0.08	97.4
6	30.7	23.1	0.09	0.60	43.0	0.06	0.23	0.06	97.9
8	32.0	25.5	0.08	0.70	39.3	0.05	0.25	0.13	98.0
10	31.4	23.7	0.09	0.66	42.7	0.05	0.23	0.12	98.9
12	30.6	20.6	0.08	0.63	47.7	0.07	0.25	0.12	100.0
14	33.6	29.1	0.10	0.70	34.5	0.06	0.15	0.08	98.2
16	33.7	29.0	0.10	0.91	34.5	0.06	0.19	0.08	98.6
18	33.0	27.1	0.08	1.19	36.8	0.05	0.18	0.13	98.6
20	33.8	29.1	0.08	0.66	34.7	0.02	0.20	0.12	98.8
22	33.5	28.8	0.07	0.57	35.2	0.05	0.21	0.09	98.5
24	32.4	25.1	0.07	1.00	40.0	0.05	0.21	0.14	99.0
26	32.6	26.6	0.09	0.60	38.6	0.05	0.13	0.06	98.7
28	31.4	24.7	0.08	0.66	41.1	0.05	0.17	0.08	98.3
30	31.2	24.7	0.08	0.88	40.6	0.06	0.19	0.10	97.9
32	29.4	20.1	0.05	0.67	49.0	0.08	0.24	0.11	99.6
33	29.6	21.2	0.06	0.56	47.1	0.06	0.15	0.09	98.8
34	30.5	22.3	0.07	0.57	44.5	0.06	0.16	0.11	98.2
35	30.5	21.8	0.08	0.70	46.5	0.05	0.22	0.09	99.9
36	31.1	24.1	0.06	0.69	42.0	0.05	0.21	0.12	98.4

Table B3: Composition of the Cu-Fe sulfide recovered from diamond PA-76 (given in wt%). The measurements were taken in 2 µm steps along the profile-line shown in Figure B1 (above).

Appendix B

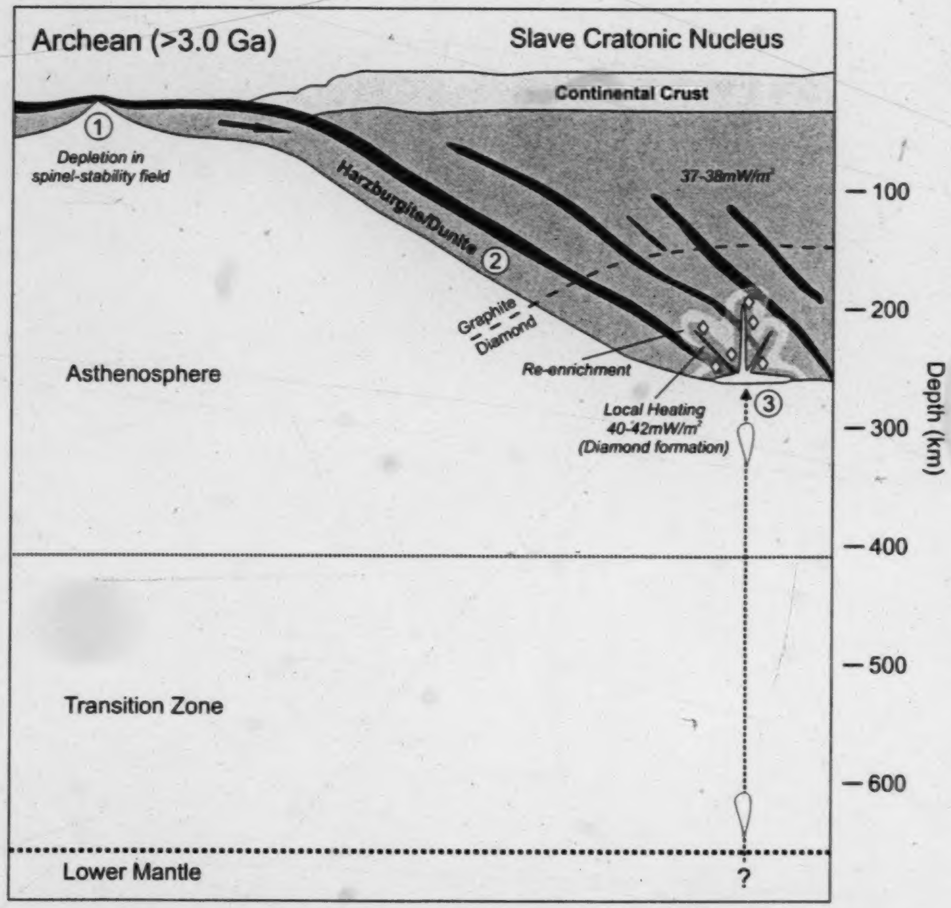
Archean (>3.0 Ga)
Slave Cratonic Nucleus
Continental Crust
①
Depletion in spinel-stability field
Harzburgite/Dunite
②
37-38mW/m²
Graphite
Diamond
Re-enrichment
Local Heating
40-42mW/m²
(Diamond formation)
③
Asthenosphere
Transition Zone
Lower Mantle
?
100
200
300
400
500
600
Depth (km)

Figure B2: Cross section through crust and upper mantle illustrating the processes that led to the formation of the lithospheric mantle beneath the Slave craton during the Archean. 1: Formation of oceanic crust and depleted mantle lithosphere in mid-ocean ridge setting. 2: Subduction and stacking of oceanic lithosphere underneath the early nucleus of the Slave craton. 3: Penetration of the deep Slave lithosphere by ascending melts, causing short term heating, re-enrichment of the depleted mantle lithosphere and diamond formation.

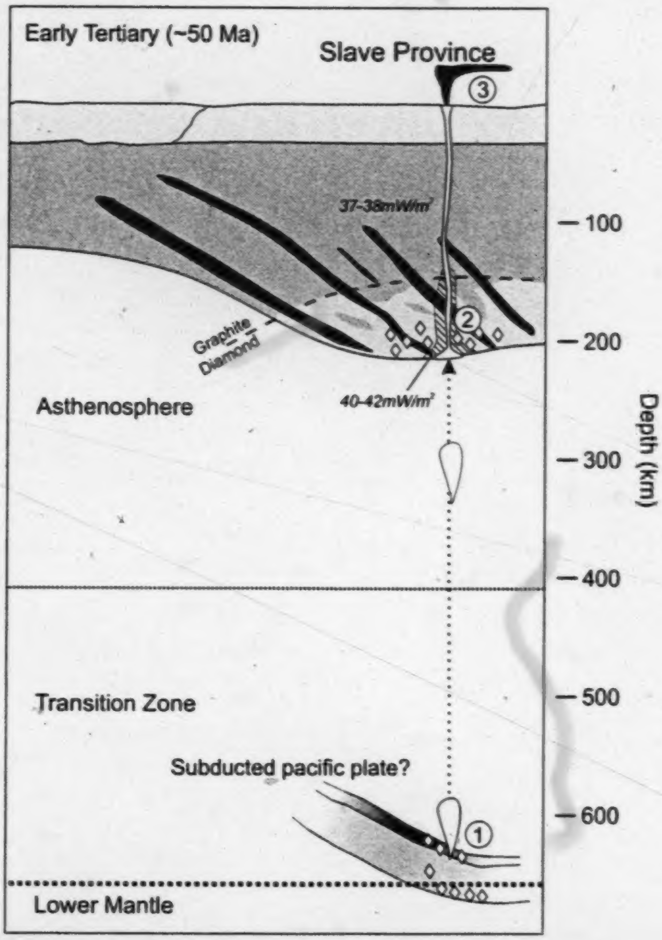
Early Tertiary (~50 Ma)
Slave Province
③
37-38mW/m²
②
Graphite
Diamond
40-42mW/m²
Asthenosphere
Transition Zone
Subducted pacific plate?
①
Lower Mantle
100
200
300
400
500
600
Depth (km)

Figure B3: Cross section through crust and upper mantle beneath the Slave craton at the time of the emplacement of the diamondiferous kimberlites in the Early Tertiary. 1: Ascending melts incorporate diamonds from the transition zone/lower mantle boundary. 2: Penetration of the lithospheric mantle by ascending melts, causing localized heating in the deeper (>150 km), more enriched part of the lithospheric mantle. Also, incorporation of lithospheric xenoliths and diamonds into the melts during their ascent. 3: Kimberlite emplacement.

APPENDIX C: BRAZIL

Table C1: Composition of mineral inclusions in diamonds from Brazil (EPMA-analyses, given in wt%)

Sample	Mineral	Parag.	Assemblage	P_2O_5	SiO_2	TiO_2	Al_2O_3	Cr_2O_3	V_2O_3	FeO	MnO	NiO	MgO	CaO	ZnO	Na_2O	K_2O	Total
AR-04A	olivine	p	ol	0.01	40.4	0.01	0.02	0.04		7.21	0.11	0.39	49.2	0.03		0.02	0.00	97.5
AR-04B	olivine	p	ol	0.00	41.5	0.01	0.01	0.04		7.03	0.09	0.40	50.6	0.02		0.01	0.00	99.7
AR-04C	olivine	p	ol	0.00	41.0	0.01	0.02	0.05		7.22	0.10	0.40	50.2	0.02		0.02	0.00	99.1
AR-05B	olivine	p	ol, qz	0.00	41.2	0.00	0.02	0.04		7.19	0.10	0.41	50.0	0.03		0.04	0.01	99.0
AR-05C	olivine	p	ol, qz	0.00	41.2	0.00	0.02	0.04		7.08	0.11	0.40	50.4	0.03		0.01	0.00	99.3
AR-05D	olivine	p	ol, qz	0.00	40.6	0.00	0.02	0.04		7.14	0.10	0.40	49.8	0.03		0.01	0.00	98.2
AR-07A	chromite	p	chr		0.30	0.32	4.12	68.0	0.19	12.3	0.24	0.09	15.1		0.034			100.8
AR-07B	chromite	p	chr		0.30	0.31	4.09	67.7	0.21	12.3	0.24	0.09	14.8		0.042			100.1
AR-08A	chromite	p	chr		0.19	0.16	3.41	66.5	0.21	13.3	0.25	0.08	14.3		0.039			98.4
AR-08B	chromite	p	chr		0.19	0.17	3.44	68.3	0.22	13.5	0.26	0.08	14.1		0.066			100.3
AR-09A	chromite	p	chr		0.18	0.03	7.93	63.8	0.20	13.9	0.24	0.11	14.1		0.044			100.5
AR-09B	chromite	p	chr		0.19	0.03	7.92	63.7	0.21	13.9	0.24	0.10	14.0		0.048			100.2
AR-09C	chromite	p	chr		0.19	0.03	7.82	63.2	0.21	13.8	0.23	0.10	13.8		0.053			99.4
AR-09D	chromite	p	chr		0.21	0.03	8.06	63.1	0.23	13.9	0.23	0.11	14.2		0.049			100.0
AR-10A	chromite	p	chr		0.14	0.08	8.84	64.5	0.11	10.5	0.20	0.09	15.8		0.034			100.3
AR-10B	chromite	p	chr		0.14	0.08	8.76	64.1	0.11	10.4	0.20	0.10	15.9		0.034			99.8
AR-11A	chromite	p	chr, amph		0.30	0.05	6.93	65.2	0.21	12.5	0.23	0.11	14.9		0.041			100.5
AR-11C	chromite	p	chr, amph		0.30	0.05	6.90	64.8	0.21	12.5	0.23	0.10	14.9		0.042			100.0
AR-11D	chromite	p	chr, amph		0.30	0.05	6.83	65.1	0.20	12.4	0.23	0.10	14.8		0.031			100.0
AR-14A	olivine	p	ol, chr	0.00	40.6	0.01	0.02	0.05		6.96	0.10	0.40	51.2	0.02		0.01	0.00	99.3
AR-14B	olivine	p	ol, chr	0.01	41.0	0.00	0.01	0.04		6.94	0.11	0.41	50.2	0.02		0.01	0.00	98.7
AR-14C	chromite	p	ol, chr		0.21	0.05	8.31	62.6	0.22	13.7	0.23	0.13	14.9		0.025			100.4
AR-14D	chromite	p	ol, chr		0.16	0.05	8.45	62.3	0.21	13.5	0.23	0.12	14.8		0.034			99.9
AR-16A	chromite	p	chr		0.20	0.32	17.4	53.9	0.20	11.8	0.21	0.13	16.9		0.048			101.1
AR-16B	chromite	p	chr		0.19	0.32	17.7	53.8	0.20	11.8	0.19	0.12	17.0		0.048			101.4
AR-18A	chromite	p	chr		0.28	0.02	5.48	65.6	0.22	14.3	0.26	0.11	13.6		0.042			99.9
AR-19A	chromite	p	chr		0.21	0.05	6.57	65.1	0.17	13.5	0.25	0.08	14.3		0.045			100.3
AR-20A	chromite	p	chr		0.29	0.01	6.77	64.1	0.25	14.1	0.25	0.11	14.2		0.039			100.1
AR-20B	chromite	p	chr		0.29	0.01	6.77	63.8	0.25	14.0	0.23	0.10	14.3		0.041			99.8
BV01-B	olivine	p	gt,ol	0.02	40.0	0.01	0.05	0.06		8.00	0.11	0.40	50.0	0.04		0.02	0.01	98.7
BV01-A	garnet	p	gt,ol	0.02	40.7	0.02	15.9	9.10		6.55	0.30	0.01	20.7	4.83		0.01	0.01	98.1

Table C1 continued

Sample	Mineral	Parag.	Assemblage	P_2O_5	SiO_2	TiO_2	Al_2O_3	Cr_2O_3	V_2O_3	FeO	MnO	NiO	MgO	CaO	ZnO	Na_2O	K_2O	Total
BV02-A	garnet	p	gt	0.01	41.8	0.03	17.2	9.73		5.76	0.28	0.02	23.5	1.71		0.02	0.01	100.0
BV03-A	garnet	p	gt	0.02	41.5	0.00	18.5	7.79		6.04	0.29	0.01	21.1	4.77		0.01	0.00	100.0
BV03-B	garnet	p	gt	0.01	41.3	0.01	18.5	7.84		6.05	0.29	0.01	21.0	4.75		0.01	0.00	99.8
BV04-A	olivine	p	ol, chr	0.00	40.2	0.00	0.02	0.05		6.22	0.10	0.40	51.1	0.01		0.02	0.00	98.2
BV04-B	chromite	p	ol, chr		0.19	0.07	9.18	62.3	0.14	12.5	0.20	0.12	15.7	0.00	0.058			100.4
BV04-C	chromite	p	ol, chr		0.22	0.07	9.23	61.7	0.13	12.5	0.20	0.12	15.6	0.00	0.064			99.8
BV05-A	chromite	p	chr		0.19	0.06	6.25	63.9	0.22	14.1	0.21	0.12	14.6	0.00	0.054			99.6
BV05-B	chromite	p	chr		0.20	0.07	6.23	64.0	0.22	14.0	0.21	0.12	14.6	0.00	0.053			99.8
BV06-A	chromite	p	chr		0.33	0.05	7.95	64.6	0.20	11.3	0.19	0.11	15.9	0.00	0.047	0.09	0.01	100.8
BV06-B	chromite	p	chr	0.00	0.33	0.03	8.05	64.7	0.21	11.4	0.20	0.12	16.1	0.00	0.046	0.05	0.01	101.3
BV07-A	chromite	p	chr		0.24	0.23	5.26	65.2	0.18	11.9	0.19	0.11	16.1	0.00	0.056			99.5
BV07-B	chromite	p	chr		0.26	0.22	5.07	64.8	0.18	11.9	0.20	0.10	15.6	0.00	0.057			98.4
BV08-A	chromite	p	chr		0.35	0.01	6.16	64.0	0.19	13.8	0.22	0.13	15.3	0.00	0.034			100.2
BV08-B	chromite	p	chr		0.34	0.00	6.08	63.9	0.18	13.8	0.20	0.13	15.3	0.00	0.045			99.9
BV08-C	chromite	p	chr		0.34	0.00	5.97	63.8	0.19	13.7	0.22	0.13	15.2	0.00	0.031			99.6
BV09-A	olivine	p	ol	0.00	40.2	0.01	0.02	0.08		7.39	0.09	0.40	50.1	0.03		0.01	0.00	98.2
BV09-B	olivine	p	ol	0.01	40.8	0.01	0.03	0.06		7.38	0.10	0.39	50.9	0.03		0.02	0.00	99.7
BV10-A	olivine	p	ol	0.00	41.0	0.01	0.02	0.04		7.43	0.10	0.38	51.0	0.04		0.03	0.00	100.1
BV10-B	olivine	p	ol	0.01	40.6	0.01	0.03	0.04		7.42	0.10	0.39	50.7	0.04		0.02	0.00	99.4
BV11-A	opx	p	opx	0.00	57.4	0.01	0.63	0.47		4.58	0.13	0.11	35.5	0.45		0.05	0.01	99.3
BV12-A	olivine	p	ol	0.00	40.3	0.00	0.02	0.07		6.85	0.09	0.38	50.7	0.04		0.03	0.01	98.5
BV12-B	olivine	p	ol	0.00	40.6	0.00	0.03	0.06		6.77	0.09	0.38	50.9	0.04		0.02	0.00	98.9
BV13-A	olivine	p	ol	0.01	40.4	0.00	0.03	0.10		6.91	0.10	0.38	51.0	0.02		0.02	0.00	99.0
BV13-B	olivine	p	ol	0.01	39.9	0.00	0.03	0.09		6.97	0.10	0.39	50.7	0.02		0.01	0.00	98.2
BV16-A	garnet	p	gt,ol	0.12	41.4	0.08	18.6	7.29		6.44	0.30	0.01	21.9	3.28		0.04	0.00	99.8
BV16-B	olivine	p	gt,ol	0.01	40.5	0.01	0.03	0.10		7.27	0.11	0.39	50.7	0.07		0.02	0.00	99.2
BV16-C	olivine	p	gt,ol	0.01	40.2	0.01	0.02	0.06		7.66	0.11	0.38	49.9	0.03		0.03	0.00	98.4
BV16-D	olivine	p	gt,ol	0.01	40.3	0.00	0.07	0.06		7.63	0.11	0.39	49.9	0.03		0.02	0.00	98.5
BV17-A	garnet	p	gt,ol	0.01	41.6	0.02	18.4	7.88		5.87	0.28	0.02	23.3	2.25		0.01	0.00	99.7
BV17-B	garnet	p	gt,ol	0.01	41.6	0.02	18.3	7.79		5.84	0.28	0.01	23.2	2.24		0.01	0.00	99.3
BV17-C	olivine	p	gt,ol	0.01	40.8	0.00	0.02	0.07		7.20	0.11	0.38	51.1	0.02		0.01	0.00	99.7

Table C1 continued

Sample	Mineral	Parag.	Assemblage	P_2O_5	SiO_2	TiO_2	Al_2O_3	Cr_2O_3	V_2O_3	FeO	MnO	NiO	MgO	CaO	ZnO	Na_2O	K_2O	Total
BV19-A	garnet	p	gt,opx	0.01	41.3	0.03	14.9	12.0		6.06	0.31	0.02	21.8	3.41		0.01	0.00	99.8
BV19-B	garnet	p	gt,opx	0.01	41.0	0.04	14.8	11.9		6.06	0.30	0.02	21.5	3.45		0.01	0.00	99.1
BV19-C	opx	p	gt,opx	0.00	57.3	0.01	0.66	0.55		4.21	0.11	0.13	35.4	0.38		0.05	0.00	98.8
BV19-D	opx	p	gt,opx	0.00	56.7	0.01	0.65	0.55		4.16	0.11	0.13	35.1	0.39		0.06	0.00	97.9
BV20-A	garnet	p	gt,ol	0.01	42.3	0.01	19.5	6.19		5.67	0.25	0.01	23.7	1.80		0.01	0.00	99.5
BV20-B	garnet	p	gt,ol	0.01	42.4	0.00	19.2	6.16		5.67	0.26	0.01	23.9	1.81		0.01	0.00	99.5
BV20-D	olivine	p	gt,ol	0.00	40.3	0.00	0.01	0.03		6.80	0.10	0.39	50.4	0.01		0.01	0.00	98.1
BV21-A	garnet	p	gt,opx	0.02	42.7	0.01	18.3	6.47		6.13	0.27	0.01	23.5	2.68		0.01	0.00	100.1
BV21-B	opx	p	gt,opx	0.00	56.8	0.00	0.51	0.25		4.24	0.10	0.14	35.1	0.43		0.02	0.00	97.5
BV21-C	opx	p	gt,opx	0.01	57.5	0.01	0.51	0.25		4.21	0.11	0.13	35.7	0.43		0.02	0.00	98.9
BV22-A	garnet	p	gt	0.02	40.2	0.22	15.8	9.84		5.88	0.26	0.02	21.8	2.93		0.01	0.00	97.0
BV23-A	garnet	p	gt	0.02	42.0	0.13	18.8	6.80		5.73	0.26	0.01	23.0	2.66		0.02	0.00	99.4
BV23-B	garnet	p	gt	0.01	40.4	0.13	17.9	6.76		5.66	0.26	0.02	22.5	2.63		0.01	0.00	96.2
BV24-A	garnet	p	gt	0.00	42.6	0.01	18.2	7.72		5.38	0.25	0.02	24.7	0.86		0.01	0.00	99.7
BV25-A	garnet	p	gt	0.01	41.1	0.08	14.8	9.96		6.54	0.29	0.02	21.6	4.10		0.04	0.00	98.4
BV26-A	olivine (-chr)	p	ol-chr,opx,chr	0.01	41.3	0.01	0.01	0.13		6.00	0.08	0.42	52.3	0.01		0.01	0.00	100.2
BV26-A	chromite (-ol)	p	ol-chr,opx,chr		0.29	0.01	6.28	64.1	0.21	13.1	0.22	0.11	14.4	0.00	0.051			98.7
BV26-B	opx	p	ol-chr,opx,chr	0.00	58.4	0.01	0.62	0.48		3.78	0.09	0.13	36.6	0.12		0.01	0.01	100.2
BV26-C	chromite	p	ol-chr,opx,chr		0.26	0.01	6.60	64.4	0.21	13.0	0.21	0.11	15.0	0.00	0.046			100.0
BV26-D	chromite	p	ol-chr,opx,chr		0.29	0.00	6.65	64.4	0.22	13.1	0.22	0.11	15.0	0.00	0.048			100.1
BV26-G	opx	p	ol-chr,opx,chr	0.00	57.1	0.00	0.68	0.56		3.79	0.09	0.13	35.8	0.12		0.01	0.00	98.3
BV26-H	opx	p	ol-chr,opx,chr	0.01	57.0	0.00	0.68	0.56		3.81	0.10	0.13	35.6	0.13		0.01	0.00	98.0
BV27-A	olivine	p	ol,chr	0.02	40.2	0.01	0.04	0.05		8.08	0.11	0.38	50.4	0.03		0.02	0.01	99.3
BV27-B	chromite	p	ol,chr	0.00	0.31	0.34	4.69	64.5	0.26	17.2	0.29	0.11	13.1	0.01	0.058	0.07	0.00	101.0
BV28-B	chromite	p	chr		0.28	0.12	7.07	64.1	0.17	13.2	0.22	0.12	14.5	0.01	0.046	0.02	0.01	99.8
BV29-A	chromite	p	chr		0.25	0.42	5.29	64.9	0.19	12.8	0.19	0.12	15.3	0.00	0.049			99.5
BV29-B	chromite	p	chr		0.27	0.42	5.35	64.9	0.19	12.8	0.20	0.12	16.3	0.00	0.038			100.5
BV30-A	chromite	p	chr		0.27	0.08	4.42	65.8	0.22	15.0	0.24	0.10	14.0	0.00	0.056			100.1
BV30-B	chromite	p	chr		0.27	0.08	4.45	65.8	0.22	14.9	0.24	0.11	14.3	0.00	0.055			100.4
BV31-A	chromite	p	chr		0.23	0.20	6.10	64.8	0.22	12.8	0.21	0.11	16.2	0.00	0.049			100.8
BV31-B	chromite	p	chr		0.23	0.11	6.35	64.2	0.21	12.6	0.20	0.11	15.5	0.00	0.045			99.5

Table C1 continued

Sample	Mineral	Parag.	Assemblage	P_2O_5	SiO_2	TiO_2	Al_2O_3	Cr_2O_3	V_2O_3	FeO	MnO	NiO	MgO	CaO	ZnO	Na_2O	K_2O	Total
BV31-C	chromite	p	chr		0.21	0.11	6.24	64.1	0.22	12.6	0.21	0.11	14.7	0.00	0.045			98.5
BV32-A	chromite	p	chr		0.30	0.05	6.46	63.6	0.13	13.1	0.22	0.12	15.2	0.00	0.048			99.2
BV32-B	chromite	p	chr		0.31	0.05	6.67	63.5	0.13	13.1	0.21	0.12	15.4	0.00	0.038			99.5
BV33-A	chromite	p	chr		0.20	0.06	5.76	64.7	0.20	13.7	0.22	0.12	14.4	0.00	0.061			99.3
BV33-B	chromite	p	chr		0.21	0.06	6.14	64.5	0.21	13.7	0.22	0.11	14.9	0.00	0.056			100.0
BV34-A	garnet	e	gt	0.15	39.1	0.97	21.3	0.06		20.0	0.40	0.00	6.68	11.94		0.26	0.00	100.8
BV34-B	garnet	e	gt	0.15	39.2	0.96	20.9	0.05		19.8	0.39	0.00	6.75	11.92		0.26	0.00	100.4
CA01-A	olivine	p	ol	0.00	39.8	0.00	0.02	0.05		8.38	0.10		50.7	0.03		0.02	0.00	99.6
CA01-B	olivine	p	ol	0.00	40.0	0.00	0.02	0.05		8.46	0.10		51.5	0.03		0.01	0.00	100.6
CA02-A	olivine	p	ol	0.01	40.1	0.01	0.03	0.05		7.03	0.10		52.6	0.02		0.01	0.00	100.3
CA03-A	olivine	p	ol	0.01	40.3	0.00	0.02	0.04		6.96	0.09		53.0	0.03		0.02	0.00	100.8
CA05-A	chromite	p	chr		0.21	0.02	5.85	64.7	0.17	13.2	0.26	0.10	15.6	0.00	0.048			100.1
CA10-A	olivine	p	ol,chr	0.01	40.4	0.00	0.02	0.11		5.76	0.08		53.5	0.02		0.02	0.00	100.3
CA10-B	chromite	p	ol,chr		0.32	0.54	4.68	65.2	0.25	11.7	0.22	0.12	16.0	0.00	0.039			99.0
CA10-C	chromite	p	ol,chr		0.36	0.54	4.73	64.6	0.22	12.0	0.21	0.12	16.3	0.00	0.034			99.0
CA12-A	chromite	p	ol,chr		0.20	0.01	0.78	71.4	0.10	11.3	0.24	0.10	14.8	0.01	0.036			99.0
CA12-B	olivine	p	ol,chr	0.01	39.9	0.00	0.02	0.11		5.63	0.07		52.8	0.01		0.01	0.00	98.9
CA12-C	olivine	p	ol,chr	0.00	40.6	0.00	0.02	0.20		5.66	0.08		53.4	0.01		0.01	0.04	100.4
CA13-B	chromite	p	chr		0.14	0.15	3.54	66.4	0.15	15.7	0.29	0.09	12.8	0.00	0.059			99.3
CA13-C	chromite	p	chr		0.15	0.12	3.94	67.6	0.21	16.0	0.28	0.08	12.4	0.00	0.059			100.8
CA14-A	e-garnet	e	gt	0.12	40.1	0.21	22.1	0.19		15.4	0.44		15.4	4.89		0.17	0.01	99.0
CA14-B	e-garnet	e	gt	0.09	40.8	0.22	22.4	0.18		15.4	0.47		15.7	4.91		0.16	0.01	100.3

Appendix C

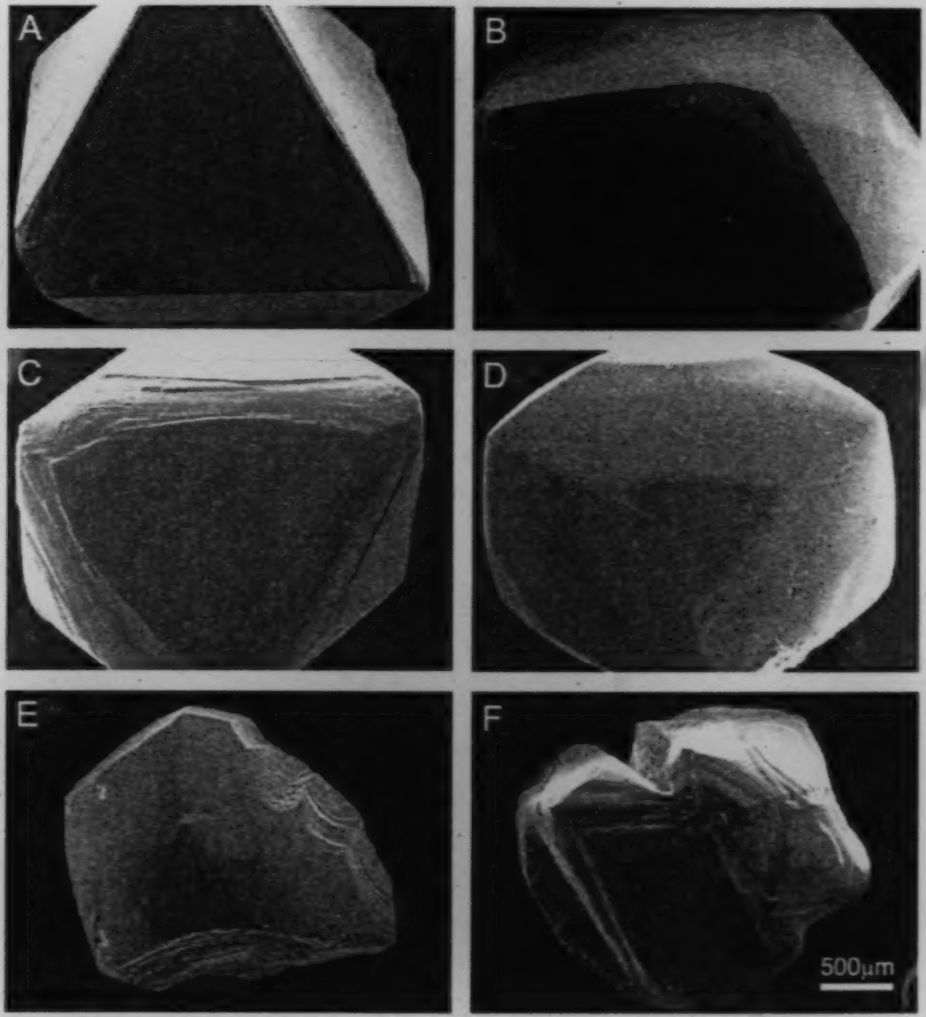

Figure C1: Crystal shapes of Brazilian diamonds (SEI images): [A] Octahedron, the primary crystal shape (BV-06). [B] Dodecahedron, the result of resorption (AR-01). [C],[D] Combinations of Octahedron and Dodecahedron (BV-03, AR-02). [E] Irregular crystal shape: cleavage chip (BV-29). [F] Complex crystal shape: Aggregate of twinned combinations of dodecahedron and octahedron (BV-28). Scale applies to all images.

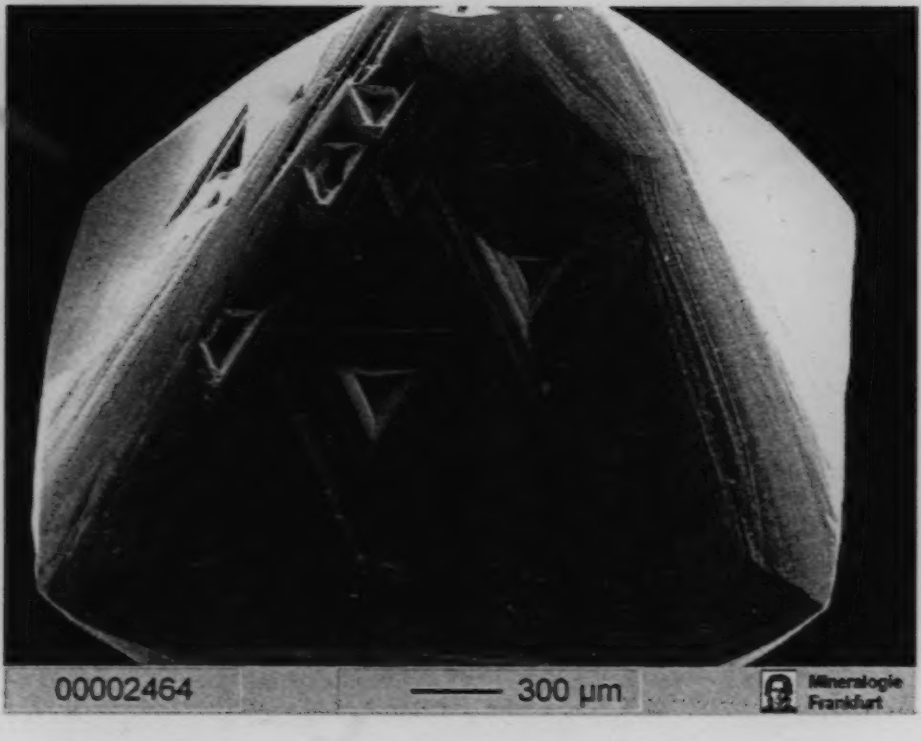
00002464
300 µm
Mineralogie
Frankfurt

Figure C2: SEI image of diamond BV-13 (Boa Vista) showing negatively oriented trigonal etch pits (trigons) developed on an octahedral, (111), crystal face.

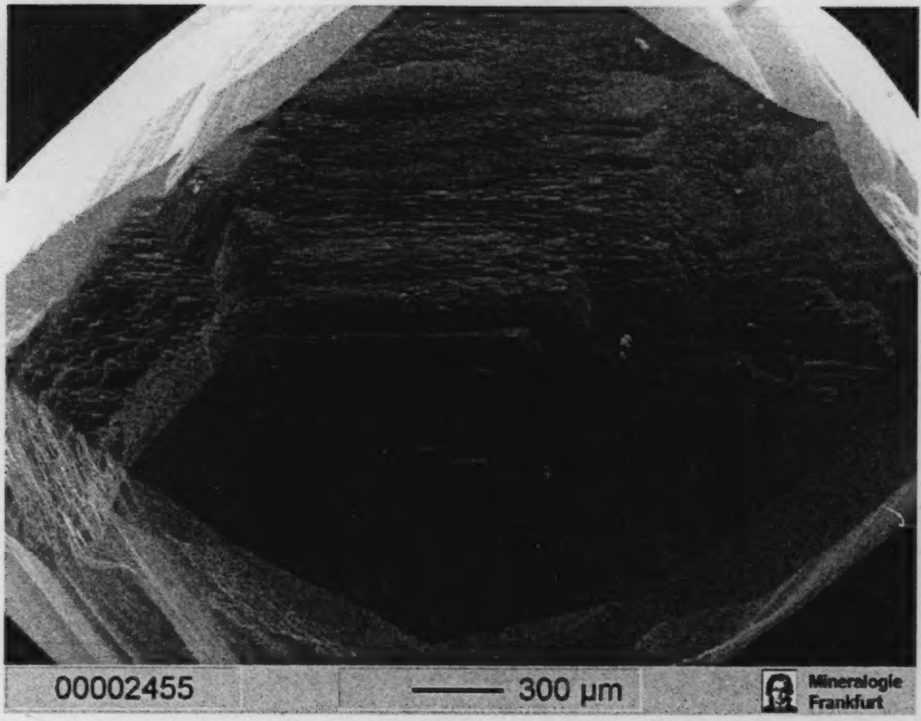
00002455
300 µm
Mineralogie
Frankfurt

Figure C3: SE image of diamond BV-09 (Boa Vista) showing hillocks on dodecahedral crystal faces.

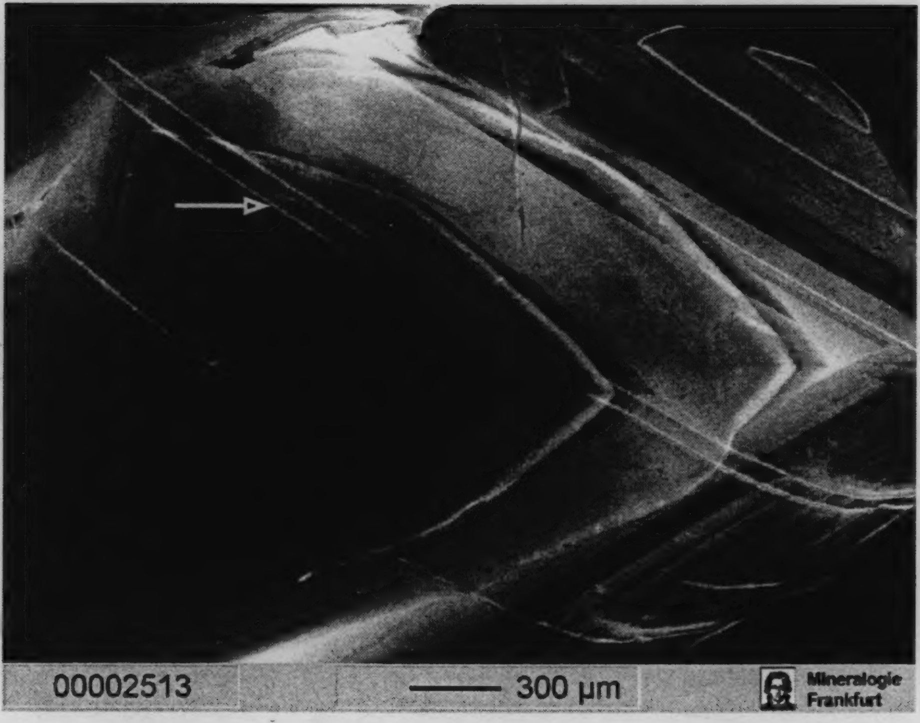
00002513
300 µm
Mineralogie Frankfurt

Figure C4: CL image of diamond CA-01 (Canastra) showing deformation lines (white arrow) parallel to (111).

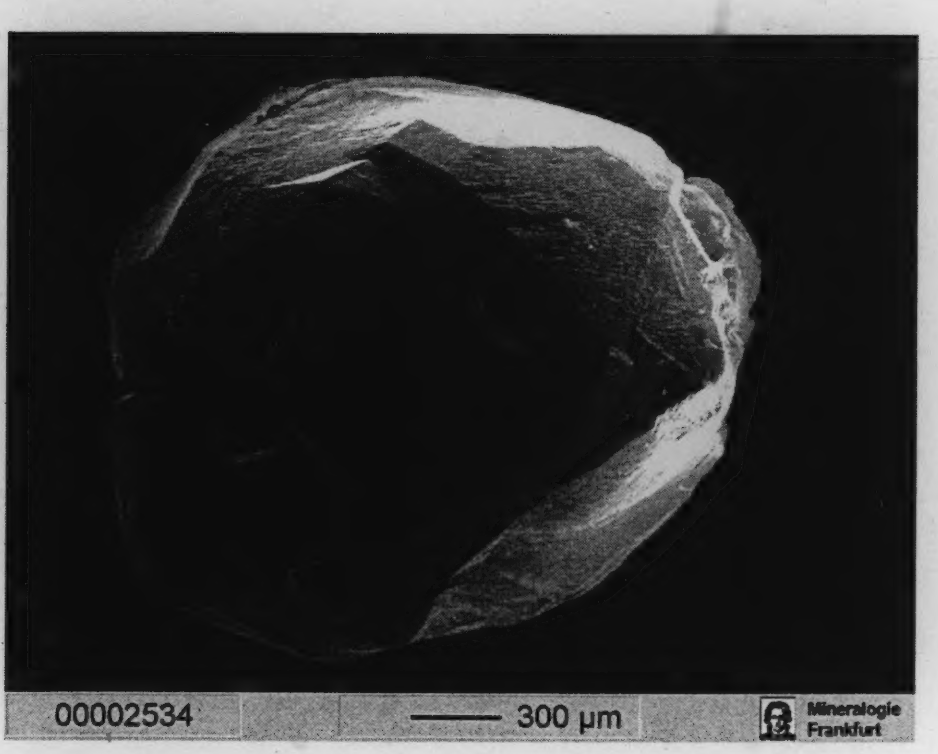
00002534
300 µm
Mineralogie Frankfurt

Figure C5: SE image of diamond CA-12 (Canastra) showing inclusion cavities on the surface.

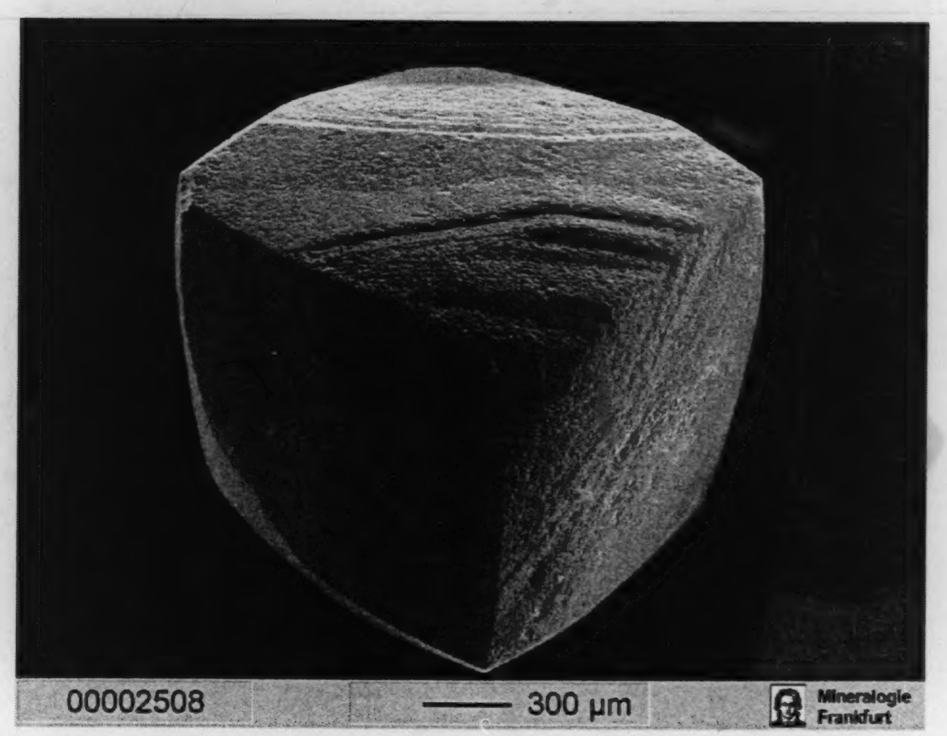
00002508
300 µm
Mineralogie Frankfurt

Figure C6: SEI image of diamond BV-33 (Boa Vista) showing a coarse frosted surface.

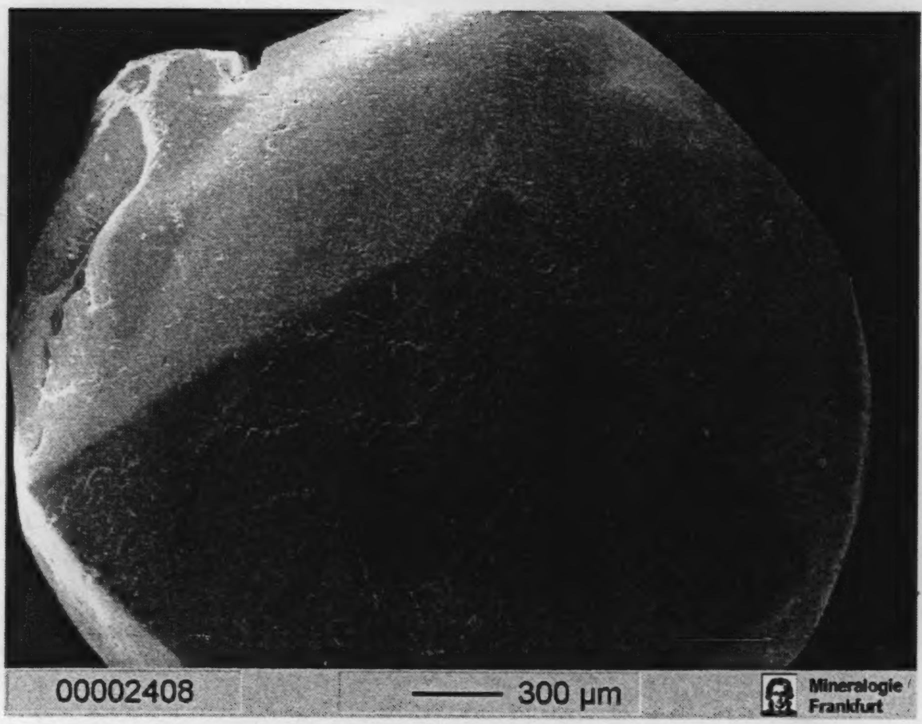
00002408
300 µm
Mineralogie
Frankfurt

Figure C7: SEI image of diamond AR-05 (Arenapolis), showing percussion marks and edge abrasion on the diamond surface.

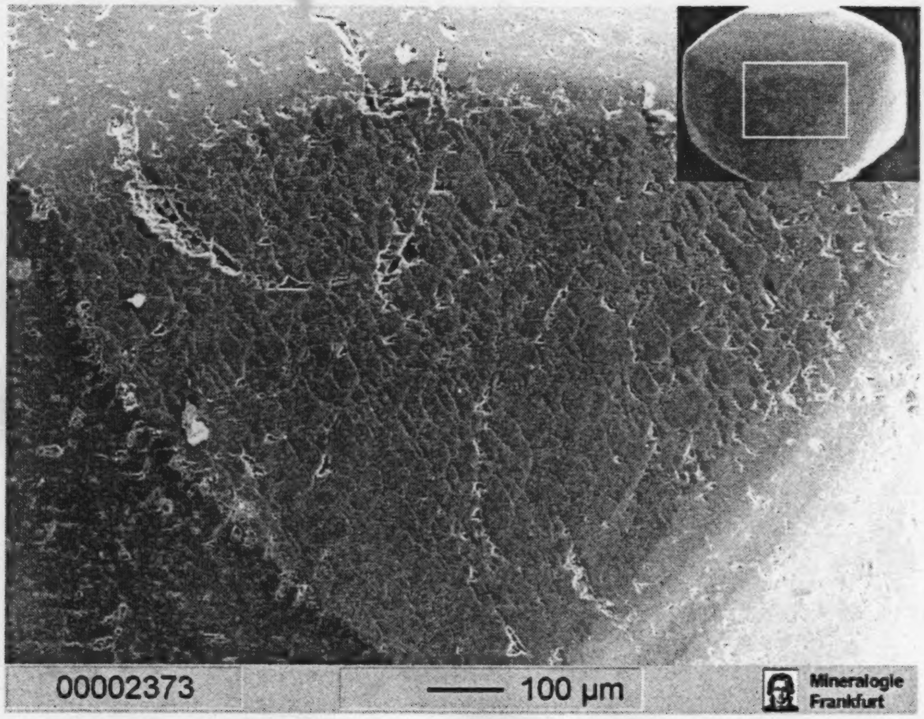
00002373
100 µm
Mineralogie
Frankfurt

Figure C8: SE image of diamond AR-02 (Arenapolis) showing network pattern and percussion marks on a (111) crystal face. *INSET*: overview

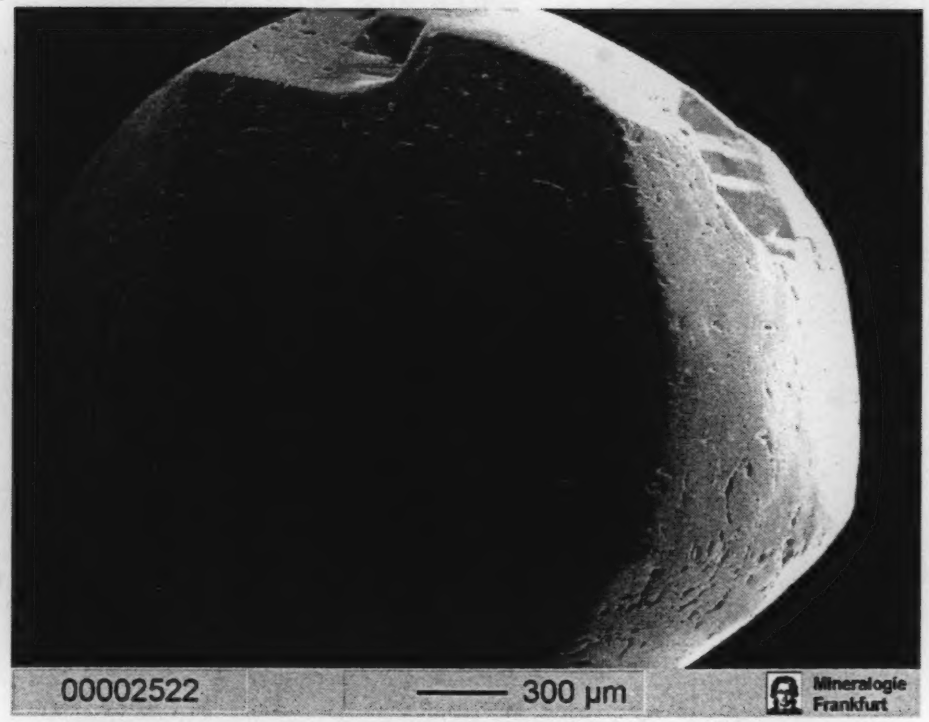
00002522
300 µm
Mineralogie
Frankfurt

Figure C9: SEI image of diamond CA-06 (Canastra) showing percussion marks and edge abrasion on the diamond surface. Abrasion textures like these are rare on Canastra diamonds.

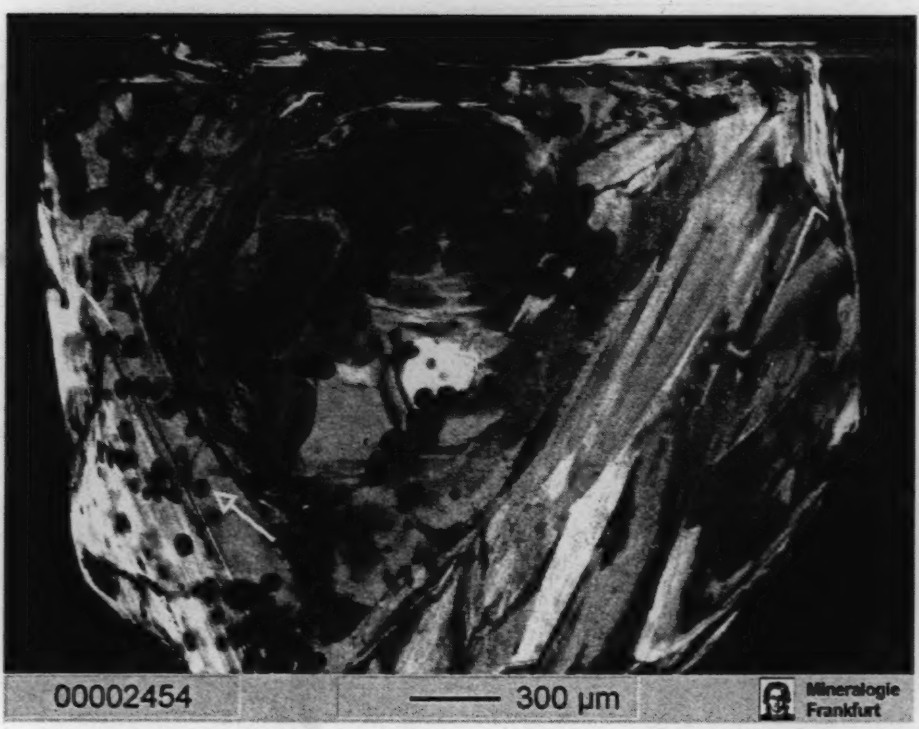
00002454
300 µm
Mineralogie Frankfurt

Figure C10: CL image of diamond BV-08 (Boa Vista). The dark spots in the CL image mark green radiation spots in visible light. Weaker spots, which do not appear in visible light, show a central dark spot and a surrounding dark rim (arrow).

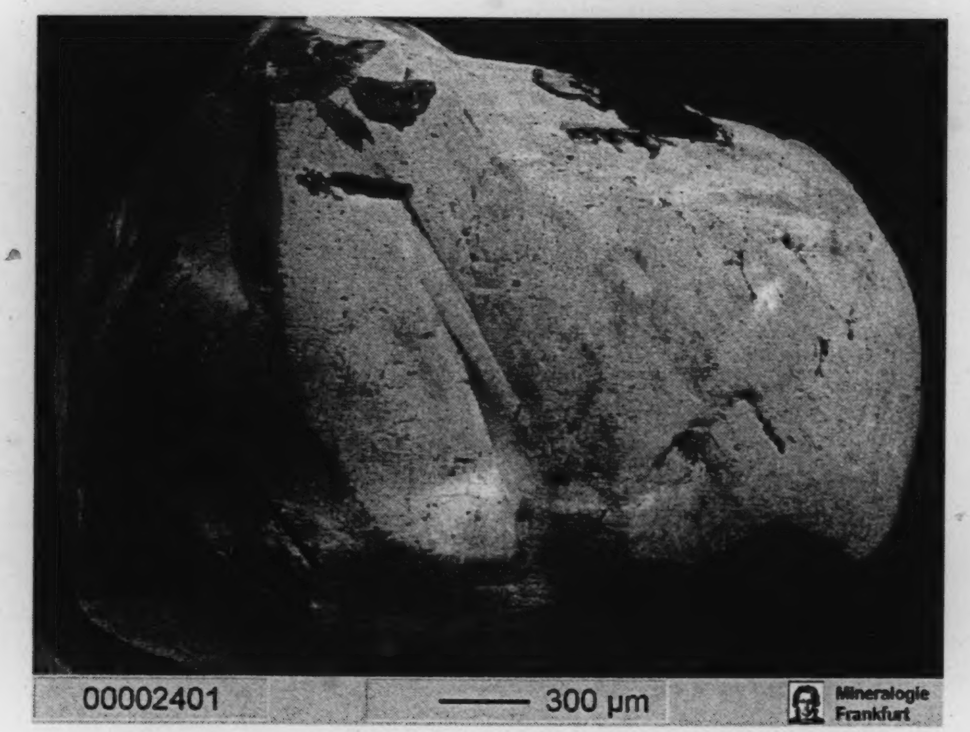
00002401
300 μm
Mineralogie
Frankfurt

Figure C11: CL image of almost un-zoned diamond AR-03 (Arenapolis).

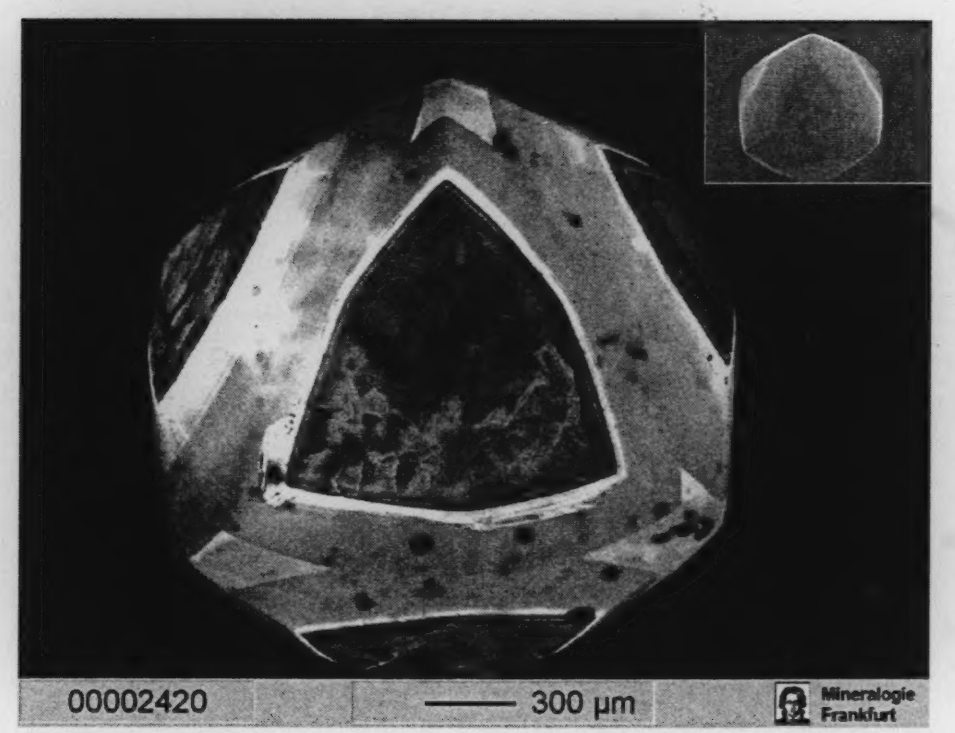
00002420
300 µm
Mineralogie
Frankfurt

Figure C12: CL image of diamond AR-17 (Arenapolis) showing regular growth zoning. *INSET*: corresponding SEI image

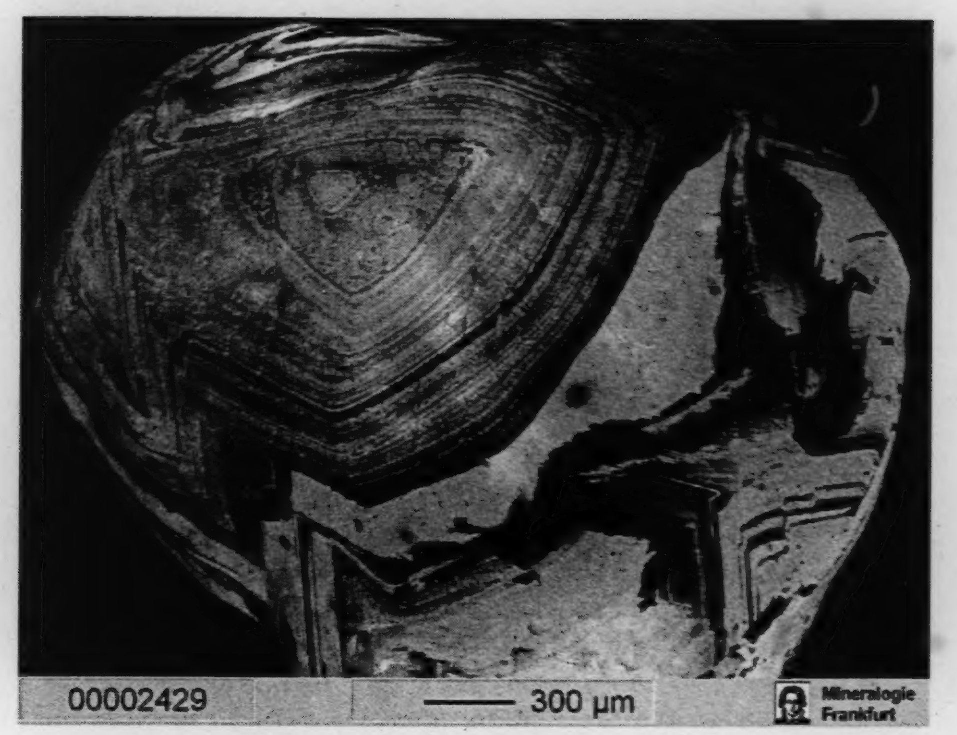
00002429
300 µm
Mineralogie
Frankfurt

Figure C13: CL image of the irregular zoning pattern of diamond BV-16 (Boa Vista).

APPENDIX D: JAGERSFONTEIN

Appendix D

Table D1: Morphological and compositional characteristic of Jagersfontein diamonds.

Sample	Weight [ct]	Color	Shape	Def.	Assemblage	Paragenesis	$\delta^{13}C$ [‰ PDB]	N [at.ppm]	B-cent. [%]	Type
JF-01	0.025	colorless	O	N	maj	deep-eclogitic	-21.2	0		II
JF-02	0.020	colorless	IA	N	ol	peridotitic	-4.9	136	6.6	IaA
JF-03	0.033	colorless	OA	N	ol	peridotitic	-6.1	171	19.5	IaAB
JF-04	0.035	colorless	FO	N	cpx,gt-cpx	eclogitic	-4.1	582	45.8	IaAB
JF-05	0.040	slightly yellow	I	N	ol	peridotitic	-7.5	199	91.8	IaB
JF-06	0.035	colorless	I	N		unknown	-14.1	0		II
JF-07	0.040	brown	I	N	opx	websteritic	-20.2	0		II
JF-08	0.053	colorless	O	N	cpx	eclogitic	-5.3	434	64.7	IaAB
JF-09	0.048	colorless	O	N	maj	deep-eclogitic	-21.8	0		II
JF-10	0.043	colorless	D	N	ol	peridotitic	-6.6	0		II
JF-11	0.050	colorless	O	N	cpx	eclogitic	-4.5	146	23.4	IaAB
JF-12	0.055	colorless	D	Y	cpx	eclogitic	-3.9	39	61.8	IaAB
JF-13	0.068	colorless	O	N	gt	eclogitic	-5.6	706	64.6	IaAB
JF-14	0.038	colorless	I	N		unknown	-15.3	60	11.8	IaAB
JF-15	0.063	colorless	I	N	gt	eclogitic	-4.4	690	39.3	IaAB
JF-16	0.070	colorless	FD	N		unknown	-4.8	728	42.7	IaAB
JF-17	0.045	colorless	O	N	opx	peridotitic	-2.6	0		II
JF-18	0.075	colorless	OA	N		unknown	-20.9	35	1.6	IaA
JF-19	0.078	slightly yellow	D	Y	SiO2,cpx	eclogitic	-19.8	133	40.9	IaAB
JF-20	0.095	slightly brown	D	Y	gt-cpx	eclogitic	-3.8	639	48.9	IaAB
JF-21	0.073	colorless	OA	N		unknown	-4.3	544	77.7	IaAB
JF-22	0.075	colorless	D	N	maj	deep-eclogitic	-17.2	34	98.5	IaB
JF-23	0.115	slightly brown	D	Y	cpx	eclogitic	-4.5	320	29.3	IaAB
JF-24	0.088	colorless	TM	N	opx	peridotitic	-4.7	14	0.0	IaA
JF-25	0.110	colorless	I	N		unknown	-3.5	49	4.5	IaA
JF-26	0.128	brown	OM	N	cpx	eclogitic	-18.4	250	39.4	IaAB
JF-27	0.130	colorless	D	N	opx	peridotitic	-6.4	220	26.6	IaAB
JF-28	0.143	colorless	D	N		unknown	-5.1	783	8.5	IaA
JF-30	0.623	colorless	DA	N	gt,opx	websteritic	-4.5	459	13.7	IaAB
JF-31	0.025	colorless	I	N	gt (ex)	eclogitic	-9.2	0		II
JF-32	0.023	colorless	I	N	gt	peridotitic	-4.1	224	52.9	IaAB
JF-33	0.033	colorless	D	Y	gt	peridotitic	-5.0	336	8.7	IaA
JF-34	0.030	colorless	OA	N	gt-cpx	eclogitic	-19.3	42	76.0	IaAB
JF-35	0.028	colorless	I	N	gt,gt-opx-chr	peridotitic	-5.0	89	3.5	IaA
JF-36	0.033	colorless	D	N	gt	peridotitic	-5.3	18	30.1	IaAB
JF-37	0.025	colorless	O	N	maj	deep-eclogitic	-21.7	23	36.0	IaAB
JF-38	0.025	colorless	I	N	gt	eclogitic	-17.9	0		II
JF-39	0.040	colorless	O	N	maj	deep-eclogitic	-17.9	54	72.4	IaAB
JF-40	0.065	slightly yellow	I	N	gt	eclogitic	-17.4	0		II
JF-41	0.060	colorless	I	N	gt	eclogitic	-15.6	13	76.7	IaAB
JF-42	0.063	colorless	O	N	maj	deep-eclogitic	-17.4	18	100.0	IaB
JF-43	0.058	colorless	I	N	maj, gt	deep-websteritic	-18.7	0		II
JF-44	0.058	yellow	I	N	maj	deep-eclogitic	-17.7	0		II
JF-45	0.090	colorless	O	N		unknown	-5.2	46	0.0	IaA
JF-46	0.060	slightly yellow	I	N	gt	peridotitic	-3.5	0		II
JF-47	0.055	colorless	I	N	gt (ex)	eclogitic	-16.0	85	57.4	IaAB
JF-48	0.068	colorless	I	N	maj	deep-eclogitic	-23.6	0		II
JF-49	0.070	colorless	I	N	gt,opx	websteritic	-17.2	122	35.3	IaAB
JF-50	0.080	colorless	O	N	maj	deep-eclogitic	-19.9	60	66.2	IaAB
JF-51	0.065	slightly yellow	I	N	gt	eclogitic	-22.6	13	97.8	IaB
JF-52	0.038	colorless	O	N	gt	eclogitic	-15.4	36	91.5	IaB
JF-53	0.133	colorless	D	N	gt,cpx	eclogitic	-4.3	24	0.0	IaA
JF-54	0.080	colorless	IA	N	gt-opx-cpx	websteritic	-17.1	0		II
JF-55	0.115	colorless	I	N	maj	deep-eclogitic	-17.6	35	99.9	IaB
JF-56	0.138	colorless	FD	N	gt-2cpx-SiO2	eclogitic	-13.0	29	63.6	IaAB
JF-57	0.163	slightly yellow	O	N	gt	peridotitic	-5.7	194	11.7	IaAB
JF-58	0.135	colorless	I	N	maj	deep-eclogitic	-23.0	0		II
JF-59	0.290	colorless	DM	N	gt,corundum	eclogitic	-4.3	427	64.7	IaAB
JF-60	0.253	colorless	D	N	opx	websteritic	-4.3	102	13.6	IaAB
JF-61	0.240	slightly brown	D	N	gt	eclogitic	-4.7	206	0.0	IaA
JF-62	0.205	colorless	DA	N	gt	peridotitic	-4.1	0		II

Appendix D

Table D1 continued

Sample	Weight [ct]	Color	Shape	Def.	Assemblage	Paragenesis	δ^{13}C [‰ PDB]	N [at.ppm]	B-cent. [%]	Type
JF-63	0.308	colorless	DA	N	gt	eclogitic	-14.3	249	92.5	IaB
JF-64	0.238	colorless	FD	N	gt	peridotitic	-4.6	55	3.8	IaA
JF-65	0.315	slightly brown	DM	Y	ol	peridotitic	-3.1	493	35.8	IaAB
JF-66	0.410	colorless	I	N	gt(ex)	eclogitic	-24.2	0		II
JF-67	0.475	colorless	I	N	gt,cpx	eclogitic	-4.1	356	24.1	IaAB
JF-68	0.430	slightly yellow	I	N	gt(ex)	eclogitic	-18.2	0		II
JF-69	0.125	colorless	I	N	gt	eclogitic	-4.4	439	23.7	IaAB
JF-70	0.138	brown	I	N	cpx	eclogitic	-16.3	106	33.6	IaAB
JF-71	0.048	colorless	I	N		unknown	-19.7	0		II
JF-72	0.070	colorless	I	N	cpx	eclogitic	-17.2	33	70.4	IaAB
JF-73	0.070	colorless	O	N	opx	peridotitic	-6.4	65	0.0	IaA
JF-74	0.415	colorless	I	N	cpx	eclogitic	-1.6	339	13.7	IaAB
JF-75	0.123	slightly yellow	D	Y		unknown	-3.9	910	43.7	IaAB
JF-76	0.078	yellow	I	N	gt	eclogitic	-5.2	45	23.3	IaAB
JF-77	0.040	colorless	O	N	cpx	eclogitic	-5.2	352	19.3	IaAB
JF-78	0.685	colorless	I	N	opx	peridotitic	-3.5	106	31.2	IaAB
JF-79	0.363	colorless	D	N	cpx (ex)	eclogitic	-5.1	1027	21.2	IaAB
JF-80	0.055	colorless	I	N	cpx	eclogitic	-22.8	38	5.5	IaA
JF-81	0.075	yellow	I	N	cpx	eclogitic	-4.9	0		II
JF-82	0.090	colorless	D	N		unknown	-5.6	921	27.9	IaAB
JF-84	0.040	colorless	D	N	maj	deep-eclogitic	-20.9	39	24.7	IaAB
JF-85	0.108	slightly brown	TM	N		unknown	-5.0	440	12.2	IaAB
JF-86	0.170	colorless	I	N	cpx	eclogitic	-4.5	56	5.6	IaA
JF-87	0.175	colorless	O	N		unknown	-4.3	372	8.2	IaA
JF-88	0.070	colorless	D	N	ol	peridotitic	-5.9	126	5.2	IaA
JF-89	0.033	colorless	O	N		unknown	-19.5	89	13.7	IaAB
JF-90	0.070	colorless	D	N	cpx	eclogitic	-4.8	23	0.0	IaA
JF-91	0.050	colorless	I	N	cpx	eclogitic	-3.6	552	23.8	IaAB
JF-92	0.168	colorless	I	N	cpx	eclogitic	-5.6	451	47.9	IaAB
JF-93	0.070	colorless	I	N		unknown	-4.4	0		II
JF-94	0.028	slightly yellow	I	N	ol	peridotitic	-1.1	0		II
JF-95	0.065	slightly yellow	OA	N	cpx	eclogitic	-5.4	683	34.0	IaAB
JF-96	0.210	colorless	I	N	cpx	eclogitic	-18.1	18	0.0	IaA
JF-97	0.130	colorless	DA	N	opx	peridotitic	-7.6	6	0.0	II
JF-98	0.053	colorless	D	N	ol	peridotitic	-5.1	0		II
JF-99	0.165	colorless	D	N		unknown	-5.7	967	38.0	IaAB
JF-100	0.695	colorless	D	N		unknown	-4.7	310	0.0	IaA
JF-101	0.025	colorless	D	N		unknown	-4.3	0		II
JF-102	0.145	colorless	O	N		unknown	-5.1	390	1.6	IaA
JF-103	0.040	colorless	OA	N	gt(ex)	eclogitic	-21.7	69	32.0	IaAB
JF-104	0.115	slightly brown	D	N		unknown	-3.3	345	33.7	IaAB
JF-105	0.325	colorless	OA	N	chr	peridotitic	-5.9	357	7.4	IaA
JF-106	0.250	colorless	D	N	chr	peridotitic	-2.6	369	11.1	IaAB
JF-107	0.178	colorless	D	N	gt(ex)	peridotitic	-5.3	269	17.8	IaAB
JF-108	0.055	colorless	DA	N		unknown	-6.3	0		II
JF-109	0.068	colorless	O	N	chr	peridotitic	-4.0	418	29.8	IaAB
JF-110	0.120	colorless	I	N	gt(ex)	eclogitic	-13.9	273	58.0	IaAB
JF-111	0.290	slightly brown	D	Y	cpx	eclogitic	-3.2	392	43.1	IaAB
JF-112	0.163	colorless	D	N	chr	peridotitic	-3.9	507	17.0	IaAB
JF-113	0.065	colorless	D	N	gt(ex)	eclogitic	-19.1	15	52.0	IaAB
JF-114	0.190	colorless	D	N	gt	peridotitic	-3.9	63	21.1	IaAB
JF-115	0.140	colorless	I	N	ol	peridotitic	-4.3	24	55.0	IaAB
JF-116	0.120	slightly greenish	I	Y	chr(ex)	peridotitic	-7.6	21	25.6	IaAB
JF-117	0.075	brown	D	Y		unknown	-4.2	100	12.7	IaAB
JF-118	0.090	colorless	I	N	chr	peridotitic	-2.0	23	0.0	IaA
JF-119	0.308	colorless	D	N		unknown	-4.2	1186	19.1	IaAB
JF-120	0.145	colorless	D	N	cpx	eclogitic	-5.1	578	10.2	IaAB
JF-121	0.040	colorless	I	N		unknown	-23.2	0		II
JF-122	0.120	slightly yellow	I	Y	gt-opx-cpx	websteritic	-15.4	45	34.7	IaAB
JF-123	0.095	colorless	O	N	chr	peridotitic	-4.3	235	27.1	IaAB
JF-124	0.250	colorless	O	N	ol	peridotitic	-5.5	104	3.6	IaA

Table D2: Composition of mineral inclusions in diamonds from the Jagersfontein kimberlite (EPMA-analyses, given in wt%)

Sample	Mineral	Parag.	Assemblage	P_2O_5	SiO_2	TiO_2	Al_2O_3	Cr_2O_3	FeO	MnO	NiO	MgO	CaO	Na_2O	K_2O	Total
JF-01A	garnet, majoritic	deep-e	2maj	0.02	42.7	0.13	19.9	0.24	12.6	0.42	0.01	17.5	6.14	0.15	0.00	99.8
JF-01B	garnet, majoritic	deep-e	2maj	0.02	42.5	0.14	20.0	0.23	12.6	0.41	0.01	17.6	6.14	0.15	0.00	99.8
JF-02A	olivine	p	ol	0.01	40.3	0.01	0.03	0.07	6.95	0.10	0.35	50.2	0.05	0.05	0.00	98.1
JF-02B	olivine	p	ol	0.02	40.8	0.02	0.05	0.09	7.00	0.09	0.34	50.7	0.05	0.04	0.00	99.1
JF-03A	olivine	p	ol	0.02	41.2	0.02	0.03	0.04	6.12	0.08	0.32	51.9	0.02	0.03	0.01	99.8
JF-03B	olivine	p	ol	0.00	41.0	0.00	0.05	0.01	6.00	0.08	0.33	51.7	0.02	0.02	0.00	99.2
JF-03C	olivine	p	ol	0.00	40.6	0.01	0.04	0.08	6.10	0.10	0.32	51.3	0.02	0.00	0.00	98.6
JF-04A	cpx	e	cpx,gt-cpx	0.03	53.3	0.67	8.25	0.03	7.49	0.09	0.03	9.93	13.9	4.38	0.16	98.3
JF-04B	cpx(-gt)	e	cpx,gt-cpx	0.02	53.5	0.66	8.29	0.02	7.61	0.10	0.03	9.94	13.9	4.47	0.14	98.7
JF-04B	garnet (-cpx)	e	cpx,gt-cpx	0.05	39.5	0.97	21.1	0.04	18.0	0.37	0.01	10.8	8.60	0.25	0.00	99.7
JF-04C	cpx	e	cpx,gt-cpx	0.02	53.8	0.64	8.30	0.02	7.51	0.09	0.03	10.0	13.9	4.48	0.15	98.8
JF-05A	olivine	p	ol	0.01	41.5	0.00	0.04	0.05	6.10	0.09	0.37	52.3	0.02	0.02	0.01	100.5
JF-07A	opx	w	opx	0.01	56.7	0.09	0.88	0.37	5.43	0.12	0.11	33.6	1.16	0.26	0.01	98.7
JF-08A	cpx	e	cpx	0.01	54.9	0.49	8.86	0.05	5.45	0.08	0.03	11.4	14.3	3.92	0.07	99.5
JF-09A	garnet, majoritic	deep-e	maj	0.02	42.4	0.09	21.0	0.08	14.1	0.40	0.01	16.2	6.11	0.20	0.01	100.6
JF-10B	olivine	p	ol	0.02	40.8	0.01	0.03	0.04	5.27	0.07	0.32	51.8	0.01	0.02	0.00	98.4
JF-11A	cpx	e	cpx	0.02	55.7	0.22	7.94	0.06	2.94	0.03	0.08	11.0	16.0	4.78	0.03	98.7
JF-11B	cpx	e	cpx	0.02	56.4	0.21	8.10	0.07	2.92	0.03	0.07	11.2	16.0	4.87	0.03	99.8
JF-12A	cpx	e	cpx	0.00	54.5	0.36	3.63	0.12	5.90	0.08	0.05	13.6	18.7	2.16	0.02	99.1
JF-13A	garnet	e	3gt	0.05	40.6	0.70	21.9	0.09	14.4	0.28	0.01	12.7	9.15	0.21	0.01	100.0
JF-13B	garnet	e	3gt	0.04	40.8	0.66	22.0	0.10	14.3	0.28	0.02	12.8	9.05	0.21	0.01	100.2
JF-13C	garnet	e	3gt	0.05	41.0	0.70	22.3	0.09	14.4	0.26	0.01	12.9	9.14	0.19	0.00	101.0
JF-15A	garnet	e	gt	0.03	41.1	0.38	22.2	0.09	14.3	0.31	0.01	14.2	7.61	0.14	0.01	100.4
JF-15B	garnet	e	gt	0.05	41.1	0.40	22.3	0.06	14.2	0.30	0.01	14.2	7.57	0.14	0.00	100.4
JF-17A	opx	p	opx	0.00	57.4	0.02	0.48	0.42	3.47	0.09	0.11	35.6	0.45	0.08	0.01	98.1
JF-17B	opx	p	opx	0.01	58.1	0.02	0.54	0.46	3.41	0.07	0.12	36.0	0.45	0.06	0.01	99.2
JF-19A	SiO_2	e	SiO_2,cpx	0.01	99.3	0.00	0.02	0.00	0.00	0.01	0.00	0.02	0.00	0.02	0.01	99.4
JF-19B	cpx	e	SiO_2,cpx	0.01	54.3	0.11	1.75	0.05	7.13	0.18	0.01	19.0	15.0	0.72	0.02	98.2
JF-20B	garnet(-cpx)	e	gt-cpx	0.02	41.1	0.27	22.3	0.17	16.1	0.30	0.01	16.8	2.91	0.12	0.01	100.1
JF-20B	cpx(-gt)	e	gt-cpx	0.02	55.0	0.27	5.73	0.15	8.38	0.14	0.07	15.2	10.5	3.50	0.13	99.1
JF-22A	garnet, majoritic	deep-e	maj	0.09	48.7	0.50	9.65	0.22	11.7	0.36	0.01	21.7	5.73	0.65	0.01	99.4
JF-23A	cpx	e	2cpx	0.02	55.1	0.33	6.12	0.14	7.68	0.13	0.05	14.3	11.6	3.56	0.22	99.2

Table D2 continued

Sample	Mineral	Parag.	Assemblage	P_2O_5	SiO_2	TiO_2	Al_2O_3	Cr_2O_3	FeO	MnO	NiO	MgO	CaO	Na_2O	K_2O	Total
JF-23B	cpx	e	2cpx	0.02	54.8	0.32	5.96	0.16	7.65	0.14	0.06	14.1	11.7	3.54	0.23	98.6
JF-24A	opx	p	opx	0.02	57.4	0.03	0.68	0.50	3.09	0.07	0.11	35.7	0.44	0.03	0.01	98.2
JF-24B	opx	p	opx	0.00	58.8	0.02	0.70	0.51	3.08	0.08	0.11	36.9	0.45	0.04	0.01	100.7
JF-24C	opx	p	opx	0.00	57.9	0.02	0.71	0.53	3.14	0.08	0.12	36.5	0.45	0.04	0.01	99.5
JF-26A	cpx	e	cpx	0.03	54.6	0.26	2.11	0.03	5.58	0.10	0.01	16.0	19.3	1.06	0.12	99.2
JF-26B	cpx	e	cpx	0.02	55.1	0.27	2.13	0.04	5.57	0.10	0.03	16.3	19.3	1.11	0.12	100.1
JF-26C	cpx	e	cpx	0.01	54.8	0.27	2.11	0.06	5.55	0.10	0.02	16.1	19.3	1.08	0.13	99.5
JF-27A	opx	p	opx	0.01	57.1	0.01	0.77	0.33	3.47	0.09	0.12	36.2	0.33	0.03	0.01	98.4
JF-27B	opx	p	opx	0.01	57.4	0.02	0.73	0.31	3.45	0.09	0.11	36.3	0.34	0.05	0.00	98.8
JF-27C	opx	p	opx	0.01	57.6	0.00	0.74	0.32	3.47	0.08	0.12	36.5	0.34	0.05	0.01	99.2
JF-30A	opx	w	2gt,opx	0.00	56.5	0.10	1.16	0.19	8.09	0.11	0.18	31.7	0.66	0.36	0.01	99.1
JF-30B	opx	w	2gt,opx	0.00	56.2	0.10	1.13	0.15	8.02	0.11	0.18	31.6	0.66	0.36	0.00	98.5
JF-30C	garnet	w	2gt,opx	0.03	42.2	0.37	22.4	1.09	10.6	0.25	0.02	20.3	2.79	0.10	0.00	100.1
JF-30D	garnet	w	2gt,opx	0.02	42.2	0.41	22.8	0.42	11.5	0.27	0.02	19.9	2.85	0.12	0.00	100.5
JF-31A	garnet(ex)	e	gt (ex)	0.19	42.1	0.27	22.1	0.11	17.9	0.40	0.01	15.7	3.42	0.30	0.00	102.5
JF-32A	garnet	p	gt	0.01	42.4	0.01	18.0	8.11	5.59	0.28	0.01	24.3	1.54	0.02	0.00	100.3
JF-32B	garnet	p	gt	0.01	43.0	0.02	18.2	8.12	5.56	0.28	0.02	24.7	1.52	0.04	0.01	101.5
JF-33A	garnet	p	gt	0.02	41.9	0.01	17.9	8.03	5.86	0.28	0.01	23.0	2.72	0.02	0.01	99.7
JF-33B	garnet	p	gt	0.01	42.8	0.02	18.4	7.99	5.78	0.30	0.01	23.4	2.66	0.02	0.00	101.3
JF-34A	garnet(-cpx)	e	gt-cpx	0.01	41.2	0.97	19.6	0.56	15.0	0.35	0.01	17.1	5.48	0.04	0.01	100.3
JF-34B	cpx(-gt)	e	gt-cpx	0.01	54.3	0.14	0.78	0.04	8.07	0.15	0.01	20.9	13.9	0.34	0.03	98.6
JF-35A	garnet	p	gt,gt-opx-chr	0.04	42.2	0.02	17.8	8.61	4.83	0.21	0.01	24.9	1.28	0.02	0.00	99.9
JF-35B	garnet(-opx-chr)	p	gt,gt-opx-chr	0.03	42.3	0.01	17.8	8.63	4.84	0.21	0.01	24.9	1.28	0.03	0.00	99.9
JF-35B	opx(-gt-chr)	p	gt,gt-opx-chr	0.01	58.1	0.02	0.57	0.45	2.94	0.06	0.15	36.6	0.10	0.03	0.01	99.1
JF-35B	chromite(-gt-opx)	p	gt,gt-opx-chr	0.01	0.22	0.02	7.37	65.6	11.8	0.17	0.13	15.0	0.02	0.04	0.00	100.4
JF-36A	garnet	p	gt	0.02	41.6	0.03	11.1	17.8	5.64	0.29	0.01	24.0	1.25	0.04	0.01	101.8
JF-37A	garnet, majoritic	deep-e	2maj	0.02	42.5	0.17	20.6	0.14	12.9	0.38	0.00	16.9	6.46	0.14	0.01	100.2
JF-37B	garnet, majoritic	deep-e	2maj	0.01	42.4	0.19	20.7	0.12	12.9	0.37	0.01	16.8	6.40	0.14	0.01	100.0
JF-38A	garnet	e	gt	0.01	41.7	0.40	21.2	0.57	14.5	0.33	0.01	17.4	4.21	0.05	0.00	100.3
JF-39A	garnet, majoritic	deep-e	maj	0.03	45.2	0.31	15.0	0.24	10.8	0.24	0.00	20.3	5.67	0.37	0.01	98.1
JF-40A	garnet	e	gt	0.02	41.5	0.38	21.7	0.46	15.4	0.36	0.01	16.6	4.15	0.06	0.00	100.5
JF-41A	garnet	e	gt	0.04	42.2	0.55	21.1	0.85	11.9	0.30	0.01	19.5	4.23	0.10	0.01	100.8

Table D2 continued

Sample	Mineral	Parag.	Assemblage	P_2O_5	SiO_2	TiO_2	Al_2O_3	Cr_2O_3	FeO	MnO	NiO	MgO	CaO	Na_2O	K_2O	Total
JF-41B	garnet	e	gt	0.04	42.1	0.53	21.1	0.85	11.8	0.29	0.01	19.3	4.19	0.09	0.01	100.3
JF-42A	garnet, majoritic	deep-e	maj	0.01	43.4	0.54	17.4	0.03	12.9	0.36	0.02	13.4	11.2	0.54	0.02	99.7
JF-43A	garnet	deep-w	maj, gt	0.00	42.3	0.39	19.8	3.60	11.0	0.34	0.00	20.1	3.12	0.02	0.00	100.7
JF-43B	garnet	deep-w	maj, gt	0.02	41.8	0.41	19.7	3.63	11.0	0.33	0.01	19.9	3.16	0.03	0.00	100.0
JF-43B	garnet, majoritic	deep-w	maj, gt	0.02	43.5	0.53	16.2	3.45	11.7	0.38	0.01	20.0	3.89	0.10	0.00	99.8
JF-43D	garnet, majoritic	deep-w	maj, gt	0.02	43.0	0.52	16.0	3.50	11.7	0.39	0.01	19.9	3.89	0.14	0.01	99.0
JF-44B	garnet, majoritic	deep-e	maj	0.02	44.1	0.32	17.9	0.31	11.7	0.30	0.01	17.7	7.97	0.18	0.01	100.6
JF-46A	garnet	p	gt	0.01	42.0	0.08	17.8	6.84	5.77	0.25	0.01	23.6	2.30	0.03	0.01	98.8
JF-47A	cpx(ex)	e	cpx (ex)	0.02	54.5	0.42	2.18	0.06	9.61	0.18	0.03	19.1	11.3	1.75	0.01	99.2
JF-48A	garnet, majoritic	deep-e	maj	0.02	42.0	0.20	21.7	0.14	13.8	0.40	0.01	16.2	5.89	0.13	0.01	100.5
JF-48B	garnet, majoritic	deep-e	maj	0.02	41.6	0.18	21.5	0.08	13.9	0.39	0.01	16.1	5.89	0.13	0.00	99.8
JF-49A	opx	w	gt,opx	0.00	56.3	0.07	0.91	0.16	10.6	0.16	0.05	30.0	1.24	0.09	0.01	99.6
JF-49C	garnet	w	gt,opx	0.01	42.2	0.47	20.5	1.84	12.6	0.30	0.01	18.8	3.78	0.05	0.02	100.6
JF-49D	opx	e	gt,opx	0.01	56.2	0.07	0.89	0.16	10.6	0.16	0.04	30.2	1.24	0.09	0.00	99.6
JF-50A	garnet, majoritic	deep-e	maj	0.02	42.5	0.09	21.0	0.15	13.2	0.36	0.01	17.7	4.87	0.19	0.01	100.1
JF-51A	garnet	e	2gt	0.03	41.1	0.14	22.0	0.05	15.3	0.38	0.01	15.0	5.97	0.22	0.01	100.2
JF-51B	garnet	e	2gt	0.01	40.9	0.22	22.1	0.08	14.7	0.40	0.00	15.3	6.12	0.08	0.01	99.9
JF-52A	garnet	e	gt	0.14	39.6	1.30	19.5	0.08	18.1	0.34	0.01	15.1	4.10	0.23	0.00	98.6
JF-53A	garnet	e	gt,cpx	0.02	40.1	0.25	22.5	0.04	20.4	0.49	0.00	14.1	3.11	0.15	0.00	101.1
JF-53B	cpx	e	gt,cpx	0.02	55.7	0.36	9.44	0.05	7.46	0.14	0.02	10.2	9.85	6.07	0.09	99.4
JF-53C	garnet	e	gt,cpx	0.03	40.2	0.24	22.2	0.04	20.2	0.48	0.02	13.8	3.13	0.13	0.00	100.5
JF-54A	opx(-gt-cpx)	w	gt-opx-cpx	0.00	56.4	0.06	0.55	0.06	11.4	0.18	0.03	31.0	1.17	0.13	0.01	100.9
JF-54A	cpx(-gt-opx)	w	gt-opx-cpx	0.01	54.6	0.08	0.90	0.17	7.45	0.17	0.02	18.9	16.8	0.68	0.00	99.8
JF-54A	garnet(-opx-cpx)	w	gt-opx-cpx	0.03	41.4	0.56	19.1	1.38	15.5	0.37	0.01	17.2	5.19	0.05	0.01	100.8
JF-55A	garnet, majoritic	deep-e	2maj	0.02	47.9	0.41	11.9	0.34	9.44	0.25	0.02	22.0	7.41	0.43	0.02	100.2
JF-55B	garnet, majoritic	deep-e	2maj	0.03	48.1	0.31	12.3	0.38	9.08	0.25	0.01	22.1	7.24	0.42	0.00	100.2
JF-56A	garnet(-cpx-SiO2)	e	gt-2cpx-SiO2	0.03	40.2	0.33	22.2	0.16	21.1	0.49	0.01	11.9	5.26	0.10	0.00	101.7
JF-56A	SiO2(-gt-cpx)	e	gt-2cpx-SiO2	0.00	100.2	0.00	0.03	0.00	0.25	0.00	0.00	0.0	0.02	0.00	0.00	100.5
JF-56A	cpx(-gt-SiO2)	e	gt-2cpx-SiO2	0.01	54.5	0.25	4.25	0.12	8.88	0.14	0.05	13.3	16.4	2.56	0.01	100.4
JF-56A	cpx(-gt-SiO2)	e	gt-2cpx-SiO2	0.00	54.4	0.25	4.02	0.09	8.47	0.14	0.05	13.1	16.6	2.53	0.01	99.7
JF-56B	cpx	e	cpx	0.02	54.4	0.37	6.18	0.12	8.82	0.14	0.03	11.2	14.2	3.34	0.50	99.3
JF-57A	garnet	p	gt	0.03	42.1	0.06	18.6	6.85	5.19	0.26	0.01	25.2	0.73	0.02	0.01	99.0

Table D2 continued

Sample	Mineral	Parag.	Assemblage	P_2O_5	SiO_2	TiO_2	Al_2O_3	Cr_2O_3	FeO	MnO	NiO	MgO	CaO	Na_2O	K_2O	Total
JF-58A	garnet, majoritic	deep-e	2maj	0.03	43.3	0.28	18.1	0.19	14.7	0.41	0.02	18.2	4.62	0.27	0.01	100.1
JF-58B	garnet, majoritic	deep-e	2maj	0.03	43.7	0.28	18.4	0.17	14.6	0.40	0.01	18.4	4.62	0.26	0.01	100.9
JF-59A	garnet	e	gt,cor	0.01	40.4	0.22	23.0	0.04	14.1	0.23	0.02	10.0	13.0	0.16	0.01	101.1
JF-59B	corundum	e	gt,cor	0.00	0.19	0.06	97.0	0.09	0.57	0.01	0.01	0.1	0.00	0.02	0.00	98.0
JF-60A	opx	w	opx	0.02	55.2	0.00	0.68	0.51	5.26	0.13	0.15	34.3	0.51	0.06	0.00	96.7
JF-61B	garnet	e	gt	0.02	39.5	0.41	21.9	0.07	21.0	0.60	0.01	12.4	4.65	0.16	0.01	100.7
JF-62A	garnet	p	gt	0.01	40.6	0.02	19.2	5.83	7.02	0.31	0.01	22.4	3.24	0.03	0.01	98.7
JF-63A	garnet	e	gt	0.07	39.6	0.67	21.3	0.31	18.6	0.40	0.01	13.5	5.34	0.22	0.00	100.0
JF-63B	garnet	e	gt	0.08	38.7	0.65	20.8	0.31	18.5	0.41	0.01	13.3	5.34	0.20	0.00	98.2
JF-64A	garnet	p	gt	0.02	41.3	0.03	20.6	4.36	5.73	0.23	0.01	24.9	1.24	0.04	0.01	98.5
JF-65A	olivine	p	ol	0.00	39.7	0.01	0.04	0.04	6.76	0.08	0.40	52.3	0.02	0.03	0.01	99.4
JF-66A	garnet(ex)	e	gt(ex)	0.01	40.8	0.32	21.9	0.12	14.3	0.40	0.02	16.1	5.29	0.05	0.01	99.3
JF-67A	garnet	e	gt,cpx	0.02	41.1	0.39	22.3	0.12	17.7	0.33	0.01	16.4	2.87	0.15	0.00	101.5
JF-67B	cpx	e	gt,cpx	0.01	54.4	0.37	6.74	0.14	8.73	0.15	0.05	13.5	9.66	4.28	0.19	98.3
JF-68A	garnet(ex)	e	gt(ex)	0.02	41.5	0.33	22.2	0.31	12.9	0.34	0.01	18.2	4.39	0.05	0.00	100.3
JF-69A	garnet	e	gt	0.04	39.7	0.39	21.9	0.22	15.7	0.31	0.01	15.0	5.93	0.13	0.01	99.3
JF-70A	cpx	e	cpx	0.00	53.9	0.13	2.34	0.11	8.12	0.16	0.02	18.4	14.2	0.95	0.02	98.4
JF-72A	cpx	e	cpx	0.02	55.4	0.05	1.87	0.13	5.13	0.12	0.02	18.1	16.6	1.70	0.16	99.4
JF-73A	opx	p	opx	0.01	57.1	0.01	0.66	0.49	3.35	0.10	0.10	36.5	0.24	0.07	0.00	98.7
JF-74A	cpx	e	cpx	0.02	54.9	0.38	8.58	0.17	5.58	0.08	0.06	11.0	13.2	4.32	0.24	98.5
JF-76A	garnet	e	gt	0.02	40.3	0.24	23.1	0.00	14.8	0.26	0.01	9.4	13.4	0.12	0.01	101.6
JF-76B	garnet	e	gt	0.03	40.4	0.25	22.8	0.05	14.7	0.26	0.01	9.1	13.5	0.14	0.01	101.3
JF-77A	cpx	e	cpx	0.01	54.6	0.29	5.66	0.20	7.34	0.13	0.07	15.3	11.4	3.07	0.11	98.1
JF-78A	opx	p	opx	0.00	56.6	0.00	0.55	0.42	3.31	0.07	0.13	36.2	0.05	0.02	0.00	97.4
JF-79A	cpx(ex)	e	cpx (ex)	0.02	56.2	0.53	9.31	0.20	5.67	0.08	0.05	10.6	11.7	5.44	0.17	100.0
JF-80A	cpx	e	cpx	0.01	54.1	0.22	2.26	0.03	10.6	0.14	0.05	13.8	16.8	1.81	0.03	99.9
JF-81A	cpx	e	cpx	0.00	55.6	0.36	6.89	0.07	9.72	0.17	0.01	11.5	10.7	5.12	0.05	100.1
JF-84A	garnet, majoritic	deep-e	maj	0.02	44.2	0.41	17.3	0.30	11.7	0.31	0.01	18.8	6.36	0.30	0.01	99.7
JF-86B	cpx	e	cpx	0.02	55.6	0.40	9.81	0.10	5.22	0.08	0.03	10.0	12.0	5.87	0.09	99.2
JF-88A	olivine	p	ol	0.01	41.4	0.00	0.03	0.03	5.66	0.07	0.35	52.3	0.02	0.03	0.00	100.0
JF-90A	cpx	e	2cpx	0.01	55.5	0.37	5.15	0.27	9.66	0.16	0.03	13.8	12.2	3.30	0.15	100.6
JF-90B	cpx	e	2cpx	0.01	55.3	0.38	5.08	0.28	9.58	0.17	0.04	13.7	12.4	3.33	0.15	100.5

Table D2 continued

Sample	Mineral	Parag.	Assemblage	P_2O_5	SiO_2	TiO_2	Al_2O_3	Cr_2O_3	FeO	MnO	NiO	MgO	CaO	Na_2O	K_2O	Total
JF-91A	cpx	e	cpx	0.01	56.0	0.29	6.07	0.18	6.64	0.12	0.06	14.4	11.9	3.87	0.22	99.8
JF-92A	cpx	e	cpx	0.01	55.1	0.47	8.95	0.07	5.65	0.09	0.03	11.1	14.5	3.84	0.07	100.0
JF-94A	olivine	p	ol	0.00	41.0	0.00	0.02	0.04	6.83	0.09	0.39	51.2	0.03	0.02	0.01	99.7
JF-95A	cpx	e	cpx	0.02	54.9	0.44	4.88	0.06	9.02	0.15	0.05	15.5	12.3	2.67	0.08	100.1
JF-96A	cpx	e	cpx	0.01	54.1	0.20	2.49	0.25	9.39	0.16	0.12	14.9	16.1	1.72	0.01	99.4
JF-96B	cpx	e	cpx	0.01	54.7	0.23	3.02	0.30	9.49	0.16	0.11	14.6	15.6	2.02	0.01	100.1
JF-97A	opx	p	2opx	0.01	57.7	0.01	0.65	0.54	2.08	0.06	0.12	37.3	0.06	0.02	0.01	98.6
JF-97B	opx	p	2opx	0.01	58.1	0.01	0.63	0.55	2.08	0.05	0.12	37.5	0.06	0.04	0.02	99.2
JF-98A	olivine	p	ol	0.01	40.2	0.01	0.02	0.03	5.73	0.08	0.38	51.7	0.02	0.01	0.00	98.1
JF-103A	garnet(ex)	e	gt(ex)	0.01	40.9	0.68	20.8	0.45	16.3	0.30	0.01	19.2	1.04	0.04	0.01	99.7
JF-105A	chromite	p	2chr	0.01	0.12	0.73	6.19	63.2	16.6	0.27	0.10	13.4	0.01	0.01	0.00	100.6
JF-105B	chromite	p	2chr	0.01	0.12	0.73	6.20	63.2	16.5	0.28	0.10	13.2	0.01	0.02	0.00	100.5
JF-106A	chromite	p	chr	0.01	0.14	0.01	5.99	66.0	13.3	0.24	0.08	15.0	0.02	0.01	0.01	100.8
JF-107A	garnet(ex)	p	gt(ex)	0.02	41.6	0.07	19.5	5.14	6.13	0.28	0.01	22.8	2.74	0.03	0.01	98.4
JF-109A	chromite	p	2chr	0.01	0.17	1.22	4.57	63.5	18.2	0.31	0.12	12.6	0.01	0.02	0.01	100.7
JF-109B	chromite	p	2chr	0.01	0.15	1.16	4.67	63.4	17.5	0.31	0.12	12.8	0.01	0.02	0.00	100.2
JF110A	garnet(ex)	e	gt(ex)	0.02	40.0	0.44	22.4	0.07	16.4	0.41	0.01	11.2	9.10	0.15	0.00	100.2
JF-111A	cpx	e	cpx	0.01	54.4	0.30	6.94	0.15	8.22	0.13	0.05	12.5	10.7	4.49	0.18	98.2
JF-112B	chromite	p	chr	0.00	0.11	0.04	9.23	63.0	13.1	0.25	0.09	15.3	0.01	0.03	0.00	101.2
JF-113A	garnet(ex)	e	gt(ex)	0.02	40.5	0.64	21.4	0.39	15.6	0.35	0.01	21.8	0.05	0.03	0.00	100.7
JF-114A	garnet	p	gt	0.01	42.0	0.04	18.3	7.10	6.04	0.28	0.01	23.3	2.57	0.02	0.01	99.7
JF-115A	olivine	p	ol	0.01	40.9	0.01	0.02	0.02	6.05	0.08	0.40	52.2	0.02	0.01	0.00	99.7
JF-116A	chromite(ex)	p	chr(ex)	0.00	0.11	0.17	8.33	63.1	12.0	0.20	0.10	16.1	0.01	0.01	0.01	100.1
JF-118A	chromite	p	chr	0.01	0.07	0.07	9.20	62.4	12.4	0.24	0.35	14.7	0.01	0.03	0.00	99.4
JF-120A	cpx	e	cpx	0.01	55.5	0.42	8.74	0.17	4.67	0.09	0.04	11.9	11.6	5.22	0.10	98.4
JF-122A	garnet(-opx-cpx)	w	gt-opx-cpx	0.03	41.2	0.35	19.7	1.24	15.7	0.38	0.01	17.1	4.75	0.04	0.00	100.5
JF-122A	opx(-gt-cpx)	w	gt-opx-cpx	0.01	55.3	0.04	0.57	0.06	11.8	0.18	0.02	30.3	1.15	0.13	0.00	99.5
JF-122A	cpx(-gt-opx)	w	gt-opx-cpx	0.01	54.0	0.05	1.01	0.17	7.84	0.18	0.01	18.4	15.9	0.82	0.01	98.5
JF-123A	chromite	p	2chr	0.01	0.12	0.01	8.83	61.5	14.0	0.24	0.10	14.9	0.01	0.02	0.00	99.8
JF-123B	chromite	p	2chr	0.01	0.11	0.01	8.98	61.0	14.0	0.24	0.08	15.0	0.01	0.02	0.00	99.4
JF-124A	olivine	p	ol	0.00	42.1	0.00	0.01	0.04	5.12	0.07	0.33	53.8	0.01	0.00	0.01	101.5

Appendix D

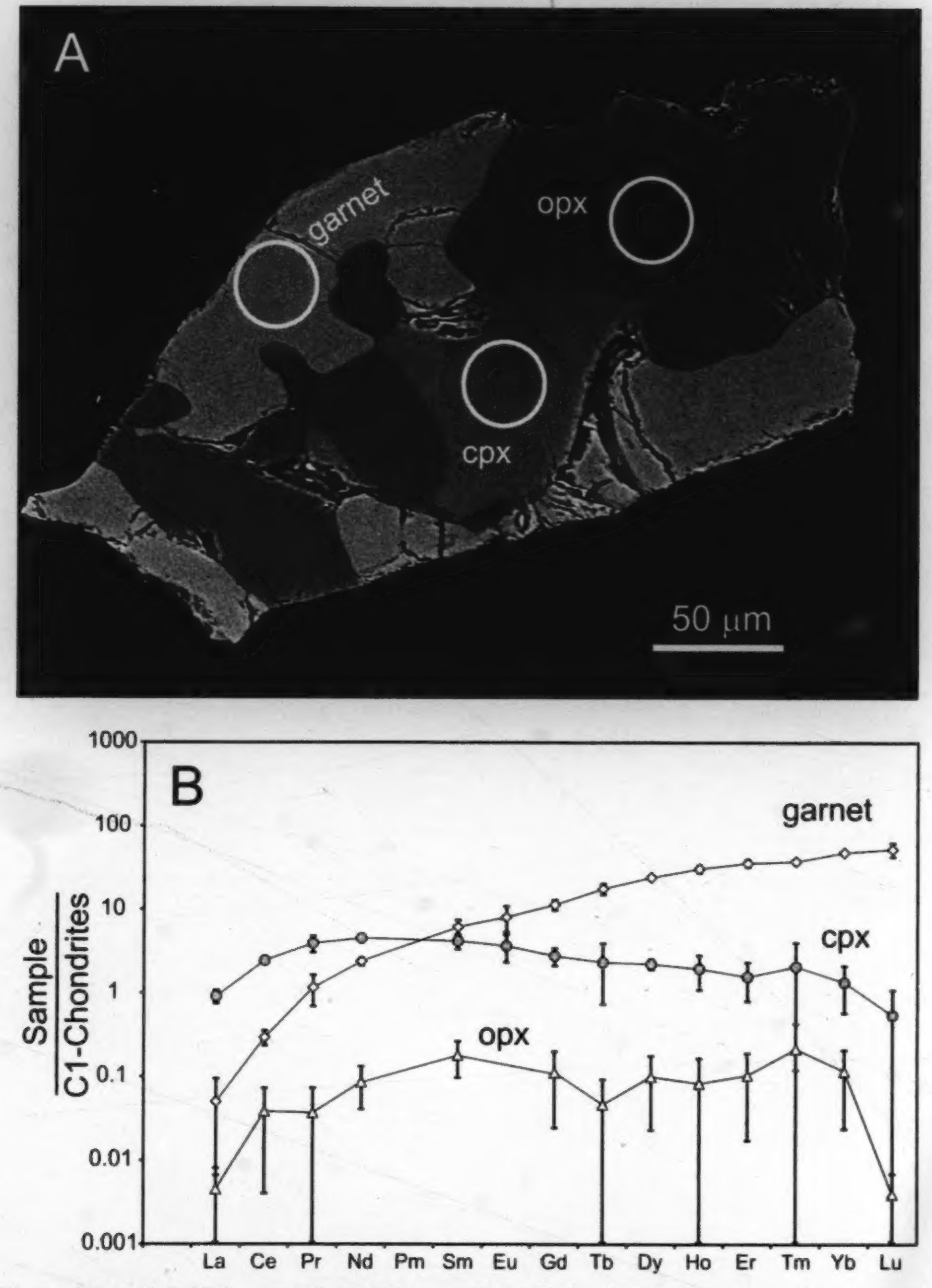

Figure D1: (A) BSE image of polyphase websteritic inclusion (gt-cpx-opx) recovered from diamond JF-122. Circles indicate position and approximate size of SIMS measurement points. (B) REE composition of the separate mineral phases. Error bars mark standard deviations of 1σ.

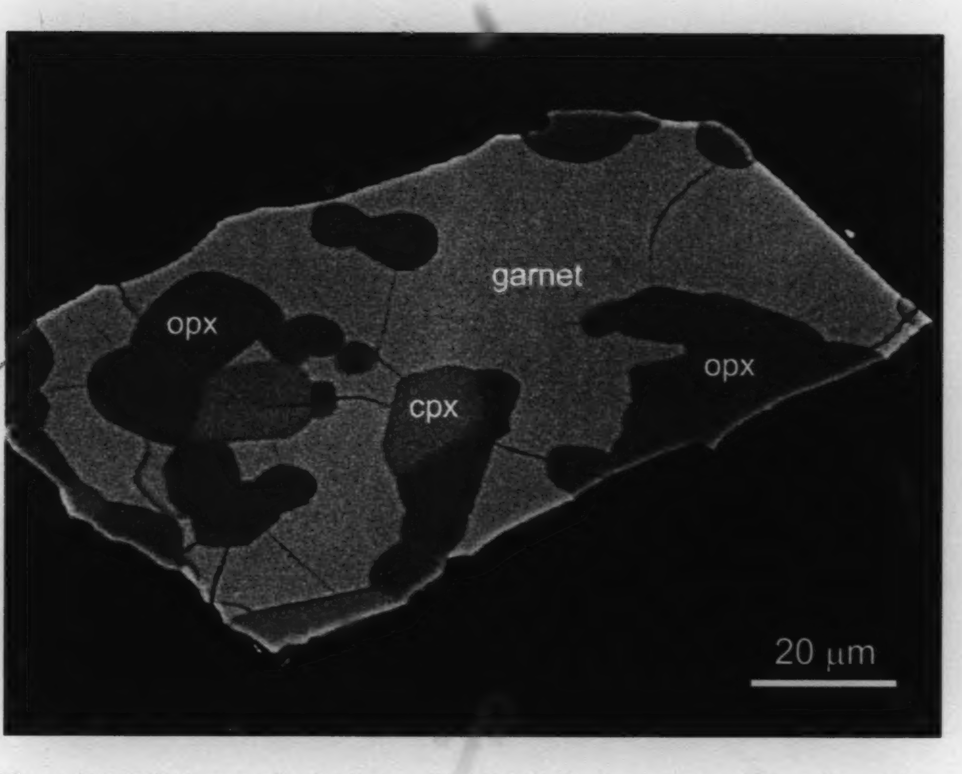
garnet
opx
opx
cpx
20 µm

Figure D2: BSE image of polyphase websteritic inclusion recovered from diamond JF-54.